Modelling the Freezing and Thawing Behaviour of Saturated Soils

Thesis Submitted in Canditure for the Degree of Doctor of Philosophy at Cardiff University

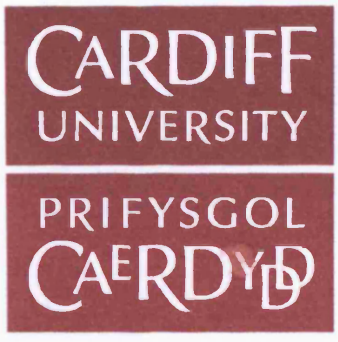

Mark Charles Glendinning

September 2007

ProQuest LLC
789 East Eisenhower Parkway
P.O. Box 1346
Ann Arbor, MI 48106-1346

CARDIFF UNIVERSITY
PRIFYSGOL CAERDYDD

DECLARATION

This work has not previously been accepted in substance for any degree and is not concurrently submitted in candidature for any degree.

Signed: M Glendinning (Mark Glendinning) **Date**: 14/09/07

STATEMENT 1

This thesis is being submitted in partial fulfilment of the requirements for the degree of PhD.

Signed: M Glendinning (Mark Glendinning) **Date**: 14/09/07

STATEMENT 2

This thesis is the result of my own independent work/investigation, except where otherwise stated. Other sources are acknowledged by explicit references.

Signed: M Glendinning (Mark Glendinning) **Date**: 14/09/07

STATEMENT 3

I hereby give consent for my thesis, if accepted, to be available for photocopying and for inter-library loan, and for the title and summary to be made available to outside organisations.

Signed: M Glendinning (Mark Glendinning) **Date**: 14/09/07

In Memory of

Margaret Ellen Glendinning

1952 – 2005

Acknowledgements

I would like to thank both my supervisors; Dr. Peter Cleall for his advice, support and encouragement throughout the course of this research period and Prof. Hywel Thomas for providing the opportunity of studying at the Geoenvironmental Research Centre. My sincere thanks to you both.

I would like to acknowledge the Engineering and Physical Sciences Research Council (EPSRC) which provided the financial support to undertake this study.

My thanks also go to all of my friends and colleagues at the Geoenvironmental Research Centre, particularly Dr. Suresh Seetharam and Dr. Deping Ding for their technical assistance and cooperation at the various stages during this study. Thanks must also be extended to my fellow numerical modelling colleagues; Yuchao Li (Kenny), Phil Vardon and Katherine Butterfield who have shared the trials and tribulations of development.

Finally I would like to thank my family and friends for enduring me during this period of study; in particular to Mum and Dad, sister Rachael and girlfriend Emma.

Abstract

This thesis presents an investigation of the thermo / hydro / mechanical behaviour of saturated soils with cryogenic suction effects.

The flow relationships accommodate a number of mechanisms: i) heat transfer by conduction, convection, and latent heat transfer; and ii) moisture transfer in the liquid phase due to pressure head, elevation head, and thermal gradients. The mechanical behaviour of the soil is modelled by an elasto-plastic work hardening modified Cam-Clay constitutive model.

A numerical solution for the theoretical formulation is presented. Standard finite element methods are used for spatial discretisation and finite difference methods are used for temporal discretisation.

Verification of the model is achieved by means of programme of tests to check the following cryogenic components; i) coupled thermo-hydraulic response, ii) deformation behaviour of the fully coupled thermo-hydro-mechanical model, iii) transient coupled liquid flow and deformation behaviour, and iv) latent heat of fusion.

Validation focused on the impact of the cryogenic related processes included within the proposed theoretical formulation. In particular the development of ice lenses and the movement of moisture under cryogenic suction were investigated. The performance of the proposed model with respect to a number of variables was subsequently explored in order to determine their effect on the magnitude and growth of ice lenses in a freezing soil.

The model was then applied to a large scale freezing experiment, namely a fully coupled thermo / hydro / mechanical simulation. The simulated results show a good correlation with the experimental results by predicting the patterns and trends of experimentally observed behaviour and the cryogenic processes that occur during the freezing and thawing of frost susceptible soils.

It was therefore concluded that the proposed model is capable of providing a good representation of the fully coupled THM behaviour of saturated soils with cryogenic effects.

Contents

Chapter 1 – Introduction

1.1. Introduction 1-1

1.2. Study Objectives 1-7

1.3. Research Background 1-8

1.4. Scope and Limitations 1-9

1.5. Thesis Overview 1-9

1.6. References 1-12

Chapter 2 – Literature Review

2.1. Introduction 2-1

2.2. Physics of Soil Freezing and Thawing 2-2

2.2.1. Mechanisms of Frost Heave 2-2

2.2.2. Primary and Secondary Frost Heave 2-7

2.2.3. Frozen Fringe 2-7

2.2.4. Soil Freezing Under Static Conditions 2-8

2.2.5. Soil Freezing Under Dynamic Conditions 2-9

2.3. Freezing Processes 2-11

2.3.1. Water Transport 2-11
2.3.2. Unfrozen Water Content and Hydraulic Conductivity 2-13
2.3.3. Equilibrium and Non Equilibrium Models 2-15
2.3.4. Separation Criterion 2-21
2.4. Thawing Processes 2-25
2.4.1. Thaw Settlement 2-25
2.4.2. Thaw Consolidation 2-27
2.4.3. Surface Temperature Variations with Time 2-30
2.4.4. Residual Stress in Thawing Soils 2-32
2.4.5. Soils with Discrete Ice Layers (Lenses) 2-35
2.4.6. Thawing Soil Slopes 2-37
2.5. Mechanical Properties and Effects 2-38
2.5.1. Freezing Effects on the Soil Structure 2-38
2.5.2. Permeability 2-38
2.5.3. Strength 2-39
2.5.4. Hydrostatic Pressure Effect on Frozen Soil Behaviour 2-40
2.5.5. Stress-Strain Behaviour of Frozen Soil 2-42
2.5.6. Creep and Creep Strength of Frozen Soils 2-43
2.5.6.1. Creep of Frozen Soils 2-43
2.5.6.2. Creep Strength of Frozen Soils 2-44
2.5.7. Ice Content Effect on Strength 2-45
2.5.8. Temperature Effect on Strength 2-45
2.6. Numerical Modelling of Freezing and Thawing Soil 2-46
2.6.1. Empirical Models 2-47
2.6.2. Hydrodynamic Models 2-47
2.6.3. The Rigid Ice Model of Frost Heave 2-47
2.6.4. Segregation Potential 2-49

2.6.5. A Model for the Prediction of Ice Lensing and Frost Heave in Soils 2-51

2.6.6. Discrete Ice Lens Theory for Frost Heave in Soils 2-52

2.6.7. Modelling of Coupled Heat, Moisture and Stress Field in Freezing Soil 2-53

2.6.8. Thermo-Mechanical Models 2-53

2.6.9. Towards Multidimensional Fully Coupled Numerical Modelling of Freezing and Thawing Soil 2-54

2.7. Periglacial Processes 2-57

2.7.1. Process Definition 2-58

2.7.2. Observations of Laboratory Experiments 2-59

2.7.3. Mechanical Changes during Freezing and Thawing 2-60

2.7.4. Mechanisms of Mass Wasting 2-61

2.8. Conclusions 2-62

2.9. References 2-65

Chapter 3 – Theoretical Formulation

3.1. Introduction 3-1

3.2. Assumptions 3-2

3.3. Moisture Transfer 3-3

3.3.1. Mechanism of Liquid Flow 3-5

3.3.2. Governing Differential Equation for Water Flow 3-9

3.4. Heat Transfer 3-12

3.5. Deformation Behaviour 3-17

3.5.1. Governing Equation for an Elasto-Plastic Approach. 3-20

3.5.2. Material Behaviour under Elastic Conditions 3-21

3.5.3. Yield Function 3-22

3.5.4. Flow Rule 3-23

3.5.5. Hardening Laws 3-25

3.5.6. Development of the Elasto-Plastic, Stress-Strain Matrix, Dep 3-25

3.6. Summary and Conclusions 3-30

3.7. References 3-32

Chapter 4 – Numerical Formulation

4.1. Introduction 4-1

4.2. Spatial Discretisation 4-1

4.2.1. Spatial Discretisation for Flow Variables 4-2

4.2.2. Spatial Discretisation for Deformation Variables 4-6

4.3. Temporal Discretisation of the Coupled Flow and Deformation Formulation 4-9

4.4. Consideration of the Frozen Fringe 4-11

4.5. Conclusions 4-13

4.6. References 4-14

Chapter 5 – Verification

5.1. Introduction 5-1

5.2. Coupled Thermo-Hydraulic Response of a Thawing Soil System 5-2

5.2.1. Analytical Solution 5-3

5.2.2. Application 5-4

5.2.3. Results and Conclusions 5-6

5.3. Heaving Strains 5-10

5.3.1. Analytical Solution 5-10

5.3.2. Application 5-10
5.3.3. Results and Conclusions 5-13
5.4. Transient Coupled Liquid Flow and Deformation Behaviour 5-15
5.4.1. Application 5-17
5.4.2. Results and Conclusions 5-18
5.5. Latent Heat of Fusion 5-21
5.5.1. Analytical Solution 5-21
5.5.2. Application 5-21
5.5.3. Results and Conclusions 5-23
5.6. Conclusions 5-25
5.7. References 5-26

Chapter 6 – Validation and Sensitivity Analysis

6.1. Introduction 1
6.2. Moisture Movement in the Frozen Fringe and Ice Lensing 2
6.2.1. Analytical Solution 2
6.2.2. Analysis 3
6.2.3. Results and Conclusions 6
6.3. One Dimensional Ramped Freezing Test 16
6.3.1. Experimental Setup 16
6.3.2. Material Parameters 17
6.3.3. Numerical Simulation 19
6.3.4. Results and Conclusions 21
6.4. Overview of Sensitivity Analysis 35
6.5. Thermal Gradient 35

6.5.1. Introduction 35
6.5.2. Results and Conclusions 36
6.6. Rate of Cooling 39
6.6.1. Introduction 39
6.6.2. Results and Conclusions 40
6.7. Hydraulic Conductivity 43
6.7.1. Introduction 43
6.7.2. Results and Conclusions 44
6.8. Segregation Freezing Temperature 47
6.8.1. Introduction 47
6.8.2. Results and Conclusions 48
6.9. Stress Level 51
6.9.1. Introduction 51
6.9.2. Results and Conclusions 52
6.10. Conclusions 54
6.11. References 56

Chapter 7 – Simulation of a Freezing and Thawing Experiment

7.1. Introduction 7-1
7.2. Experimental Setup 7-2
7.3. Material Parameters 7-3
7.4. Numerical Simulation 7-6
7.5. Results 7-8
7.5.1. Temperature 7-9
7.5.2. Pore Water Pressure 7-10

7.5.3. Displacement 7-13
7.5.4. Effective Stress and Void Ratio 7-16
7.5.5. Numerical Difficulties 7-18
7.6. Conclusions 7-19
7.7. References 7-25

Chapter 8 – Conclusions and Further Work

8.1. Introduction 8-1
8.2. Current State of the Art 8-2
8.3. Theoretical Formulation and Numerical Solution 8-3
8.4. Verification of the Numerical Model 8-3
8.5. Validation and Sensitivity of the Numerical Model 8-4
8.6. Simulation of Freezing Experiments at Caen 8-5
8.7. Overall Summary and Conclusions 8-6
8.8. Suggestions for Further Research 8-7
8.9. References 8-10

List of Figures

Figure 2.2 1 - Positive prints of X-rays taken during ice lensing (Penner 1966)..... 2-4

Figure 2.3 1 – Cooling curve for soil water and ice (After Lundardini; Anderlsand and Ladanyi, 2003) 2-14

Figure 2.3 2 – Schematic drawing of a steadily-growing ice layer in a freezing soil. (Nakano 1990)..... 2-17

Figure 2.3 3 – Computed profiles in T, u_w, u_i and σ_n across the frozen fringe at the moment when σ_n surpasses P. (O'Neil and Miller 1985) 2-22

Figure 2.3 4 - Idealised distribution of temperature and ice pressure within the freezing fringe, adopted in the calculation. (Shen and Ladanyi 1987) 2-24

Figure 2.4 1 – Typical void ratio versus pressure curve for frozen soils subject to thawing (Andersland and Ladanyi 2003)..... 2-26

Figure 2.4 2 – One-dimensional thaw consolidation (Morgenstern and Nixon 1971).... 2-28

Figure 2.4 3 – Excess pore pressure a) $\sigma' = 0$ (weightless material) b) $P_0 = 0$ (no applied load) (Morgenstern and Nixon 1971)..... 2-30

Figure 2.4 4 – Neumann and linearly increasing surface temperature solutions for thaw depth (Lunardini 1997)..... 2-31

Figure 2.4 5 – Stress path in a closed system freeze-thaw cycle (schematic) (Nixon and Morgenstern 1973) 2-33

Figure 2.4 6 – Measurement of residual stress for reconstituted Athabasca clay: (a) increasing consolidation pressure; (b) constant consolidation pressure. (Nixon and Morgenstern 1973) 2-34

Figure 2.4 7 – Thawing in a soil ice profile: (a) thaw plane in soil; (b) thaw plane in ice. (Nixon 1973) 2-35

Figure 2.4 8 – Pore pressure at a soil-ice interface (Nixon 1973)..... 2-37

Figure 2.5 1 – a) A set of σ-ε curves of ice-poor saturated Lanzhou silt at various strain rates (w=15.5%, γ_d=17.25kN/m3). b) Typical elastic-plastic σ-ε curves. 1 – Elastic-strain hardening, 2 – Elastic-ideal plastic, 3 – Elastic-strain softening. (Zhu et al. 1991)..... 2-43

Figure 2.5 2 – Constant-stress (creep) test: (a) creep-curve variations; (b) basic creep curve; (c) true strain rate versus time. (Andersland and Ladanyi 2003)..... 2-44

Figure 2.6 1 - Schematic diagram of the frozen fringe, with ice lens above (O'Neill and Miller 1985)..... 2-48

Figure 2.6 2 – Relation between water intake velocity and temperature gradient across the active system during the formation of the final ice lens. (Konrad and Morgenstern 1981)..... 2-50

Figure 2.6 3 – Interaction mechanism in a fully coupled THM system (Neaupane et al. 1999)..... 2-55

Figure 2.7 1 – Profiles of soil movement following seven cycles of soil freezing and thawing as revealed by excavation of buried columns. (Harris and Davies 2000)..... 2-60

Figure 3.5 1 A general two dimensional stress system..... 3-18

Figure 3.5 2 a) Typical isotropic compression and recompression curves..... 3-21

Figure 3.5 3 – Modified Cam-clay yield locus..... 3-23

Figure 5.2 1 – Mesh used in simulation..... 5-5

Figure 5.2 2 – Thaw depth vs. square root of time – T_s = 273.05K, T_{Step} = 0.5K..... 5-8

Figure 5.2 3 – Relative Thaw depth vs. square root of time – T_s = 273.10K, T_{Step} = 0.5K..... 5-8

Figure 5.2 4 – Relative Thaw depth vs. square root of time – T_s = 273.10K, T_{Step} = 2.0K..... 5-9

Figure 5.2 5 – Temperature profile across sample during thaw – T_s = 273.10K, T_{Step} = 2.0K..... 5-9

Figure 5.3 1 – Mesh Used in Simulation..... 5-11

Figure 5.3 2 – Temperature time curve applied to nodes in heaving strain exercise5-13

Figure 5.3 3 – Plot of Development of Void Ratio Due to Freezing..... 5-14

Figure 5.4 1 – Plot of dissipation of analytical and numerical pore water pressure against time..... 5-20

Figure 5.4 2 – Plot of analytical and numerical settlement of surface and mid layer over time..... 5-20

Figure 5.5 1 – Mesh used in Simulation 5-22

Figure 5.5 2 – System fully frozen. 5-24

Figure 6.2 1 – Mesh used in Simulation 6-3

Figure 6.2 2 – Initial temperature profile through sample for mass balance test. 6-5

Figure 6.2 3 - Temperature curve applied to top and bottom of sample in mass balance test. 6-5

Figure 6.2 4 – Temperature profiles – undrained freezing test; a) moisture flow including cryogenic suction. b) moisture flow defined by Darcy's law 6-11

Figure 6.2 5 – Pore water pressure profiles – undrained freezing test; a) moisture flow including cryogenic suction. b) moisture flow defined by Darcy's law 6-12

Figure 6.2 6 – Displacement profiles – undrained freezing test; a) moisture flow including cryogenic suction. b) moisture flow defined by Darcy's law 6-13

Figure 6.2 7 – Mean effective stress profiles – undrained freezing test; a) moisture flow including cryogenic suction. b) moisture flow defined by Darcy's law. 6-14

Figure 6.2 8 – Void ratio profiles – undrained freezing test; a) moisture flow including cryogenic suction. b) moisture flow defined by Darcy's law 6-15

Figure 6.3 1 – Frost cell used to explore aspects of ice lens growth in soils (Penner 1986) 6-17

Figure 6.3 2 – Variation of hydraulic conductivity with temperature and volumetric ice content used for the ramped freezing test. 6-19

Figure 6.3 3 – Mesh used in Simulation 6-20

Figure 6.3 4 – Temperature curve applied to top and bottom of sample in ramped freezing test. 6-21

Figure 6.3 5 – Temperature profiles – ramped freezing test; a) moisture flow including cryogenic suction. b) moisture flow defined by Darcy's law 6-28

Figure 6.3 6 – Pore water pressure profiles – ramped freezing test; a) moisture flow including cryogenic suction. b) moisture flow defined by Darcy's law 6-29

Figure 6.3 7 – Displacement profiles – ramped freezing test; a) moisture flow including cryogenic suction. b) moisture flow defined by Darcy's law 6-30

Figure 6.3 8 – Mean effective stress profiles – ramped freezing test; a) moisture flow including cryogenic suction. b) moisture flow defined by Darcy's law 6-31

Figure 6.3 9 – Void rato profiles – ramped freezing test; a) moisture flow including cryogenic suction. b) moisture flow defined by Darcy's law 6-32

Figure 6.3 10 – Comparison of calculated surface heave with experimental data by Penner (1986) 6-33

Figure 6.3 11 – Comparison of calculated frost penetration with experimental data by Penner (1986) 6-33

Figure 6.3 12 - Increase in heave rate during growth history of ice lenses, run No. 1, soil No. 1, ramped temperature rate 0.02°C/day (Penner 1986). 6-34

Figure 6.5 1 – Thermal gradient profile through sample after 12 hours. 6-36

Figure 6.5 2 – Magnitude of surface heave with varying thermal gradient. 6-38

Figure 6.5 3 – 10 day displacement profiles through sample (variable thermal gradient). 6-38

Figure 6.6 1 – Variation of surface temperature for rate of cooling tests 6-40

Figure 6.6 2– Magnitude of surface heave with varying rate of cooling. 6-42

Figure 6.6 3 – End of simulation displacement profiles through sample (variable rate of cooling). 6-42

Figure 6.7 1 – Variation of hydraulic conductivity with temperature for simulations 6-44

Figure 6.7 2– Magnitude of surface heave with varying hydraulic conductivity. ... 6-46

Figure 6.7 3– 10 day displacement profiles through sample (variable hydraulic conductivity). 6-46

Figure 6.8 1– Magnitude of surface heave with varying segregation freezing temperature. 6-50

Figure 6.8 2– 10 day displacement profiles through sample (variable segregation freezing temperature). 6-50

Figure 6.9 1– Magnitude of surface heave with varying segregation freezing temperature. 6-53

Figure 6.9 2– 10 day displacement profiles through sample (variable effective stress). 6-53

Figure 7.2 1 – Diagram of apparatus; TM, thermistors; T, semiconductor temperature sensors; PWP. Porewater pressure transducers (Harris et. al 1996) 7-3

Figure 7.3 1 – Variation of hydraulic conductivity with temperature and volumetric ice content used for the freezing and thawing experiment. 7-5

Figure 7.4 1 – Mesh used in Simulation 7-6

Figure 7.4 2 – Temperature time curve applied to surface and base of slope in simulation 7-8

Figure 7.5 1 – Temperature profile a) with time, b) with depth 7-21

Figure 7.5 2 – Pore water pressure a) with time, b) with depth 7-22

Figure 7.5 3 – Displacement profile a) with time, b) with depth 7-23

Figure 7.5 4 – Effective stress profile with depth 7-24

Figure 7.5 5 – Void ratio profile with depth 7-24

List of Tables

Table 2.6 1 – Classification of frost heave models (Kujala 1997) 2-46

Table 3.5 1 – Comparison between segregation potential, osmotic model and proposed model. 3-9

Table 5.1 1 – Summary of verification exercises 5-2

Table 5.2 1 – Thermal Constants Used in Simulation 5-6

Table 5.3 1 – Heaving strain test conditions 5-12

Table 5.3 2 – Simulated End of Run Results for Test H1 – H4 5-14

Table 5.3 3 – Simulated vs. Analytical Void Ratio 5-14

Table 5.5 1 – Thermal Constants Used in Calculation 5-22

Table 5.5 2 – Energy Requirements 5-23

Table 5.5 3 – Predicted vs. Simulated Finish Temperatures 5-23

Table 6.2 1 – Thermal Constants Used in Calculation 6-4

Table 6.5 1 – Thermal gradient tests 6-36

Table 6.6 1 – Rate of cooling tests 6-39

Table 6.7 1 – Hydraulic conductivity tests 6-43

Table 6.8 1 – Segregation freezing tests 6-47

Table 6.9 1 – Insitu stress level tests 6-51

Table 7.3 1 – Test Soil Geotechnical Properties (Harris et al 2001) 7-4

Table 7.3 2 – Thermal Constants Used in Calculation 7-4

Nomenclature

A	Defined in equation 2.3-6
A	Defined in equation 2.4-7
A	Defined in equation 2.5-5
A_0	Thaw strain parameter. Defined in equation 2.4-3
A_T	Defined in equation 3.5-14
$\mathbf{A}$	Defined in equation 3.5-37
$\mathbf{A}$	Defined in equation 4.3-3
B	Defined in 2.4-7
$\mathbf{b}$	Body force vector
$\mathbf{B}$	Defined in equation 4.3-3
c_v	Coefficient of consolidation
c'	Effective cohesion
C_{ll}	Defined in equation 3.3-31
C_{lT}	Defined in equation 3.3-32
C_{lu}	Defined in equation 3.3-30
c_i	Specific heat capacity of ice
c_l	Specific heat capacity of liquid
c_s	Specific heat capacity of soil solids
C_{TT}	Defined in equation 3.4-23
C_{Tu}	Defined in equation 3.4-22
C_{ul}	Defined in equation 3.5-35
C_{uT}	Defined in equation 3.5-52
C_{uu}	Defined in equation 3.5-51
$\mathbf{C}$	Defined in equation 4.3-3
$\mathbf{C}_{ll}$	Defined in equation 4.2-13
$\mathbf{C}_{lT}$	Defined in equation 4.2-14

$\mathbf{C_{lu}}$	Defined in equation 4.2-12
$\mathbf{C_{TT}}$	Defined in equation 4.2-20
$\mathbf{C_{Tu}}$	Defined in equation 4.2-19
$\mathbf{C_{ul}}$	Defined in equation 4.2-39
$\mathbf{C_{uT}}$	Defined in equation 4.2-38
$\mathbf{C_{uu}}$	Defined in equation 4.2-37
d	Vertical thickness of thaw
D	Normalised excess pore water pressure
D_1	Empirically determined transport function. Defined in equation 2.3-3
D_2	Empirically determined transport function. Defined in equation 2.3-6
$\hat{D}_1$	Empirically determined transport functions. Defined in equation 2.3-10
$\hat{D}_2$	Empirically determined transport functions. Defined in equation 2.3-10
$\mathbf{D}$	Elasticity matrix
$\mathbf{D_{ep}}$	Elasto-plastic matrix
e	void ratio
e_f	Frozen void ratio
e_0	Initial void ratio
e_{th}	Thawed void ratio
E	Young's modulus
E_i	Ice sink source term
E_l	Liquid sink source term
f	Liquid water flux
F	Yield function as defined in equation 3.5-19
$\mathbf{f_L}$	Defined in equation 4.2-17
$\mathbf{f_T}$	Defined in equation 4.2-23
$\mathbf{f_u}$	Defined in equation 4.2-23
g	Gravitational constant
G_{ff}	Thermal gradient in frozen fringe

h_i	Initial ice layer thickness
H	Thickness of the element of soil strata
H_c	Heat capacity of the soil
H_f	Thickness of the frozen element of soil strata
H_{th}	Thickness of the thawed element of soil strata
J_l	Defined in equation 3.3-35
J_T	Defined in equation 3.4-26
k	hydraulic conductivity
k_l	Effective permeability of pore-liquid
k_0	Defined by equation 2.3-6
k_u	Unfrozen hydraulic conductivity
k_f	Frozen hydraulic conductivity
$\bar{k}$	Apparent hydraulic conductivity. Defined in equation 3.5-16
K	Bulk modulus
K_l	Bulk modulus of water
K_{ll}	Defined in equation 3.3-33
K_{lT}	Defined in equation 3.3-34
K_{Tl}	Defined in equation 3.4-25
K_{TT}	Defined in equation 3.4-24
K_0	Insitu at rest earth pressure coefficient
K_0	Saturated hydraulic conductivity
K_1	Defined by equation 2.3-11
K_2	Defined by equation 2.3-11
$\hat{K}_1$	Defined by equation 2.3-12
$\hat{K}_2$	Defined by equation 2.3-12
$\mathbf{K}_{ll}$	Defined in equation 4.2-15
$\mathbf{K}_{lT}$	Defined in equation 4.2-6
$\mathbf{K}_{Tl}$	Defined in equation 4.2-21
$\mathbf{K}_{TT}$	Defined in equation 4.2-22
L	Latent heat of fusion
L_w	Latent heat of water
L_s	Latent heat of soil

m	Test parameter. Defined by equation 2.5-5
m_v	Coefficient of compressibility
M	Slope of the critical state line
$\mathbf{m}$	Unit vector
n	Porosity
n_0	Location of the frost front
$\dot{n}_0$	Velocity of the frost front
n_l	Location of the lensing front
N_r, N_s	Shape functions
$\mathbf{N}$	Matrix of shape functions
p_i	Ice pressure
p_l	Liquid water pressure
p_0	Preconsolidation stress
p_w	Liquid water pressure
p'	Effective stress
P	Local mean stress
P_i	Ice pressure
P_0	Applied loading
P_{OB}	Overburden pressure
P_{SEP}	Separation pressure
P_l	Liquid water pressure
P_2	Ice pressure
$\mathbf{P}$	Strain-displacement matrix
q	Deviatoric stress
q_i	Ice flux
q_l	Liquid flux
q_s	Soil solids flux
$\mathbf{Q}$	Heat flux per unit area
$\mathbf{Q_c}$	Convective heat flux per unit area
Q	Plastic potential for yield surface (equation 3.5-20)
r_p	Effective pore radius of the soil
R	Mean radius of soil particles. Defined in equation 2.3-21
R	Thaw consolidation ratio

R_f	Mostly frozen part of the soil
R_0	Unfrozen zone. Defined in figure 2.3-2
R_1	Frozen fringe. Defined in figure 2.3-2
R_2	Ice layer. Defined in figure 2.3-2
R_Ω	Residual error introduced due to approximation
S_i	Degree of saturation of pore-ice
S_l	Degree of saturation of pore-liquid
t	Time
t_f	Time to thaw ice layer
T	Temperature
T_r	Reference temperature
T_f	Freezing temperature
T_s	Segregation freezing temperature
T_v	Time factor
T_0	Absolute temperature in Kelvin
T_1	Temperature of lensing front. Defined in figure 2.3-2
$\hat{T}$	Approximate value of temperature
$\mathbf{T}_s$	Nodal value of temperature
$\mathbf{TL}_{abs}$	Matrix of absolute tolerances
$\mathbf{TL}_{rel}$	Matrix of percentage tolerances
u_i	Pore ice pressure
u_l	Pore water pressure
$\hat{u}_l$	Approximate value of pore-water pressure
$\hat{\mathbf{u}}$	Approximate value of displacement
$\mathbf{u}$	Displacement vector
$\mathbf{u}_{ls}$	Nodal value of pore-water pressure
$\mathbf{u}_s$	Nodal value of displacement
v	Poisson's ratio
v_0	Initial specific volume
V	Volume
V_{ff}	Pore water velocity in the frozen fringe
V_s	Volume of solids

V_0	Initial volume
$\mathbf{v_l}$	Velocity of liquid
$\mathbf{v_i}$	Velocity of ice
w	Water content
w^*	Equilibrium water content
w_u	Unfrozen water content
w_i	Ice content
X, X_0	Distance to thaw plane from surface
Z	Dimensionless depth variable
x, y, z	Global Cartesian coordinates
α	Soil parameter defined in equation 2.3-5
α	Constant determined in the solution of the heat conduction problem. Defined in equation 2.4-5
α_q	Parameter for non-associated flow rule
α_T	Coefficient of thermal expansion
β	Soil parameter defined in equation 2.3-5
χ	Fluidity parameter controlling the plastic flow rate (plastic multiplier)
χ	Stress partition function
ε	Total strain
ε^e	Elastic component of strain
ε^p	Plastic component of strain
$\varepsilon^{(c)}$	Creep strain
ε_0	Instantaneous strain
ε_q^e	Elastic deviatoric strain
ε_q^p	Plastic deviatoric strain
ε_T^e	Elastic component of strain due to temperature changes
ε_v	Volumetric strain
ε_p^p	Volumetric plastic strain due to stress changes
ε_σ^e	Elastic component of strain due to stress changes
ε_r	Radial strain
ε_θ	Circumferential strain

ε_x, ε_y, ε_z	Normal strains
ϕ'	Effective angle of internal shearing resistance
ϕ_l	Defined in equation 4.3-4
γ	Defined in equation 2.3-15
γ_l	Unit weight of liquid
γ'	Effective soil unit weight
γ_{xy}, γ_{yx}	Shear strain
κ	Stiffness parameter for changes in effective stress in the elastic region
λ	Stiffness parameter for changes in effective stress for virgin states of the soil
λ_i	Thermal conductivity of pore ice
λ_l	Thermal conductivity of pore liquid
λ_s	Thermal conductivity of soil solids
λ_T	Thermal conductivity of soil
μ_l	Absolute viscosity of liquid
θ	Defined in equation 2.3-5
θ	Volumetric water content. Defined by equation 3.3-1
θ_i	Volumetric ice content of the soil
θ_l	Volumetric liquid content of the soil
θ_0	Initial water content
ξ	Moving coordinate. Defined in equation 2.3-13
ρ_i	Density of ice
ρ_l	Density of pore liquid
ρ_s	Density of soil solids
σ	Total stress
σ'	Effective stress
σ_e	Normal stress of the soil grains
σ_{iw}	Interfacial tension of the ice / water interface
σ_n	Neutral stress
σ_0	Applied stress. Defined in figure 2.4-1
σ_r	Radial stress

σ_θ	Circumferential stress
$\sigma_x, \sigma_y, \sigma_z$	Normal stresses
τ_{xy}, τ_{yx}	Shear stresses
ϖ	Integration constant
Γ^e	Element boundary surface
ϑ	Defined in equation 4.3-4
Ω	Heat content of moist soil
Ω^e	Element domain
φ	Variable vector
∇	Gradient operator

Chapter 1

Introduction

1.1. Introduction

The effects of climate change and global warming are leading to increases in average temperatures. In permafrost regions these rises in temperature are predicted to be more pronounced (Matsuoka, 2001) and have the potential to alter the stability of slopes, road bases and foundations, potentially resulting in increased pre-failure strains and possibly failure. It is of considerable importance to be able to quantify the change in rates of displacement, pore water pressure, and temperature and change in strength due to such climatic changes in these environments. With increasing temperatures these regions are experiencing an increase to the active layer depth, resulting in parts of the ground that would have normally been frozen starting to thaw. The development of models capable of representing these processes will lead to an improved ability to assess the effects of climate change on a variety of engineering and geological problems.

On a different note ground freezing has been applied to many geotechnical applications through necessity, pressure and energy resources which have driven the need to construct in the cold regions of the world. The development of ground freezing techniques have allowed construction using temporary frozen earth support systems to take place and the greater understanding of the behaviour and performance of frozen ground have been applied to the design of earth structures and foundations in permafrost regions (Andersland and Ladanyi 2003). The similarities between

construction ground freezing, cold regions engineering and periglacial processes all benefit from the development of numerical techniques for stability and deformation.

Artificial Ground Freezing (AGF) has been in use for more than a century with the first recorded application of AGF on a mineshaft project near Swansea, South Wales, in 1862 (Li et al, 2006). With AGF the ground surrounding the site of the proposed excavation is frozen using a series of heat pipes which radially freezes the soil around each pipe and subsequently join and form a strong, watertight barrier of frozen earth. The ground can then be safely excavated and, once construction is completed, thawed to return to its initial condition with the new structure in place. The ground freezing process is largely dependent on the time and temperature, factors such as the structure, grain size and permeability having minimal effect allowing the reuse of the refrigeration equipment from job to job.

While AGF uses freezing to give favourable ground conditions to construct on or in, there are locations where frozen ground causes extremely unfavourable ground conditions and additional steps must be taken while constructing in these areas. In general, pavements, airports and pipelines are among the infrastructures most affected by the presence of frost susceptible materials in arctic climates (Padilla et al 1997). Where buildings and structures are constructed in cold regions care has to be taken to ensure that foundations are placed at a sufficient depth to avoid problems resulting from frost heave. Warming effects from buildings can cause the ground to thaw and in cases of frost susceptible soil water can accumulate in the form of ice lenses providing there is free water available. The forces created by this process can be considerable and the magnitude of heave forces is generally difficult to determine and the impracticalities of fully restraining heave forces mean that proper design should be used to eliminate it (Andersland and Ladanyi 2003).

Engineering design can be used to control and limit the effects of frost heave, measures to control frost penetration particularly in heated buildings utilise insulation beneath the building to reduce the thermal losses through the ground; in unheated buildings, insulating the ground may reduce frost penetration considerably (Andersland and Ladanyi 2003). Replacement of the frost susceptible soil is another means to limit the frost heave and frost stable coarse granular material without ice

inclusions are the best materials for foundations in cold regions. From a phenomenological point of view, frost heave mechanics can be regarded as a problem of impeded drainage to an ice-water interface in the frozen soil at the segregation-freezing front (Konrad and Shen, 1996). Thus frost heaving in sands and gravels is generally negligible as the permeability of these materials is so high that they freely drain.

Significant problems with the ground in cold regions do not generally occur during the freezing phase but rather at thaw. Differential heave during freezing is the most common fault with spatial variations in the ground conditions resulting in varying heave amounts while thaw brings high moisture contents and instabilities which have far more severe consequences. Pavements must be designed to offer uninterrupted use at any time guarding against both differential heave during freeze and reduction in load supporting capacity during thaw. The critical phase in the seasonal variation in temperature is during thaw and pavements are at their weakest and most vulnerable to cracking at this time. Pavement structures are composed of one or more layers that are required to provide a strong working platform and to help transfer and distribute the vehicular loading when applied at the surface to the underlying natural subgrade soils (Hadi and Arfiadi, 2001). A variety of methods can be employed in the design of pavements to reduce the effects of freezing and thawing but ultimately cost is the major consideration in the design and adopted solution. Again frost susceptible soils are the trickiest of soils to design for given their propensity to heave and accumulate ice lenses.

In cold regions it is the natural thermal regime that controls the evolution of the ground and dominates in the whole. There are however instances where human intervention is controlling the thermal regime and the shaping the landscape. Chilled buried gas pipelines are considered to be practical for transporting natural gas from the arctic region over the discontinuous permafrost region to the warmer populated regions of the world. Proper design and construction of such pipelines requires consideration of some important processes that govern the behaviour of freezing soils (Razaqpur and Wang, 1996). Buried chilled gas and oil pipelines are particularly prevalent across Canada and Alaska carrying large volumes of oil and gas across huge

distances. In the northern most parts the ground is permanently frozen becoming discontinuous and sporadic further south. The variation in ground thermal regime offers design challenges from both freezing and thawing of the surrounding soil around the pipe depending on the geographic location. Where the pipe passes through permafrost regions the temperature of pipe contents may be warmer than the surrounding soil and thawing commences which results in thaw settlement. Insulation can be placed around the pipe or the contents chilled before entering the ground. The reverse occurs when the buried pipe passes through discontinuous and sporadic permafrost and the chilled pipe causes the surrounding soil to freeze, at the frost front ice lenses accumulate and frost heave occurs. Elegant designs for conveying the pipe above ground to prevent freezing and thawing of the soil result in a zigzag design to counter the effects of thermal expansion due to the pipe transition from frozen to unfrozen ground and seasonal variations.

Broadening the scope and considering all areas of the world which are permanently or seasonally frozen leads into another research area that has attracted considerable interest and attention from a geological perspective. Much of these regions are mountainous, are continually changing and evolving due to the thermal regime yet despite being uninhabited provide important information on cryogenic processes that impact on other disciplines within the frozen ground remit. The stability of soil masses are affected by freeze–thaw action which induces downslope displacement of soils in these cold, non-glacial environments, where vegetation is lacking or sparse (Ballantyne and Harris 1994). This process, broadly referred to as solifluction, operates slowly, in general at a rate of at most 1 m per year. Solifluction collectively represents slow mass wasting (movements) associated with freeze–thaw action, with the saturated soil movement associated with ground thawing designated as gelifluction. Its widespread distribution on mountain slopes means that solifluction contributes greatly to the evolution of mountain landscapes. Moreover, landforms and subsurface structures resulting from solifluction are strongly dependent on climatic conditions (Matsuoka 2001).

Extensive research has been carried out in the field to monitor and evaluate the conditions which cause the gradual mass wasting of slopes. For this purpose, field

measurements have been undertaken in a variety of geographical situations ranging from polar hill slopes to tropical high mountains and, as a result, a large number of data-sets of solifluction rates and associated parameters have been obtained (Matsuoka 2001). Laboratory simulations using full scale and centrifuge modelling have further contributed to the understanding of the mechanisms that are involved in the solifluction processes (Harris and Davies 2000; Harris et al. 1997; Harris et al. 2003; Harris et al. 1993). Despite extensive field studies, progress in understanding gelifluction processes has been limited.

While field studies, large scale laboratory experiments and centrifuge modelling offer a good understanding they are however expensive and time consuming activities to undertake. Adopting a numerical modelling approach permits considerable time savings to be made as months and years of time can pass in a matter of hours and days. The ability to forecast and predict into the future is one potential application of numerical models as well as finding use as a design tool for engineering structures in cold regions. Inevitably the complexity of the available numerical models has increased as developments in understanding and computing power have grown.

Numerical modelling of freezing and the associated frost heave that accompanies freezing has attracted attention since the 1970s with many studies and models proposed. These models have nearly all been based on coupled heat and moisture transfer (Harlan, 1973; Taylor and Luthin, 1978) or conceptual models such as the segregation potential (Konrad and Morgenstern 1981; Nixon 1991). The major limitation to these models was the inability to consider the effect of external loading on the freezing process and it was assumed that there was no applied loading and the ice was under atmospheric pressure (the segregation potential was later modified to account for external loads).

One of the first models to incorporate applied loading was by Hopke (1980) with further advancements in understanding presented by Gilpin (1980) allowing the prediction of ice lens location and the introduction of the rigid ice model considered the application of external loading (O'Neill and Miller, 1985). These three models were still limited as the applied loading was only considered as a factor influencing the frost heave, while the stress field in the soil due to loading, volumetric expansion

and creep heave not considered and calculated in these models (Shen and Ladanyi, 1987). Traditionally, frost heave modelling has been one-dimensional however the theory is being extended to include continuum models with three-dimensions (e.g. Talamucci, 1997; Selvadurai et al, 1999; Mikkola and Hartikainen, 2001).

Modelling of frozen soils requires knowledge of the complex thermo-hydro-mechanical processes that occur as a result of freezing and thawing in soil in order to provide a model that can be applied to practical applications. The adaptability and reliability of these developments, for practical application to problems such as frost heave induced mechanics of civil engineering structures is as yet unproven and currently, there appears to be no satisfactory model which can accommodate these aspects in a comprehensive fashion (Selvadurai et al, 1999). Numerical modelling of such complicated processes nearly always results in simplifying assumptions and under highly idealised conditions.

The principal aim of this thesis is to develop, and implement via a numerical solution, a coupled heat, moisture and deformation model for saturated soil, which is commonly referred to as a thermo / hydro / mechanical (THM) model, which incorporates cryogenic effects. The numerical model developed uses as a starting point a numerical programme called COMPASS (COde for Modelling PArtially Saturated Soils) (Seetharam et al, 2007). COMPASS is a transient finite element code which can solve problems involving the coupled flow of heat, moisture, air, multiple contaminant gases and multiple contaminant chemicals as well as the mechanical behaviour of the soil. The model developed in this study uses the framework for transient THM analysis provided by COMPASS to implement the numerical solution of the proposed model.

In this model, the flow of heat due to conduction, convection and latent heat of fusion is governed by the equation of conservation of energy. The flow of moisture is considered to only take place in the liquid phase and the law of conservation of mass is utilised to produce the governing equation. The movement of liquid water caused by pressure gradients is governed by Darcy' law and the movement of liquid water due to cryogenic suctions is based on irreversible thermodynamics (Ratkje et al. 1982).

The stress / strain behaviour of the soil is modelled by an elasto-plastic work hardening modified Cam-Clay constitutive model. The governing equation for deformation is derived from considerations of stress equilibrium.

The complexities of the physical processes involved and the subsequent governing equations derived means that a direct analytical solution is unavailable. In order to solve these equations a numerical solution scheme is required. In this work spatial discretisation of the equations is performed by the finite element method, whilst a finite difference time-stepping algorithm is used to achieve temporal discretisation.

A verification and validation programme is conducted to test the integrity and soundness of the model. The verification exercises focuses on the cryogenic processes that have been incorporated into the existing COMPASS numerical model. A step by step approach against subsets of the full model is implemented before the completed numerical code is validated on an experimental example.

A sensitivity analysis on key model variables is performed to explore the model performance in order to determine their effect on the magnitude and growth of ice lenses in a freezing soil. The effect each key variable contributes to ice lensing in a freezing soil is explored based on the validation exercise from the preceding chapter.

The numerical model is then applied to experimental work carried at Caen (Harris 2007, personal comment) on one, one sided freezing test. The objective of this work is to gain an improved confidence in the ability of the developed model to solve thermo / hydro / mechanical problems in freezing / thawing soils. Comparisons between the experimental and numerical results are presented and discussed.

1.2. Study Objectives

The main objectives for this study are summarised as follows;

i. The investigation and development of a coupled theoretical model of saturated soil with cryogenic effects including the effects of moisture flow, heat flow and deformation.

ii. The development of two-dimensional thermo / hydro / mechanical governing equations.

iii. The development of a numerical solution of the theoretical formulation.

iv. The development of a computer programme, based on the existing model COMPASS, of the numerical solution for saturated soil with cryogenic effects.

v. To verify and validate the numerical code via comparisons with analytical solutions and existing experimental results.

vi. To investigate the cryogenic behaviour of frost susceptible soils.

1.3. Research Background

Extensive research has been carried out at Cardiff University in the field of developing both theoretical and numerical models of unsaturated soil. The theoretical model was initially developed as a coupled transient heat and moisture transfer model in unsaturated soil, including gravity effects by Thomas (1985). Development of the model continued with deformation behaviour introduced in the theoretical formulation by Thomas and He (1995) and multi-component reactive chemical transport by Seetharam (2003). A full review of the previous work in the modelling of unsaturated soil behaviour can be found in Seetharam (2003).

This work continues the development of the COMPASS code with the addition of cryogenic effects in saturated soil. The development undertaken in this work is a new area of research in the university and considerable changes to the theoretical formulation have been made. Due to the difference in formulation from previous research areas, the existing COMPASS code has been used as a framework which the current theoretical formulation has been integrated into. The data file manipulation, finite element implementation and solvers have remained unchanged from previous versions.

1.4. Scope and Limitations

The limitations of the model are as follows;

i. One of the principal assumptions of the model is that the soil is homogeneous. It is known that soils exhibit some heterogeneity and this may be partly accommodated as the assumption of homogeneity only applies within an individual element. Therefore, different soil types may be used within an analysis.

ii. The theoretical formulation has been presented in a two dimensional form, which may represent plane strain, plane stress or axisymmetric analysis. However, the numerical code, COMPASS, is also capable of modelling three dimensional problems.

iii. Temperatures in excess of 100°C cannot be modelled. This limitation is included as the phenomenon of boiling is not included in the model.

iv. Approximate numerical methods are needed to solve the theoretical governing equations. The finite element method is used for spatial discretisation, whilst a finite difference method is used for temporal discretisation.

v. Salinity and other chemical effects are not considered.

vi. The soil-ice composite material is assumed to deform elasto-plastically.

1.5. Thesis Overview

A brief description of each chapter is presented below.

Chapter 2 presents a comprehensive review of recent developments in the numerical modelling of coupled heat and mass transport in a deformable saturated freezing soil. The review considers in depth the freezing and thawing processes that take place, the mechanisms by which they occur and the assumptions that these are based on. The development of numerical models of freezing and thawing soils is discussed from

early implementations to current practice. The final section of the review considers the freezing and thawing processes from a geological point of view with a summary of the processes that need to be defined to formulate a model for frost heave.

Chapter 3 describes the theoretical formulation for thermal / hydro / mechanical behaviour of saturated frozen soil. A set of governing equations have been proposed to represent the flow of moisture, heat in a deformable saturated soil which may be subjected to freezing. The equations have been formulated in terms of three unknown primary variables, namely; pore water pressure (u_l), temperature (T), and deformation ($\boldsymbol{u}$).

In chapter 4 an approximate solution to the developed coupled flow and deformation formulation is presented. Spatial discretisation of the governing differential equations for moisture, heat and deformation has been accomplished through the use of the Galerkin weighted residual finite element method. Temporal discretisation has been achieved by employing a backwards difference mid-interval time stepping algorithm.

Chapter 5 presents the verification of the numerical model against analytical solutions. The COMPASS code has been extensively verified by previous authors using a series of test cases involving coupled moisture, air, heat and deformation, this chapter focuses on the additions that have been made to the code to incorporate the cryogenic processes that occur during freezing and thawing of saturated porous media. Verification tests have been carried out to check the following cryogenic components; i) coupled thermo-hydraulic response, ii) deformation behaviour of the fully coupled thermo-hydro-mechanical model, iii) transient coupled liquid flow and deformation behaviour, and iv) latent heat of fusion.

Chapter 6 validates the numerical model by considering the components of the moisture equation that have been introduced into the theoretical formulation to represent cryogenic suction and compares the findings against published experimental data. The model performance with respect to a number of variables in order to determine their effect on the magnitude and growth of ice lenses in a freezing soil is also explored. This is achieved using the validation test presented earlier in the chapter and individually varying key model parameters; thermal gradient, rate of

cooling hydraulic conductivity, segregation freezing temperature, and stress level in the soil.

Chapter 7 considers a large scale freezing experiment conducted at the Caen CNRS Centre de Géomorphologie in Caen, France. The results from a numerical simulation of the experiment are presented and compared against the experimental data.

Chapter 8 presents the conclusions that can be drawn from this work, and suggestions are made for further research.

1.6. References

Andersland, O. B. and Ladanyi, B. 2003. "Frozen ground engineering". 2nd Edition. New York ; Chichester: Wiley.

Ballantyne, C.K and Harris, C. "The Periglaciation of Great Britain". *Cambridge University Press,* 1994.

Gilpin, R. R. 1980. "A model for the prediction of ice lensing and frost heave in soils". *Water Resources Research* 16(5), pp. 918-930.

Hadi M. N. S. and Arfiadi Y., 2001 "Optimum rigid pavement design by genetic algorithms" *Computers and Structures*, **79**, 1617-1624

Harlan, R. L. 1973. "Analysis of coupled heat-fluid transport in partially frozen soil". *Water Resources Research* 9(5), pp. 1314-1323.

Harris, C. and Davies, M. C. R. 2000. "Gelifluction: Observations from Large-Scale Laboratory Simulations". *Arctic Antarctic and Alpine Research* 32(2), pp. 202-207.

Harris, C. Davies, M.C.R. and Coutard J-P. 1997. "Rates and Processes of Periglacial Solifluction: An Experimental Approach". *Earth Surface Processes and Landforms* 22(9), pp. 849-868.

Harris, C. Davies, M.C.R. and Rea, B.R. 2003. "Gelifluction: Viscous Flow or Plastic Creep?" *Earth Surface Processes and Landforms* 28(12), pp. 1289-1302.

Harris, C. Gallop, M. and Coutard, J-P. 1993. "Physical Modelling of Gelifluction and Frost Creep: Some Results of a Large-scale Laboratory Experiment". *Earth Surface Processes and Landforms* 18(5), pp. 383.

Harris, C. Davies, M.C.R. and Coutard J-P. 1996. "An Experimental Design for Laboratory Simulation of Periglacial Solifluction Processes". *Earth Surface Processes and Landforms* 21(1), pp. 67-76.

Harris, C. 2007. Personal comment. School of Earth, Ocean and Planetary Sciences, Cardiff University, Cardiff, UK.

Hopke, S. W. 1980. "A model for frost heave including overburden". *Cold Regions Science and Technology* 3(2-3), pp. 111-127.

Kirkby, M. J. 1995. "A model for variations in gelifluction rates with temperature and topography: implications for global change". *Geografiska Annaler Series A* 77(4), pp. 269-278.

Konrad, J. M. and Morgenstern, N. R. 1981. "The segregation potential of a freezing soil" *Canadian Geotechnical Journal* 18, pp. 482-491.

Konrad. J. -M., and Shen, M., 1996 "2-D frost action modelling using the segregation potential of soils" *Cold Regions Science and Technology*, **24**, 263-278

Li, S., Lai, Y., Zhang, M. and Zhang, S., 2006 "Minimum ground pre-freezing time before excavation of Guangzhou subway tunnel" *Cold Regions Science and Technology*, **46**, 181-191

Matsuoka, N., 2001. "Solifluction rates, processes and landforms: a global review". *Earth Science Reviews* 55(1-2), pp. 107-134.

Matsuoka, N. Hirakawa, K. Watanabe, T. Moriwaki, K. 1997. "Monitoring of Periglacial Slope Processes in the Swiss Alps: the First Two Years of Frost Shattering, Heave and Creep". *Permafrost and Periglacial Processes* 8(2), pp. 155-178.

Mikkola, M. and Hartikainen, J. 2001. "Mathematical model of soil freezing and its numerical implementation". *International journal for numerical methods in engineering.* 52: pp 543-557

Nixon, J. F. 1991. "Discrete ice lens theory for frost heave in soils". *Canadian Geotechnical Journal* 28, pp. 843-859.

O'Neill, K. and Miller, R. D. 1985. "Exploration of a rigid ice model of frost heave". *Water Resources Research* 21(3), pp. 281-296.

Padilla, F., Villeneuve, J-P., and Stein, J., 1997 "Simulation and analysis of frost heaving in subsoils and granular fills of roads" *Cold Regions Science and Technology*, **25**, 89-99

Ratkje, S. K., Yamamoto, H., Takashi, T., Ohrai, T. and Okamoto, J., (1982) "The hydraulic conductivity of soils during frost heave". *Frost i Jord*, **24**, 22-26

Razaqpur, A. G., and Wang, D., 1996 "Frost-induced deformations and stresses in pipelines" *International Journal of Pressure Vessels and Piping*, **69**, 105-118

Seetharam, S. C. 2003 "An Investigation of the Thermo / Hydro / Chemical / Mechanical Behaviour of Unsaturated Soils" Ph.D thesis. University of Wales, Cardiff. UK.

Seetharam, S. C., Thomas, H. R., Cleall, P. J. 2007 "Coupled Thermo / Hydro / Chemical / Mechanical Model For Unsaturated Soils - Numerical Algorithm" *International Journal for Numerical Methods in Engineering* **70 (12)**,1480-1511

Selvadurai, A.P.S., Hu, J. and Konuk, I. 1999. "Computational modelling of frost heave induced soil-pipeline interaction". *Cold regions science and technology*. 29: pp 215-228.

Shen, M. and Ladanyi, B. 1987. "Modelling of coupled heat, moisture and stress field in freezing soil". *Cold regions science and technology*, 14: pp 237-246

Talamucci, F. 1997. "Some recent mathematical results on the problem of soil freezing" In: Knutsson, S (Ed) 1997. *Ground freezing and frost action in geotechnical engineering Lulea; Sweden: Balkema*, pp 179-186.

Taylor, G.S. and J.N. Luthin, 1978. "A model for coupled heat and moisture transfer during soil freezing". *Canadian Geotechnical Journal*, 15: pp 548-555.

Thomas, H.R., 1985 "Modelling two-dimensional heat and moisture transfer in unsaturated soils, including gravity effects", *International Journal of Analytical Methods in Geomechanics*, **9**, 573-588.

Thomas, H.R., and He, Y., 1995 "Analysis of coupled heat, moisture and air transfer in a deformable unsaturated soil" *Geotechnique* **45 (4)**, 677-689

Chapter 2

Literature Review

2.1. Introduction

This chapter presents a review of developments and understanding in the field of freezing soil behaviour. Experimental, theoretical and numerical studies are covered in the context of the development of models to represent the behaviour of freezing and thawing soils. There have been a number of theoretical developments in the field of freezing and thawing soil over the past decades with many researchers adding contributions. In order to formulate numerical models of freezing and thawing soil it is imperative to identify the processes that occur, the mechanisms by which they occur and the assumptions that these are based on.

Section 2.2 covers the physics of soil freezing, the mechanisms that occur as soil freezes and thaws. In particular the concepts that define the pivotal elements of freezing and thawing processes in saturated soils are introduced. Consideration of soil freezing under static and dynamic conditions is explored as a preface to further discussion in proceeding sections.

Section 2.3 considers the freezing processes that take place as soil systems freeze. The movement of moisture to and within the transitional phase change zone is presented. Discussions on the nature of the development of the processes that take place in the transitional zone and the mechanisms that cause large heaving strains in freezing soils are also examined.

Section 2.4 deals with the thawing processes of ice poor and ice rich soils. The settlements and consolidation of these systems and their evolution with time to variations in temperature are presented. Mechanical changes in the soil as a result of thawing, thawing of discrete layers of ice within the soil structure and slope stability are also considered.

Section 2.5 deals with the mechanical properties and effects freezing and thawing cause. Soil structure, permeability, strength, stress – strain relationships are discussed with their associated implications. The effect of temperature, hydrostatic pressure and ice content on the problem is also presented.

Section 2.6 details developments in the numerical modelling of freezing and thawing soil. The developments of the model capabilities are reviewed and specific examples are given before their relative merits and drawbacks are summarised.

Section 2.7 explores the freezing and thawing processes from a geological point of view. Background to the problem is discussed from observations in the field to work conducted in the laboratory including recent advances in centrifuge modelling. The application of numerical modelling to the field conditions and laboratory experiments is proposed and discussed.

Finally, in section 2.8 overall conclusions are drawn from the discussion presented.

2.2. Physics of Soil Freezing and Thawing

2.2.1. Mechanisms of Frost Heave

The capillary theory for ice lens growth in non-colloidal soils proposed in the sixties initially showed promising advances. This theory was based upon the capillary suction present at a curved ice / water interface to provide the means by which water could move to a growing ice lens. This suction can be derived from the Kelvin equation:

$$p_i - p_l = 2\left(\frac{\sigma_{iw}}{r_p}\right) \qquad \textbf{2.2-1}$$

in which: p_i = ice pressure

p_l = liquid pressure

σ_{iw} = the interfacial tension of the ice / water interface

r_p = the effective pore radius of the soil

The Kelvin equation relates the equilibrium ice pressure of water to the curvature of the water –ice interface. Following a thermodynamic approach the Kelvin equation can be derived by equating the chemical potential of each of the phases.

This model predicts the growth of an ice lens only at the freezing front as its development is contingent on the inability of an ice / water interface to penetrate, at a given temperature, a pore which has a radius smaller than r_p. This type of model is termed as a 'Primary frost heave' model (Miller 1972).

Research carried out in the early seventies showed that the capillary model severely underestimated the force of frost heave and the maximum heaving pressure in non-colloidal soils (Miller 1972).

Feldman (1967) was perhaps the first to propose that an ice lens grows behind the freezing front, so that moisture movement not only takes place in the unfrozen soil but also in a region of frozen soil. Independently the concept of secondary heaving for non-colloidal soils was developed from earlier experimental work in the laboratory (Miller 1972). In this model ice could move by means of a regelation process. The whole model was considered to be a continuous rigid phase moving as a whole in the thermal field.

Experimental research confirmed the presence of the growing ice lens behind the freezing front. Loch and Kay (1978) used a double beam γ-scanning system to find the location of the growing ice lens in a non-colloidal sample and Penner (1986) photographed a growing ice lens in a soil behind a frozen fringe (Figure 2.2-1).

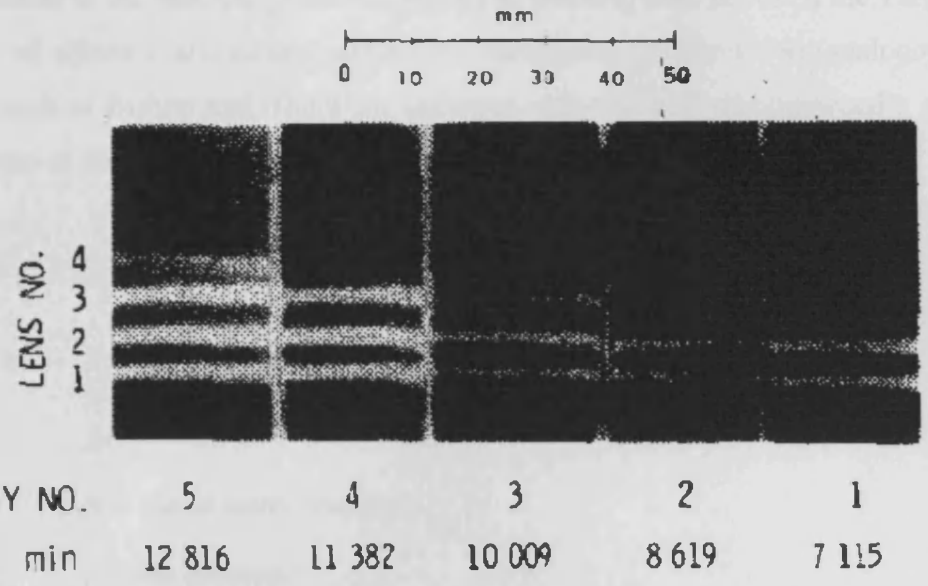

Figure 2.2-1 - Positive prints of X-rays taken during ice lensing (Penner 1966)

Penner (1977) who strongly supported the capillary theory concluded from their experimental work that the theory of secondary frost heave is realistic. It was also found that this zone increased in thickness as the overburden pressure was increased (Penner and Walton 1978).

The presence of the base of the ice lens at a temperature lower than that of the freezing front was able to explain the high heaving pressures that had been measured in silty materials, which capillary theory was unable to explain. The movement of appreciable amounts of water in frozen soils in response to imposed thermal gradients was shown by experiments in the US, Canada and Soviet Union. Williams (1977) recognised the possibility that water movement in frozen soil from a temperature gradient could result in considerable heaving pressure developing as a result of this migration. It was emphasised that despite the slow movement of moisture, the results may be significant over long periods of time.

The model in which ice lenses grow behind the frost front and mass transport takes place in a frozen zone was becoming accepted by an increasing number of researchers (Loch 1981). Much of the development of frost heave knowledge was accredited to R. D. Miller and the research group around him.

An extension to the secondary heaving model of freezing soil, in which the Tergazhi concepts of effective and neutral stress were introduced (Miller 1978) (analogous to the approach of Bishop and Blight for unfrozen soil) where it was proposed a stress distribution of the pore content of frozen soil by means of the equation;

$$\sigma_n = \chi p_l - (1-\chi) p_i \qquad \textbf{2.2-2}$$

in which σ_n = the neutral stress

χ = a stress partition function

p_l = liquid water pressure

p_i = ice pressure

Having introduced these stress variables, (Miller 1978) it is possible to determine where in the changing thermal field, and where, with respect to the location of the frost front during frost penetration, a new ice lens will start to form.

It was stated that an observed characteristic of frost heave, both in the field and in a laboratory test, is the non-steady nature of the thermal field and, consequently, the fact that frost penetration and heave by ice lens growth takes place simultaneously at nearly any rate of heat extraction.

Further model developments often used a Clausius-Clapeyron relation which had been derived for thermodynamic equilibrium between ice and water in porous media (Loch 1981). This equation relates the water potential in the unfrozen pore water to the local pore ice pressure and temperature. The equation has the following form:

$$\frac{dp_l}{\rho_l} - \frac{dp_i}{\rho_i} = L\frac{dT}{T_0} \qquad \textbf{2.2-3}$$

in which p_l, p_i = the pressure of water and ice phases respectively

ρ_l, ρ_i = the density of water and ice respectively

L = the latent heat of fusion of water

T_0 = the absolute temperature in Kelvin (273.15K)

$dT = T_0 - T$ is difference between the normal freezing temperature of pure water, T_0, and the actual temperature, T, of the system.

The Clausius-Clapeyron equation is derived from consideration of thermodynamic equilibrium which requires a balance of thermal, mechanical, and chemical forces. Thermal equilibrium is reached when temperatures are equal, mechanical equilibrium is reached when there is a balance of mechanical forces, and chemical equilibrium is reached when the chemical potentials of all components of the system are equal (Henry 2000).

For a system in chemical equilibrium containing more than one phase of a substance, the chemical potentials of the substance in all phases must be equal. The Clausius-Clapeyron equation describes the local equilibrium at any location in the mass-conducting soil, it has been used to derive the gradient of water potential and ice pressure, when there is a steady gradient of temperature in the frozen soil. A pressure difference and a temperature difference may compensate each other, thereby maintaining a constant chemical potential (Henry 2000).

Considering the effects of overburden pressure and incorporating this into a model has presented problems where the load is distributed between the soil matrix and the liquid and ice phases. For the situation in the frozen fringe, Miller attempted to solve this by means of equation 2.2-3.

Some researchers still accepted the capillary theory as the actual mechanism of frost heave (Loch 1981) and this created a disagreement about the maximum heaving pressure that can exist in a soil. The capillary theory led to the proposal that a 'shutoff' pressure exists for each soil, defined as the effective pressure at which no moisture flow occurs across the freezing front. At pressure greater than the shutoff pressure, water is expelled from the freezing front. Experiments by others indicated that the observed water expulsion may only be temporary and precedes the stage of water intake for segregation of ice lenses.

It was found that in all experiments where the overburden pressure was increased, the heave rate was found to decrease. Studies also indicated that the definite maximum heaving pressure may not exist in theory as a characteristic for a soil. Using this reasoning the pressure can build up slowly but almost for an indefinite period as long as the process is given an ample (geological) length of time.

2.2.2. Primary and Secondary Frost Heave

Modes of heaving that can be observed in a soil depend upon the properties of the soil and the boundary conditions of the narrow zone in which freezing takes place. Three possibilities can exist in the soil (O'Neill and Miller 1985); primary heave, secondary heave and no heave.

Primary heave consists of a layer of ice growing on top of some uniform soil, through which liquid water is drawn to join the ice. This system may or may not be overlain by frozen soil. In either case, essentially no ice penetrates the remaining unfrozen soil, and all freezing contributes directly to the surface heave.

The secondary mode of frost heave is where ice penetrates the soil; at the same time the liquid flow towards the ice feeds an accumulation of ice within the frozen soil. Lenses of pure segregated ice grow within forced discontinuities in the frozen soil fabric.

At the opposite extreme from primary heave, soil freezing may result in no heave at all when all ice formed penetrates the soil. Between these two limiting possibilities lies the secondary mode.

2.2.3. Frozen Fringe

Through research into frozen soils it is accepted that mass transport through a frozen zone underneath an ice lens occurs. The theory of secondary heave was introduced (O'Neill and Miller 1985) where an ice lens in a freezing soil grows somewhere in the frozen soil, slightly behind the frost front, i.e., the warmest isotherm at which ice can exist in the soil pores. Pore size, applied pressure and solute concentration primarily dictate the temperature of this warmest isotherm.

In silts, which are of the greatest interest due to their high frost susceptibility, the average pore size is relatively large and the frost front is then close to the 0°C isotherm.

The temperature at the base of the ice lens (or freezing front) is often referred to as the segregation-freezing temperature, T_s, because the segregation heaving process takes place at that isotherm (Konrad and Morgenstern 1980; Konrad and Morgenstern 1981). The zone of frozen soil between frost front and the freezing front is called the frozen fringe with evidence of its existence being published (Konrad and Morgenstern 1982a, b).

Published experimental data (Mageau and Morgenstern 1979) indicated that the apparent suction effect developed in the frozen soil on the cold side of the warmest ice lens had little or no effect on the rate of water migration to that lens. That is, an ice lens acts as a cut-off with regard to water flow.

2.2.4. Soil Freezing Under Static Conditions

As a preface to the consideration of soil freezing as a dynamic process, it is useful to consider the soil components under static or equilibrium conditions. Important insights have been gained while studying soils at sub zero temperatures and have been essential to the studies on the dynamics of heat and mass transfer in soils. The fundamental importance is the assumption that under dynamic conditions, 'local' equilibrium exists.

Relationships between variables which can be experimentally determined under static conditions are assumed to be equally applicable, on a local basis, under dynamic conditions when hysteresis is taken into account. The validity of this assumption depends on the magnitude of the departure of the system from an overall equilibrium condition. The magnitude of gradients under field conditions, and the size of the fluxes involved lead to an intuitive conclusion that relationships between variables should apply under both static and dynamic conditions in frozen soils.

Transport of water in the liquid phase was generally accepted to satisfy the Clausius – Clapeyron relationship (2.2-3). Although strictly applicable to static states due its

formulation on equilibrium conditions, it also applies under steady state dynamic conditions, i.e. conditions under which local pressure and temperature are not changing with time.

The Clausius – Clapeyron relationship can be used to express the energy status of the ice. Measurements of p_i are readily made providing the ice exists as large segregated regions (lenses). When ice exists as pore ice the values of p_i are not easily measured, however it is the extent of ice formation in this condition which is the most important for the transport of water in frozen soils (Kay and Perfect 1988).

The content of ice is normally measured as the difference between total water content and unfrozen water content. Measuring the total water content can be destructive using methods such as sectioning and gravimetric determination of water content or by non-destructive methods such as dual gamma-ray attenuation and thermal neutron radiography.

The vapour component in frozen soils, by means of the relative vapour pressure can be used to calculate the energy status of water in the vapour phase. Water vapour is only normally studied under static conditions in order to give a means of determining more about the ice and liquid water phases.

When solutes are present in unfrozen water it can be seen that they tend to be excluded from ice as the water freezes and as a result accumulate in the unfrozen water. Solute behaviour is of importance to the energy status of unfrozen water (Equation 2.2-3) and therefore to the unfrozen water content. The influence of solutes on liquid water pressure and on unfrozen water content can have major effects on the transport of water in freezing soils.

2.2.5. Soil Freezing Under Dynamic Conditions

Heat and mass transfer in freezing soils occurs through both direct and coupled transport mechanisms. Despite the basic framework for frozen soils, the processes responsible for the heat and mass transfer in frozen soil have been examined in less detail than that for unfrozen soil.

Liquid water flow in frozen soils containing pore ice only can be described by Darcy's law (Kay and Perfect 1988). This process is the direct driving force of water and results due to a liquid pressure gradient; the transport characteristic is the hydraulic conductivity. Equation 2.2-3 predicts that a temperature gradient within a partially frozen soil can induce a liquid pressure gradient. Values of apparent hydraulic conductivity have been determined from laboratory measurements by various ways and by several authors and have been found to be reasonably consistent (Kay and Perfect 1988).

It was observed between 0°C and -1°C that the apparent hydraulic conductivity function decreases rapidly from unfrozen values in the order of 10^{-8} m/s to values between 10^{-12} and 10^{-14} m/s. Below -1°C conductivity values appear to remain relatively constant (Ratkje et al 1982).

A vapour phase may be present in frozen soil and transport of water in the vapour phase may take place. The extent of transport, relative importance of the vapour phase, and extent of coupling that occurs is lacking evidence (Kay and Perfect 1988).

As a result of water transport in the liquid, solid or vapour phases a change in water content will arise. In soils with a very high ice water content, considerable water accumulation can be observed but without visible ice lenses. This condition is common in soils near the ground surface that are seasonally frozen. Water accumulation may also occur in the form of needle ice or ice lenses which are soil free. Needle ice is a transient surficial phenomenon which occurs when thermal conditions are such so that ice crystals are unable to penetrate beyond the first few millimetres of the surface.

Ice lenses within the soil produce a rhythmic or stratified pattern of ice bodies. The formations may be laminar in shape, orientated perpendicular to the direction of heat flow or may be more polygonal in shape with some lenses orientated almost parallel to the direction of heat flow. Ice lenses in layered soils typically occur on the face of the finest textured layer encountered by the freezing front (Penner 1986).

Water accumulation in the form of ice in homogenous soil was initially described in terms of a divergence of water flux (Harlan 1973). This formulation could account for ice enriched zones; however it could not account for the formation of ice lenses which were free of soil grains. Additionally there was no means to distribute the applied load between the components, therefore making it difficult to determine p_w (a requirement for the prediction of the water flux).

The limitations to these approaches were solved by introducing a lensing criterion to specify the location where an ice lens will form. Use of the stress partition function and each ice lens forms at a specific location where the effective stress is zero or the neutral stress equals the applied load is one such example (Miller 1978).

Analysis of cores of frozen silt loam taken during different times throughout the year indicated that very little air exists behind the freezing front; this indicates that lens formation normally forms under saturated conditions. This transitional zone containing pore ice and unfrozen water separating segregated ice from the zero isotherm has been well documented. It has been found that the growth of the lens adjoining this zone depends on the properties of the zone and the cooling rate (Nakano 1986).

2.3. Freezing Processes

2.3.1. Water Transport

Water in frozen soil is accepted to exist in three phases; vapour, liquid water and ice. The liquid water content is generally referred to as the unfrozen water content and is mobile in the soil at temperatures below 0°C. The unfrozen water content of the soil is mainly dependant on the soil type and the temperature although unfrozen water versus temperature curves usually exhibit minor hysteresis depending on cooling and warming cycles (Nakano et al. 1982).

The presence of a freezing front in soils is believed to create a suction force that draws the water in the soil beneath the front upwards to provide water for the process

of ice lens formation. The process of cryogenic suction was explained by microscopic physics and chemistry (Blanchard and Fremond 1982). Their work investigated the thermal and hydraulic aspects of the freezing of soils but did not detail mechanical aspects such as heaving.

The question however exists in the literature as to whether the water flux in the frozen fringe is driven by a thermal gradient or by water pressure alone, i.e. the water flux is described by Darcy's law. The two differing opinions can be summarised as follows

$$f = f(p_w),\ f \neq f(T) \qquad \textbf{2.3-1}$$

$$f = f(p_w, T) \qquad \textbf{2.3-2}$$

A series of experiments was carried out to investigate the mechanisms of water transport through unsaturated frozen soils (Nakano and Tice 1987, 1990; Nakano et al. 1984a, b, c; Nakano et al. 1982, 1983). The studies into the transport of water in frozen clay under isothermal conditions found that the mass flux of water, f, is given by:

$$f = -\rho D_1(w,T)\frac{\partial w}{\partial x} \qquad \textbf{2.3-3}$$

where w is the content of water in all phases. Their work validated equation 2.3-3 with a series of experiments using two long soil columns with different but uniform initial water contents w, which were connected and exposed to a constant negative temperature, T.

It was their findings from the data collected that equation 2.3-3 describes the redistribution law of water and that the presence of the gradient of w alone does not necessarily generate the flux of water when $w(x)$ is not less than the equilibrium unfrozen water content w^* at a point x.

Nakano (1991) concluded that a temperature gradient is an important driving force of water in unsaturated frozen soils. Under isothermal conditions, both the gradient of

water content and temperature are the major driving forces for the transport of water in unsaturated frozen soils. The relationship between water content and temperature was then considered to determine if the two driving forces are dependant.

2.3.2. Unfrozen Water Content and Hydraulic Conductivity

When a fine grained soil is frozen, not all of the water within the soil pores freezes at 0°C. In some clay soils up to 50% of the moisture may exist as a liquid at temperatures of -2°C. This unfrozen water is mobile and can migrate under the action of a potential gradient (Morgenstern 1981).

The cooling curve for soil water (Figure 2.3-1) shows an ice phase forming in soil particles at a freezing temperature T_f. Current practice neglects the vapour phase and the total water content, w, is the sum of the unfrozen water, w_u, and ice contents, w_i.

$$w = w_u + w_i \qquad \textbf{2.3-4}$$

Experimental data for the unfrozen water content in frozen soils has been represented by a simple power curve of the form (Andersland and Ladanyi 2003)

$$w_u = \alpha\theta^{\beta} \qquad \textbf{2.3-5}$$

where α and β are characteristic soil parameters and θ is temperature, expressed as a positive number in degrees Celsius below freezing, e.g. $\theta = 3$ if $T = -3$°C.

A number of other means have been proposed to estimate the unfrozen water content in soils, the two-points method (Xu Xiaozu et al. 1985) is just one of a variety of other possible means.

The hydraulic conductivity is closely related to the unfrozen water content and under a potential gradient a considerable amount of water may be able to migrate in the frozen soil. These relationships often take the form of some power or exponential type law.

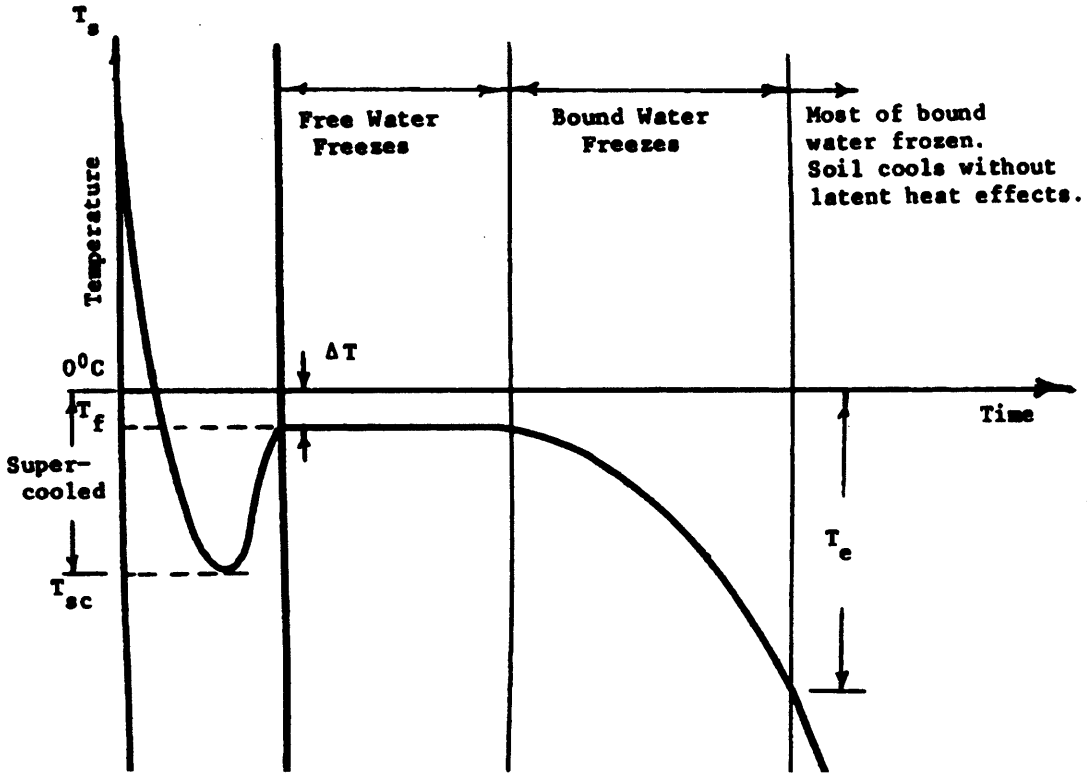

Figure 2.3-1 – Cooling curve for soil water and ice (After Lundardini; Anderlsand and Ladanyi, 2003)

Nixon (1991) describes the hydraulic conductivity of frozen soil by

$$k = \frac{k_0}{(-T)^A} \qquad \textbf{2.3-6}$$

where k_0 is the hydraulic conductivity at -1°C, T the temperature in degrees Celsius and A is the slope of the relationship between k and $(-T)$ on a log-log plot.

Using regression analysis on experimental results, the relationship between the hydraulic conductivity and temperature can be determined. Horiguchi and Miller proposed the relationship for one particular soil in the form (Shen and Ladanyi, 1987)

$$k = \begin{cases} 3.072\times10^{-11}e^{13.438T} & -0.3°C < T < T_f \\ 5.453\times10^{-13} & T \le 0.3°C \end{cases} m/s \qquad \textbf{2.3-7}$$

Shen and Ladanyi also proposed a relationship for Caen Silt in a similar form as (Selvaduari et al., 1999)

$$k = \begin{cases} 1.075\times10^{-9}e^{23.99T} & -0.3°C < T < T_f \\ 8.0499\times10^{-13} & T \le 0.3°C \end{cases} m/s \qquad \textbf{2.3-8}$$

2.3.3. Equilibrium and Non Equilibrium Models

Two possible forms for the mass flux of water were posed by Nakano (1991); if temperature, T, and water content, w, are independent the mass flux can be written in the general form:

$$f = -\rho D_1 \frac{\partial w}{\partial x} - \rho D_2 \frac{\partial T}{\partial x} \qquad \textbf{2.3-9}$$

where D_1 and D_2 are independent empirically determined transport functions that generally depend on temperature and water content. If temperature, T, and water content, w, are dependent, f is given by:

$$f = -\rho \hat{D}_1 \frac{\partial w}{\partial x} - \rho \hat{D}_2 \frac{\partial T}{\partial x} \qquad \textbf{2.3-10}$$

where $\hat{D}_1$ and $\hat{D}_2$ are dependent empirically determined transport functions.

During a series of experiments studying the transport of water in unsaturated frozen clay under temperature gradients (Nakano and Tice 1988, 1990) it was observed that equation 2.3-9 holds true. If equation 2.3-10 was to hold true, a flow of water in the direction of lower temperature would be observed. The experiments undertaken however showed that as water moves towards the cold end, the initial uniformity of w breaks down and a gradient of water content build up in the column acts against the driving force of water movement due to a temperature gradient.

The two driving forces of water movement were found to balance each other out over time while the profile of water content in the column asymptotically approaches the

stationary profile with increasing time. The results from the experimental work confirmed the validity of equation 2.3-9 and it was subsequently proposed that in saturated frozen soils the two major driving forces for the transport of water are the gradient of temperature T under uniform pressure fields and the gradient of unfrozen water pressure P_l under isothermal conditions (Nakano 1991).

Experimentally it was shown (Mageau and Morgenstern 1979) that the gradient of temperature causes the movement of water in the direction of lower temperature under uniform pressure. Data determined experimentally (Horiguchi and Miller 1983) confirmed that the flux of water is proportional to the gradient of pressure under isothermal conditions.

The mass flux, f, in saturated soil in one direction can then be written in the general form as:

$$f = -K_1 \frac{\partial P_l}{\partial x} - K_2 \frac{\partial T}{\partial x} \qquad \textbf{2.3-11}$$

where x is the space coordinate, K_1 and K_2 are the properties of a given soil that generally depend on temperature and the composition of the soil. Where temperature, T, and liquid water pressure, P_l, are dependant, 2.3-11 may be rewritten as:

$$f = -\hat{K}_1 \frac{\partial P_l}{\partial x} - \hat{K}_2 \frac{\partial T}{\partial x} \qquad \textbf{2.3-12}$$

where $\hat{K}_1$ and $\hat{K}_2$ are the properties of a given soil that generally depend on T and the composition of the soil.

Determining if these two forces are dependant of each other has proved difficult to validate directly, but indirect mathematical and experimental studies have investigated into the water transport through the frozen fringe was considered in a series of papers (Nakano 1990, 1994b; Nakano and Takeda 1991; Takeda and Nakano 1990).

One-dimensional freezing of a soil saturated with water was considered under the assumption that the constituents of the soil are incompressible during the freezing

process. Under this assumption all dependant variables are functions of two independent variables; the space coordinate x, and time, t. For their analysis the soil was divided into two parts, an unfrozen part R_0 and a mostly frozen part R_f, by the 0°C isotherm $x = n_0(t)$ (Figure 2.3-2).

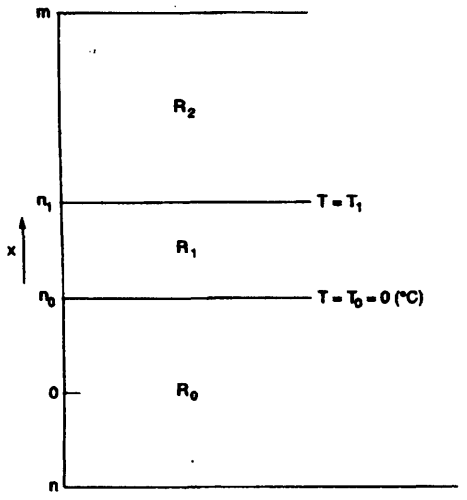

Figure 2.3-2 – Schematic drawing of a steadily-growing ice layer in a freezing soil. (Nakano 1990).

A special case was considered in which the velocity of the frost front $\dot{n}_o = (dn_0 / dt)$ is constant and that all dependant variables are described by a moving coordinate ξ alone, defined as:

$$\xi = x - \dot{n}_0 t \qquad \textbf{2.3-13}$$

A solution satisfying the two conditions described above is commonly referred to as a travelling wave solution.

The velocity of the frost front, $\dot{n}_0$, relative to the coordinate x, was shown to vanish when the stable growth of an ice layer occurs (Nakano 1986). The vanishing velocity of a front has been confirmed experimentally by Takeda (Nakano 1990). When $\dot{n}$ vanishes, the coordinates ξ and x coincide, x is used hereafter.

To investigate the problem the equations of heat and mass transfer that must be satisfied by a travelling wave solution to the quasi-steady problems in freezing soils

were derived. The problem of steady state ice layer growth was subsequently analysed using a particular case of the general quasi-steady problems in freezing soils (Nakano 1986).

Many hypotheses had been proposed in the literature with no consensus among the researchers as to the exact nature of water transport in the frozen fringe. The validity of the Clausius – Clapeyron equation (Equation 2.2-3) during the phase equilibrium has been confirmed (Radd and Oertle 1973) but questions still exist over its applicability to the freezing processes that occur in the frozen fringe. The difference of opinions comes essentially from experimental difficulties; for instance; the phase equilibrium is achieved in a long time interval, generally months (Talamucci 1997).

Some modellers assume that the heat and mass transfer in the frozen fringe are so slow that Equation 2.2-3 can be considered a good approximation even if the thermal and phase equilibrium is not reached (Gilpin 1980; Hopke 1980; Nixon 1991; Shen and Ladanyi 1987) and 2.2-3 is extended to the whole fringe. These models are classified as equilibrium models. The other opinion is that the phase equilibrium is only reached at the base of the lens and it is stated that equation 2.2-3 is only valid under these conditions and is not valid throughout the whole fringe even if phase equilibrium has been reached (Konrad and Morgenstern 1981; Loch 1981; Nakano 1990). Furthermore, under this assumption no relationship exists between the temperature and water pressure in the frozen fringe and these models fall into the category of non-equilibrium models.

Using three distinct and representative hypotheses, the properties of a frozen fringe with steady growth of an ice layer were studied (Nakano 1990). The objective of the work was to show the important differences among the three hypotheses by using the knowledge of the properties of each hypothetical model obtained by mathematical analysis.

During the mathematical derivations of the basic equations, restrictions were imposed to the transport equation (2.3-11) in order to provide sufficient conditions for the recovery of the generalised Clausius-Clapeyron (2.2-3) when f vanishes. These restrictions are given as:

$$\frac{K_2}{K_1} \to \gamma \text{ as } f \to 0 \qquad \textbf{2.3-14}$$

$$\lim_{x \to n_1} P_l(x) = P_2(n_1) \qquad x \text{ in } R_l \qquad \textbf{2.3-15}$$

$$\gamma = \frac{\rho_i L}{T_0}$$

Under the stable growth of an ice layer, the frozen soil R_f may be considered to consist of two parts, i.e. the frozen fringe R_1 and the ice layer R_2 (Figure 2.3-2). The models that had been proposed to date could be placed into two categories depending on whether ice is permitted to grow in the frozen fringe, R_1. They could also be distinguished depending on whether the pressure of unfrozen water P_1 is independent of the temperature T. Thus a total of four types of models could be defined and termed by Nakano (1990) as M_1, M_2, M_3 and M_4.

Model M_1 considers a fringe where ice may exist, but does not grow and f is given by 2.3-11, under the restrictions of 2.3-14 and 2.3-15. When ice does not grow at any interior point of R_1, ice grows at the interface n_1 between R_1 and R_2. Model M_2 considers a fringe where ice may exist, but does not grow and f is given by 2.3-12. Model M_3 considers a fringe where ice grows and f is given by 2.3-12. Finally model M_4 considers a fringe where ice may grow and f is given by 2.3-11 under the restrictions of 2.3-14 and 2.3-15.

Model M_1 is a generalisation of several models, including that by Ratkje et al. (1982) based on the thermal osmosis of irreversible thermodynamics, the concept of segregation potential (Konrad and Morgenstern 1980, 1982b), and on the osmotic pressure effects in a diffused double layer (Horiguchi 1987). Model M_2 is the generalisation of models including those by Harlan (1973), Kay et al (1977), and Hopke (1980). Model M_3 is essentially the same as the rigid ice model (O'Neill and Miller 1985).

The accuracy of the models was studied (Nakano 1990) based on previous experimental work (Radd and Oertle 1973; Takashi et al. 1981). Radd and Oertle

studied the relationship between P_2 and T of an ice layer by using a water-permeable, constant-volume cell in which the unfrozen part of a soil column was connected with a water reservoir subjected to an atmospheric pressure $P_1 = 0.1$ MPa. It was found that for a given T_1 and P_1 a unique pressure P_2 exists when an existing ice layer neither grows or melts and the flux of water vanishes, and that the measured values, P_2, T_1 and P_1, satisfy the equation given as:

$$\sigma' = P_2 - P_1 = -\gamma T_1 \quad \text{if} \quad f = 0 \qquad \textbf{2.3-16}$$

2.3-16 is a generalised form of the Clausius-Clapeyron equation introduced previously (2.2-3). The validity of equation 2.3-16 between the effective stress σ' and T_1 was confirmed (Takashi et al. 1981) using a closed constant-volume cell.

From 2.3-16 it can be seen (Nakano 1990) that T_1 is negative when σ' is positive. When $\sigma' > 0$, the frozen fringe R_1 therefore does not disappear even if f vanishes. When f vanishes, the water pressure in the unfrozen part R_0 must become equal to the constant pressure of water reservoir P_1 if the gravitational effect is neglected. 2.3-16 hence relates the pressure P_2 of R_2 and the temperature T_1 at n_1 to the pressure of water P_1 in R_0.

Common to the experimental work (Radd and Oertle 1973; Takashi et al. 1981) is that the system is not under thermal equilibrium when the phase equilibrium is attained and f vanishes. When $\sigma' > 0$ a temperature gradient exists in R_1 and the steady transport of heat takes place through R_1 at the phase equilibrium of water.

For model M_1 (Nakano 1990) it was shown that 2.3-11, with conditions of 2.3-14 and 2.3-15, is reduced to 2.3-16 at the phase equilibrium when f vanishes. When f vanishes in models M_2 and M_3 there are only two possibilities;

1) The temperature gradient in R_1 must vanish regardless of σ', and

2) The frozen fringe itself must vanish regardless of σ'.

These two possibilities contradict the experimental observations by Radd and Oertle (1973) and Takashi et al (1981) that a frozen fringe does not disappear when $\sigma' > 0$ even if f vanishes.

A series of freezing tests were subsequently conducted (Takeda and Nakano 1990) on three different kinds of soils to empirically determine the steady growth condition of an ice layer. The study clearly showed (Nakano and Takeda 1991) that the model M_1 is consistent with results obtained. Models M_2 and M_3 contradict the experimental data. These findings imply that 2.3-11 is consistent with experimental data while 2.3-12 contradicts them.

Considering the liquid water pressure and temperature to be independent in the fringe under dynamic conditions where unfrozen water is flowing through the fringe and an ice layer is growing, Ratkje et al. (1982) proposed the transport equation of water in the frozen fringe based on irreversible thermodynamics as

$$f = -K_1(\nabla u_l + \gamma \nabla T) \qquad \textbf{2.3-17}$$

where $\gamma = \dfrac{\rho_i L}{T_0}$

According to Ratkje et al (1982), P_1 approaches the pressure of an ice layer P_2, as x approaches the interface $n_1(t)$ between R_1 and R_2 so that 2.3-17 is reduced to an approximate form of the generalised form of the Clausius – Clapeyron equation (2.3-16), when f vanishes at the phase equilibrium of water.

2.3.4. Separation Criterion

In order for an ice lens to form in the soil the structure of the soil must split to allow for water to accumulate, freeze and grow. Determining the mechanism by which conditions are sufficient to permit the growth of an ice lens is not simple and many hypotheses have been proposed. A relationship between the overburden pressure, liquid pressure and the stress of the porous matrix is needed to be found in order to prescribe such a separation criteria (Talamucci 1997).

One proposal considers the mechanical balance in the frozen fringe and follows Terzaghi's stress partition idea of unsaturated soils which states that the overburden pressure (P) causes a stress tensor in the solid matrix and pore material (ice and water):

$$P = \sigma_n + \sigma_e \qquad \textbf{2.3-18}$$

where the neutral stress, σ_n, represents the reaction of the pore material and the effective stress, σ_e, is the normal stress of the soil grains. O'Neil and Miller (1985) divided the neutral stress in two components (2.2-2) with a suitable stress partition function (χ). χ is empirically determined as a function of the volumetric ice content, S_i. The soil separates when the effective stress vanishes and the normal stress exerted exceeds the overburden pressure.

$$P = \chi p_w - (1-\chi)p_i \qquad \textbf{2.3-19}$$

If it is assumed that the water pressure is sub-atmospheric (Talamucci 1997), the ice pressure, p_i, is an important factor in the frozen fringe. From (2.3-19) the ice pressure must exceed the overburden pressure and the ice exerts a separation force (Figure 2.3-3).

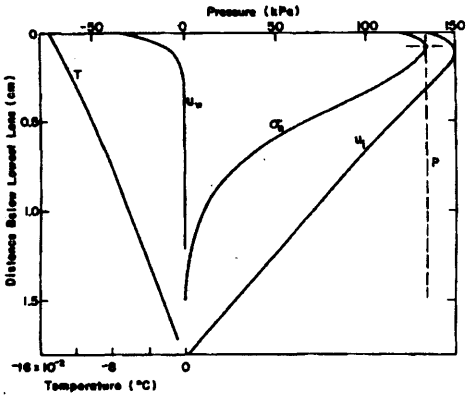

Figure 2.3-3 – Computed profiles in T, u_w, u_i and σ_n across the frozen fringe at the moment when σ_n surpasses P. (O'Neil and Miller 1985)

Sheng and Knuttson used a simplified stress partition factor (Talamucci 1997) which was a function of the porosity and volumetric ice content.

$$\chi = n(1 - S_i) \qquad \textbf{2.3-20}$$

The equilibrium and capillary model by Gilpin (1980) assumed that soil separates when the ice pressure exceeds the overburden pressure and an additional separation pressure.

$$p_i = P + 2\sigma_{iw}\frac{f(P_R)}{R} \qquad \textbf{2.3-21}$$

where R represents the mean radius of the soil particles and $f(P_R)$ is an empirical function. This criterion was simplified by Nixon (1991) to be dependent on soil properties (via R) but not on the temperature. Hopke (1980) simply set the separation pressure to the overburden pressure and an ice lens forms when the ice pressure equals the overburden pressure.

It has also been proposed that the weight of the soil is entirely supported by the stress transmitted through the intergranular contacts of the soil particles (Konrad and Morgenstern 1980; Nakano 1990). Within the frozen fringe the fact that the thermodynamic processes occur at a constant porosity would confirm such a hypothesis (Talamucci 1997). Ice forming within the pores of the frozen fringe would therefore not be subjected to the stress transmitted by the overburden pressure. Under this assumption the ice would be at atmospheric pressure and there would be no need to introduce the ice pressure into the mechanical balance and the separation criteria simply becomes (Nakano 1986; Nakano 1990):

$$u_l = \sigma \qquad \textbf{2.3-22}$$

Konrad and Morgenstern (1980) used a segregation freezing temperature (T_s) to determine where a growing ice lens would occur. At the segregation freezing temperature the hydraulic conductivity would become so small that the water flux

stops and water would accumulate at this location, the height of this location becoming the position of the new lens and the base of the frozen fringe. The segregation temperature is essentially dependant on soil properties.

The frozen fringe was regarded as a series of equivalent connected pumps in the model by Konrad and Duquennoi (1993). The ice lens grew while the mass transfer to the lower ice lens is provided by the available energy.

The critical ice content was introduced by Kay et al (1977) where the soil would expand and heaving would take place when the volume of ice in the pores reached a critical value. Ice was assumed to be under atmospheric pressure and the critical ice content was set equal to the porosity of the soil minus the unfrozen water content. A similar approach was chosen by Shen and Ladanyi (1987) where a critical ice content of 0.85% was used. This model differed from the previous model as it assumed a linear distribution of ice pressure in the frozen fringe from $p_i = 0$ at the base of the fringe and $p_i = P$ at the top (Figure 2.3-4).

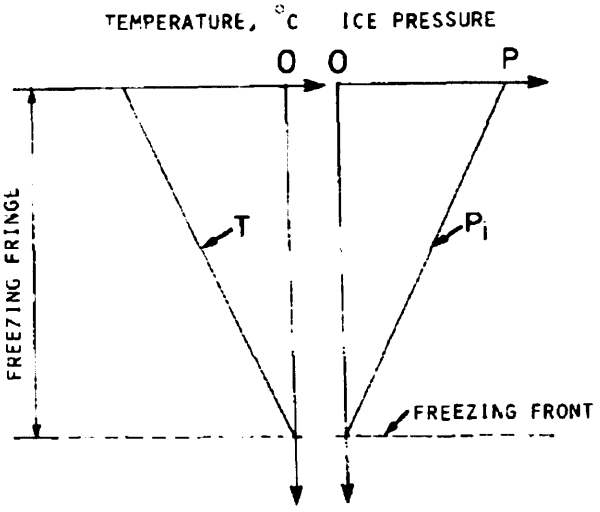

Figure 2.3-4 - Idealised distribution of temperature and ice pressure within the freezing fringe, adopted in the calculation. (Shen and Ladanyi 1987)

2.4. Thawing Processes

Frozen ground contains ice in several forms, ranging from coatings on soil particles and individual ice inclusions to ice with soil inclusions. On thawing, the ice will melt and change in phase to water, and for existing overburden pressures the soil skeleton must now adapt itself to a new equilibrium void ratio (Andersland and Ladanyi 2003).

In this section the thawing process is describe in relation to the settlement attributed to thawing soils, consolidation effects and that of layered soil and ice systems.

2.4.1. Thaw Settlement

As thawing of a frozen soil takes place a volume change will occur, this volume change is caused by the phase change of ice to water and from the flow of excess water from the soil. When a soil freezes under saturated and closed drainage conditions, in equilibrium with the overburden pressure, the soil will expand as the pore water changes state. The associated volumetric strain, ε_v, can be expressed as:

$$\varepsilon_v = 0.09n \qquad \textbf{2.4-1}$$

where

n = porosity of the soil

and 0.09 is determined from the ratio of the densities of liquid water and ice

Upon thawing under undrained conditions the soil will return to its initial volume, V_0. Additional volume changes can be observed in drained conditions when the soil thaws which result from mechanical effects such as consolidation and soil structure changes that took place during previous freezing cycles.

Frost susceptible soils, such as silts and clays (fine grained soils) exhibit discrete layers of ice forming within the soil structure under suitable freezing conditions which generally depend on the transport of water to the growing ice lens and the temperature gradient, i.e. freezing rate. In general, with all else being equal, the slower the freezing rate, the greater the formation of ice lenses.

The process of the formation of discrete ice lenses is irreversible and upon thawing more liquid water is generated than the soil matrix can absorb. Subsequent drainage of this liquid water results in further settlement. The most frost susceptible soils, silts and clayey silts, are, by definition the most ice-rich soils and exhibit the greatest thaw settlements. Ice-rich permafrost is common in alluvial plains, some till deposits, and glacio-lacustrine basins (Andersland and Ladanyi 2003).

Determination of the magnitude of thaw settlement can be estimated from a visual inspection of the formation of ice lenses within a sample. This however can lead to significant errors, so a representative sample is tested in the laboratory under recreated field conditions. Testing of the samples can be undertaken in a triaxial apparatus or more commonly in a one-dimensional consolidation device (Andersland and Ladanyi 2003).

Results from a typical thaw-settlement experiment are shown in Figure 2.4-1. It can be seen that a small decrease in void ratio occurs under frozen conditions for an increase in load (point *a* to *b*). Upon thawing, a large decrease is observed (*b* to *c*) due to phase change and drainage of excess water. The pressure σ_0 is usually selected on the basis of the effective overburden pressure for the field sample.

Under an increase in load, $\Delta\sigma$, consolidation will take place until a new equilibrium void ratio is reached (point *d*).

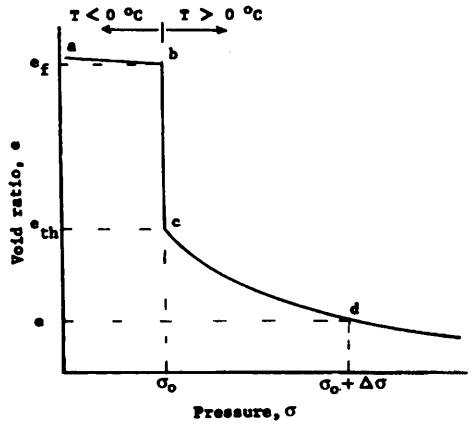

Figure 2.4-1 – Typical void ratio versus pressure curve for frozen soils subject to thawing (Andersland and Ladanyi 2003)

The vertical strain of the soil element thawed under a stress σ_0 and loaded to (σ_0 + $\Delta\sigma$) is

$$\frac{\Delta H}{H} = A_0 + m_v \Delta\sigma \qquad \textbf{2.4-2}$$

m_v = coefficient of volume compressibility

H = thickness of the element of soil strata

A_0 = thaw-strain parameter and defined below as

$$A_0 = \frac{e_f - e_{th}}{1 + e_f} \qquad \textbf{2.4-3}$$

e_f = frozen soil void ratio

e_{th} = thawed void ratio

Settlement is given by

$$\Delta H = A_0 H_f + m_v \Delta\sigma H_{th} \qquad \textbf{2.4-4}$$

Other methods have been proposed to predict the thaw settlement that will occur. These methods include using the soil dry densities and fitting an empirical relationship to the experimental data (Andersland and Ladanyi 2003).

2.4.2. Thaw Consolidation

When a mass of frozen soil is subjected to a temperature increase on or near the ground surface, thawing will commence in a manner that is controlled by the temperature boundary conditions and the thermal properties of the soil (Morgenstern and Nixon 1971). The solution to such a problem in heat conduction may be found analytically (Carslaw and Jaeger 1959) or by a variety of numerical methods which depend on the complexity of the problem.

In the problem of a thawing soil, the freeze-thaw interface is taken as the 0°C isotherm. As frozen soil does not transmit pore pressures or participate in any significant deformation, this interface forms the lower boundary of the thaw-consolidation problem. The thaw interface advances into the soil according to some function *X(t)*. With the water flow from the thawed soil impeded, settlement with time will be controlled by the thaw plane location (Andersland and Ladanyi 2003). As the thaw plane moves with time the solution to this problem is governed by a moving boundary condition.

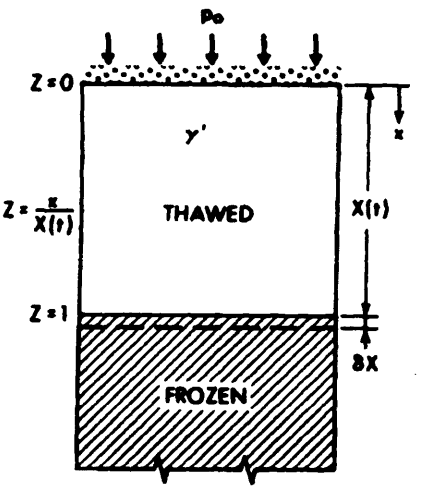

Figure 2.4-2 – One-dimensional thaw consolidation (Morgenstern and Nixon 1971)

The solution to the problem (Morgenstern and Nixon 1971) used the classical theory of consolidation by Terzaghi. The limitations of this theory when applied to other problems in soil mechanics are also applicable to problems in thawing soils. The linear void ratio – effective stress relationship may grossly be in error if the frozen soil contains much ice in excess of the pore volume normally present (Morgenstern and Nixon 1971). The thawed soil is also assumed to be saturated and therefore the solutions obtained may also over estimate the magnitude of the pore pressure in the soil if an air phase is present.

The solution to the heat conduction problem is attributed to Neumann (Carslaw and Jaeger 1959). The movement of the thaw plane is given by:

$$X(t) = \alpha t^{\frac{1}{2}} \qquad \textbf{2.4-5}$$

α = constant determined in the solution of the heat conduction problem

X = the distance to the thaw plane from the soil surface

In the thawed region, it is assumed that the soil is compressible and that the theory of consolidation is valid. When the applied stress does not vary with time it may be shown (Morgenstern and Nixon 1971) that

$$c_v \frac{\partial^2 u}{\partial x^2} = \frac{\partial u}{\partial t} \qquad \textbf{2.4-6}$$

$u(x,t)$ = excess pore pressure

x = depth measured from the ground surface

c_v = coefficient of consolidation

The upper surface of the soil is taken to be free draining and as thawing proceeds, a flow of water occurs upwards from the thaw line if there is any excess pore pressure. A change in soil volume must result from flow from the thaw line.

Morgenstern and Nixon (1971) found a solution to 2.4-6 in the form

$$u(x,t) = A \cdot erf\left(\frac{x}{2\sqrt{c_v t}}\right) + Bx \qquad \textbf{2.4-7}$$

$erf\left(\frac{x}{2\sqrt{c_v t}}\right)$ = the error function

$$A = \frac{P_0}{erf(R) + \frac{e^{-R^2}}{\sqrt{\pi} R}}, \quad B = \frac{\gamma'}{1 + \frac{1}{2R^2}}$$

$R = \frac{\alpha}{2\sqrt{c_v}}$ = thaw consolidation ratio

It is convenient to introduce the dimensionless depth variable

$$Z = \frac{x}{X(t)} \qquad \textbf{2.4-8}$$

Considering a weightless material, $\gamma' = 0$, the second term in 2.4-7 drops out and the first term represents the pore pressures generated under the applied loading, P_0 (Figure 2.4-3a). The second term gives the pore pressures maintained in a soil thawing and settling under the action of its own weight, $P_0 = 0$ (Figure 2.4-3b).

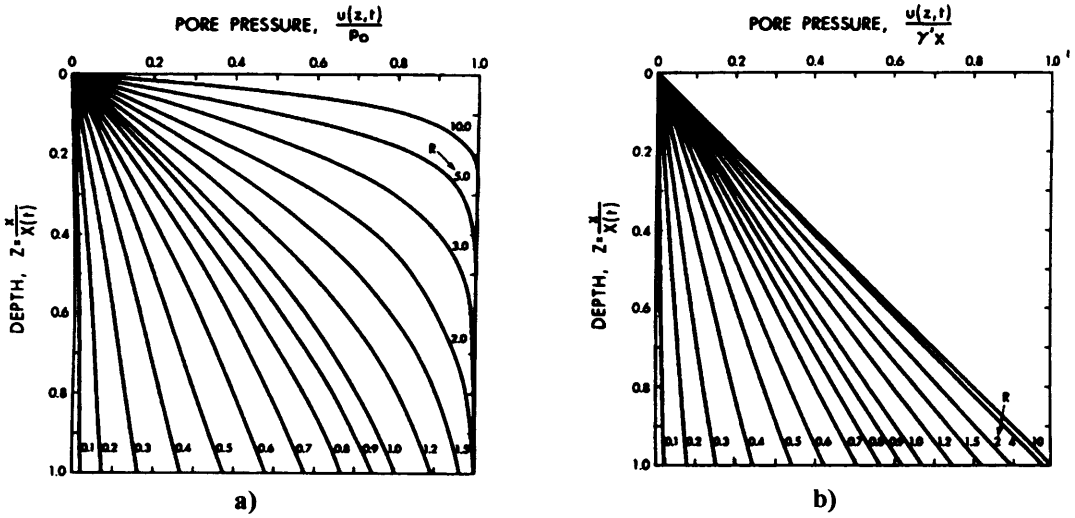

Figure 2.4-3 – Excess pore pressure a) $\gamma' = 0$ (weightless material) b) $P_0 = 0$ (no applied load) (Morgenstern and Nixon 1971)

It can be seen that an increase of the pore pressure will increase with an increase in the thaw consolidation ratio R for both loading situations. Dimensionless pore pressures represented in Figure 2.4-3 are independent of time. When R exceeds unity, the pore pressures at the thaw plane approach their maximum value and effective stresses tend towards zero. The range of α values in practice falls within 0.2 to 1.0 mm/s$^{1/2}$ and can be calculated to an accuracy close to ±10% (Nixon and McRoberts 1973). The coefficient c_v may vary from 10 (sandy silts) to 0.01 mm^2/s (clays) (Andersland and Ladanyi 2003).

2.4.3. Surface Temperature Variations with Time

A thawing soil with a linearly increasing surface temperature can be considered (Lunardini 1991; Lunardini 1997). It was found that the Neumann solution, when

used with an equivalent surface temperature can give reliable total freeze/thaw depth, however it is significantly in error at intermediate times. An analytical solution to a linear surface temperature increase was presented and compared to the Neumann solution.

It was found that when the Stefan number (dimensionless ratio of the sensible heat to the latent heat) is small, the growth of the thawed zone is nearly linear in time, but as the Stefan number increases, it becomes increasingly nonlinear. The Neumann solution therefore was found to greatly exaggerate the thermal changes during the early growth and underpredict them during the latter part of the warming. As a result this can lead to significant errors in calculating the effects of warming on frozen ground as the Neumann solution will model a variable surface temperature if the total phase-change depth is desired but will not give comparable intermediate values for the phase-change depth or rate (Lunardini 1991).

The approach adopted uses a simple approximate solution to the Neumann problem through the use of the heat-balance integral (HBI) method as described in equation 2.4-9. In the investigated case (Lunardini 1997), a linear temperature surface profile was used, however the HBI can be used for a variety of surface temperature profiles and yields results close the exact solution.

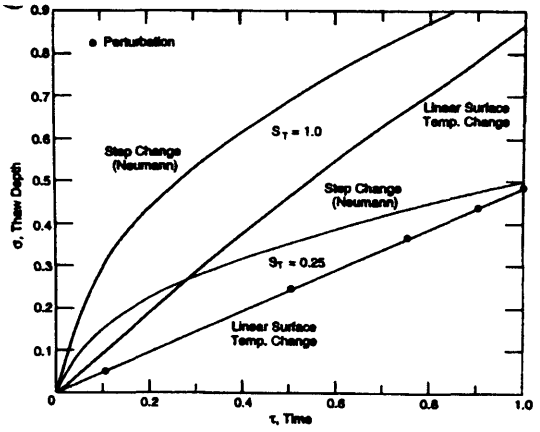

Figure 2.4-4 – Neumann and linearly increasing surface temperature solutions for thaw depth (Lunardini 1997)

$$\frac{d}{dt}\int_0^X T_1(x,t)dx - T_f\frac{dx}{dt} - \alpha_1\left[\frac{\partial T_1(X,t)}{\partial x} - \frac{\partial T_1(0,t)}{\partial x}\right] = 0 \qquad \text{2.4-9}$$

2.4.4. Residual Stress in Thawing Soils

The maintenance of excess pore pressures and the development of settlements have been shown to be dependant mainly on the thaw-consolidation ratio, R, which is a measure of the balance between the rate of generation of excess pore fluids, and the ability of the soil to expel these fluids from the pore space (Nixon and Morgenstern 1973).

At the thaw line the boundary condition equates any flow from the thaw line with a change in volume of the soil, only departures from the residual stress will result in volume change (Nixon and Morgenstern 1973). In ice-rich soils it is reasonable to assume the residual stress is small and is taken as zero, however for ice-poor soils with a high void ratio in the thawed, undrained state, a significant residual stress may exist in the undrained soil on thawing.

A sample of unfrozen fine grained soil was prepared with a known stress history by consolidating slurry in an oedometer to a known stress P_0 (Nixon and Morgenstern 1973). The sample was left to dissipate all excess pore pressures so P_0 was an effective stress. The sample was subsequently frozen under undrained conditions with a small increase in the average void ratio observed from point A to B due to the volume expansion of water to ice in the soil pores (Figure 6.4 1). If the sample is allowed to thaw under undrained conditions, it will return to point A.

During the experiments an elevation of the pore water pressure was observed, in cases of high initial void ratios, the pore pressure may approach or equal the total stress on the sample. At this point the effective stress is considerably reduced and may approach zero. The test on the sample (Figure 2.4-5) resulted in a net decrease in volume from $A \rightarrow C$ under a constant external stress. It is well known that negative pore water pressures build up in fine grained soils and the formation of small ice layers and inclusions often occur even when free water is not available. As the test conditions required the total water quantity to remain constant, the soil layers between

ice inclusions must be over-consolidated with respect to the constant external total stress. Soil between ice inclusions have experienced an effective stress greater than P_0, shown by the dashed curve ($A \rightarrow D$) in Figure 2.4-5.

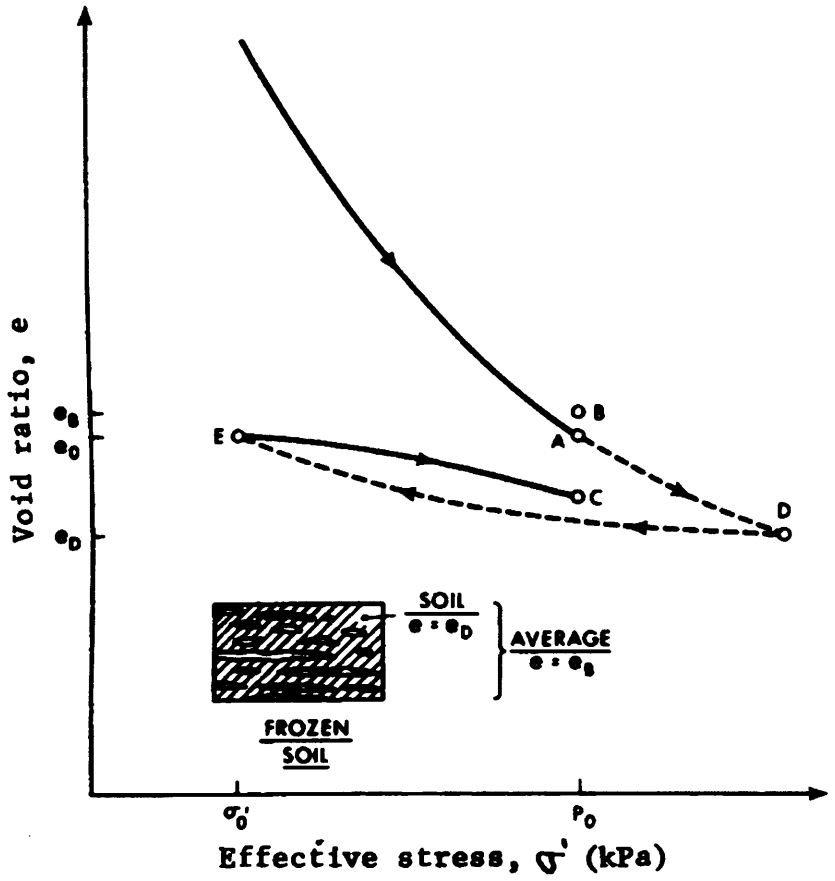

Figure 2.4-5 – Stress path in a closed system freeze-thaw cycle (schematic) (Nixon and Morgenstern 1973)

As thawing progresses a quantity of local free water is available from the thawed ice segments and the soil swells almost instantaneously to absorb the excess water in the macropores. The soil swells along the path $D \rightarrow E$. If the soil is capable of absorbing all the free water, then the remaining effective stress is the residual stress. If free water still exists when the soil swells to a zero effective stress condition, the residual stress is zero and excess water remains in the soil. Allowing the soil to reconsolidate under drained conditions returns to the effective stress, P_0 (Path $E \rightarrow C$). Reloading is similar that that of an overconsolidated unfrozen soil. The net strain from the frozen to the fully thawed consolidated state ($B \rightarrow C$) is the net strain and often called the thaw strain.

Stress, thermal history, and drainage conditions prior to permafrost formation will influence its behaviour. After removal of a soil sample from frozen ground, the first measurement in the thawed state corresponds to the residual stress. Prediction of excess pore water pressures must be made relative to this stress.

A series of tests using a special oedometer with a saturated soil using two different methods was conducted (Nixon and Morgenstern 1973). The first method kept the total load σ applied to the sample constant, the second the method the total stress is adjusted so that the excess pore water pressure remains zero.

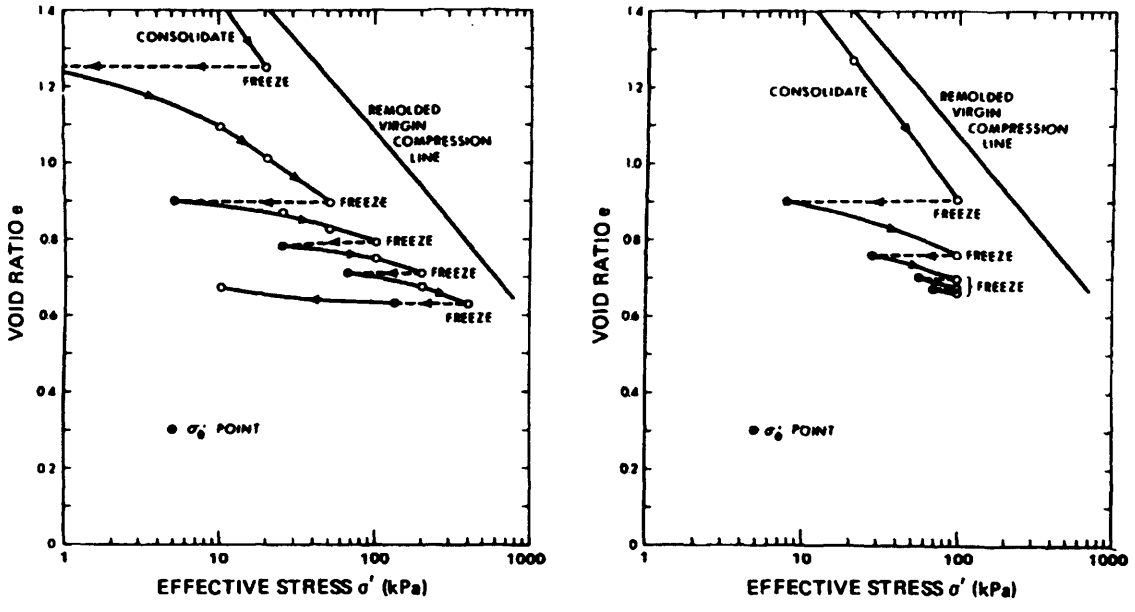

Figure 2.4-6 – Measurement of residual stress for reconstituted Athabasca clay: (a) increasing consolidation pressure; (b) constant consolidation pressure. (Nixon and Morgenstern 1973)

Following completion of the first test, the soil was remoulded, consolidated to a higher stress level and then refrozen. Once thawing had finished again the residual stress was recorded. For each cycle the residual stress was seen to increase as shown in Figure 2.4-6a as a series of solid points. For the second experiment, the sample was reconsolidated to the same stress (98.0 kPa), as is shown in Figure 2.4-6b. For each freeze-thaw cycle a similar increase was noted in the residual stress. The consolidation that occurred for each reloading cycle decreased steadily.

Both test series demonstrated that if the residual stress is close to the effective overburden stress in the thawed soil; subsequent consolidation settlement will be small. A strong correlation between the thawed void ratio and the logarithm of the residual stress was found (Nixon and Morgenstern 1973). This relationship appeared to be independent of previous stress and thermal history effects. From their results it was expected that the undrained strength of the thawed soil would increase with depth and for a given loading, the volumetric strain would decrease with depth.

2.4.5. Soils with Discrete Ice Layers (Lenses)

In soils with silt sized particles, segregated ice in the form of discrete layers or bands often occur depending on the conditions in the soil. In the finer grained plastic soils, ice banding is also found, with the bands orientated perpendicularly to the maximum principal stress (Nixon 1973).

Analysis of a compressible soil with discrete ice layers considered a solution for a layer of saturated compressible soil overlying a layer of ice that extends downwards indefinitely (Figure 2.4-7) (Nixon 1973). It was subsequently shown that the procedure could be modified to include any ice layer of finite thickness.

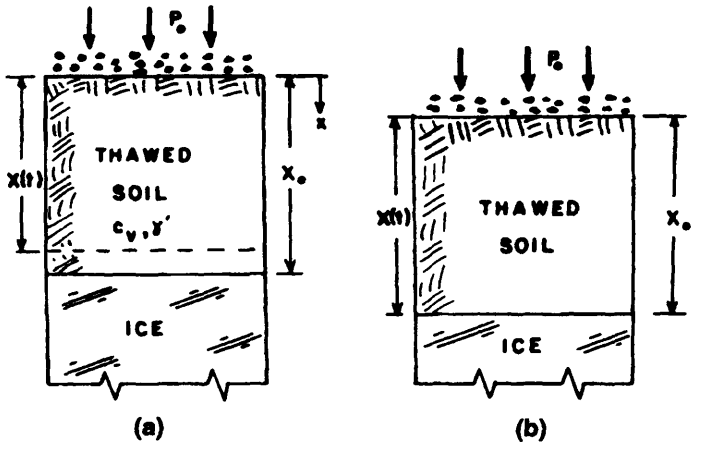

Figure 2.4-7 – Thawing in a soil ice profile: (a) thaw plane in soil; (b) thaw plane in ice. (Nixon 1973)

It was shown that the thaw rate in the ice is proportional to time, whereas in the soil the rate is proportional to the square of time. The rate of thaw is also reduced when

the ice layer is encountered as the latent heat of water L_w is greater than the latent heat of soil L_s.

For ice of a finite thickness, the time to thaw an ice layer is given by (Nixon 1973)

$$t_f = \frac{h_i X_0 L_w}{k_u (T_s - T_0)} \qquad \textbf{2.4-10}$$

h_i = initial ice layer thickness

t_f = time required to thaw the ice layer

Converting into a time factor yields

$$T_v = \frac{c_v t_f}{X_0^2} = \frac{c_v h_i L_w}{k_u (T_s - T_o) X_0} \qquad \textbf{2.4-11}$$

Knowing the time factor at the conclusion of thawing of the ice lens, Figure 2.4-8 may be used to determine the final (and usually the worst) pore pressure conditions over the ice layer (Nixon 1973). From Figure 2.4-8, for values of D less than unity the normalised excess pore pressures will rise to the D value, where D is greater than unity, the stability of the soil is only assured for the finite time shown by Figure 2.4-8. After the finite time, the excess pore pressure will exceed the effective overburden pressure and instability will result.

The relationship expressed in 2.4-11 shows that T_v is directly proportional to h_i and inversely proportional to X_0. The implication of this is that ice layers near the surface can only be tolerated if they are thin whereas thicker ice layers at greater depths can be thawed safely.

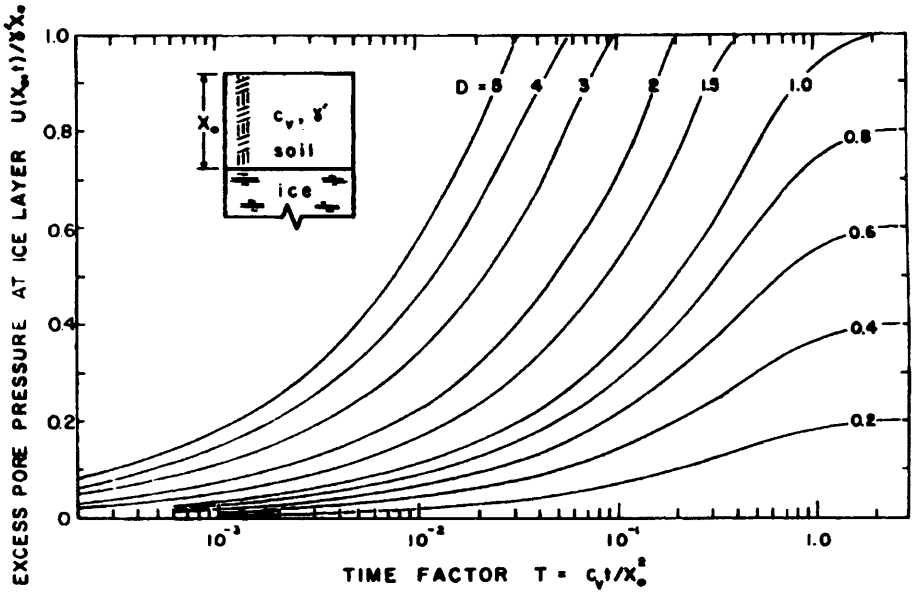

Figure 2.4-8 – Pore pressure at a soil-ice interface (Nixon 1973)

2.4.6. Thawing Soil Slopes

An important observation of slopes in thawing permafrost, be it solifluction, skin flows or lobes of bimodal flows is instabilities of slopes with low angles. Geotechnical experience in temperate regions suggests that it is entirely appropriate to consider the stability of long shallow slopes using an infinite slope analysis (Andersland and Ladanyi 2003). In this analysis the conventional theory of slope stability should be modified to include the pore pressures generated at the thaw front (2.4-7) (McRoberts and Morgenstern 1974).

Infinite slope analysis of unfrozen soils of thickness d (measured vertically) and angle i, occurring in a c', ϕ' soil with groundwater flow parallel to the slope surface, gives a factor of safety

$$FS = \frac{c'}{\gamma d \sin i \cos i} + \frac{\gamma'}{\gamma}\frac{\tan\phi'}{\tan i} \qquad \textbf{2.4-12}$$

c' and ϕ' = effective soil shear parameters

d = vertical thickness of flow, $d = \dfrac{X(t)}{\cos i}$ in a thawing slope

γ' = effective soil unit weight

Considering the effects of the excess pore pressures generated through thawing the following expression was obtained (McRoberts and Morgenstern 1974):

$$FS = \frac{c'}{\gamma d \sin i \cos i} + \frac{\left(\frac{\gamma'}{\gamma}\right)}{1+2R^2} \frac{\tan \phi'}{\tan i} \qquad \textbf{2.4-13}$$

Infinite slope analysis is only valid for a long shallow planar form of a thawing slope. In some cases the thawing slope may only have a limited lateral extent and a 'thaw plug' flow may occur within a narrow width of slope where an increase in side resistance will be experienced. Such a case may be where there is a downslope pipeline construction (Andersland and Ladanyi 2003)

2.5. Mechanical Properties and Effects

2.5.1. Freezing Effects on the Soil Structure

Fine-grained soils exposed to freeze-thaw cycles show changes in volume, changes in strength and compressibility, redistribution of pore water, densification and exhibit microstructural changes such as formation of cracks and particle movement. In addition, the Atterberg limits can be affected as well as the bearing capacity reduced due to large pore water pressures when the frozen soil thaws (Viklander and Knutsson 1997).

2.5.2. Permeability

Changes due to freezing and thawing often lead to a change in permeability, especially in fine-grained soils which are strongly affected and are normally found to increase in permeability as a result of freezing and thawing. The largest effects of permeability are recorded after the first cycle; however it has been shown that changes still occur up to 10-15 cycles and beyond (Viklander and Knutsson 1997).

Permeability changes depend on several factors, such as void ratio, degree of compaction, water content, plastic limit, frost susceptibility, content of stones and type of clay mineral.

A series of experiments on fine-grained till was undertaken (Viklander and Knutsson 1997) to investigate if the permeability in the vertical direction was affected by repeated cycles of freezing and thawing. It was found that the permeability in a fine-grained till exposed to a maximum of 10 cycles of freezing and thawing is significant. For loose structure samples with a high initial void ratio a permeability decrease between 1.4 and 50 times was noticed. For dense structures, small void ratios, a permeability increase of 1 – 11 times was observed. For all samples a residual void ratio (e_{res}) is reached after a number of freeze/thaw cycles had occurred. Dense and loose samples ended up with the same residual void ratio.

2.5.3. Strength

Frozen soil is usually stronger than unfrozen soil or ice; it displays time-dependant creep behaviour similar to ice and like unfrozen soil, frozen soils display a frictional behaviour (Hohmann-Porebska and Czurda 1997). Frozen soils at high confining pressures will show a strength decrease after a reaching a maximum value. The strength of a frozen soil is a combination of the cohesion of the ice matrix and the frictional resistance of the soil particles. The composite strength of the frozen soil may not necessarily be the sum of the structural components (Hohmann-Porebska and Czurda 1997).

Strength properties and stress-strain behaviour of granular soils at subzero temperatures are well analysed with parameters for these materials published in literature. However, for clays and silts there has not been the same amount of research conducted as that of granular soils. Frozen clays and silts differ from granular soils in several aspects (Hohmann-Porebska and Czurda 1997). The soil skeleton consists of smaller particles with more surface area, hence greater unfrozen water contents.

Tests on five fine-grained soils to study the effect of shear strength changes after freezing in open and closed systems were conducted (Hohmann-Porebska and Czurda

1997). After the samples were prepared and frozen, they were sheared in a standard direct shear apparatus. Several conclusions were drawn as a result of the testing;

- The melting of ice must occur at an increase in load to particle contact (increase in effective stress). Melting continues until equilibrium conditions are re-established.
- On thawing, the ice matrix disappears and the soil skeleton must adapt itself to a new equilibrium void ratio under existing loads.
- Shear strength is dependant on time.
- The resistance to shearing decreases with duration of the applied stress (loading).
- The temperature effects on the shear strength are mainly reflected in the cohesion. The frictional component of the strength does not vary significantly.
- There are still few conclusions on ice-soil interaction, due to influences of cations on the strength behaviour of clayey soils.

It was concluded that the variations in shear strength of frozen soils with time and temperature results primarily from variations in the ice cohesion, and that the frictional resistance may be regarded as essentially constant. Further work is needed to characterise the mechanical behaviour, near and within the frozen fringe for applications involving seasonally frozen ground (Hohmann-Porebska and Czurda 1997).

2.5.4. Hydrostatic Pressure Effect on Frozen Soil Behaviour

The behaviour of a frozen soil under an increase of hydrostatic pressure is considered to be the result of combined mechanical and thermodynamical effects (Andersland and Ladanyi 2003), the former governing the stress sharing and the latter the pressure melting phenomena. Considering the soil grains to be bonded by ice results in a greatly reduced compressibility of the soil skeleton. As a result, a sudden increase in hydrostatic pressure can cause the unfrozen water in a frozen soil to be stressed much less than that of the ice, having important thermodynamic consequences.

Under non-isothermal conditions, the pressure-temperature relationship for ice and water in the soil matrix is considered to be accurately defined by the Clausius – Clapeyron equation:

$$\frac{dp_w}{\rho_w} - \frac{dp_i}{\rho_i} = L\frac{dT}{T} \qquad \textbf{2.5-1}$$

Substituting ρ_w = 1000 kg/m^3 and ρ_i = 916.8 kg/m^3 for the density of water and ice respectively, L = 3.336 x 10^5 J/kg as the latent heat of water and $dT = T_0 - T$ as the difference between the normal freezing temperature of pure water, T_0 = 273.15 K, and the actual temperature, T, of the system gives:

$$dp_w = 1.091\ dp_i + 1.221\ dT \qquad \textbf{2.5-2}$$

p in MPa and T in K

Most frequently it is assumed that at the ice-water interface, $dp_w = dp_i = dp$ (Andersland and Ladanyi 2003), which yields the freezing point depression for ice as:

$$\frac{dT}{dp} = -0.0743 \text{ K/MPa} \qquad \textbf{2.5-3}$$

In an isothermal case, $dT = 0$ and 2.5-2 yields

$$dp_w = 1.091\ dp_i \qquad \textbf{2.5-4}$$

According to the above equation, providing that no phase change occurs, changes in pore-water pressure will follow closely the changes in pore ice pressure.

It follows that a frozen soil under a hydrostatic confining pressure that localised pressure melting at the particle-to-particle contacts will occur and that there will be some water migration toward lower-stress regions. To depress the freezing point of water by 1 K, equation 2.5-3 predicts that a pressure of about 13.5 MPa is required. Consequently under ordinary pressures there would be very little melting were it not

for stress concentration at ice-particle contacts, which may increase the pressure by a factor of 10 to 500 (Andersland and Ladanyi 2003).

Observations at very high confining pressures, where the grain structure collapses, resulted in a total pressure melting of the pore ice occurring, even in sands.

2.5.5. Stress-Strain Behaviour of Frozen Soil

The stress-strain relation of frozen soil was proposed by Vyalov in 1962 in a simple power-form from results of constant strain rate tests:

$$\sigma = A\varepsilon^m \qquad \text{2.5-5}$$

σ = stress

ε = strain

A and m are test parameters

This relationship has been widely used to describe the σ-ε behaviour of various kinds of frozen soils (Chen and Su 1991). Zhu et al (1991) found that the σ-ε relations for frozen soils of various types in uniaxial compression at different strain rates and temperature do not all obey equation 2.5-5. A total of nine basic types of σ-ε relations were classified; the main σ-ε behaviours of frozen soils being viscoelastic-plastic (VEP), elastic-plastic with elastic-strain hardening (EP-I), or with elastic-ideal plastic (EP-II) or with elastic-strain softening (EP-III).

Zhu et al (1991) concluded that it is inappropriate to use a simple power equation for describing the σ-ε behaviour of a range of frozen soils at various strain rates and temperatures. The σ-ε behaviour of frozen soil is very complicated and has been found to mainly vary with strain rate and temperature.

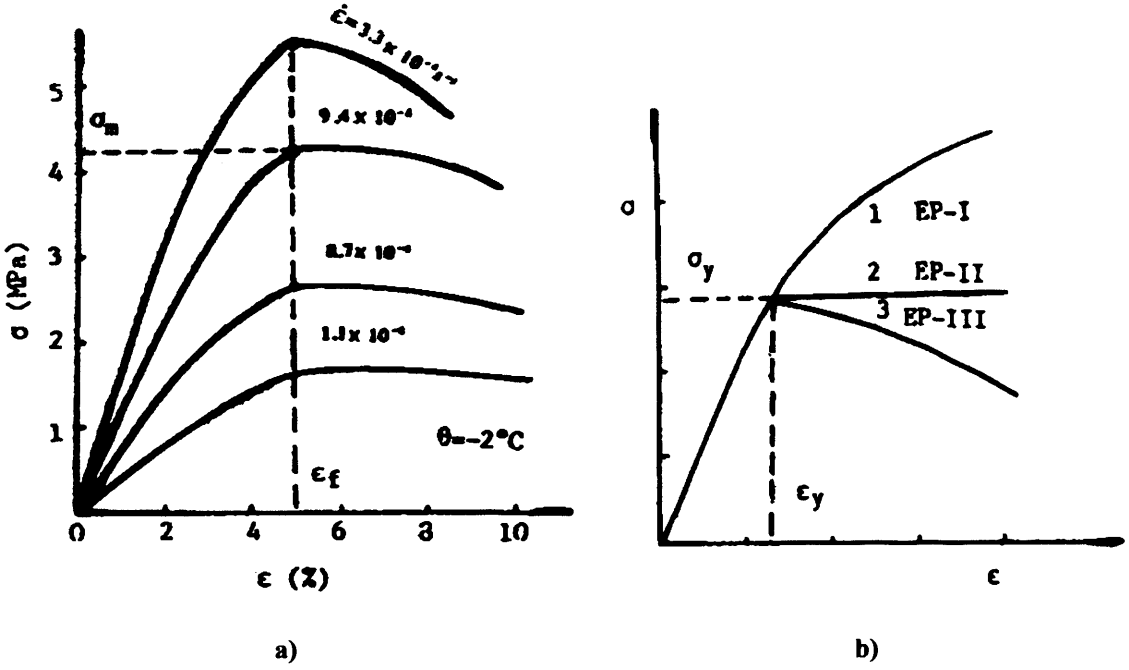

Figure 2.5-1 – a) A set of σ-ε curves of ice-poor saturated Lanzhou silt at various strain rates (w=15.5%, γ_d=17.25kN/m^3). b) Typical elastic-plastic σ-ε curves. 1 – Elastic-strain hardening, 2 – Elastic-ideal plastic, 3 – Elastic-strain softening. (Zhu et al. 1991)

2.5.6. Creep and Creep Strength of Frozen Soils

2.5.6.1. Creep of Frozen Soils

In frozen soil mechanics the total strain, ε resulting from a deviatoric stress is usually assumed to be composed of an instantaneous strain, ε_0, and a delayed or creep strain, $\varepsilon^{(c)}$ (Ladanyi 1997).

$$\varepsilon = \varepsilon_0 + \varepsilon^{(c)} \qquad \text{2.5-6}$$

The instantaneous strain, ε_0, may contain elastic and plastic portions; however at service loads, excluding instantaneous failure, the plastic component may not be present. Creep strain is composed of primary and secondary (steady-state) creep, although the latter may only be seen as an inflection point on the creep curve, preceding tertiary creep (Figure 2.5-2).

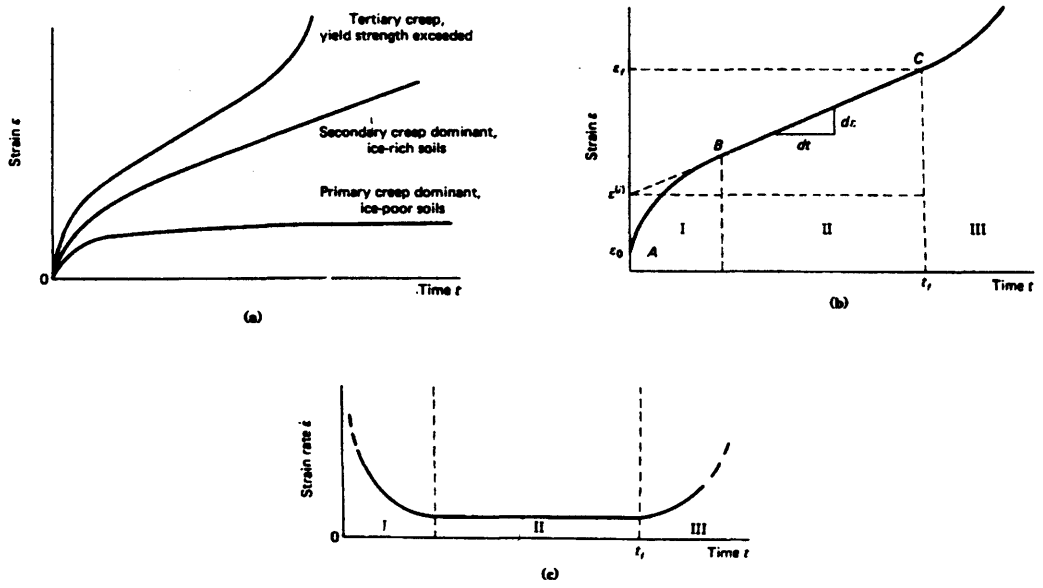

Figure 2.5-2 – Constant-stress (creep) test: (a) creep-curve variations; (b) basic creep curve; (c) true strain rate versus time. (Andersland and Ladanyi 2003)

In applications such as ground freezing, the strain ε_0 in equation 2.5-6 is considered to be governed by Hooke's law, while the creep strain, $\varepsilon^{(c)}$, is usually defined by an empirical primary creep formulation (Andersland and Ladanyi 2003). For problems over long time periods, such as foundations in permafrost, the short-term response – including elastic, plastic and primary creep portions is sometimes lumped together to form a pseudo-instantaneous plastic strain, $\varepsilon^{(i)}$ (Ladanyi 1972). The magnitude of this strain is determined from the intersection on the strain axis (Figure 2.5-2) when the slope at the minimum or steady-state creep rate is extrapolated back to $t = 0$.

2.5.6.2. Creep Strength of Frozen Soils

Failure in frozen soils exhibit similar properties as in unfrozen soils including both rupture and excessive deformation. Depending on soil type, temperature, strain rate and confining pressure, the mode of failure may vary from brittle, similar to that in a weak rock, through brittle-plastic, with a formation of a single failure plane or several slip planes, to purely plastic failure without any visible strain discontinuities (Ladanyi 1997). The last type of failure by excessive creep deformation is typical for permafrost problems involving ground temperatures of only a few degrees below the melting point of ice.

Creep strength is defined as the stress level at which, after a finite time interval, either rupture or instability leading towards rupture occurs in the material. In tensile creep testing, the creep strength is mostly taken as the stress at which actual rupture occurs. In compression creep testing, however, especially ductile materials such as high temperature metals and frozen soils, in which only a plastic type of failure occurs that is much clearly defined, the creep strength is most often identified with the moment of the test at which the first sign of instability occurs. In constant stress creep testing, this moment coincides with the passage from the steady state creep to accelerating creep of the material (Figure 2.5-2c) (Ladanyi 1972).

2.5.7. Ice Content Effect on Strength

The mechanical characteristics of frozen soils depend to an extent on the pore ice content which occupies most of the pore space and binds the soil grains together. It is now generally agreed that most of the ice found in soil pores is of a polycrystalline type with a random crystal orientation, whereas crystals within ice lenses are usually elongated in the direction of heat flow during freezing (Andersland and Ladanyi 2003).

Ice strength is dependent on many factors, the most important of which are temperature, pressure and strain rate, as well as the size, structure and orientation of grains. As temperature decreases an increase in the strength of ice is observed. Failure of ice is strain-rate dependent, varying with temperature, its response to loading is found to vary from viscous to brittle. In permafrost soils, ice exists at very high homologous temperatures, mostly above 90% of the fusion temperature, which limits its deformation mechanism to a narrow area, characterised by a power law type of creep, resulting mainly from the motion of dislocations (Andersland and Ladanyi 2003).

2.5.8. Temperature Effect on Strength

Temperature has a marked effect on all aspects of the mechanical properties of frozen soils as a result of its direct influence on the strength of intergranual ice and on the amount of unfrozen water. Similar to the observations of ice, a decrease in

temperature results in an increase in strength with a corresponding increase in brittleness. The effect of the decreased temperature on brittleness can be seen in the larger drop of strength after the peak strength and an increase in the ratio of compressive strength to tensile strength (Andersland and Ladanyi 2003).

Down to about -10°C, the embrittlement effect of temperature is observed more in a frozen sand or silt than in frozen clay, which at that temperature still contains enough unfrozen water to keep it plastic. In general the strength of frozen soil varies with strain rate, temperature and time if concerning long term strength (Chen and Su, 1991).

2.6. Numerical Modelling of Freezing and Thawing Soil

It is difficult to classify models into categories due to the approaches taken in development, for instance physical models which can be further split into deterministic and stochastic models, and scientific or operative models. The majority of frost heave models developed to date are coupled heat and mass transfer models. Models can also be classified as empirical, semi-empirical, hydrodynamic, rigid-ice, and thermomechanical models, according to the state of development of frost heave phenomena research (Kujala, 1997) (Table 2.6-1).

2.6.1. Empirical Models

These are frost heave models that have been developed based on a purely empirical observation using field observations and frost heave tests. Some models have been classified as semi-empirical, because the physical nature of frost heave has been used as a basic for the models. At their best these models function as important design tools in evaluating the magnitude of frost heave as a basis for dimensioning (Kujala 1997).

Table 2.6-1 – Classification of frost heave models (Kujala 1997)

		Empirical Model	Semi-empirical Model	Hydrodynamic Model	Rigid ice Model	Thermomechanical Model
Temperature	Frost penetration	*	*	*	*	*
	Thawing depth		*	*	*	*
Displacement	Frost heave		*	*	*	*
	Thawing settlement			*		*
Ice and Moisture Content	Water content			*	*	*
	Ice content			*	*	*
	Pore pressure			*	*	*
Stress and Strain	Stress and					*
	Strain					*

2.6.2. Hydrodynamic Models

Advances in computing capacity in the early seventies permitted the calculation of complex partial differential equations by numerical methods which enabled the first frost heave models to be developed. The first model was presented by Harlan (1973) using coupled heat and mass transfer in freezing soil. The model was based on an analogy between water transport in unsaturated soils and water transport in partially frozen soil. An apparent thermal capacity was used to combine the equations. As a result several models were subsequently developed based on this concept however they are unable to describe the formation of discrete ice lenses. It was not possible for overburden pressure to be taken into consideration in several of these models either.

Frost heaving occurs in these models when the volume of pore ice exceeds a given percentage of pore content. The formation of the ice enriched zone is located at a depth where the divergence of the water flux is greatest. The model developed by Guymon for seasonal freezing and thawing of nonplastic soils was considered to be the most developed hydrodynamic model to date (Kujala, 1997).

2.6.3. The Rigid Ice Model of Frost Heave

Introduced by O'Neill and Miller (1985), this model is based on the theory of secondary frost heave. In this model the ice lenses form at some distance behind the frost front with the zone between the frost front and lens filled with ice and water. The model was unique when it was presented in that the stress between phases is dealt with by a neutral stress, which constitutes the second factor in Terzaghi's total stress.

The underlying principle of the rigid ice model is based on the behaviour of isolated grains embedded in ice and that liquid water is attracted by the grain surface more strongly than is rigid crystalline ice. Applying a temperature gradient, the thermal equilibrium of water and ice at the interface becomes inconsistent with the mechanical equilibrium in the hydrostatic field induced by surface adsorption forces. The result of this process is to transport the grain up the temperature gradient. As individual grains migrate through the stationary rigid ice, travelling up a temperature gradient, the rigid ice that fill interstices between stationary grains ought to migrate down the temperature gradient. If the ice is inherently rigid, this movement is not flow but continuous regelation.

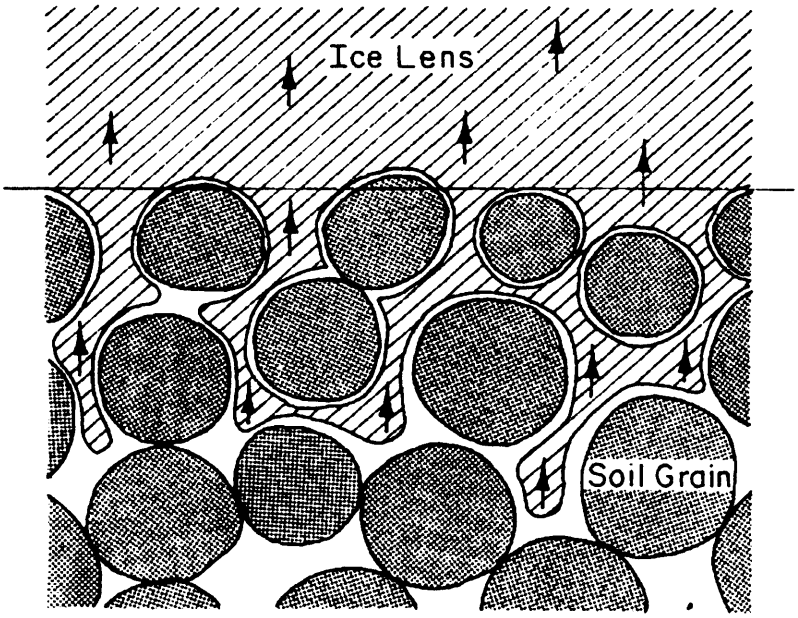

Figure 2.6-1 - Schematic diagram of the frozen fringe, with ice lens above (O'Neill and Miller 1985).

The rigid-ice model was further developed (O'Neill and Miller 1985) and has been simplified by researchers (Holden 1983; Ishizaki and Nishio 1998), Sheng (1994) presented a development to the rigid-ice model, which is capable of handling field conditions, such as stratified soils, unsaturation and insulation layers. The model was verified against field data and was found to correlate well with the measured observations (Kujala 1997).

2.6.4. Segregation Potential

A conceptual model was developed to account for the general characteristics of frost heave observed when fine grain soils freeze (Konrad and Morgenstern 1980; Konrad and Morgenstern 1981; Konrad and Morgenstern 1982a, b). The model was developed on the assumption that the frozen soil behind the formed ice lens is passive with regards to mass transfer but water is able to be transported from the unfrozen soil through a region of thin frozen soil called the frozen fringe to the developing ice lens.

In its simplest form the segregation potential theory of frost heave states that the velocity of water arriving, V_0, at the advancing frost front is related to the temperature gradient in the frozen soil just behind the frost front (Equation 2.6-5) (Konrad and Morgenstern 1980, 1982a).

$$V_o = SP \cdot \nabla T \qquad \textbf{2.6-1}$$

The proportionality factor SP is termed the segregation potential, its value determined by the gradient of the slope between the water intake velocity and temperature gradient (Figure 2.6-2). The segregation potential was found to be a function of the total suction potential at the freezing front, p_w, the suction potential at the frozen-unfrozen interface, p_u, the segregation freezing temperature, T_s, and the overall hydraulic conductivity in the frozen fringe (Konrad 1987).

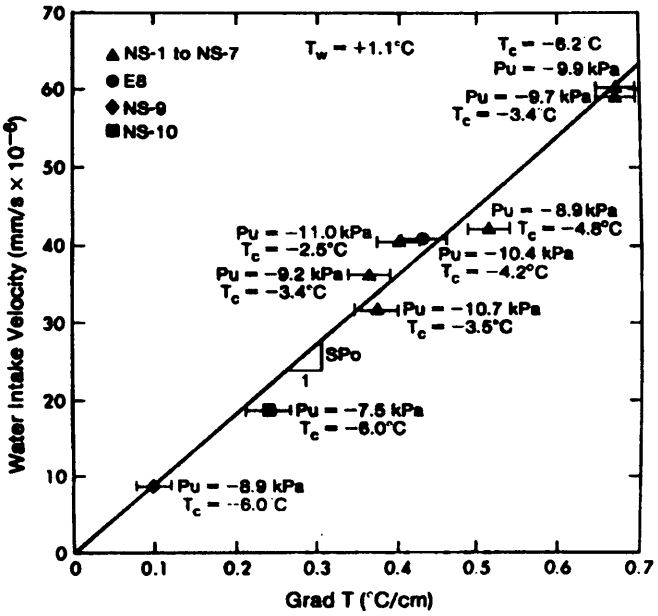

Figure 2.6-2 – Relation between water intake velocity and temperature gradient across the active system during the formation of the final ice lens. (Konrad and Morgenstern 1981)

Researchers have used the *SP* model to analyse frost heave data from field and laboratory tests, however their results suggest that the accuracy of the *SP* model is only sufficient for engineering purposes (Kujala 1997). The segregation potential is advantageous in that it can be calculated from the insitu frost heave observations when the temperature gradient is known. Through use over several years, shortcomings and limitations to this method have become apparent (Nixon 1991);

1. The Current SP approach does not predict the pore-water expulsion that is commonly observed at early times in laboratory tests on soils.
2. The heave rate is sensitive to the rate of cooling over a range of cooling rates applied in the laboratory, but cooling rate does not appear to affect heave rates at field rates of cooling.
3. The heave rate is sensitive to the suction at the advancing frost front and it is necessary to apply a theoretical method to understand the dependence of heave rate on suction at the freezing front.
4. The SP semi-empirical approach does not explicitly predict the SP parameter in terms of more fundamental soil parameters.

5. The current SP approach assumes that the overburden pressure and suction at the frost front affect the heave rate independently.

2.6.5. A Model for the Prediction of Ice Lensing and Frost Heave in Soils

An attempt was made to develop a simpler frost heave model than that proposed by O'Neill and Miller yet still exhibit all of the observed characteristics associated with frost heave (Gilpin 1980). It acknowledged the model by O'Neill and Miller; the rigid ice model, as being the most complete frost heave model developed to date as it treats all the essential features of frost heave however the rigid ice model is complex and computationally difficult (Gilpin 1980).

It is stated that water in the liquid layer is flowing to a lower potential region close to the substrate surface and not being sucked as previously reported in literature. It is this flow that creates the pressure required to separate the ice lens and the soil particles. Separation of particles in this model occurs when the separation pressure, P_{sep}, exceeds the overburden pressure, P_{ob}, plus the tensile force between the two particles (2.6-2).

$$P_{sep} = P_{OB} + \frac{2\sigma_{lw}}{R} f(P_R) \qquad \textbf{2.6-2}$$

σ_{SL} = ice water interfacial tension

R = radius of soil particle

$f(P_R)$ = separation pressure function

The results from the model were found to be in general agreement with experimental observations as to the effects of the various parameters and the predicted heave rates were of the right order of magnitude. Through the use of the model four factors were found that limited the rate of frost heave

1. The rate of heat conduction away from the freezing front.

2. The hydraulic resistance in the frozen fringe.
3. The hydraulic resistance at the ice lens.
4. The hydraulic resistance in the unfrozen soil.

Of these factors it was noted that the first two are most likely to be the controlling factors.

2.6.6. Discrete Ice Lens Theory for Frost Heave in Soils

This model returned to a more basic formulation of the problem in order to understand the mechanism of frost heave in terms of fundamental soil properties, in which the relationship between heave rate and temperature gradient is not assumed but rather derived (Nixon 1991). The approach adopted was able to predict the discrete location of the ice lenses within the soil matrix.

The segregation approach (Konrad and Morgenstern 1980, 1982a) strongly relied on the assumption that the relationship between the SP parameter and rate of cooling, suction at the freezing front, and effective stress was unique. Previous work (Nixon 1991) demonstrated that the SP should be redefined as

$$SP = \frac{V_{ff}}{G_{ff}} = \frac{dh}{dt} \cdot \frac{1}{1.09 G_{ff}} \qquad \textbf{2.6-3}$$

where V_{ff} the pore-water velocity in the frozen fringe, G_{ff} the thermal gradient in the fringe and dh/dt is the heave rate. This definition is preferred because, for an incompressible soil in the freezing fringe, it is the water velocity in the fringe, and therefore the heave rate, which is driven by the thermal gradient, and not the water velocity in the unfrozen soil.

The theory proposed (Nixon 1991) appeared to be capable of predicting the response of laboratory test specimens, once a set of more fundamental frost heave parameters were established. The separation pressure which governs the formation of a new ice lens was shown to be important in controlling the size and separation of the ice lenses

but did not greatly affect the overall heave rate prediction. These features were considered to be a significant advance from the semi empirical SP approach, which requires an extensive series of testing to map out a multidimensional surface and does not predict or explain many of the features outlined above.

2.6.7. Modelling of Coupled Heat, Moisture and Stress Field in Freezing Soil

Further developments to the rigid ice model included stress and strain; however Shen and Ladanyi (1987) did not couple the effects with the heat and mass transfer equations. A finite difference method was adopted to solve the heat and moisture equations with the mechanical equation subsequently solved using the finite element method. The ability to calculate stress and deformation fields in a freezing soil on the basis of temperature, moisture and stress states was seen to be an important step towards a more accurate prediction of stability of structures in frozen soils (Shen and Ladanyi, 1987).

Due to the poor understanding of the ice pressure some simplifying assumptions were made to be able to use the Clausius – Clapeyron equation (2.2-3). At the freezing front the ice pressure is assumed to be zero and equal to the local mean pressure at the coldest side of the frozen fringe (Figure 2.3-4). The criterion for ice lensing was chosen to occur when the ice content exceeds a value of 85% of the porosity. Agreement between the simulated and experimental results was found to be good with the simulation able to predict the amount of ice accumulation behind the frost front. The model was not capable of predicting the position of discrete ice lenses.

2.6.8. Thermo-Mechanical Models

These models are the next evolution of frost heave models in which the mechanical properties of frozen soil are taken into consideration with the heat and water transfer (Fremond and Mikkola 1991; Mikkola and Hartikainen, 2001). Development of these models is on going with significant advances needing to be made to produce operative models.

Fully coupled modelling of these processes are only recently being undertaken as the ability of modern computing power to process these complex coupled problems are making these simulations viable. In order to simplify computations heat and mass transfer equations have been uncoupled from the mechanical equations (Konrad and Shen, 1996). Expressions such as Equation 2.6-4 have been used to define the volumetric strain due to ice lensing and phase change when this approach has been adopted (Selvadurai et al, 1999)

$$\varepsilon_v = 0.09(\theta_0 + \Delta\theta - n) + \Delta\theta - (\theta_0 - n) \qquad \textbf{2.6-4}$$

where

θ_0 is the initial water content (m^3/m^3)

$\Delta\theta$ is the increment of water content by moisture migration (m^3/m^3)

n the porosity of the soil

It is not necessary with fully coupled models to introduce expressions such as Equation 2.6-4 into the mechanical equation as the cross coupling from the moisture equation, which has components due to the density difference of liquid water and ice, will result in pore water pressure changes and through the coupling terms deformation.

By virtue of the coupling the effects of the stress field on the thermal and moisture fields which is explicitly defined, the need to introduce arbitrary expressions is no longer required, i.e. the effect of overburden pressure on ice lens formation.

2.6.9. Towards Multidimensional Fully Coupled Numerical Modelling of Freezing and Thawing Soil

As a minimum requirement for models that deal with freezing and thawing is the ability to handle latent heat effects. These are for the most very large and can be very troublesome computationally, especially as they enter via nonlinearities (O'Neill, 1983). In general, it is quite difficult for approximate techniques and finite mesh

spacings to deal with discontinuities much less with moving discontinuities (O'Neill, 1983).

Traditionally, frost heave modelling has been one-dimensional however the theory is being extended to include continuum models with three-dimensions (e.g. Konrad and Shen, 1996; Talamucci, 1997; Selvadurai et al, 1999; Mikkola and Hartikainen, 2001). The developments of multidimensional fully coupled models in the literature are few, in no small part to the complex dependency of the interrelated processes (Figure 2.6-3). These include (Konrad and Shen, 1996): (1) hydraulic conductivity - unfrozen water content relationships; (2) stress-strain relationships for both unfrozen and frozen soils; (3) relations between frost heave and stresses; and (4) moving boundary problems associated with the growth of a freezing front.

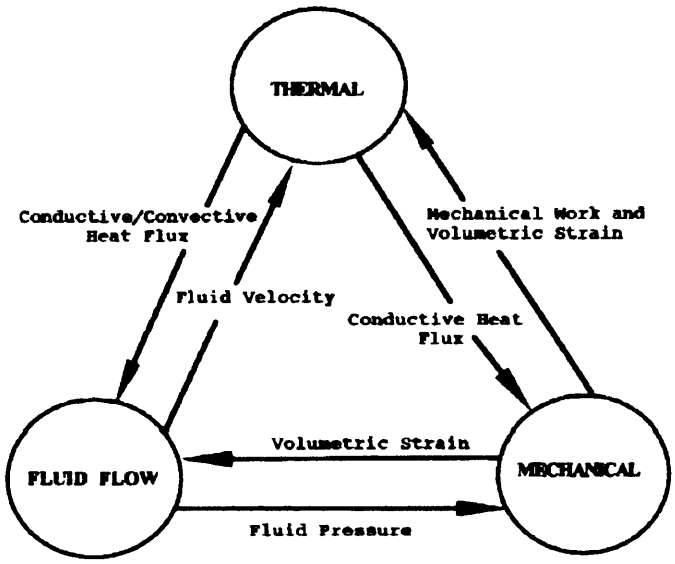

Figure 2.6-3 – Interaction mechanism in a fully coupled THM system (Neaupane et al. 1999)

The equations that describe freezing and thawing in these models are highly nonlinear and are computationally intensive, especially given the dependence of the hydraulic and thermal conductivity on the thermal regime. Various simplifications and assumptions are usually made such as (Konrad and Shen, 1996): (1) heat transport is governed by conduction and neglects convection; (2) phase change effects may be uncoupled from the governing transport equations; (3) frozen zones are nondeformable, (4) frozen fringe characteristics are only temperature dependent and

not related to stresses; (5) moisture flow in the frozen zone on the cold side of the active ice lens is negligible; (6) hysteresis effects on unfrozen water are not considered; and (7) uncoupling of the heat and mass transfer equations from the mechanical equations.

In order to formulate a model for frost heave certain questions must be answered about the behaviour of the frozen fringe. The properties of the frozen fringe have been discussed early in this chapter and the salient points pertaining to the development of freezing and thawing numerical models are drawn upon here to summarise the decisions that must be taken to develop these models.

The mass flux, f, in saturated soil in one direction can be written in a general form as:

$$f = -K_1 \frac{\partial u_l}{\partial x} - K_2 \frac{\partial T}{\partial x} \qquad \textbf{2.6-5}$$

While it is an accepted view that $K_1 \equiv K_0$, $K_2 \equiv 0$ within the unfrozen soil (Darcy's law), the question about water flux in the frozen fringe in controversial. In the literature, there are two possibilities that exist.

$K_2 \equiv 0$ (O'Neill and Miller 1985), and

$K_2 > 0$ (Nakano 1991) **2.6-6**

A common point of view is that the generalised Clausius-Clapeyron equation holds at the phase equilibrium (Equation 2.3-16). If T and u_l are dependent (equilibrium models) (O'Neill and Miller 1985), equation 2.6-5 is claimed to hold even during the freezing process. In the non-equilibrium models, T and u_l are independent and equation 2.6-5 holds only at the phase equilibrium (Forland et al. 1988; Nakano 1986).

In capillary models (Gilpin 1980), the most relevant interfacial effects due to the contacts among the three constituents (water, ice, and soil grains) of the frozen fringe

are water-ice effects: $u_i - u_l = \phi(S_i)$. In other models (Nakano 1990), water-soil grains effects prevail.

Main theories of the mechanism of ice segregation are Terzaghi's stress partition idea, the existence of a segregation temperature T_s, (the permeability K_l is so small at $T = T_s$ that water tends to accumulate somewhere (Konrad and Morgenstern 1988). In other models (Nakano, 1986), the stress balance on the top of the frozen fringe is simply $u_l = \sigma$ and the lens starts to form simply when the speed of the upper boundary of the frozen fringe vanishes. The use of critical ice contents has also found use in some models (Kay et al, 1977; Shen and Ladanyi, 1987) and lensing forms when the critical value of pore ice has been exceeded.

The final consideration is ice at rest with respect to the porous matrix. For some modellers, ice can move through the porous space by means of regelation. In this case, a common position is $q_i = q_i(t)$ (O'Neill and Miller 1985). Many assume that regelation does not occur and there is no need to introduce further complexities (Konrad and Morgenstern 1981; Shen and Ladanyi 1987; Nakano 1990).

2.7. Periglacial Processes

A number of studies from a geological perspective have been made to explore the periglacial processes that take place in cold regions. A better understanding of these processes has been obtained through the use of field studies, large scale physical modelling and centrifuge modelling. This section explores the recent developments in this field and presents the findings from those investigations.

The effects of climate change and global warming are leading to increases in average temperatures. In periglacial environments these rises in temperature have the potential to alter the stability of slopes, potentially resulting in increased pre-failure strains and possibly failure. It is of considerable importance to be able to quantify the change in solifluction rates due to such climatic changes in these environments. With increasing temperatures slopes are experiencing an increase to the active layer depth, resulting in

parts of the slope that would have normally been frozen starting to thaw and move. The development of models capable of representing these processes will lead to an improved ability to assess the effects of climate change on such slopes.

Freeze–thaw action induces downslope displacement of soils in cold, non-glacial environments, where vegetation is lacking or sparse (Ballantyne and Harris 1994). This process, broadly referred to as solifluction, operates slowly, in general at a rate of at most 1m $year^{-1}$. Its widespread distribution on mountain slopes means that solifluction contributes greatly to the evolution of mountain landscapes. Moreover, landforms and subsurface structures resulting from solifluction are strongly dependent on climatic conditions (Matsuoka 2001).

Rates and processes of solifluction depend on climate, hydrology, geology and topography. Prediction of landscape evolution in periglacial mountains requires quantitative relationships between the rate of solifluction and these variables (Kirkby 1995). For this purpose, field measurements have been undertaken in a variety of geographical situations ranging from polar hill slopes to tropical high mountains and, as a result, a large number of data-nets on solifluction rates and associated parameters have been obtained (Matsuoka 2001).

Extensive research has been carried out in the field to monitor and evaluate the conditions which cause the gradual mass wasting of slopes. Laboratory simulations using full scale and centrifuge modelling have further contributed to the understanding of the mechanisms that are involved in the solifluction processes (Harris and Davies 2000; Harris et al. 1997; Harris et al. 2003; Harris et al. 1993) .

2.7.1. Process Definition

The term 'solifluction' has not yet been defined unequivocally (Matsuoka 2001). The original meaning was defined as the slow downslope movement of saturated soil occurring in cold regions. It has been subsequently shown that it is not a necessary requirement for the soil to be saturated for slow mass movements to occur. Generally accepted today is that solifluction represents collectively slow mass wasting

associated with freeze–thaw action, and the saturated soil movement associated with ground thawing is designated as gelifluction (Ballantyne and Harris 1994).

Solifluction precludes rapid slope failures that reflect slide or flow over a shear plane, such as active-layer detachment slides and skinflows (Ballantyne and Harris 1994). Solifluction is most prevalent in sandy to silty soils having low liquid limits and plasticity indices (Matsuoka 2001).

Solifluction is classified into needle ice creep, frost creep, gelifluction and plug-like flow, using the criteria of the locus of particles and the vertical extent of movement that reflects the depth at which ice lenses develop during frost heaving (Matsuoka 2001).

2.7.2. Observations of Laboratory Experiments

Despite extensive field studies, progress in understanding gelifluction processes has been limited. Controlled laboratory simulation experiments offer an alternative and potentially extremely effective approach (Harris and Davies 2000). An experiment was conducted (Harris and Davies 2000) on a 12° slope formed of two natural soils, one a fine sandy silt derived from slate bedrock, the second a gravelly silty sand derived from mudstone bedrock.

Results from two-dimensional vectors of soil surface movement with evidence from excavated displacement columns suggest that gelifluction occurred only during the thaw consolidation of the upper parts of the soil profile: thawing of the deeper layers caused thaw consolidation but little downslope displacement (Harris and Davies 2000). It was also observed that the cryogenic processes caused a decrease in void ratio and moisture content with depth with an increase in the shear strength within the continuous soil matrix that separates ice lenses.

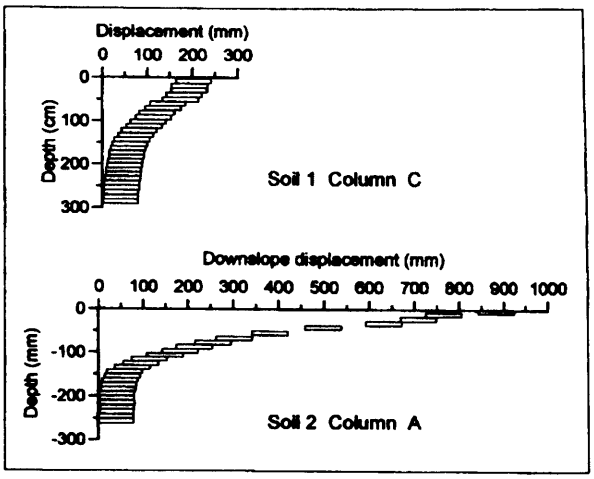

Figure 2.7-1 – Profiles of soil movement following seven cycles of soil freezing and thawing as revealed by excavation of buried columns. (Harris and Davies 2000)

2.7.3. Mechanical Changes during Freezing and Thawing

For each freeze-thaw cycle that the soil goes through, a change in the mechanical properties occur due to the stress changes resulting from the freezing and thawing process. It is well documented that ice segregation leads to a negative pore water pressure gradient which flows towards the growing ice lens. As a result this raises the effective stress in the continuous matrix of soil surrounding the ice lens so consolidation results in the soil matrix (Morgenstern and Nixon 1971). The increase in effective stress is reinforced by heaving pressures transmitted downwards into the unfrozen soil (Harris and Davies 2000). Ice segregation causes an overall increase in the void ratio and the void ratio of soil between the lenses actually decreases.

If the soil is normally consolidated or slightly over consolidated, the freezing process will result in an increase in the pre-consolidation pressure and irreversible plastic deformation will occur. Upon thawing the deformation is non-recoverable and a lower void ratio will remain. With each freeze-thaw cycle accompanies a further decrease in void ratio however for each cycle is subsequently less than the previous (Nixon and Morgenstern 1973). On thawing the effective stress acting on the soil is a large proportion of the self weight stress (Harris and Davies 2000) and this results in a progressive reduction in average void ratio as the thaw front travels deeper into the frozen soil. A corresponding reduction in moisture content also occurs. The viscosity

of soil also increases with decreasing moisture content (Harris et al. 1997). At the end of the thaw period the soil is overconsolidated throughout the active layer.

It was stated that for slopes of low angles and low overburden stress, the rate of thaw induced shear strain is highly sensitive to changes in soil shear strength and viscosity (Harris and Davies 2000). The potential for gelifluction is therefore likely to decrease with depth.

2.7.4. Mechanisms of Mass Wasting

In order to formulate constitutive equations, the timings and mechanisms of soil displacements during gelifluction have only rarely been measured in the field (Matsuoka et al. 1997). Due to the complexity of field conditions, determining good quality data to use in the formulation of constitutive equations is difficult and efforts are directed towards laboratory based studies. In the laboratory the material properties and conditions can be controlled and offer the most effective approach to process understanding (Harris et al. 1996; Matsuoka 2001).

Two scaled physical modelling experiments at elevated gravity were conducted in the geotechnical centrifuge (Harris et al. 2003). Their investigation was to test the hypothesis that gelifluction may be modelled by assuming soils flow as viscosity controlled fluids. Anderson in 1906 originally defined solifluction as 'slow flowing from higher to lower ground of masses of waste saturated with water' (Harris et al. 2003) and several authors have used 'viscous flow' to described gelifluction.

If gelifluction is a viscosity-controlled flow process scaling conflicts will arise and the rates of displacement will subsequently not correctly scale to the prototype. Scaling laws in geotechnical centrifuge modelling have been discussed in previous literature (Harris and Davies 2000; Harris et al. 2003). If however, no scaling conflicts are observed, it can be concluded (Harris et al. 2003) that gelifluction is not controlled by viscosity, but rather by elasto-plastic soil deformation in which frictional shear strength depends on effective stress, itself a function of the thaw consolidation process.

When the two models and volumetric soil transports were scaled to the prototype, the pore water pressures, displacement rates and displacement profiles reflecting accumulated shear strain were virtually identical (Harris et al. 2003). The displacement rates and profiles were also similar to those observed in previous laboratory experiments (Harris and Davies 1998; Harris et al. 1996, 1997; Harris et al. 1995; Harris et al. 1993). It was concluded that gelifluction is not a time-dependent viscosity-controlled flow phenomenon, but rather elasto-plastic in nature (Harris et al. 2003). A flow law was then proposed based on the 'Cam Clay' constitutive model for soil as a first approximation gelifluction model.

Numerical modelling is the next step in the development and understanding of these processes. Large scale experiments and centrifuge modelling offer a good understanding and give good agreement with field conditions but are however expensive and time consuming activities to undertake. Numerical models can be developed in conjunction with observations from field and laboratory testing to be useful tools in the prediction of changes in periglacial environments as well as in the more traditional areas of application of pavement design and buried chilled pipelines.

2.8. Conclusions

This chapter set out to present a review of developments and understanding in the field of freezing soil behaviour in the numerical modelling of coupled heat and mass transport in freezing and thawing soil. The freezing and thawing was divided into separate components in order to explore the processes that take place, the mechanisms by which they occur and the assumptions that these are based on.

A pivotal part in the ability to model freezing and thawing soil is the understanding of the frozen fringe. A significant amount of work has gone into studying this physically small, but vital part of the problem and yet, despite the number of years of research, no definitive answer to date has been reached. Whilst there are of course many agreements on certain aspects there are still disagreements on other fundamental processes from others. For instance it is agreed that the Clausius – Clapeyron equation

is valid in freezing and thawing soil systems but where in the frozen fringe it is valid is still open to discussion with experimental work available to support the varying arguments.

The freezing and thawing of soil is a highly coupled problem even though at first sight it may seem to be driven by the temperature field and to an extent it is as the processes only exists when the soil is at the correct temperature but is far more complex than simply accounting for the energy release due to the latent heat of fusion. With the presence of the frozen fringe and ice and water coexisting together a complex thermo-hydro-mechanical system is active with a variety of controlling factors.

The freezing and thawing aspects of soil systems are just as different as they are similar; while the latent heat of fusion and frozen fringe play a significant role in both the freezing and thawing there are two very distinct processes that occur during freezing and thawing. It is the ice lensing that defines the uniqueness in freezing systems with the attraction and large accumulation of solid water in the soil matrix whereas the uniqueness of thawing soils is the conditional stability while the excess water that has accumulated thaws and dissipates, too fast and the soil suffers from major strength losses and certain failure will result.

With such complex processes to consider the numerical developments of solutions have changed considerably over time. Most of this in part is due to the equipment that is available to solve the problems, such complex systems require a large amount of computing power and the balance between complexity and time taken to solve has to be addressed. The very first models were coupled thermo-hydraulic and it was not for some time that more sophisticated techniques were employed, the use of highly coupled finite element analysis involving moving boundary problems were simply to costly to run. Still recently these models were developed for one-dimensional use and did not employ full coupling between variables and opted to solve the equations sequentially.

The final section considered the freezing and thawing processes from a geological point of view. With the current situation with global warming; temperatures are rising

and this has very significant bearing on those parts of the world which are covered in permafrost and those that experience seasonal freezing and thawing. Extensive field and laboratory work has been carried out to obtain an in-depth understanding of the processes and it is now that numerical models are finding use in this area of research as the next step in understanding geological problems.

The need is clearly there for numerical models that are able to be applied to a variety of scenarios where freezing and thawing of soil is concerned; be it periglacial environments, pavement design or buried chilled pipelines a numerical model that has the physical processes defined in a generic way is applicable to all these types of problems and an extremely useful tool.

2.9. References

Andersland, O. B. and Ladanyi, B. 2003. "Frozen ground engineering". 2nd Edition. New York ; Chichester: Wiley.

Ballantyne, C. K. and Harris, C. 1994. "The periglaciation of Great Britain". Cambridge: Cup.

Blanchard, D. and Fremond, M. 1982. "Cryogenic suction in soils". *3rd International Symposium on Ground Freezing.* Hanover, New-Hampshire.

Carslaw, H. S. and Jaeger, J. C. 1959. "Conduction of heat in solids". Oxford: Clarendon Press.

Chen, X. and Su, L. 1991 "General report on mechanical properties". *6th International Sympiosium on Ground Freezing.* Beijing: Balkema. **2** 429-435.

Fremond, M. and Mikkola, M. 1991. "Thermodynamical modelling of freezing soil", *6th International Symposium on Ground Freezing.* Beijing: Balkema. **1,** 17-24

Feldman, G. M. 1967. "Moisture migration and stratified texture in freezing soils" *Journal of Engineering Physics*, **13**, 425-429

Gilpin, R. R. 1980. "A model for the prediction of ice lensing and frost heave in soils". *Water Resources Research* **16(5)**, 918-930.

Harlan, R. L. 1973. "Analysis of coupled heat-fluid transport in partially frozen soil". *Water Resources Research* **9(5)**, 1314-1323.

Harris, C. and Davies, M. C. R. 1998. "Pressures recorded during laboratory freezing and thawing of a natural silt-rich soil", *International conference on permafrost*; Permafrost Yellowknife, Canada: International Permafrost Association Canadian National Committee

Harris, C. and Davies, M. C. R. 2000. "Gelifluction: Observations from Large-Scale Laboratory Simulations". *Arctic Antarctic and Alpine Research* **32(2)**, 202-207.

Harris, C., Davies, M. C. R, Coutard, J. P. 1996. "An Experimental Design for Laboratory Simulation of Periglacial Solifluction Processes". *Earth Surface Processes and Landforms* **21(1)**, 67-76.

Harris, C., Davies, M. C. R., Coutard, J. P. 1997. "Rates and Processes of Periglacial Solifluction: An Experimental Approach". *Earth Surface Processes and Landforms* **22(9)**, 849-868.

Harris, C, Davies, M. C. R, Rea, B. R.. 2003. "Gelifluction: Viscous Flow or Plastic Creep?" *Earth Surface Processes and Landforms* **28(12)**, 1289-1302.

Harris, C., Davies, M. C. R., Coutard, J. P. 1995. "Laboratory Simulation of Periglacial Solifluction: Significance of Porewater Pressures, Moisture Contents and Undrained Shear Strengths During Soil Thawing". *Permafrost and Periglacial Processes* **6(4)**, 293-312.

Harris, C., Gallop, M., Coutard, J. P. 1993. "Physical Modelling of Gelifluction and Frost Creep: Some Results of a Large-scale Laboratory Experiment". *Earth Surface Processes and Landforms* **18(5)**, 383.

Henry, K. S., 2000. "A Review of the Thermodynamics of Frost Heave" *Technical Report ERDC/CRREL TR-00-16.* US Army Corps of Engineers. Cold Regions Research and Engineering Laboratory (CRREL).

Hohmann-Porebska, M. and Czurda, K. A. 1997. "Cryogenical alterations of fabric and shear strength of clayey soils" *Ground freezing and frost in geotechnical engineering* Lulea; Sweden: Balkema. 317-326

Holden, J. T. 1983. "Approximate solutions for Miller's theory of secondary heave" *4th International Conference on Permafrost*: Fairbanks Alaska. 498-503

Hopke, S. W. 1980. "A model for frost heave including overburden". *Cold Regions Science and Technology* **3**, 111-127.

Horiguchi, K. 1987. "An osmotic model for soil freezing". *Cold Regions Science and Technology* **14(1)**, 13-22.

Horiguchi, K. and Miller, R. D. 1983. "Hydraulic conductivity functions of frozen materials" *4th International Conference on Permafrost*. 504-508

Hult, J. A. 1966. "Creep in engineering structures". Waltham, Mass.:Blaisdell.

Ishizaki, T. and Nishio, N. 1998. "Experimental study of frost heaving of a saturated soil" *5th International Symposium on Ground Freezing* Balkema. 65-72

Kay, B. D., Sheppard, M. I. and Loch, J. P. G. 1997 "A preliminary comparison of simulated and observed water redistribution in soils freezing under laboratory and field conditions" *Proceedings of the International Symposium on Frost Action in Soils*, Lulea. 42-53

Kay, B. D. and Perfect, E. 1988. "State of the art: Heat and mass transfer in freezing soils" *5th International Symposium on Ground Freezing;* Balkema. 3-21

Kirkby, M. J. 1995. "A model for variations in gelifluction rates with temperature and topography: implications for global change". *Geografiska Annaler Series A* **77(4),** 269-278.

Konrad, J-M. and Morgenstern, N. R. 1980. "A mechanistic theory of ice lens formation in fine-grained soils". *Canadian Geotechnical Journal* **17**, 473-486.

Konrad, J-M. and Morgenstern, N. R. 1981. "The segregation potential of a freezing soil". *Canadian Geotechnical Journal* **18**, 482-491.

Konrad, J-M. and Morgenstern, N. R. 1982a. "Effects of applied pressure on freezing soils". *Canadian Geotechnical Journal* **19**, 494-505.

Konrad, J-M. and Morgenstern, N. R. 1982b. "Prediction of frost heave in the

laboratory during transient freezing". *Canadian Geotechnical Journal* **19**, 250-259.

Konrad, J-M..and Shen, M. 1996. "2-D frost action modelling using the segregation potential of soils" *Cold Regions Science and Technology*, **24**, 263-278

Kujala, K. 1997. "Estimation of frost heave and thaw weakening by statistical analyses and physical models" *Ground freezing and frost in geotechnical engineering* Lulea; Sweden: Balkema. 31-42

Ladanyi, B. 1972. "An engineering theory of creep of frozen soils". *Canadian Geotechnical Journal* **9**, 63-80.

Ladanyi, B. 1997. "Mechanical properties data base for ground freezing applications" *Ground freezing and frost in geotechnical engineering* Lulea; Sweden: Balkema. 43-52

Loch, J. P. G. 1981. "State-of-the-art report - frost action in soils". *Engineering Geology* **18**, 213-224.

Lunardini, V. J. 1991. "Heat transfer with freezing and thawing". Amsterdam ; New York: Elsevier Science Pub. Co.

Lunardini, V. J. 1997. "Thawing of frozen soil with a linearly increasing surface temperature" *Ground freezing and frost in geotechnical engineering* Lulea; Sweden: Balkema. 127-130

Mageau, D. W. and Morgenstern, N. R. 1979. "Observations on moisture migration in frozen soils". *Canadian Geotechnical Journal* **17**, 54-60.

Matsuoka, N. 2001. "Solifluction rates, processes and landforms: a global review." *Earth Science Reviews* **55(1-2)**, 107-134.

Matsuoka, N. Hirakawa, K. Watanabe, T. Moriwaki, K. 1997. "Monitoring of Periglacial Slope Processes in the Swiss Alps: the First Two Years of Frost Shattering, Heave and Creep." *Permafrost and Periglacial Processes* **8(2)**, 155-178.

McRoberts, E. C. and Morgenstern, N. R. 1974. "The stability of thawing slopes." *Canadian Geotechnical Journal* **11(4)**, 447-469.

Miller, R. D. 1972. "Freezing and heaving of saturated and unsaturated soils." *Highway Research Record* **393**, 1-11.

Miller, R. D. 1978. "Frost heaving in non-colloidal soils" *3rd International Conference on Permafrost*; Edmonton, Alberta:

Morgenstern, N. R. 1981. "Geotechnical engineering frontier resource development." *Geotechnique* **31(3)**, 305-365.

Morgenstern, N. R. and Nixon, F. M. 1971. "One-dimensional consolidation of thawing soils." *Canadian Geotechnical Journal* **8**, 558-565.

Nakano, Y. 1986. "On the stable growth of segregated ice in freezing soil under negligible overburden pressure". *Advances in Water Resources* **9(4)**, 223-235.

Nakano, Y. 1990. "Quasi-steady problems in freezing soils: I. Analysis on the steady growth of an ice layer." *Cold Regions Science and Technology* **17**, 207-226.

Nakano, Y. 1991. "Transport of water through frozen soils" *6th International Symposium on Ground Freezing* Beijing: Balkema. 65-70

Nakano, Y. 1994. "Quasi-steady problems in freezing soils: IV. Traveling wave solutions". *Cold Regions Science and Technology* **23(1)**, 1-17.

Nakano, Y. and Takeda, K. 1991. "Quasi-steady problems in freezing soils: III. Analysis of experimental data" *Cold Regions Science and Technology* **19(3)**, 225-243.

Nakano, Y. and Tice, A. 1987. "Transport of water in frozen soil VI. Effects of temperature." *Advances in Water Resources* **10(1)**, 44-50.

Nakano, Y. and Tice, A. 1988. "A method for measuring the rate of water transport due to temperature gradient in unsaturated frozen soils" *5th International Conference on Permafrost* Tronheim, Norway: Tapir Press. 412-417

Nakano, Y. and Tice, A. 1990. "Transport of water due to a temperature gradient in unsaturated frozen clay." *Cold Regions Science and Technology* **18(1)**, 57-75.

Nakano, Y. Tice, A. Jenkins, T. 1984a. "Transport of water in frozen soil: V, Method for measuring the vapor diffusivity when ice is absent." *Advances in Water Resources* **7(4)**, 172-179.

Nakano, Y. Tice, A. Oliphant, J. 1984b. "Transport of water in frozen soil IV. Analysis of experimental results on the effects of ice content." *Advances in Water Resources* **7(2)**, 58-66.

Nakano, Y. Tice, A. Oliphant, J. 1984c. "Transport of water in frozen soil: III. Experiments on the effects of ice content." *Advances in Water Resources* **7(1)**, 28-34.

Nakano, Y. Tice, A. Oliphant, J. Jenkins, T. 1982. "Transport of water in frozen soil: I: Experimental determination of soil-water diffusivity under isothermal conditions." *Advances in Water Resources* **5(4)**, 221-226.

Nakano, Y. Tice, A. Oliphant, J. Jenkins, T. 1983. "Transport of water in frozen soil II. Effects of ice on the transport of water under isothermal conditions." *Advances in Water Resources* **6(1)**, 15-26.

Neaupane, K. M. Yamabe T. and Yoshinaka R. 1999. "Simulation of a fully coupled thermo-hydro-mechanical system in freezing and thawing rock". *International Journal of Rock Mechanics and Mining Sciences* **36**, 563-580.

Nixon, F. M. 1973. "Thaw-consolidation of some layered systems." *Canadian Geotechnical Journal* **10**, 617-631.

Nixon, F. M. and McRoberts, E. C. 1973. "A study of some factors affecting the thawing of frozen soils." *Canadian Geotechnical Journal* **10**, 439-452.

Nixon, F. M. and Morgenstern, N. R. 1973. "The residual stress in thawing soils." *Canadian Geotechnical Journal* **10(4)**, 571-580.

Nixon, J. F. 1991. "Discrete ice lens theory for frost heave in soils." *Canadian Geotechnical Journal* **28**, 843-859.

O'Neill, K. 1983. "The physics of mathematical frost heave models: A review" *Cold Regions Science and Technology*, **6**, 275-291

O'Neill, K. and Miller, R. D. 1985. "Exploration of a rigid ice model of frost heave." *Water Resources Research* **21(3)**, 281-296.

Penner, E. 1977 "Fundamental aspects of frost action" *Frost Action in Soils.* International Symposium University Lulea, Sweden, **2** 17-28

Penner, E and Walton, T. 1978 "Effects of temperature and pressure on frost heaving" *International Symposium on Ground Freezing*, Ruhr University, Bochum.

Penner, E. 1986. "Ice lensing in layered soils." *Canadian Geotechnical Journal* **23**, 334-340.

Penner, E. 1986 "Aspects of Ice Lens Growth in Soils". *Cold Regions Science and Technology* **13**, 91-100.

Radd, F. J. and Oertle, D. H. 1973. "Experimental pressure studies of frost heave mechanism and growth-fusion behaviour of ice" *2nd International Conference on Permafrost.* 377-384

Selvadurai, A. P. S., Hu, J, Konuk, I, 1999 "Computational modelling of frost induced soil-pipeline interaction I. Modelling of frost heave". *Cold Regions Science and Technology*, **29**. 215-228

Shen, Mu. Ladanyi, B. 1987 "Modelling of coupled heat, moisture and stress field in freezing soil" *Cold Regions Science and Technology* **14**, 237-246

Sheng, D. 1994 "Thermodynamics of Freezing Soils - Theory and Application" PhD Lulea University of Technology, Lulea, Sweden, February 1994

Takashi, T., Ohrai, T., Yamamoto, H., Okamoto, J., 1981. "Upper limit of heaving pressure derived by pore-water pressure measurements of partially frozen soil." *Engineering Geology* **18(1-4)**, 245-257.

Takeda, K. and Nakano, Y. 1990. "Quasi-steady problems in freezing soils: II. Experiment on the steady growth of an ice layer." *Cold Regions Science and Technology* **18(3)**, 225-247.

Talamucci, F. 1997. "Analysis of coupled heat-mass transport in freezing porous media" *Surveys on Mathematics for Industry* **7(2)**, 93-140.

Talamucci, F. 2003. "Freezing processes in porous media: Formation of ice lenses, swelling of the soil" *Mathematical and Computer Modelling* **37(5-6)**, 595-602.

Viklander, P. and Knutsson, S. 1997. "Permeability changes in a fine-grained till due to cycles of freezing and thawing" *Ground freezing and frost in geotechnical engineering* Lulea; Sweden: Balkema. 193-202

Zhu, Y. Zhang, J. Peng, W. Sheng, Z. Miao, L. 1991. "Constitutive relations of frozen soil in uniaxial compression" *6th International Symposium on Ground Freezing* Beijing: Balkema. 211-216

Chapter 3

Theoretical Formulation

3.1. Introduction

This chapter describes the theoretical formulation for thermal / hydro / mechanical behaviour of saturated soil subjected to freezing and thawing. The governing equations are expressed in terms of three primary variables: pore water pressure (u_l), temperature (T) and displacement ($\boldsymbol{u}$).

The assumptions the numerical model has been formulated on are presented in section 3.2.

The law of conservation of mass is utilised to produce the governing equation for moisture flow in section 3.3. The flow of moisture in this study is considered to only take place in the liquid phase.

The equation of conservation of energy is used to produce the governing equation for heat transfer in section 3.4. Heat transfer is assumed to be driven by conduction, convection and latent heat of fusion.

In section 3.5 the elasto-plastic stress-strain behaviour of soil is discussed. The response of the soil is modelled by an elasto-plastic work hardening modified Cam-Clay constitutive model. The governing equation for deformation is derived from considerations of stress equilibrium.

A summary of the governing equations describing flow and deformation is presented in section 3.6

3.2. Assumptions

The model is based on the following assumptions;

1. The variation of temperature with respect to time is slow (quasi-steady assumption).

2. Temperature and pore water pressure are independent in the frozen fringe.

3. The empirical functions K_1 and K_2 appearing in the water flux law depend only on T; they are strictly positive, increasing functions, and vanishing for very low temperatures.

4. The effect of the vapour phase on moisture transfer is negligible.

5. The degree of ice saturation, S_i, is a function of temperature and varies between 0 and 1. At the freezing temperature, T_0, S_i is equal to 0 and at the segregation freezing temperature, T_s, is equal to 1. The gradient of the function is less than 0. This can be mathematically described as;

$$S_i = S_i(T),\ 0 \le S_i \le 1,\ S_i(T_0) = 0,\ S_i(T_s) = 1,\ \frac{\partial S_i(T)}{\partial T} < 0.$$

6. No capillary effects are present.

7. Pore ice in the frozen fringe is at rest with respect to the porous matrix (no regelation).

8. The quantities λ_s, λ_l, λ_i (thermal conductivities), c_s, c_l, c_i (specific heat capacities), ρ_s, ρ_l, ρ_i (specific densities), and L (latent heat per unit volume) are constant.

9. The thermal conductivity, specific heat capacity and density in the frozen fringe depend on the temperature T as a function of the volumetric ice content, S_i.

These assumptions follow the approach proposed by Nakano (1986, 1990).

3.3. Moisture Transfer

In this study moisture transfer in frozen soil is considered to take place under saturated conditions. In saturated freezing soils two phases can coexist, liquid and ice, although it assumed that the transfer of moisture in the ice phase does not occur it is necessary to include this in the initial formulation of the moisture transport equation.

The volumetric water content, θ, is defined as the sum of the liquid and ice phases;

$$\theta = \theta_l + \theta_i \qquad \textbf{3.3-1}$$

where θ_l is the volumetric liquid content and θ_i is the volumetric ice content.

Using equation 3.3-1 the liquid and ice phases can be split and treated separately in order to obtain the law of conservation of mass for moisture.

The law of conservation of mass dictates that the time derivative of the liquid content is equal to the gradient of the liquid flux.

Mathematically this can be expressed as;

$$\rho_l \frac{\partial \theta_l \partial V}{\partial t} + \rho_l \partial V \nabla \cdot \mathbf{v}_l = E_l \partial V \qquad \textbf{3.3-2}$$

where t is time, $\boldsymbol{v}_l$ is the velocity of liquid, ρ_l is the density of liquid, E_l is the liquid sink source term, ∇ is the gradient operator and ∂V is the incremental volume.

Similarly for the ice phase, the law of conservation of mass states that the time derivative of the ice content is equal to the gradient of the ice flux.

Mathematically this can be expressed as;

$$\rho_i \frac{\partial \theta_i \partial V}{\partial t} + \rho_i \partial V \nabla \cdot \mathbf{v}_i = E_i \partial V \qquad \textbf{3.3-3}$$

where $\boldsymbol{v}_i$ is the velocity of ice, ρ_i is the ice density, E_i is the ice sink source term.

Considering that the production of water or ice is due to the change of phase, we have,

$$E_l = -E_i \qquad \textbf{3.3-4}$$

Substituting equations (3.3-2), (3.3-3) into equation (3.3-4), gives the equation of conservation of mass for moisture as;

$$\frac{\partial}{\partial t}(\theta_l \rho_l)\partial V + \frac{\partial}{\partial t}(\theta_i \rho_i)\partial V + \nabla(\rho_l \mathbf{v}_l)\partial V + \nabla(\rho_i \mathbf{v}_i)\partial V = 0 \qquad \textbf{3.3-5}$$

The volumetric liquid and ice contents may be expressed in terms of porosity as;

$$\theta_l = nS_l \qquad \textbf{3.3-6}$$

$$\theta_i = nS_i \qquad \textbf{3.3-7}$$

where S_l is the degree of saturation of pore water and S_i is the degree of saturation of pore ice. The two are related by means of equation (3.3-1);

$$S_l = 1 - S_i \qquad \textbf{3.3-8}$$

The term ∂V, the incremental volume, is a summation of the void volume and solid volume. Hence it can be shown that;

$$\partial V = (1+e)\partial V_s \qquad \textbf{3.3-9}$$

where V_s is the volume of the solids.

Assuming that the ice does not move relative to the soil grains (regelation), $\mathbf{q}_i = 0$, and substituting (3.3-9) gives:

$$\frac{\partial}{\partial t}((1-S_i)n\rho_l)(1+e)\partial V_s + \frac{\partial}{\partial t}(nS_i\rho_i)(1+e)\partial V_s + \nabla(\rho_l \mathbf{v}_l)(1+e)\partial V_s = 0 \qquad \textbf{3.3-10}$$

The term V_s can be eliminated from (3.3-10) since the volume of the soil solid is assumed to remain constant. Noting by definition the porosity, $n = \frac{e}{(1+e)}$ and making these two changes gives;

$$\frac{\partial}{\partial t}((1-S_i)e\rho_l)+\frac{\partial}{\partial t}(eS_i\rho_i)+\nabla(\rho_l \mathbf{v}_l)(1+e)=0 \qquad \textbf{3.3-11}$$

3.3.1. Mechanism of Liquid Flow

The following mechanisms are considered to cause the flow of water (Mitchell, 1993):

- pressure head,
- elevation head, and
- thermal gradients.

The flow of liquid water due to electrical gradients is not considered.

The first two of these mechanisms; pressure head, and elevation head, may be combined to give the hydraulic head gradient. This is considered to be a driving potential for water flow. These mechanisms may be described by Darcy's law (1856). For flow in saturated soil, Darcy's law may be expressed as;

$$\mathbf{v}_l = -\frac{K_l}{\mu_l}\left[\nabla\left(\frac{u_l}{\gamma_l}\right)+\nabla z\right] = -k_l\left[\nabla\left(\frac{u_l}{\gamma_l}\right)+\nabla z\right] \text{ (m/s)} \qquad \textbf{3.3-12}$$

where

$\mathbf{v}_l$ is the liquid velocity due to pressure and elevation heads,

K_l is the effective permeability,

μ_l is the absolute viscosity of pore liquid,

k_l is the saturated hydraulic conductivity,

γ_l is the unit weight of liquid and z is the elevation.

The variation of the hydraulic conductivity within the frozen fringe is dependent on the quantity of ice contained within the pore space. As the temperature decreases the ice retards the ability of the liquid water to flow, and as more ice is produced the retardation becomes more pronounced. Power and exponential type relationships have been proposed (Chapter 2, Section 3.2) which vary the hydraulic conductivity according to ice content and hence are a function of temperature. An exponential relationship has been adopted following the approach presented by Shen and Ladanyi (1987)

$$k = \begin{cases} k_u e^{\alpha T} & T_s < T < T_0 \\ k_f & T \le T_s \end{cases} \qquad \textbf{3.3-13}$$

where

k_u, k_f is the unfrozen and frozen hydraulic conductivity respectively

α is a constant determined from regression analysis on experimental results

T is the temperature in degrees centigrade

T_0, T_s is the freezing and segregation freezing temperature respectively

In saturated freezing soils it has been experimentally shown that the gradient of temperature causes the movement of water in the direction of lower temperatures under uniform pressure fields (Mageau and Morgenstern 1980, Perfect and Williams 1980). This is sometimes referred to as the effect of cryogenic suctions. Following the approach presented by Nakano (1990) that the pressure and temperature are independent driving forces for moisture flow, the mass flux of water ignoring the flow due to elevation head in freezing soils can be expressed as

$$\mathbf{v}_1 = -K_1 \nabla u_l - K_2 \nabla T \qquad \textbf{3.3-14}$$

where K_1 and K_2 are independent transport coefficients of a given soil that generally depend on temperature and the composition of the soil. Ratkje et al (1982) proposed the transport equation of water based on irreversible thermodynamics as;

$$\mathbf{v}_l = -K_l(\nabla u_l + \gamma \nabla T) \qquad \textbf{3.3-15}$$

where $\gamma = \frac{\rho_i L}{T_0}$, L is the latent heat of fusion, and T_0 is the freezing temperature of pure water in Kelvin.

In terms of Darcian velocity and hydraulic conductivity, equation (3.3-15) can be rewritten as

$$\mathbf{v}_l = -\frac{k_l}{\gamma_l}(\nabla u_l + \gamma \nabla T) \qquad \textbf{3.3-16}$$

Consideration of equation 3.3-12 and equation 3.3-16 yields an expression for liquid flow in terms of pressure head, thermal gradient and elevation head as;

$$\mathbf{v}_l = -k_l\left[\nabla\left(\frac{u_l}{\gamma_l}\right) + \gamma\nabla\left(\frac{T}{\gamma_l}\right) + \nabla z\right] \qquad 0 < S_i < 1 \qquad \textbf{3.3-17a}$$

$$\mathbf{v}_l = -k_l\left[\nabla\left(\frac{u_l}{\gamma_l}\right) + \nabla z\right] \qquad S_i = 0,\ S_i = 1 \qquad \textbf{3.3-17b}$$

The term in equation 3.3-17a representing cryogenic suction has been derived through considerations of the thermo-dynamic equilibrium at phase change using the Clausius-Clapeyron equation.

The assumptions on which the proposed model is based (Section 3.2) are consistent with the approaches adopted in consideration of the concept of the segregation potential (Konrad and Morgenstern 1980, 1982), and the osmotic pressure effects in a diffused double layer (Horiguchi 1987).

Konrad and Morgenstern (1980) proposed that the flow of water to the growing ice lens is proportional to the overall temperature gradient in the frozen soil and the rate of heave is given by.

$$\frac{dh}{dt} = SP \cdot \nabla T \qquad \textbf{3.3-18}$$

The segregation potential, *SP*, is defined as the ratio of the water migration rate to the overall gradient in the frozen fringe.

According to the osmotic pressure effects in a diffused double layer (Horiguchi, 1987) the Segregation Potential corresponds to;

$$SP = \frac{\bar{k}L}{gT_0} \qquad \textbf{3.3-19}$$

where $\bar{k}$ is the apparent hydraulic conductivity of the frozen fringe.

Using published values (Konrad and Morgenstern, 1981) a comparison was made between the two models with a good agreement shown and their equivalence was suggested (Horiguchi, 1987).

The flow of moisture is governed by equation 3.3-17 in which moisture will flow due to pressure head, thermal gradient and elevation head. The flow of water in the frozen fringe due to pressure and thermal gradients are independent (Section 3.2). The initial approach considered is where the strain due to ice lensing is represented by the thermal gradient term in equation 3.3-17.

According to this assumption the Segregation Potential corresponds to;

$$SP = \frac{\bar{k}L\rho_i}{gT_0\rho_l} \qquad \textbf{3.3-20}$$

Table 3.3-1 shows a comparison between segregation potential, osmotic model and the proposed model, test numbers, $\bar{k}$ and *SP* are quoted from Konrad and Morgenstern (1981). A good agreement can be seen between the models suggesting the equivalence between all three models and that the initial approach adopted is consistent with previously published work.

Table 3.3-1 – Comparison between segregation potential, osmotic model and proposed model.

Test	$\bar{k}$ (10^{-10} cm/s)	Segregation Potential	Osmotic Pressure	Proposed Model
		SP (10^{-5} mm^2/s°C)	$\frac{\bar{k}L}{gT_0}$ (10^{-5} mm^2/s°C)	$\frac{\bar{k}L\rho_i}{gT_0\rho_l}$ (10^{-5} mm^2/s°C)
E-4	5.72	61.2	70.9	65.4
E-5	11.10	132.1	137.6	126.9
E-6	11.60	138.0	143.8	132.6
E-7	6.60	72.7	81.8	75.4
E-8	8.30	94.6	102.9	94.9

3.3.2. Governing Differential Equation for Water Flow

In this section the liquid flow is incorporated into the mass conservation equation. Rewriting the mass conservation equation in terms of the primary variables yields the governing differential equation for saturated moisture flow with phase change.

This section expands and develops the terms in order to express the equation of mass conservation in terms of these primary variables.

Substituting the equation for moisture flow (3.3-17) into the mass conservation equation (3.3-11) gives;

$$\frac{\partial}{\partial t}\left((1-S_i)e\rho_l\right)+\frac{\partial}{\partial t}\left(eS_i\rho_i\right)-\nabla\left(\begin{array}{l}\frac{\rho_l k_l}{\gamma_l}\nabla u_l+\rho_l k_l\nabla z\\ +\frac{\rho_l k_l}{\gamma_l}\left(\frac{\rho_i L}{T_0}\right)\nabla T\end{array}\right)(1+e)=0 \qquad \text{3.3-21}$$

Expanding and grouping terms

$$\frac{\partial}{\partial t}\left((1-S_i)e\rho_l+S_i e\rho_i\right)-\nabla\left(\frac{\rho_l k_l}{\gamma_l}\nabla u_l\right)(1+e)-\nabla\left(\frac{\rho_l k_l}{\gamma_l}\left(\frac{\rho_i L}{T_0}\right)\nabla T\right)(1+e) \qquad \text{3.3-22}$$
$$-\nabla\left(\rho_l k_l\nabla z\right)(1+e)=0$$

Considering the first term of (3.3-22);

$$\frac{\partial}{\partial t}\left((1-S_i)e\rho_l + eS_i\rho_i\right) = \left((1-S_i)\rho_l + S_i\rho_i\right)\frac{\partial e}{\partial t} + e(\rho_i - \rho_l)\frac{\partial S_i}{\partial t} + (1-S_i)e\frac{\partial \rho_l}{\partial u_l}\frac{\partial u_l}{\partial t} \quad \textbf{3.3-23}$$

where $\frac{\partial \rho_l}{\partial u_l}$ is the compressibility of water and is defined after Massey (1989) as;

$$\frac{\partial \rho_l}{\partial u_l} = \frac{\rho_l}{K_l} \quad \textbf{3.3-24}$$

where K_l is the bulk modulus of water.

Substituting (3.3-23), and (3.3-24) into (3.3-22)

$$\left((1-S_i)\rho_l + S_i\rho_i\right)\frac{\partial e}{\partial t} + e(\rho_i - \rho_l)\frac{\partial S_i}{\partial t} + (1-S_i)e\frac{\rho_l}{K_l}\frac{\partial u_l}{\partial t} = \nabla\left(\frac{\rho_l k_l}{\gamma_l}\nabla u_l\right)(1+e) + \nabla\left(\frac{\rho_l k_l}{\gamma_l}\left(\frac{\rho_i L}{T_0}\right)\nabla T\right)(1+e) + \nabla(\rho_l k_l \nabla z)(1+e) \quad \textbf{3.3-25}$$

Noting that S_i can be expressed with respect to time and space as

$$\frac{\partial S_i}{\partial t} = \frac{\partial S_i}{\partial T}\frac{\partial T}{\partial t} \text{ and } \nabla S_i = \frac{\partial S_i}{\partial T}\nabla T \quad \textbf{3.3-26}$$

Dividing (3.3-25) by $(1+e)$, substituting (3.3-26), and noting

$$\frac{\partial e}{(1+e)\partial t} = \frac{\partial \varepsilon_v}{\partial t} \quad \textbf{3.3-27}$$

where ε_v is the volumetric strain yields;

$$\begin{aligned}&\left((1-S_i)\rho_l + S_i\rho_i\right)\frac{\partial \varepsilon_v}{\partial t} + n(\rho_i - \rho_l)\frac{\partial S_i}{\partial T}\frac{\partial T}{\partial t} + (1-S_i)n\frac{\rho_l}{K_l}\frac{\partial u_l}{\partial t} \\ &= \nabla\left[\frac{\rho_l k_l}{\gamma_l}\nabla u_l\right] + \nabla\left[\frac{\rho_l k_l}{\gamma_l}\left(\frac{\rho_i L}{T_0}\right)\nabla T\right] + \nabla\left[\rho_l k_l \nabla z\right]\end{aligned} \qquad \textbf{3.3-28}$$

The term, $\frac{\partial \varepsilon_v}{\partial t}$ can be shown to be

$$\frac{\partial \varepsilon_v}{\partial t} = \mathbf{m}^T \frac{\partial \boldsymbol{\varepsilon}}{\partial t} = \mathbf{m}^T \mathbf{P} \frac{\partial \mathbf{u}}{\partial t} \qquad \textbf{3.3-29}$$

where **P** is the strain matrix given as;

$$\mathbf{P} = \begin{bmatrix} \frac{\partial}{\partial x} & 0 \\ 0 & \frac{\partial}{\partial z} \\ \frac{\partial}{\partial z} & \frac{\partial}{\partial x} \\ 0 & 0 \end{bmatrix} \qquad \textbf{3.3-30}$$

The vector **m** is defined for two dimensional plane stress or plane strain analysis as;

$$\mathbf{m}^T = (1,1,0,0) \qquad \textbf{3.3-31}$$

Writing (3.3-28) in concise form yields the governing differential equation for saturated moisture flow with phase change.

$$C_{lu}\frac{\partial \mathbf{u}}{\partial t} + C_{ll}\frac{\partial u_l}{\partial t} + C_{lT}\frac{\partial T}{\partial t} = \nabla\left[K_{ll}\nabla u_l\right] + \nabla\left[K_{lT}\nabla u_l\right] + J_l \qquad \textbf{3.3-32}$$

where

$$C_{lu} = \left[(1-S_i)\rho_l + S_i\rho_i\right]\mathbf{m}^T\mathbf{P} \qquad \textbf{3.3-33}$$

$$C_{ll} = n\frac{\rho_l}{K_l}(1-S_i) \qquad \textbf{3.3-34}$$

$$C_{IT} = n(\rho_i - \rho_l)\frac{\partial S_i}{\partial T} \qquad \textbf{3.3-35}$$

$$K_{ll} = \frac{\rho_l k_l}{\gamma_l} \qquad \textbf{3.3-36}$$

$$K_{lT} = \frac{\rho_l k_l}{\gamma_l}\left(\frac{\rho_i L}{T_0}\right) \qquad \textbf{3.3-37}$$

$$J_l = \nabla \rho_l k_l \nabla z \qquad \textbf{3.3-38}$$

3.4. Heat Transfer

The transfer of heat occurs via three principle methods, (Jakob 1949); conduction, convection and radiation. Transfer via radiation is assumed to be negligible and has not been considered. The latent heat of fusion is included to account for the liquid-solid phase change.

The law of conservation of energy for heat flow dictates that the temporal derivative of heat content, Ω, is equal to the spatial derivative of the heat flux $\mathbf{Q}$.

This can be written as;

$$\frac{\partial(\Omega \partial V)}{\partial t} + \nabla \cdot \mathbf{Q}(\partial V) = 0 \qquad \textbf{3.4-1}$$

The heat content of saturated soil per unit volume is assumed to be the sum of the soil heat capacity and the latent heat of fusion. Denoting by T the soil temperature, and T_r the soil reference temperature, the heat content per unit volume is:

$$\Omega = H_c(T - T_r) - LnS_i\rho_i \qquad \left(J/m^3\right) \qquad \textbf{3.4-2}$$

where L is the latent heat of fusion and H_c, the equivalent heat capacity, is given by

$$H_c = (1-S_i)n\rho_l c_l + nS_i\rho_i c_i + (1-n)\rho_s c_s$$
$$= \rho_s c_s + n((1-S_i)\rho_l c_l + S_i\rho_i c_i - \rho_s c_s) \qquad \textbf{3.4-3}$$

The heat flux per unit area, **Q** is determined by:

$$\mathbf{Q} = -\lambda_T \nabla T + \mathbf{Q_c} \qquad \textbf{3.4-4}$$

where λ_T is the thermal conductivity of saturated soil. Following the approach of Talamucci (1997) the thermal conductivity can be considered as a function of the ice content as;

$$\lambda_T = \lambda_s(S_i) = (1-S_i)n\lambda_l + nS_i\lambda_i + (1-n)\lambda_s \qquad \textbf{3.4-5}$$

where λ_l, λ_i, and λ_s are the thermal conductivities of water, ice and dry soil, respectively.

The first term on the right-hand side of (3.4-4) represents the conduction term, while the second one, $\mathbf{Q_c}$, is the convective contribution, due to the possible movement of the components:

$$\mathbf{Q_c} = (c_l\rho_l\mathbf{q_l} + c_i\rho_i\mathbf{q_i} + c_s\rho_s\mathbf{q_s})(T - T_r) \qquad \textbf{3.4-6}$$

Recalling the assumption that ice does not move relative to the soil grains (regelation), $\mathbf{q_i} = 0$, the convective term reduces to

$$\mathbf{Q_c} = (c_l\rho_l\mathbf{q_l})(T - T_r) \qquad \textbf{3.4-7}$$

Substituting (3.4-2), (3.4-4), and (3.4-7) into (3.4-1) yields:

$$\frac{\partial}{\partial t}[H_c(T - T_r) - LnS_i\rho_i]\partial V - \nabla[\lambda_T \nabla T]\partial V + \nabla[(c_l\rho_l\mathbf{q_l})(T - T_r)]\partial V = 0 \qquad \textbf{3.4-8}$$

Repeating

$$\partial V = (1+e)\partial V_s \qquad \textbf{3.4-9}$$

and substituting into 3.4-8 gives:

$$\begin{aligned}&\frac{\partial}{\partial t}[H_c(T-T_r)-LnS_i\rho_i](1+e)-\nabla[\lambda_T\nabla T](1+e)\\&+\nabla[(c_l\rho_l\mathbf{q}_l)(T-T_r)](1+e)=0\end{aligned} \qquad \textbf{3.4-10}$$

Considering the first part of the storage component of (3.4-10) separately and substituting for H_c from equation (3.4-3) yields;

$$\begin{aligned}&\frac{\partial}{\partial t}[H_c(T-T_r)](1+e)=\\&\quad\frac{\partial}{\partial t}[\rho_s c_s+n((1-S_i)\rho_l c_l+S_i\rho_i c_i-\rho_s c_s)](T-T_r)(1+e)\end{aligned} \qquad \textbf{3.4-11}$$

noting $n(1+e)=e$, the first component of equation (3.4-11) can be expressed as

$$\frac{\partial}{\partial t}(\rho_s c_s(T-T_r)(1+e))=(1+e)\rho_s c_s\frac{\partial T}{\partial t}+\rho_s c_s(T-T_r)\frac{\partial e}{\partial t} \qquad \textbf{3.4-12}$$

and the second, third and fourth as

$$\begin{aligned}&\frac{\partial}{\partial t}([(1-S_i)\rho_l c_l+S_i\rho_i c_i-\rho_s c_s](T-T_r)e)=\\&[(1-S_i)\rho_l c_l+S_i\rho_i c_i-\rho_s c_s](T-T_r)\frac{\partial e}{\partial t}+e(T-T_r)(\rho_i c_i-\rho_l c_l)\frac{\partial S_i}{\partial t}\\&+e[(1-S_i)\rho_l c_l+S_i\rho_i c_i-\rho_s c_s]\frac{\partial T}{\partial t}\end{aligned} \qquad \textbf{3.4-13}$$

Substituting (3.4-12) and (3.4-13) back into (3.4-11) and recalling $\frac{\partial S_i}{\partial t}=\frac{\partial S_i}{\partial T}\frac{\partial T}{\partial t}$ yields

$$\frac{\partial}{\partial t}[H_c(T-T_r)](1+e)=[(1-S_i)\rho_l c_l+S_i\rho_i c_i](T-T_r)\frac{\partial e}{\partial t}$$
$$+\left[\begin{array}{l}e(T-T_r)(\rho_i c_i-\rho_l c_l)\frac{\partial S_i}{\partial T}\\+[(1+e)\rho_s c_s+e((1-S_i)\rho_l c_l+S_i\rho_i c_i-\rho_s c_s)]\end{array}\right]\frac{\partial T}{\partial t} \qquad \textbf{3.4-14}$$

The second part of the storage component of (3.4-10) can be written as;

$$\frac{\partial}{\partial t}[-LnS_i\rho_i](1+e)=-L\rho_i\left(e\frac{\partial S_i}{\partial T}\frac{\partial T}{\partial t}+S_i\frac{\partial e}{\partial t}\right) \qquad \textbf{3.4-15}$$

Substituting (3.4-14) and (3.4-15) into (3.4-10), diving through by $(1+e)$, substituting $n=\frac{e}{(1+e)}$, and noting $\frac{\partial e}{(1+e)\partial t}=\frac{\partial \varepsilon_v}{\partial t}$ and the definition of H_c (3.4-3) gives;

$$[[(1-S_i)\rho_l c_l+S_i\rho_i c_i](T-T_r)-L\rho_i S_i]\frac{\partial \varepsilon_v}{\partial t}$$
$$+\left[[n(T-T_r)(\rho_i c_i-\rho_l c_l)-L\rho_i n]\frac{\partial S_i}{\partial T}+H_c\right]\frac{\partial T}{\partial t} \qquad \textbf{3.4-16}$$
$$-\nabla[\lambda_T\nabla T]+\nabla[(c_l\rho_l\mathbf{q}_l)(T-T_r)]=0$$

Taking and expanding the convective term of (3.4-16) gives

$$\nabla[(\rho_l c_l\mathbf{q}_l)(T-T_r)]=-\nabla(T-T_r)\left[c_l\rho_l k_l\nabla\left(\frac{u_l}{\gamma_l}\right)\right]$$
$$-\nabla(T-T_r)\left[\frac{c_l\rho_l k_l}{\gamma_l}\left(\frac{\rho_i L}{T_0}\right)\nabla T\right]-\nabla(T-T_r)(c_l\rho_l k_l\nabla z) \qquad \textbf{3.4-17}$$

Considering the first term of equation (3.4-17) gives

$$\nabla(T-T_r)\left[c_l\rho_l k_l\nabla\left(\frac{u_l}{\gamma_l}\right)\right]=\frac{c_l\rho_l k_l}{\gamma_l}[(T-T_r)\nabla^2 u_l+\nabla u_l\nabla T] \qquad \textbf{3.4-18}$$

and considering the second term of equation (3.4-17) gives

$$\nabla(T-T_r)\left[\frac{c_l\rho_l k_l}{\gamma_l}\left(\frac{\rho_i L}{T_0}\right)\nabla T\right]=\frac{c_l\rho_l k_l}{\gamma_l}\left(\frac{\rho_i L}{T_0}\right)\left[(T-T_r)\nabla^2 T+\nabla^2 T\right] \qquad \textbf{3.4-19}$$

and considering the third term of equation (3.4-17) gives

$$\nabla(T-T_r)(c_l\rho_l k_l\nabla z)=c_l\rho_l k_l\left[(T-T_r)\nabla^2 z+\nabla z\nabla T\right] \qquad \textbf{3.4-20}$$

Using (3.4-16), (3.4-18) and (3.4-19) the governing partial differential equation can be expressed as:

$$\begin{aligned}
&\left[\left((1-S_i)\rho_l c_l+S_i\rho_i c_i\right)(T-T_r)-L\rho_i S_i\right]\frac{\partial\varepsilon_v}{\partial t}\\
&+\left[\left[n(T-T_r)(\rho_i c_i-\rho_l c_l)-L\rho_i n\right]\frac{\partial S_i}{\partial T}+H_c\right]\frac{\partial T}{\partial t}\\
&-\nabla\left[\lambda_T\nabla T\right]-c_l\rho_l k_l\left(\frac{\nabla u_l}{\gamma_l}+\left(\frac{\rho_i L}{T_0}\right)\frac{\nabla T}{\gamma_l}+\nabla z\right)\nabla T\\
&-\nabla\left[\frac{c_l\rho_l k_l}{\gamma_l}\left(\frac{\rho_i L}{T_0}\right)(T-T_r)\nabla T\right]-\nabla\left[\frac{c_l\rho_l k_l}{\gamma_l}(T-T_r)\nabla u_l\right]\\
&-\nabla c_l\rho_l k_l(T-T_r)\nabla z=0
\end{aligned} \qquad \textbf{3.4-21}$$

Writing (3.4-21) in the concise form:

$$C_{Tu}\frac{\partial\mathbf{u}}{\partial t}+C_{TT}\frac{\partial T}{\partial t}=\nabla\left[K_{TT}\nabla T\right]+\nabla\left[K_{Tl}\nabla u_l\right]+J_T \qquad \textbf{3.4-22}$$

where

$$C_{Tu}=\left[\left((1-S_i)\rho_l c_l+S_i\rho_i c_i\right)(T-T_r)-L\rho_i S_i\right]\mathbf{m}^{\mathrm{T}}\mathbf{P} \qquad \textbf{3.4-23}$$

$$C_{TT}=H_c+\left(n(T-T_r)(\rho_i c_i-\rho_l c_l)-L\rho_i n\right)\frac{\partial S_i}{\partial T} \qquad \textbf{3.4-24}$$

$$K_{TT}=\lambda_T+c_l\rho_l k_l\left(\frac{u_l}{\gamma_l}+\left(\frac{\rho_i L}{T_0}\right)\frac{T}{\gamma_l}+z\right)+\frac{c_l\rho_l k_l}{\gamma_l}\left(\frac{\rho_i L}{T_0}\right)(T-T_r) \qquad \textbf{3.4-25}$$

$$K_{Tl} = \frac{c_l \rho_l k_l}{\gamma_l}(T - T_r) \qquad \textbf{3.4-26}$$

$$J_T = \nabla c_l \rho_l (T - T_r) k_l \nabla z \qquad \textbf{3.4-27}$$

3.5. Deformation Behaviour

In this section an approach is presented to describe changes in volume due to applied stress, phase change and temperature in a saturated medium. Deformations resulting from unsaturated soil behaviour, such as suction and osmotic effects, are not considered in this derivation.

It is worth noting that volumetric deformations due to phase change are controlled by pore water pressure variations, induced by density changes, in the governing equation for moisture transfer. As such they are represented in the following approach via the inclusion of pore water pressure in the definition of effective stress. Volumetric deformations due to cryogenic suctions are represented in a similar way. It is also worth considering the deformation behaviour of the frozen soil. In this approach, on reaching a fully frozen state the extremely low value of hydraulic conductivity of the ice – soil composite results in an effectively undrained condition and therefore no volume change will occur.

It is recognised that further developments of the model could be made to include a more complex approach for the frozen material; for example considering possible creep behaviour of the frozen composite; but this is beyond the scope of this study.

The Modified Cam-Clay elasto-plastic model developed by Schofield and Wroth (1968) has been adopted in this work. This model uses effective stress, σ' as the independent stress state variable. The effective stress is defined as

$$\sigma' = \sigma - u_l \qquad \textbf{3.5-1}$$

where σ is the total stress and u_l the pore water pressure. A compression positive sign convention has been adopted in this work for stress, σ, with u_l defined as positive in compression.

A body under the action of external forces in a state of equilibrium has been described by Wang (1953) as *'at rest or moving in a straight line with constant velocity'*. It is known that two types of external forces act on a body; those through the centroid of the body known as body forces and those that act on the surface of the body known as surface forces.

Considering an element of soil with a unit length and cross sectional area *dxzdz* under a system of two dimensional stresses and body forces, it can be seen that the two dimensional stresses σ_x, σ_z, τ_{xz} and τ_{zx} are independent of y (Figure 3.5-1). The body forces b_x and b_z are likewise independent of y with b_y assumed to be zero.

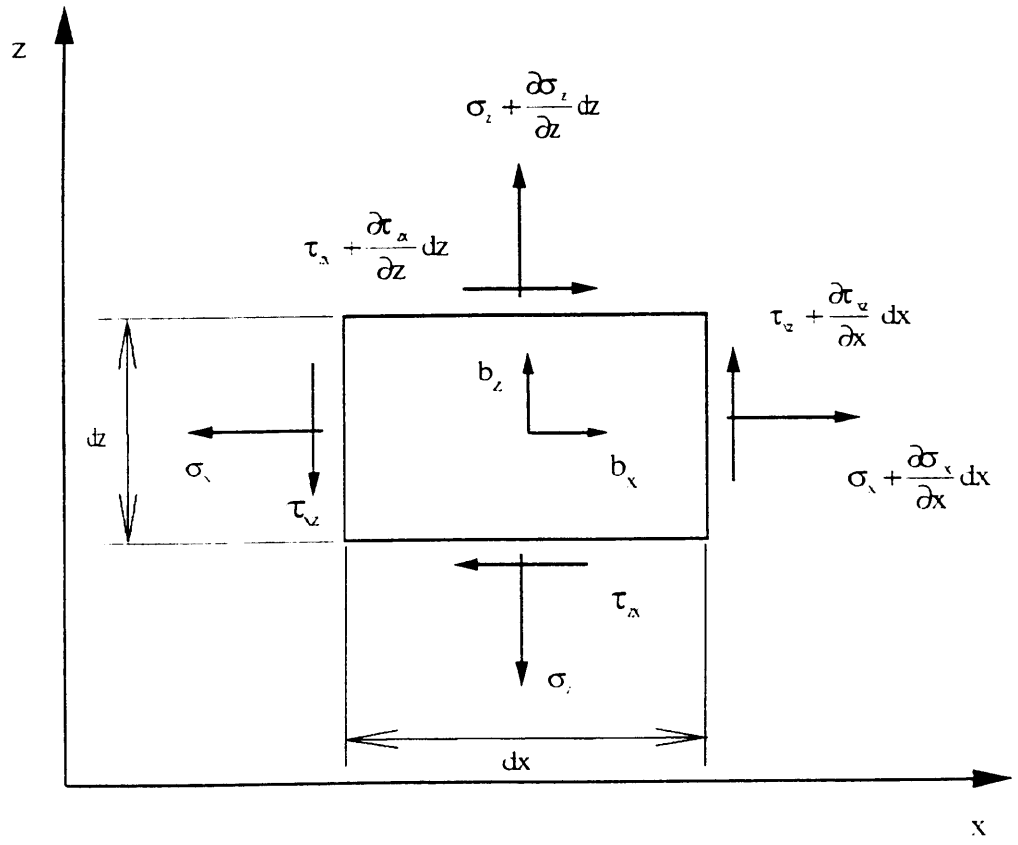

Figure 3.5-1 A general two dimensional stress system.

Newton's Law states that the resultant force acting in the x-direction must be zero, therefore;

$$\left(\sigma_x + \frac{\partial \sigma_x}{\partial x} dx\right) dz + \left(\tau_{zx} + \frac{\partial \tau_{zx}}{\partial z} dz\right) dx - \sigma_x dz - \tau_{zx} dx + b_x dx dz = 0 \qquad \textbf{3.5-2}$$

Rearranging and substituting into the total stress equation, yields;

$$\left(\frac{\partial \sigma'}{\partial x} + \frac{\partial u_l}{\partial x} + \frac{\partial \tau_{zx}}{\partial z} + b_x\right) dx dz = 0 \qquad \textbf{3.5-3}$$

It is not necessarily the case that *dxdz* is equal to zero and so equation (3.5-3) can be reduced to;

$$\frac{\partial \sigma'}{\partial x} + \frac{\partial u_l}{\partial x} + \frac{\partial \tau_{zx}}{\partial z} + b_x = 0 \qquad \textbf{3.5-4}$$

Likewise for the z direction;

$$\frac{\partial \sigma'}{\partial z} + \frac{\partial u_l}{\partial z} + \frac{\partial \tau_{xz}}{\partial x} + b_z = 0 \qquad \textbf{3.5-5}$$

Applying the principle of superposition equations (3.5-4) and (3.5-5) can be combined to yield, in incremental form;

$$\mathbf{P} d\sigma' + \mathbf{m}\mathbf{P} du_l + \mathbf{d}b = 0 \qquad \textbf{3.5-6}$$

where **b** is the vector of body forces and **P** is the strain matrix given as;

$$\mathbf{P} = \begin{bmatrix} \frac{\partial}{\partial x} & 0 \\ 0 & \frac{\partial}{\partial z} \\ \frac{\partial}{\partial z} & \frac{\partial}{\partial x} \\ 0 & 0 \end{bmatrix} \qquad \textbf{3.5-7}$$

The vector **m** is defined for two dimensional plane stress or plane strain analysis as;

$$\mathbf{m}^T = (1,1,0,0) \qquad \textbf{3.5-8}$$

for axisymmetric analysis, and three dimensional analysis;

$$\mathbf{m}^T = (1,1,0,1) \qquad \textbf{3.5-9}$$

3.5.1. Governing Equation for an Elasto-Plastic Approach.

Elasto-plastic constitutive modelling requires that a series of relationships are defined in order to model this behaviour. These are defined below (Britto and Gunn, 1987; Wood, 1990; Owen and Hinton, 1980);

- A yield function for the material in stress space.
- A relationship between the directions of the principal plastic strain increments and the principal stresses.
- A flow rule for the material to specify the relative magnitudes of the incremental plastic strains when the material is yielding.
- A hardening law for the material; the relationship between the amount a material hardens and the plastic strain the material undergoes.

Soils that display elasto-plastic behaviour are characterised by the production of both recoverable and irrecoverable strains. The recoverable strains are defined as elastic and the irrecoverable strains as plastic (Owen and Hinton, 1980). The total strain can therefore be defined as;

$$d\varepsilon = d\varepsilon^e + d\varepsilon^p \qquad \textbf{3.5-10}$$

where $d\varepsilon^e$ is the incremental elastic component of strain, and $d\varepsilon^p$ is the incremental plastic component of strain.

The elastic strain increment can be written considering the individual components as;

$$d\varepsilon^e = d\varepsilon_p^e + d\varepsilon_T^e \qquad \textbf{3.5-11}$$

where ε is the strain vector, and the subscripts p, and T, represent the contributions due to changes in stress, and temperature.

Employing Hooke's law the incremental stress-strain relationship can be described;

$$d\sigma' = \mathbf{D}\left(d\varepsilon - d\varepsilon_T^e - d\varepsilon^p\right) \qquad \textbf{3.5-12}$$

The following sections will now present the four components for the elasto-plastic constitutive model.

3.5.2. Material Behaviour under Elastic Conditions

It is assumed that the elastic deformation in this model occurs due to changes in effective stress under isothermal conditions and follows compressions and recompression curves as shown in (Figure 3.5-2a). This behaviour can be idealised in the compression curves shown in (Figure 3.5-2b) where the slope of the virgin compression curve has a value of $-\lambda$ and the recompression curve a slope of $-k$.

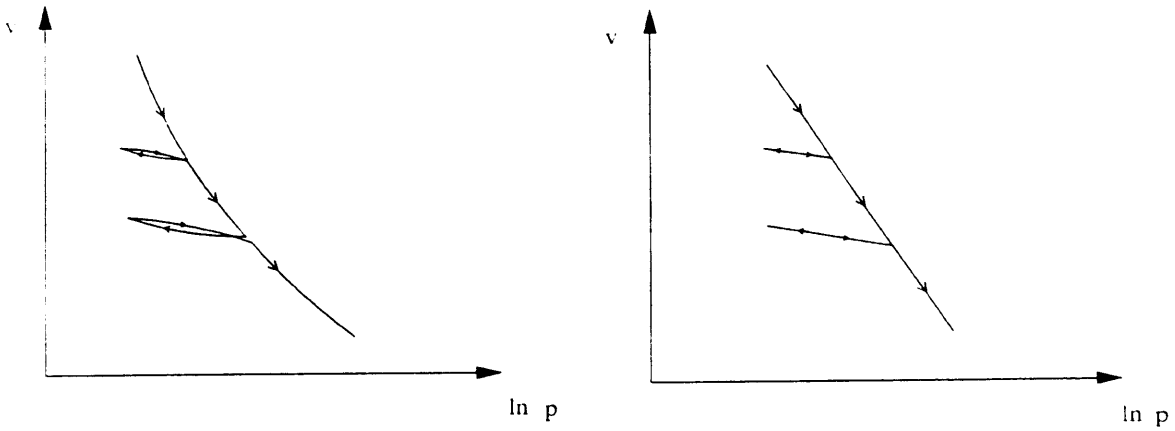

Figure 3.5-2 a) Typical isotropic compression and recompression curves

b) Idealised curves

It is assumed that recoverable changes in volume accompany any changes in mean effective stress p' according to the expression (Wood, 1990)

$$dv = -k\frac{dp'}{p'} \qquad \textbf{3.5-13}$$

in terms of elastic volumetric strain the expression becomes;

$$d\varepsilon_p^e = \frac{dv}{v} = -\frac{k}{v}\frac{dp'}{p'} \qquad \textbf{3.5-14}$$

Temperature effects are only considered due to thermal expansion and are written as;

$$d\varepsilon_T^e = \frac{\alpha_T}{v_0}dT = A_T dT \qquad \textbf{3.5-15}$$

where α_T is the coefficient of thermal expansion, and v_0 is the initial specific volume.

Changes in deviatoric stress can be expressed in terms of incremental deviatoric strain as, (Wood 1990);

$$d\varepsilon_q^e = \frac{1}{3G}dq \qquad \textbf{3.5-16}$$

where q is the deviatoric stress, and G is the shear modulus.

3.5.3. Yield Function

The onset of plastic deformation is described by a set of elliptical yield functions, all having the same shape controlled by the slope of the critical of the critical state line, *M*, pass through the origin and have their sizes controlled by the preconsolidation pressure, p_o'.

The modified CamClay yield locus (Figure 3.5-3) is adopted in this work and is given as (Britto and Gunn, 1987);

$$F(p', q, p_0') = q^2 - M^2 p'(p_o' - p') = 0 \qquad \textbf{3.5-17}$$

where

M is the slope of the critical state line (CSL)

p' is the effective stress

p_0' is the preconsolidation pressure

q is the deviator stress

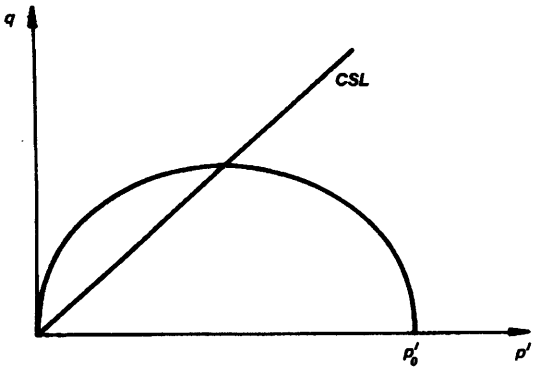

Figure 3.5-3 – Modified Cam-clay yield locus.

3.5.4. Flow Rule

The flow rule for a plastic material gives the ratio of the plastic strain increments when the material is yielding in a particular stress state. The flow rule describes the relative sizes of the individual strain increments, but not their absolute sizes (Britto and Gunn, 1987). Adopting the same function for the yield locus as the plastic potential function results in an associated flow rule or one of normality as the vector of plastic strain is normal to the yield locus. Where the yield function and plastic strain function is not equal the plastic flow rule is said to be non-associated.

In conventional critical state models the at rest earth pressure coefficient, K_o, is often over estimated (Gens and Potts, 1982). Alonso et al. (1990) proposed the introduction of a correction factor, α_q. A non-associated plastic flow rule has been assumed.

The plastic potential can be expressed as;

$$Q = \alpha_q q^2 - M^2 p'(p_0' - p') \qquad \textbf{3.5-18}$$

α_q is a constant derived from the 'at rest' stress state for which there is no lateral deformation. The pressure coefficient has been defined by, (Jaky, 1948);

$$K_o = 1 - \sin\phi' = \frac{(6-2M)}{(6+M)} \qquad \textbf{3.5-19}$$

With the assumption that the elastic strain increment is equal to zero, α_q is given as follows;

$$\alpha_q = \frac{M(M-9)(M-3)}{6(6-M)} \frac{1}{\left(1-\frac{k}{\lambda}\right)} \qquad \textbf{3.5-20}$$

The plastic strain component is assumed to be proportional to the stress gradient of the plastic potential, the incremental plastic strain can be written as;

$$d\varepsilon^p = \chi \frac{dQ}{d\sigma'} \qquad \textbf{3.5-21}$$

χ is a plastic multiplier determined through plasticity conditions (Alonso et al., 1990). The incremental plastic strain can be further split into its volumetric and deviatoric components;

$$d\varepsilon_p^p = \chi \frac{dQ}{dp'} = \chi M^2 (2p' - p_0') \qquad \textbf{3.5-22}$$

$$d\varepsilon_q^p = \chi \frac{dQ}{dq} = \chi 2\alpha_q q \qquad \textbf{3.5-23}$$

3.5.5. Hardening Laws

It is assumed that the yield loci expand at constant shape, the size being controlled by the tip stress p_0' and that the expansion of the yield loci, the hardening of the soil, is linked with the normal compression of the soil (Wood, 1990). The rate of plastic straining after yield is dependent on the plastic volumetric strain increment $d\varepsilon_p^p$.

$$\frac{dp_0'}{p_0'} = \frac{v}{\lambda - k} d\varepsilon_p^p \qquad \textbf{3.5-24}$$

3.5.6. Development of the Elasto-Plastic, Stress-Strain Matrix, Dep

The elastic incremental constitutive matrix **D** relates the elastic strain increment to the stress increment. This has to be extended for an elasto-plastic approach and is described below.

The elastic matrix **D** is defined for a two dimensional plane strain problem in terms of Young's modulus, *E*, and Poisson's ration, v, as (Smith, 1982);

$$\mathbf{D} = \frac{E(1-v)}{(1+v)(1-2v)} \begin{bmatrix} 1 & \frac{v}{1-v} & 0 \\ \frac{v}{1-v} & 1 & 0 \\ 0 & 0 & \frac{1-2v}{2(1-v)} \end{bmatrix} \qquad \textbf{3.5-25}$$

In two dimensional plane strain problems, $\varepsilon_y = \gamma_{xy} = \gamma_{zy} = 0$

The bulk modulus may be expressed as;

$$K = \frac{d\sigma'}{d\varepsilon_p} \qquad \textbf{3.5-26}$$

Assuming a constant Poisson's ratio Young's modulus may be expressed as;

$$E = 3(1-2v)K \qquad \textbf{3.5-27}$$

Changes in stress produced as a result of changes in strain due to the application of load are predicted using the elastic stiffness matrix. This is valid only while the material is behaving elastically. Application of the elastic stiffness matrix to materials that are plastically deforming will result in an over-prediction of the changes in stress. To take account of the changes in plastic strain, the elastic stiffness matrix must be modified.

As plastic yielding occurs the stress must remain on the yield surface and the consistency condition must be satisfied as follows;

$$dF = \left(\frac{\partial F}{\partial \sigma'}\right)^T d\sigma' + \frac{\partial F}{\partial k_h} dk_h = 0 \qquad \textbf{3.5-28}$$

where F is the yield function, and k_h is the hardening parameter.

The consistency condition is given as follows;

$$dF = \left(\frac{\partial F}{\partial \sigma'}\right)^T d\sigma' + \frac{\partial F}{\partial p_0'} dp_0' = 0 \qquad \textbf{3.5-29}$$

Through superposition the total change in strain due to the application of load can be split into the contributions from elastic and plastic components;

$$d\varepsilon_\sigma = d\varepsilon_\sigma^e + d\varepsilon_\sigma^p \qquad \textbf{3.5-30}$$

This can be written as;

$$d\varepsilon_\sigma = \mathbf{D}^{-1} d\sigma' + \chi \frac{dQ}{d\sigma'} \qquad \textbf{3.5-31}$$

where ε_σ is the strain due to the application of load.

Multiplying Equation (3.5-31) through by $\left(\frac{\partial F}{\partial \sigma'}\right)^T \mathbf{D}$ gives;

$$\left[\left(\frac{\partial F}{\partial \sigma'}\right)^T \mathbf{D}\right] d\varepsilon_\sigma = \left(\frac{\partial F}{\partial \sigma'}\right)^T d\sigma' + \left[\left(\frac{\partial F}{\partial \sigma'}\right)^T \mathbf{D}\right] \chi \frac{dQ}{d\sigma'} \qquad \textbf{3.5-32}$$

Noting: $dp_0' = \frac{\partial p_0'}{\partial \varepsilon_p^p} d\varepsilon_p^p$, rearrangement of Equation (3.5-29) yields;

$$\left(\frac{\partial F}{\partial \sigma'}\right)^T d\sigma' = -\frac{\partial F}{\partial p_0'} dp_0' \qquad \textbf{3.5-33}$$

Using Equation (3.5-31), Equation (3.5-33) can be rewritten as;

$$\left(\frac{\partial F}{\partial \sigma'}\right)^T d\sigma' = -\frac{\partial F}{\partial p_0'}\left(\frac{dp_0'}{\partial \varepsilon_\sigma^p}\right)^T \frac{dQ}{d\sigma'} \chi = \mathbf{A}\chi \qquad \textbf{3.5-34}$$

Substitution of equation (3.5-34) into (3.5-32) with rearrangement gives;

$$\left(\frac{\partial F}{\partial \sigma'}\right)^T \mathbf{D} d\varepsilon_\sigma = \mathbf{A}\chi + \left(\frac{\partial F}{\partial \sigma'}\right)^T \mathbf{D}\chi \frac{dQ}{d\sigma'} \qquad \textbf{3.5-35}$$

Rearrangement in terms of χ gives;

$$\chi = \frac{\left(\frac{\partial F}{\partial \sigma'}\right)^T \mathbf{D} d\varepsilon_\sigma}{\mathbf{A} + \left(\frac{\partial F}{\partial \sigma'}\right)^T \mathbf{D} \frac{dQ}{d\sigma'}} \qquad \textbf{3.5-36}$$

Substituting equation (3.5-36) back into (3.5-31) yields;

$$d\varepsilon_\sigma = \mathbf{D}^{-1}d\sigma' + \frac{\left(\frac{\partial F}{\partial \sigma'}\right)^T \mathbf{D}d\varepsilon_\sigma}{\mathbf{A} + \left(\frac{\partial F}{\partial \sigma'}\right)^T \mathbf{D}\frac{dQ}{d\sigma'}}\frac{dQ}{d\sigma'} \qquad \textbf{3.5-37}$$

Rearranging in terms of $d\sigma$ gives;

$$d\sigma' = \left(\mathbf{D} - \frac{\mathbf{D}\left(\frac{\partial F}{\partial \sigma'}\right)^T \mathbf{D}\frac{dQ}{d\sigma'}}{\mathbf{A} + \left(\frac{\partial F}{\partial \sigma'}\right)^T \mathbf{D}\frac{dQ}{d\sigma'}}\right)d\varepsilon_\sigma \qquad \textbf{3.5-38}$$

After Owen and Hinton, (1980) the complete elasto-plastic incremental stress-strain relationship may now be formulated;

$$d\sigma' = \mathbf{Dep}d\varepsilon \qquad \textbf{3.5-39}$$

where;

$$\mathbf{Dep} = \mathbf{D} - \frac{\mathbf{D}\left(\frac{\partial F}{\partial \sigma'}\right)^T \mathbf{D}\frac{dQ}{d\sigma'}}{\mathbf{A} + \left(\frac{\partial F}{\partial \sigma'}\right)^T \mathbf{D}\frac{dQ}{d\sigma'}} \qquad \textbf{3.5-40}$$

The plastic modulus A may be defined as;

$$\mathbf{A} = -\frac{dQ}{\partial p_0'}\left(\frac{\partial p_0'}{\partial \varepsilon_\sigma}\right)^T \frac{\partial F}{d\sigma'} \qquad \textbf{3.5-41}$$

With substitution from equation (3.5-24) the plastic modulus can be reformulated as;

$$\mathbf{A} = -\frac{dQ}{\partial p_0'}\left(\frac{v}{\lambda - k}p_0'\right)\frac{\partial F}{dp'} \qquad \textbf{3.5-42}$$

Differentiating equation (3.5-18) with respect to p_0' and equation (3.5-17) with respect to p', equation (3.5-42) may be reformulated to give;

$$\mathbf{A} = M^2 p' p_0' \left(\frac{v}{\lambda - k}\right)\left(M^2(2p' - p_o')\right) \qquad \textbf{3.5-43}$$

The stress-strain relationship given in (3.5-12) can now be written in terms of the individual components of plastic strain increments due to changes in stress;

$$d\sigma' = \mathbf{Dep}\left(d\varepsilon - d\varepsilon_T^e\right) \qquad \textbf{3.5-44}$$

Using equations (3.5-14), (3.5-15), and (3.5-16) to substitute into equation (3.5-44) gives;

$$d\sigma' = \mathbf{Dep}\left(d\varepsilon - A_T dT\right) \qquad \textbf{3.5-45}$$

With substitution from equation (3.5-45), the stress equilibrium equation (3.5-6) can be written to yield;

$$\mathbf{PDep}\left(\mathbf{P}^T d\mathbf{u} - A_T dT\right) + \mathbf{m}\mathbf{P} du_l + \mathbf{d}b = 0 \qquad \textbf{3.5-46}$$

The governing differential equation for this approach can be written as;

$$C_{uu} d\mathbf{u} + C_{uT} dT + C_{ul} du_l + \mathbf{d}b = 0 \qquad \textbf{3.5-47}$$

where:

$$C_{uu} = \mathbf{PDepP}^T \qquad \textbf{3.5-48}$$

$$C_{uT} = -\mathbf{PDep}A_T \qquad \textbf{3.5-49}$$

$$C_{ul} = \mathbf{mP} \qquad \textbf{3.5-50}$$

3.6. Summary and Conclusions

In the above section a set of developed governing equations have been proposed to represent the flow of moisture, heat in a deformable saturated soil which may be subjected to freezing and thawing. The equations have been formulated in terms of three unknown primary variables, namely; pore water pressure (u_l), temperature (T), and deformation ($\boldsymbol{u}$).

A summary of the final governing equations are presented below

Moisture Transfer:

$$C_{lu}\frac{\partial \mathbf{u}}{\partial t}+C_{ll}\frac{\partial u_l}{\partial t}+C_{lT}\frac{\partial T}{\partial t}=\nabla\left[K_{ll}\nabla u_l\right]+\nabla\left[K_{lT}\nabla u_l\right]+J_l \qquad \textbf{3.6-1}$$

Heat Transfer:

$$C_{Tu}\frac{\partial \mathbf{u}}{\partial t}+C_{TT}\frac{\partial T}{\partial t}=\nabla\left[K_{TT}\nabla T\right]+\nabla\left[K_{Tl}\nabla u_l\right]+J_T \qquad \textbf{3.6-2}$$

Deformation:

$$C_{uu}d\mathbf{u}+C_{uT}dT+C_{ul}du_l+\mathbf{d}b=0 \qquad \textbf{3.6-3}$$

Considering the special cases of when the system is in a completely frozen or unfrozen state i.e. there is no phase change occurring and no latent heat effects, the governing equations can be simplified and are presented for the completely unfrozen state (Equations 3.6-4 to 3.6-6) and completely frozen state (Equations 3.6-7 to 3.6-9).

Unfrozen State

Moisture Transfer

$$\rho_l \mathbf{m}^{\mathrm{T}} \mathbf{P} \frac{\partial \mathbf{u}}{\partial t} + n \frac{\rho_l}{K_l} \frac{\partial u_l}{\partial t} = \nabla \left[\frac{\rho_l k_l}{\gamma_l} \nabla u_l \right] + \nabla [\rho_l k_l \nabla z] \qquad \textbf{3.6-4}$$

Heat Transfer

$$\begin{aligned} &[\rho_l c_l (T - T_r)] \mathbf{m}^{\mathrm{T}} \mathbf{P} \frac{\partial \mathbf{u}}{\partial t} + H_c \frac{\partial T}{\partial t} = \nabla [\lambda_T \nabla T] \\ &+ c_l \rho_l k_l \left(\frac{\nabla u_l}{\gamma_l} + \nabla z \right) \nabla T + \nabla \left[\frac{c_l \rho_l k_l}{\gamma_l} (T - T_r) \nabla u_l \right] \\ &+ \nabla c_l \rho_l k_l (T - T_r) \nabla z \end{aligned} \qquad \textbf{3.6-5}$$

Deformation:

$$C_{uu} d\mathbf{u} + C_{uT} dT + C_{ul} du_l + \mathbf{d}b = 0 \qquad \textbf{3.6-6}$$

Frozen State

Moisture Transfer

$$\rho_l \mathbf{m}^{\mathrm{T}} \mathbf{P} \frac{\partial \mathbf{u}}{\partial t} = \nabla \left[\frac{\rho_l k_l}{\gamma_l} \nabla u_l \right] + \nabla [\rho_l k_l \nabla z] \qquad \textbf{3.6-7}$$

Heat Transfer

$$\begin{aligned} &[\rho_i c_i (T - T_r) - L \rho_i] \mathbf{m}^{\mathrm{T}} \mathbf{P} \frac{\partial \mathbf{u}}{\partial t} + H_c \frac{\partial T}{\partial t} = \nabla [\lambda_T \nabla T] \\ &+ c_l \rho_l k_l \left(\frac{\nabla u_l}{\gamma_l} + \nabla z \right) \nabla T + \nabla \left[\frac{c_l \rho_l k_l}{\gamma_l} (T - T_r) \nabla u_l \right] \\ &+ \nabla c_l \rho_l k_l (T - T_r) \nabla z \end{aligned} \qquad \textbf{3.6-8}$$

Deformation:

$$C_{uu} d\mathbf{u} + C_{uT} dT + C_{ul} du_l + \mathbf{d}b = 0 \qquad \textbf{3.6-9}$$

3.7. References

Alonso, E.E., Gens, A., and Josa, A., 1990 "A constitutive model for partially saturated soils", *Geotechnique* **40**, No. 3, 405-430.

Britto, A.M., and Gunn, M.G., 1987 "Critical state soil mechanics via finite elements", Ellis Horwood Ltd.

Darcy, H., 1856 "Les fontaines publiques de la ville de Dijon", V. Dalmont, Paris, 590-594.

Gens, A., and Potts, D.M., 1982 "Application of critical state models to the prediction of the behaviour of a normally consolidated low plasticity clay", *Proceedings of the 1st International Symposium on Numerical Modelling and Geomechanics*, Zurich, 312-323.

Horiguchi, K. 1987. "An osmotic model for soil freezing". *Cold Regions Science and Technology* **14(1)**, 13-22.

Jakob, M., 1949 "Heat transfer: Vol 1", Wiley.

Jaky, J., 1948 "Pressure in soils", *Proceedings of the 2nd International Conference on Soil Mechanics and Foundation Engineering*, **1**, 103-107.

Konrad, J. M. and Morgenstern, N. R., 1980. "A mechanistic theory of ice lens formation in fine-grained soils". *Canadian Geotechnical Journal* **17**, 473-486.

Konrad, J. M. and Morgenstern, N. R., 1981. "The segregation potential of a freezing soil". *Canadian Geotechnical Journal* **18**, 482-491.

Konrad, J. M. and Morgenstern, N. R., 1982. "Prediction of frost heave in the laboratory during transient freezing". *Canadian Geotechnical Journal* **19**, 250-259.

Massey, B. S., 1989 "Mechanics of Fluids", Sixth Edition, London: Van Nostrand Reinhold

Mageau, D. W. and Morgenstern, N. R., 1980. "Observations on moisture migration in frozen soils". *Canadian Geotechnical Journal* **17**, 54-60.

Mitchell, J.K., 1993 "Fundamentals of soil behaviour" John Wiley, New York.

Nakano, Y., 1986. "On the stable growth of segregated ice in freezing soil under negligible overburden pressure". *Advances in Water Resources* **9(4)**, 223-235.

Nakano, Y., 1990 "Quasi-steady problems in freezing soils: 1. Analysis on the steady growth of an ice layer". *Cold Regions Science and Technology* **17,** 207-226.

Owen, D.R.J., and Hinton, E., 1980 "Finite elements in plasticity: Theory and practice" Pineridge Press Ltd., Swansea.

Perfect, E. and Williams, P. J., 1980 "Thermally induced water migration in saturated frozen soils". *Cold Regions Science and Technology* **3**, 101-109.

Ratkje, S. K., Yamamoto, H., Takashi, T., Ohrai, T. and Okamoto, J., 1982 "The hydraulic conductivity of soils during frost heave". *Frost i Jord*, **24**, 22-26

Schofield, A. N. and Wroth, P. 1968 "Critical State Soil Mechanics". McGraw-Hill, London.

Selvadurai, A. P. S., Hu, J. and Konuk, I. 1999 "Computational Modelling of Frost Heave Induced Soil – Pipeline Interaction. 1 Modelling of Frost Heave". *Cold Regions Science and Technology* **29**, 215-228.

Smith, I.M., 1982 "Programming the finite element method with application to geomechanics", John Wiley and Sons Ltd, USA.

Wang, C., 1953 "Applied Elasticity", McGraw-Hill Book Co.

Wood, D.M., 1990 "Soil behaviour and critical state soil mechanics", Cambridge University Press, Cambridge.

Chapter 4

Finite Element Formulation

4.1. Introduction

The governing differential equations describing moisture and heat flow in a deformable saturated frozen soil were present in Chapter 3. By the very nature and complexities of these sets of equations a direct analytical solution is unavailable. In order to solve these equations a numerical solution scheme is required. In this work spatial discretisation of the equations is performed by the finite element method, whilst a finite difference time-stepping algorithm is used to achieve temporal discretisation. This chapter presents the formulation of this solution.

4.2. Spatial Discretisation

The Galerkin weighted residual approach is employed in this study. This approach has been described in detail elsewhere (Zienkiewicz and Taylor, 1991) and has been successfully applied to examine transient coupled problems, where it has been found to be effective and robust (Zienkiewicz and Taylor, 1989; Thomas et al., 1998). The spatial discretisations of the governing equations are subsequently shown in a summarised form.

4.2.1. Spatial Discretisation for Flow Variables

The spatial discretisation of the flow variables follows similar lines and so the discretisation of only one of the flow variables is shown in detail. The governing equation for moisture flow has been chosen for this.

The primary unknowns and their derivatives may be approximated using the shape function approach for an eight noded isoparametric quadrilateral element as;

$$\hat{u}_{\text{var}} = \sum_{s=1}^{8} N_s \hat{u}_{\text{var}\,s} \qquad \textbf{4.2-1}$$

$$\nabla\hat{u}_{\text{var}} = \sum_{s=1}^{8} (\nabla N_s)\hat{u}_{\text{var}\,s} \qquad \textbf{4.2-2}$$

where $\hat{u}_{\text{var}}$ represents any of the primary variables, (u_l, T, $\mathbf{u}$), N_s is the shape function, the subscript $_s$ represents nodal points and the symbol, $\hat{}$, signifies an approximate form.

Using the shape function approximations of equations (4.2-1) and (4.2-2) to substitute for the primary unknown for the governing differential equation for moisture flow, may be rewritten as;

$$\left[-C_{lu}\frac{\partial\hat{\mathbf{u}}}{\partial t} - C_{ll}\frac{\partial\hat{u}_l}{\partial t} - C_{lT}\frac{\partial\hat{T}}{\partial t} + \nabla\left[K_{ll}\nabla\hat{u}_l\right] + \nabla\left[K_{lT}\nabla\hat{T}\right] + J_1 \right] = R_\Omega \qquad \textbf{4.2-3}$$

where R_Ω is the residual error introduced by substitution of the approximate values of the variables.

The error is minimised over the elemental volume by employing the Galerkin weighted residual approach, for example;

$$\int_{\Omega^e} N_r \left[\begin{array}{l} -C_{lu}\dfrac{\partial\hat{\mathbf{u}}}{\partial t} - C_{ll}\dfrac{\partial\hat{u}_l}{\partial t} - C_{lT}\dfrac{\partial\hat{T}}{\partial t} \\ +\nabla\left[K_{ll}\nabla\hat{u}_l\right] + \nabla\left[K_{lT}\nabla\hat{T}\right] + J_1 \end{array} \right] d\Omega^e = 0 \qquad \textbf{4.2-4}$$

Employing integration by parts yields the weak form of equation (4.2-4). Considering the fourth term it can be expressed as;

$$\int_{\Omega^e} N_r\left[\nabla\left(K_{II}\nabla\hat{u}_I\right)\right]d\Omega^e = \int_{\Omega^e}\nabla\left(N_r K_{II}\nabla\hat{u}_I\right)d\Omega^e - \int_{\Omega^e} K_{II}\nabla\hat{u}_I\nabla N_r d\Omega^e \qquad \textbf{4.2-5}$$

Similarly the sixth term J_l can be expressed, with substitution from Chapter 3, as;

$$\begin{aligned}\int_{\Omega^e} N_r\left[J_l\right]d\Omega^e &= \int_{\Omega^e} N_r\rho_l\nabla\left[k_l\nabla z\right]d\Omega^e \\ &= \int_{\Omega^e}\nabla\left(N_r\rho_l k_l\nabla z\right)d\Omega^e - \int_{\Omega^e} k_l\rho_l\nabla z\nabla N_r d\Omega^e\end{aligned} \qquad \textbf{4.2-6}$$

Applying a similar process to the other terms, equation (4.2-4) can therefore be expressed as;

$$\int_{\Omega^e}\left[\begin{array}{l}\nabla\left(N_r K_{II}\nabla\hat{u}_I\right) - K_{II}\nabla\hat{u}_I\nabla N_r + \nabla\left(N_r K_{IT}\nabla\hat{T}\right) - K_{IT}\nabla\hat{T}\nabla N_r \\ +\nabla\left(N_r\rho_l k_l\nabla z\right) - k_l\rho_l\nabla z\nabla N_r \\ +N_r\left[-C_{lu}\dfrac{\partial\hat{\mathbf{u}}}{\partial t} - C_{II}\dfrac{\partial\hat{u}_I}{\partial t} - C_{IT}\dfrac{\partial\hat{T}}{\partial t}\right]\end{array}\right]d\Omega^e = 0 \qquad \textbf{4.2-7}$$

To reduce the second order terms to first order terms the Gauss-Green Divergence theorem is applied. This method introduces surface integrals. These integrals will cancel on adjacent elements, leaving only a contribution on the limit of the domain. Application of this theorem means equation (4.2-7) can be expressed as;

$$\int_{\Omega^e}\left[\begin{array}{l}-K_{II}\nabla\hat{u}_I\nabla N_r - K_{IT}\nabla\hat{T}\nabla N_r \\ -k_l\rho_l\left(1-S_l\right)\nabla z\nabla N_r \\ -N_r\left[C_{lu}\dfrac{\partial\hat{\mathbf{u}}}{\partial t} + C_{II}\dfrac{\partial\hat{u}_I}{\partial t} + C_{IT}\dfrac{\partial\hat{T}}{\partial t}\right]\end{array}\right]d\Omega^e + \int_{\Gamma^e} N_r\left[\begin{array}{l}K_{II}\nabla\hat{u}_I \\ +K_{IT}\nabla\hat{T} \\ +k_l\rho_l\nabla z\end{array}\right]\underline{n}d\Gamma^e = 0 \qquad \textbf{4.2-8}$$

where Γ^e is the element boundary surface and $\underline{n}$ is the direction cosine normal to the surface. The surface integral in equation (4.2-8) is equal to the liquid flux normal to the boundary surface and may be expressed as;

$$\begin{aligned}&\int_{\Gamma^e} N_r \left[K_{ll}\nabla\hat{u}_l + K_{lT}\nabla\hat{T} + k_l\rho_l\nabla z\right]\underline{n}d\Gamma^e \\ &= \int_{\Gamma^e} N_r\left[\rho_l k_l\left(\frac{1}{\gamma_l}\nabla\hat{u}_l + \nabla z\right) + \frac{\rho_l k_l}{\gamma_l}\left(\frac{\rho_i L}{T_0}\right)\nabla\hat{T}\right]\underline{n}d\Gamma^e \\ &= \int_{\Gamma^e}\mathbf{N}^T\left[\rho_l\hat{\mathbf{v}}_{ln}\right]d\Gamma^e\end{aligned} \qquad \textbf{4.2-9}$$

where $\underline{\hat{\mathbf{v}}}_{ln}$ is the approximate liquid velocity normal to the boundary surface.

Introducing the expressions for the derivatives of the primary variables yields;

$$\begin{aligned}&\int_{\Omega^e}\left[K_{ll}\nabla\mathbf{N}^T\nabla\mathbf{N}\right]d\Omega^e\mathbf{u}_{ls} + \int_{\Omega^e}\left[K_{lT}\nabla\mathbf{N}^T\nabla\mathbf{N}\right]d\Omega^e\mathbf{T}_s \\ &+ \int_{\Omega^e}\left[C_{lu}\mathbf{N}^T\mathbf{N}\right]d\Omega^e\frac{\partial\mathbf{u}_s}{\partial t} + \int_{\Omega^e}\left[C_{ll}\mathbf{N}^T\mathbf{N}\right]d\Omega^e\frac{\partial\mathbf{u}_{ls}}{\partial t} + \int_{\Omega^e}\left[C_{lT}\mathbf{N}^T\mathbf{N}\right]d\Omega^e\frac{\partial\mathbf{T}_s}{\partial t} \\ &+ \int_{\Omega^e}\left[k_l\rho_l\nabla\mathbf{N}^T\nabla z\right]d\Omega^e - \int_{\Gamma^e}\mathbf{N}^T\left[\rho_l\hat{\mathbf{v}}_{ln}\right]d\Gamma^e = 0\end{aligned} \qquad \textbf{4.2-10}$$

where $\mathbf{N}$ is the shape function matrix, $\mathbf{u}_{ls}$ is the pore water pressure vector, $\mathbf{T}_s$ is the temperature vector, and $\mathbf{u}_s$ is the displacement vector.

This can be rewritten in concise matrix notation as;

$$\mathbf{C}_{lu}\frac{\partial\mathbf{u}_s}{\partial t} + \mathbf{C}_{ll}\frac{\partial\mathbf{u}_{ls}}{\partial t} + \mathbf{C}_{lT}\frac{\partial\mathbf{T}_s}{\partial t} + \mathbf{K}_{ll}\mathbf{u}_{ls} + \mathbf{K}_{lT}\mathbf{T}_s = \mathbf{f}_l \qquad \textbf{4.2-11}$$

where;

$$\mathbf{C}_{lu} = \sum_{e=1}^{m}\int_{\Omega^e}\left[C_{lu}\mathbf{N}^T\mathbf{N}\right]d\Omega^e \qquad \textbf{4.2-12}$$

$$\mathbf{C}_{ll} = \sum_{e=1}^{m}\int_{\Omega^e}\left[C_{ll}\mathbf{N}^T\mathbf{N}\right]d\Omega^e \qquad \textbf{4.2-13}$$

$$\mathbf{C}_{\mathrm{lT}} = \sum_{e=1}^{m} \int_{\Omega^e} [C_{lT} \mathbf{N}^T \mathbf{N}] d\Omega^e \qquad \textbf{4.2-14}$$

$$\mathbf{K}_{\mathrm{ll}} = \sum_{e=1}^{m} \int_{\Omega^e} [K_{ll} \nabla \mathbf{N}^T \nabla \mathbf{N}] d\Omega^e \qquad \textbf{4.2-15}$$

$$\mathbf{K}_{\mathrm{lT}} = \sum_{e=1}^{m} \int_{\Omega^e} [K_{lT} \nabla \mathbf{N}^T \nabla \mathbf{N}] d\Omega^e \qquad \textbf{4.2-16}$$

$$\mathbf{f}_{\mathrm{l}} = \sum_{e=1}^{m} \int_{\Omega^e} [k_l \rho_l \nabla \mathbf{N}^T \nabla z] d\Omega^e - \sum_{e=1}^{m} \int_{\Gamma^e} \mathbf{N}^T m [\rho_l \hat{\mathbf{v}}_{\mathrm{ln}}] d\Gamma^e \qquad \textbf{4.2-17}$$

where m is the total number of nodes

Repeating the process for the governing equation for the temperature field yields;

$$\mathbf{C}_{\mathrm{Tu}} \frac{\partial \mathbf{u}_s}{\partial t} + \mathbf{C}_{\mathrm{TT}} \frac{\partial \mathbf{T}_s}{\partial t} + \mathbf{K}_{\mathrm{Tl}} \mathbf{u}_{\mathrm{l}s} + \mathbf{K}_{\mathrm{TT}} \mathbf{T}_s = \mathbf{f}_{\mathrm{T}} \qquad \textbf{4.2-18}$$

where;

$$\mathbf{C}_{\mathrm{Tu}} = \sum_{e=1}^{m} \int_{\Omega^e} [C_{Tu} \mathbf{N}^T \mathbf{N}] d\Omega^e \qquad \textbf{4.2-19}$$

$$\mathbf{C}_{\mathrm{TT}} = \sum_{e=1}^{m} \int_{\Omega^e} [C_{lT} \mathbf{N}^T \mathbf{N}] d\Omega^e \qquad \textbf{4.2-20}$$

$$\mathbf{K}_{\mathrm{Tl}} = \sum_{e=1}^{m} \int_{\Omega^e} [K_{Tl} \nabla \mathbf{N}^T \nabla \mathbf{N}] d\Omega^e \qquad \textbf{4.2-21}$$

$$\mathbf{K}_{\mathrm{TT}} = \sum_{e=1}^{m} \int_{\Omega^e} [K_{TT} \nabla \mathbf{N}^T \nabla \mathbf{N}] d\Omega^e \qquad \textbf{4.2-22}$$

$$\mathbf{f}_{\mathrm{T}} = \sum_{e=1}^{m} \int_{\Omega^e} [C_{pl} \rho_l k_l \nabla \mathbf{N}^T \nabla z] d\Omega^e - \sum_{e=1}^{m} \int_{\Gamma^e} \mathbf{N}^T [\mathbf{F}_h] d\Gamma^e \qquad \textbf{4.2-23}$$

In the above, $\mathbf{F}_h$ is the approximate heat flux normal to the boundary surface.

4.2.2. Spatial Discretisation for Deformation Variables

The same method is used to spatially discretise the governing equation for deformation as was employed for the flow variables. Presented below is the development of the governing equation for deformation in an elasto-plastic saturated freezing soil.

The governing equation for deformation was derived in Chapter 3 as;

$$C_{uu}d\mathbf{u} + C_{uT}dT + C_{ul}du_l + \mathbf{d}b = 0 \qquad \textbf{4.2-24}$$

Using shape functions to approximate the primary unknowns and derivatives as adopted previously, the governing equation may be expressed with substitution from equations (4.2-1) and (4.2-2) as;

$$C_{uu}d\hat{\mathbf{u}} + C_{uT}d\hat{T} + C_{ul}d\hat{u}_l + \mathbf{d}b = R_\Omega \qquad \textbf{4.2-25}$$

Minimising the error over the elemental volume by using the Galerkin weighted residual approach gives;

$$\int_{\Omega^e} N_r \left[C_{uu}d\hat{\mathbf{u}} + C_{uT}d\hat{T} + C_{ul}d\hat{u}_l + \mathbf{d}b\right]d\Omega^e = 0 \qquad \textbf{4.2-26}$$

Integration by parts yields the weak form of Equation (4.2-26). The first term of the equation may be written as;

$$\int_{\Omega^e} N_r C_{uu}d\hat{\mathbf{u}}d\Omega^e = -\int_{\Omega^e} N_r \left[\mathbf{P}N_r\left[\mathbf{DepP}^T\right]d\hat{\mathbf{u}}\right]d\Omega^e + \int_{\Omega^e} P\left[N_r\mathbf{DepP}^T d\hat{\mathbf{u}}\right]d\Omega^e \qquad \textbf{4.2-27}$$

where, $\mathbf{P}N_r$ can be mathematically written as;

$$\mathbf{B} = \begin{bmatrix} \dfrac{\partial N_r}{\partial x} & 0 \\ 0 & \dfrac{\partial N_r}{\partial z} \\ \dfrac{\partial N_r}{\partial z} & \dfrac{\partial N_r}{\partial x} \\ 0 & 0 \end{bmatrix} \qquad \textbf{4.2-28}$$

Considering the second term of Equation (4.2-26), integration by parts yields;

$$\int_{\Omega^e} N_r C_{uT} d\hat{T} d\Omega^e = \int_{\Omega^e} N_r [\mathbf{PDep}(-A_T)] d\hat{T} d\Omega^e = - \int_{\Omega^e} [\mathbf{BDep}(-A_T) d\hat{T}] d\Omega^e + \int_{\Omega^e} \mathbf{P}[N_r \mathbf{Dep}(-A_T) d\hat{T}] d\Omega^e \qquad \textbf{4.2-29}$$

Considering the third term of Equation (4.2-26), integration by parts yields;

$$\int_{\Omega^e} N_r C_{ul} d\hat{u}_l d\Omega^e = \int_{\Omega^e} N_r [-\mathbf{mP}] d\hat{u}_l d\Omega^e = - \int_{\Omega^e} [\mathbf{B}(-\mathbf{m}) d\hat{u}_l] d\Omega^e + \int_{\Omega^e} \mathbf{P}[N_r (-\mathbf{m}) d\hat{u}_l] d\Omega^e \qquad \textbf{4.2-30}$$

Substituting equations (4.2-27) to (4.2-30), into equation (4.2-26) yields;

$$\begin{aligned} &- \int_{\Omega^e} [\mathbf{BDepP}^T d\hat{\mathbf{u}}] d\Omega^e + \int_{\Omega^e} P[N_r \mathbf{DepP}^T d\hat{\mathbf{u}}] d\Omega^e \\ &- \int_{\Omega^e} [\mathbf{BDep}(-A_T) d\hat{T}] d\Omega^e + \int_{\Omega^e} \mathbf{P}[N_r \mathbf{Dep}(-A_T) d\hat{T}] d\Omega^e \\ &- \int_{\Omega^e} [\mathbf{B}(-\mathbf{m}) d\hat{u}_l] d\Omega^e + \int_{\Omega^e} \mathbf{P}[N_r (-\mathbf{m}) d\hat{u}_l] d\Omega^e + \int_{\Omega^e} N_r d\mathbf{b} d\Omega^e = 0 \end{aligned} \qquad \textbf{4.2-31}$$

To produce surface integrals, the Gauss Green divergence theorem is applied to equation (4.2-31).

$$
\begin{aligned}
&-\int_{\Omega^e}\left[\mathbf{BDepP}^T d\hat{\mathbf{u}}\right]d\Omega^e + \int_{\Gamma^e}\left[N_r\mathbf{DepP}^T d\hat{\mathbf{u}}\right]\underline{n}d\Gamma^e \\
&-\int_{\Omega^e}\left[\mathbf{BDep}(-A_T)d\hat{T}\right]d\Omega^e + \int_{\Gamma^e}\left[N_r\mathbf{Dep}(-A_T)d\hat{T}\right]\underline{n}d\Gamma^e \\
&-\int_{\Omega^e}\left[\mathbf{B}(-\mathbf{m})d\hat{u}_l\right]d\Omega^e + \int_{\Gamma^e}\left[N_r(-\mathbf{m})d\hat{u}_l\right]\underline{n}d\Gamma^e + \int_{\Omega^e}N_r d\mathbf{b}d\Omega^e = 0
\end{aligned}
\qquad \textbf{4.2-32}
$$

Simplifying the surface integrals in equation (4.2-32);

$$
\begin{aligned}
&\int_{\Gamma^e}\left[N_r\mathbf{DepP}^T d\hat{\mathbf{u}}\right]\underline{n}d\Gamma^e + \int_{\Gamma^e}\left[N_r\mathbf{Dep}(-A_T)d\hat{T}\right]\underline{n}d\Gamma^e + \int_{\Gamma^e}\left[N_r(-\mathbf{m})d\hat{u}_l\right]\underline{n}d\Gamma^e \\
&= \int_{\Gamma^e}N_r\left[\mathbf{DepP}^T d\hat{\mathbf{u}} + \mathbf{Dep}(-A_T)d\hat{T} - \mathbf{m}d\hat{u}_l\right]\underline{n}d\Gamma^e = \int_{\Gamma^e}N_r\underline{\hat{T}}_r d\Gamma^e
\end{aligned}
\qquad \textbf{4.2-33}
$$

where, $\underline{\hat{T}}_r$ is the approximate traction.

Using the derivatives of the shapes function from equation (4.2-2), equation (4.2-32) can be written as;

$$
\begin{aligned}
&-\int_{\Omega^e}\left[\mathbf{BDepB}^T\right]d\Omega^e d\mathbf{u}_s - \int_{\Omega^e}\left[\mathbf{BDep}(-A_T)\mathbf{N}\right]d\Omega^e d\mathbf{T}_s \\
&-\int_{\Omega^e}\left[\mathbf{B}(-\mathbf{m})\mathbf{N}\right]d\Omega^e d\mathbf{u}_{ls} + \int_{\Omega^e}\mathbf{N}^{\mathrm{T}}d\mathbf{b}d\Omega^e + \int_{\Gamma^e}\mathbf{N}^{\mathrm{T}}\underline{\hat{T}}_r d\Gamma^e = 0
\end{aligned}
\qquad \textbf{4.2-34}
$$

By replacing the increments of the primary variables with the time differential of the primary variables multiplied by the time increment the incremental form of the solution may be used in the transient analysis. Thus writing equation (4.2-34) in concise notation gives;

$$
\mathbf{C}_{uu}\frac{\partial\mathbf{u}_s}{\partial t} + \mathbf{C}_{uT}\frac{\partial\mathbf{T}_s}{\partial t} + \mathbf{C}_{ul}\frac{\partial\mathbf{u}_{ls}}{\partial t} = \mathbf{f}_u
\qquad \textbf{4.2-35}
$$

where;

$$
\mathbf{C}_{uu} = \sum_{e=1}^{m}\int_{\Omega^e}\left[\mathbf{BDepB}^T\right]dtd\Omega^e
\qquad \textbf{4.2-36}
$$

$$\mathbf{C}_{uT} = \sum_{e=1}^{m} \int_{\Omega^e} [\mathbf{BDep}(-A_T)\mathbf{N}] dt d\Omega^e \qquad \text{4.2-37}$$

$$\mathbf{C}_{ul} = \sum_{e=1}^{m} \int_{\Omega^e} [\mathbf{B}(\mathbf{m})\mathbf{N}] dt d\Omega^e \qquad \text{4.2-38}$$

$$\mathbf{f}_u = \int_{\Omega^e} \mathbf{N}^T d\mathbf{b} d\Omega^e + \int_{\Gamma^e} \mathbf{N}^T \hat{\underline{T}}_r d\Gamma^e \qquad \text{4.2-39}$$

4.3. Temporal Discretisation of the Coupled Flow and Deformation Formulation

The spatially discretised equations for moisture and heat flow in a deformable freezing soil can be given in matrix form as

$$\begin{bmatrix} \mathbf{K}_{ll} & \mathbf{K}_{lT} & - \\ \mathbf{K}_{Tl} & \mathbf{K}_{TT} & - \\ - & - & - \end{bmatrix} \begin{bmatrix} \mathbf{u}_{ls} \\ \mathbf{T}_s \\ \mathbf{u}_s \end{bmatrix} + \begin{bmatrix} \mathbf{C}_{ll} & \mathbf{C}_{lT} & \mathbf{C}_{lu} \\ - & \mathbf{C}_{TT} & \mathbf{C}_{Tu} \\ \mathbf{C}_{ul} & \mathbf{C}_{uT} & \mathbf{C}_{uu} \end{bmatrix} \begin{bmatrix} \dot{\mathbf{u}}_{ls} \\ \dot{\mathbf{T}}_s \\ \dot{\mathbf{u}}_s \end{bmatrix} + \begin{bmatrix} \mathbf{f}_l \\ \mathbf{f}_T \\ \mathbf{f}_u \end{bmatrix} = 0 \qquad \text{4.3-1}$$

The terms $\dot{\mathbf{u}}_{ls}, \dot{\mathbf{T}}_s, \dot{\mathbf{u}}_s$ in equation (4.3-1) are the time differentials of the primary variables, with simplification of this equation yields

$$\mathbf{A}\varphi + \mathbf{B}\frac{\partial \varphi}{\partial t} + \mathbf{C} = \{0\} \qquad \text{4.3-2}$$

where φ represents the variable vector.

A fully implicit mid-interval backward difference time-stepping scheme has been adopted to achieve temporal discretisation in this analysis. This has been found to produce good results for this class of problems (Cook, 1981; Thomas et al, 1998).

The algorithm can be expressed in general form as;

$$\mathbf{A}^{\phi_l}\left[\varpi\boldsymbol{\varphi}^{n+1}+(1-\varpi)\boldsymbol{\varphi}^{n}\right]+\mathbf{B}^{\phi_l}\left[\frac{\boldsymbol{\varphi}^{n+1}-\boldsymbol{\varphi}^{n}}{\Delta t}\right]+\mathbf{C}^{\phi_l}=\{0\} \qquad \textbf{4.3-3}$$

where ϖ is the integration constant (ϖ=1, 0.5, 0 represents implicit, Crank-Nicholson or explicit time integration schemes respectively) and the superscript $^{\phi_l}$ is the level at which the matrices **A**, **B**, and **C** are evaluated, expressed as;

$$\phi_l=\vartheta(n+1)+(1-\vartheta)(n) \qquad \textbf{4.3-4}$$

The constant ϑ determines the level of evaluation. Utilising a fully implicit mid-interval backward difference time-stepping scheme the constants ϖ and ϑ take the values of 1 and 0.5 respectively.

With the introduction of these values, equation (4.3-3) yields;

$$\mathbf{A}^{n+1/2}\boldsymbol{\varphi}^{n+1}+\mathbf{B}^{n+1/2}\left[\frac{\boldsymbol{\varphi}^{n+1}-\boldsymbol{\varphi}^{n}}{\Delta t}\right]+\mathbf{C}^{n+1/2}=\{0\} \qquad \textbf{4.3-5}$$

If the matrices A, B and C can be evaluated at the time interval $^{n+1/2}$, then a solution to the vector $\boldsymbol{\varphi}^{n+1}$ can be produced. A predictor-corrector algorithm is utilised to achieve this.

The following steps are employed in this method:

1. At time^{n}, the matrices **A**, **B** and **C** are evaluated producing a first estimate called the predictor.

2. Using the predictor and the previous time step values, the matrices A, B and C are then evaluated at time$^{n+1/2}$ producing an estimate called the corrector.

3. A further check for elasto-plastic yielding is then required. If the developed strain rate is greater than the specified tolerance then plastic straining will occur and hardening parameters developed.

4. A check for convergence is conducted using either of the following checks;

$$\left|\boldsymbol{\varphi}_{iC}^{n+1} - \boldsymbol{\varphi}_{(i-1)C}^{n+1}\right| < TL_{abs} \qquad \textbf{4.3-6}$$

$$\left|\frac{\boldsymbol{\varphi}_{iC}^{n+1} - \boldsymbol{\varphi}_{(i-1)C}^{n+1}}{\boldsymbol{\varphi}_{(i-1)C}^{n+1}}\right| < TL_{rel} \qquad \textbf{4.3-7}$$

where I is the iteration level, c represents the fact that it is a corrector value and $\mathbf{TL_{abs}}$ and $\mathbf{TL_{rel}}$ are the absolute and relative error tolerance matrices for each variable. The residual force is checked using stress equilibrium against a tolerance value. After Owen and Hinton (1980), the residual force, ξ, can be calculated as:

$$\int_{\Omega} \mathbf{B}^{\mathbf{T}} \Delta\sigma d\Omega - \Delta F = \xi \qquad \textbf{4.3-8}$$

where ΔF is the increment of applied force. The algorithm returns to step 2 if the variables do not converge, or the residual is too large. The corrector then becomes the predictor and the iteration is repeated.

5. Upon convergence being reached the algorithm advances to the next time step and starts from step 1.

The size of the time step dictates the number of corrector iterations required to reach convergence. Utilising a variable time stepping scheme an efficient solution algorithm can be achieved. If convergence has not been reached in a maximum number of iterations the scheme will reduce the time step by a preset factor and re-evaluate the matrices with the new time step. If convergence is reached quickly, i.e. the minimum number of iterations is not reached then the time step size is increased for the next time step. This procedure leads to an efficient solution algorithm.

4.4. Consideration of the Frozen Fringe

The nature of the problem considered results in very steep gradients of variables within the small spatial area occupied by the frozen fringe due to both the latent heat effects and the development of cryogenic related pore water pressure changes. This

results in a problem that is numerically challenging to address. A number of options can be considered;

1) Use of a very fine mesh

2) Adaptive meshing techniques

3) Coincident node technique (Lewis et al. 1988)

4) Pre-determination of the thermal field (pre-run)

5) Use of a small time step

The coincident node technique can be used to simulate very small transitional zones such as extremely thin insulators or barriers. When a finite element mesh is used to simulate these rapid changes in the domain then ill conditioning of the matrices occur due to the very narrow elements necessary (Lewis et al, 1988). The technique assigns spatially coincident nodes on common interfaces such that they are assigned exclusively to each element. The element topography has to be expanded to account for these coincident nodes and it has been shown that the coincident node technique is an effective method to solve the coupled heat and mass transfer problem when a relatively thin material appears on the spatial domain (Lewis et al. 1988).

The use of a very fine mesh, small time step or adaptive meshing utilises a considerable amount of computational power, time or significant amount of additional coding requirements respectively. The coincident node technique first found use in simulating a thin vapour barrier to prevent the penetration of water in an insulating container and later in mold metal casting processes. Both of these involve a stationary boundary and only limited literature has been published involving the moving boundary problem of heat and mass transfer in freezing and thawing soils and the coincident node technique.

The possibility of predetermination of an estimate of the most significant variable in the system to improve the predictor-corrector scheme has been considered in this study. In particular a pre-run was introduced into the model with the objective of enabling the determination of an initial approximation to the thermal field across the domain. With a good approximation to the thermal field known it is possible to

predict to a significantly improved accuracy the latent heat effects that occur during any given time step. The pre-run is only used where phase change is occurring within the domain.

Finally it should be noted that in spite of any pre-run that each time step is calculated in full and complete convergence is achieved. In essence the pre-run allows a significantly improved initial estimate in the predictor-corrector scheme.

4.5. Conclusions

This chapter has presented an approximate solution to the coupled flow and deformation formulation developed in Chapter 3. Spatial discretisation of the governing differential equations for moisture, heat and deformation has been accomplished through the use of the Galerkin weighted residual finite element method. Temporal discretisation has been achieved by employing a backwards difference mid-interval time stepping algorithm. A pre run has been incorporated to improve the initial estimate in the predictor-corrector scheme.

COMPASS (Code for Modelling PArtially Saturated Soils), an existing computer code developed at the Geoenvironmental Research Centre, Cardiff University (Thomas et al. 1998), has been used to incorporate the latest developments of the proposed model.

4.6. References

Cook, R.D., 1981 "Concepts and applications of finite element analysis", Wiley, New York.

Lewis, R. W., Sze, W. K., Huang, H. C., 1988 "Some novel techniques for the finite element analysis of heat and mass transfer problems", *International Journal for Numerical Methods in Engineering,* **25**, 611-624.

Owen, D.R.J., and Hinton, E., 1980 "Finite elements in plasticity: Theory and practice", Pineridge Press Ltd., Swansea.

Thomas, H.R., and He, Y., 1995 "Analysis of coupled heat, moisture and air transfer in a deformable unsaturated soil", *Geotechnique*, **45**, (4), 677-689.

Thomas, H.R., He, Y., and Onofrei, C., 1998 "An examination of the validation of a model of the hydro/thermo/mechanical behaviour of engineered clay barriers", *International Journal of Numerical and Analytical Methods in Geomechanics*, **22**, 49-71.

Zienkiewicz, O.C., and Taylor, R.L., 1989 "The finite element method", McGraw Hill, 4th edition.

Chapter 5

Verification

5.1. Introduction

This chapter details the verification of the numerical model developed in Chapter 3 and 4. The exercises focus on the cryogenic processes that have been incorporated into an existing numerical model, COMPASS. By applying the model to controlled problems allows particular aspects of the model to be explored in a piecewise manner. The integrity of the model is verified in a step by step approach against subsets of the full model.

It should be noted that whilst the COMPASS code has been extensively verified and validated by previous authors (Mitchell 2002), those exercises have focused on unsaturated soil behaviour. In this study significant additions have been made to the code to incorporate the cryogenic processes that occur during freezing and thawing of porous media.

The four verification exercises are detailed in sections 5.2 to 5.5 where the numerical results have been compared against analytical solutions.

Section 5.2 examines the coupled thermo-hydraulic response of a thawing soil system. The numerical results are compared with two analytical solutions (Andersland and Ladanyi, 2003 and Nixon and McRoberts, 1973).

Deformation behaviour of the fully coupled thermo-hydro-mechanical model of a freezing soil in one and two dimensions is addressed in section 5.3. The numerical results are compared against an analytical solution.

Section 5.4 investigates the transient coupled liquid flow and deformation behaviour in a saturated one dimensional soil. The numerical results are compared against Terzaghi's one dimensional theory of consolidation.

The energy involved due to the latent heat of fusion released during the freezing of a saturated soil is considered in section 5.5. Analytical values are compared against the numerical results obtained.

Finally conclusions from the verification exercises are drawn in section 5.6. A summary of the verification exercises is given in Table 5.1-1.

Table 5.1-1 – Summary of verification exercises

Section	Aspect of model investigated.
5.2	One dimensional coupled thermo-hydraulic thawing response.
5.3	Phase change heaving strains; one and two dimensional functionality.
5.4	Transient coupled liquid flow and deformation.
5.5	Latent heat of fusion.

5.2. Coupled Thermo-Hydraulic Response of a Thawing Soil System

This exercise considers a completely frozen mass of soil subject to a step rise in the surface temperature. When a mass of frozen ground is subjected to a temperature increase on or near the ground surface, thawing will commence in a manner that is controlled by the temperature boundary conditions and the thermal properties of the soil. The solution to the heat conduction problem is attributed to Neumann and is given by Carslaw and Jaeger (1959). The moving boundary problem in frozen soil under a stepped surface temperature is a special case of the Neumann solution and often referred to as the Stefan solution (Carslaw and Jaeger, 1959).

5.2.1. Analytical Solution

Two analytical solutions were considered for this test, the original solution due to Stefan and a modified version by Nixon and McRoberts (1973). Both solutions assume the latent heat is released at a single temperature and ignores the volumetric heat effects of the frozen and unfrozen soil. The initial temperature of the sample is at the phase change temperature and therefore only the unfrozen soil properties are used.

The motion of the thaw interface is given as (Andersland and Ladanyi 2003)

$$X = \alpha\sqrt{t} \qquad \textbf{5.2-1}$$

where X (m) is the thaw depth, t (s) is the time and α (m/$\sqrt{s}$) is a constant.

Nixon and McRoberts (1973) noted that the relationship between depth (X) and the square root of time $\sqrt{t}$ is determined by seven variables (λ_u, λ_f, c_u, c_f, T_g, T_s, and L). As the temperature in the ground is close to the melting temperature ($T_g \approx 0°C$) it is reasonable to assume that the rate of thaw is not affected by the temperature distribution in the frozen zone and the complexity of the problem can be greatly reduced. Andersland and Ladanyi (2003) reported that the solution to the thaw problem can be approximated to a high degree of accuracy by

$$\alpha = 2\sqrt{\alpha_u}\left(\frac{Ste}{2}\right)^{\frac{1}{2}}\left(1-\frac{Ste}{8}\right) \qquad \textbf{5.2-2}$$

where α_u is the unfrozen soil thermal diffusivity, $Ste = c_u T_s (L)^{-1}$ is Stefan's number (the ratio of sensible heat to latent heat), c_u unfrozen volumetric heat capacity, T_s the applied constant surface temperature and L the volumetric latent heat of the soil.

For soils, the total energy involved in the phase-change process will depend on the total water contained in a given soil volume and the fraction of this water that changes phase. For a given soil,

$$L = \rho_d L' \frac{w - w_u}{100} \qquad \textbf{5.2-3}$$

where L (kJ/m^3) is the soil volumetric latent heat of fusion, L' is the latent heat of pure water, ρ_d (kg/m^3) the dry soil density, w the total water content and w_u the unfrozen water content (percent dry mass)

For those soils (sands and gravels) with little or no unfrozen water, the w_u term will be very small. For many practical problems, the assumption that w_u is zero will give acceptable L values for estimation purposes (Andersland and Ladanyi, 2003).

Assuming a linear temperature distribution in the thawed zone and again recognising that $T_g \approx 0$°C in the frozen zone, Nixon and McRoberts (1973) obtained a solution (originally due to Stefan) that is often used for prediction of the thaw depth, of

$$X = \left(\frac{2\lambda_u T_s}{L}\right)^{\frac{1}{2}} \sqrt{t} \qquad \rightarrow \qquad \alpha = \left(\frac{2\lambda_u T_s}{L}\right)^{\frac{1}{2}} \qquad \textbf{5.2-4}$$

5.2.2. Application

A 2m high vertical column was arbitrarily chosen for this exercise. The column was discretised with 150, 8 noded isoparametric quadrilateral elements. A fine mesh concentration was chosen at the top of the column where the greatest change in temperature would take place. The top 0.25m of the column was divided into 100 uniform elements with the remaining 50 elements uniformly spaced over the lower 1.75m of the column (Figure 5.2-1). The column width was set at 2mm in order to keep the upper elements square in shape. A time step of 5000 seconds was chosen and this was allowed to vary according to the time stepping algorithm employed with a maximum time step of 5000s. These spatial and temporal discretisations were used after a thorough investigation was undertaken to ensure converged results were obtained.

Representative frost susceptible soil material properties were chosen (Table 5.2-1 and equation 5.2-5) with an initial pore water pressure of 0 kPa and an initial temperature

set to just below the segregation freezing temperature (T_s) for the particular simulation. The temperature of the base of the sample was held constant during the simulation at the initial sample temperature and the pore water pressure at the top of the column was held constant at the initial sample pressure.

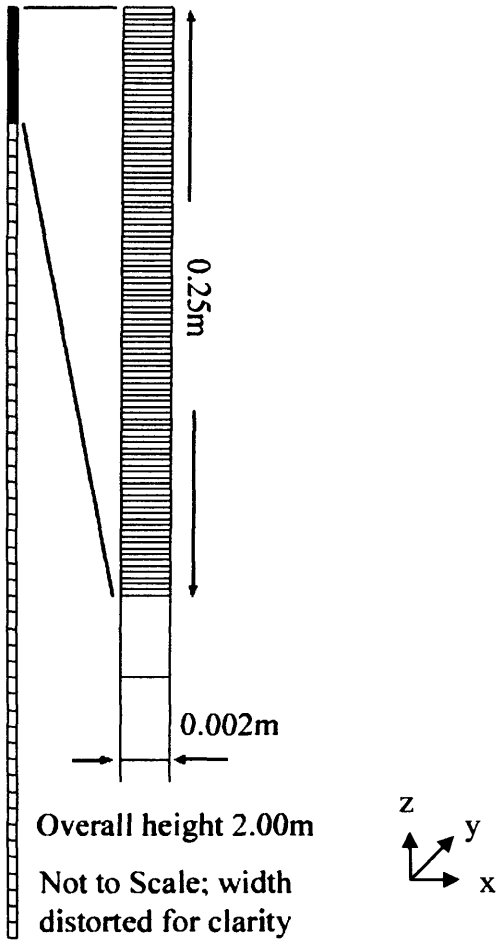

Figure 5.2-1 – Mesh used in simulation

Four segregation freezing temperatures (T_s) were chosen, 273.050K, 273.100K, 273.140K, and 273.145K to give a freezing range of 0.100K, 0.050K, 0.010K and 0.005K respectively. Three temperature steps (T_{Step}) were applied at the surface 0.5K, 2.0K, and 5.0K to give a total of 12 simulations. While the analytical solution is based on the phase change occurring at a single temperature and the segregation freezing temperature should be as close to 273.15K as possible, a range of temperatures were considered to explore the effect on the results when considering the secondary mode of heaving and latent heat being released over a temperature range. The temperature step was applied to the top of the column over two time steps at the beginning of the simulation.

Table 5.2-1 – Thermal Constants Used in Simulation

	Soil	Liquid	Ice
c (J/m^3°C)	1000	4180	2050
ρ (kg/m^3)	2000	1000	917
λ (W/m°C)	1.00	0.58	2.22

$n = 0.4, \quad k = 1\text{x}10^{-8}$ m/s $\quad k \rightarrow 0$ as $S_i \rightarrow 1$ **5.2-5**

5.2.3. Results and Conclusions

The results for the simulations are presented in Figure 5.2-2 to Figure 5.2-5. Only the analytical solution of equation 5.2-2 has been presented in the results as equation 5.2-2 and equation 5.2-4 yield almost identical results under the temperature steps that have been considered in the exercise. Trends in the results show that the accuracy of the simulations with respect to the analytical solution is subject to the segregation temperature range and the temperature step applied to the surface. These two variables and their effect on the results will now be explored.

The analytical solution assumes that the latent heat of fusion is liberated at the 273.15K isotherm (primary heave) and as a result is numerically difficult to model due to the very sharp changes that are present at the frost front. As the segregation freezing temperature tends to the freezing temperature of pure water the relative errors generally reduce. In the Stefan formula, both the heat capacity of the frozen layer and the heat flow from the underlying zone are neglected, these act to retard penetration of the frost or thawing plane and as a result the frost or thaw plane will be overestimated (Johnston 1981). The results from the simulations generally show that the thaw depth is over estimated by the model in the early stages of the analysis and towards the end of the analysis the trend of the simulated thaw rate will be under predicted at longer simulation times.

It has also been noted that at small temperature steps the relative error significantly increases where the ratio of temperature step to freezing range is similar. In the most pronounced example the temperature step applied is the same as the freezing range of the soil and therefore doesn't represent the conditions on which the analytical solution

was derived. As the temperature step increases the freezing temperature range becomes less significant and the results reflect this.

If the freezing range is accounted for, then the frost penetration will be increased while thaw penetration will be decreased (Johnston 1981). This is particularly clear in Figure 5.2-2 where the ratio of temperature step to freezing range is high and the thaw penetration is higher than the simulated value. When the freezing range is reduced as in Figure 5.2-3 and Figure 5.2-4 the simulated thaw penetration agrees much better with the analytical value. Development of the thermal profile can be seen in Figure 5.2-5.

The second variable of interest in this simulation is the temperature step applied to the surface. At small temperature steps the errors produced are believed to be attributed to the temperature range of the frozen fringe as the simulation is less representative of the analytical solution it is being compared against. At higher temperature steps the effects of errors caused by the frozen fringe become less dominant and the relative errors reduce significantly over those of smaller temperature steps. With the effects of the frozen fringe being negligible at higher temperature steps, it can be seen from Figure 5.2-2 to Figure 5.2-4 that the numerical model is capable of accurately dealing with rapid rates of latent heat changes due to high thermal gradients.

This verification exercise confirms that the proposed numerical model is capable of predicting the thaw rate of a soil system under a step temperature rise and varied frozen fringe temperature range. It should be noted that when small frozen fringe temperature ranges are used that a sufficiently refined mesh density is used to ensure spatial convergence. Both analytical solutions presented in equation 5.2-2 and equation 5.2-4 can be used to estimate the thaw depth; equation 5.2-4 is the simpler of the two to use.

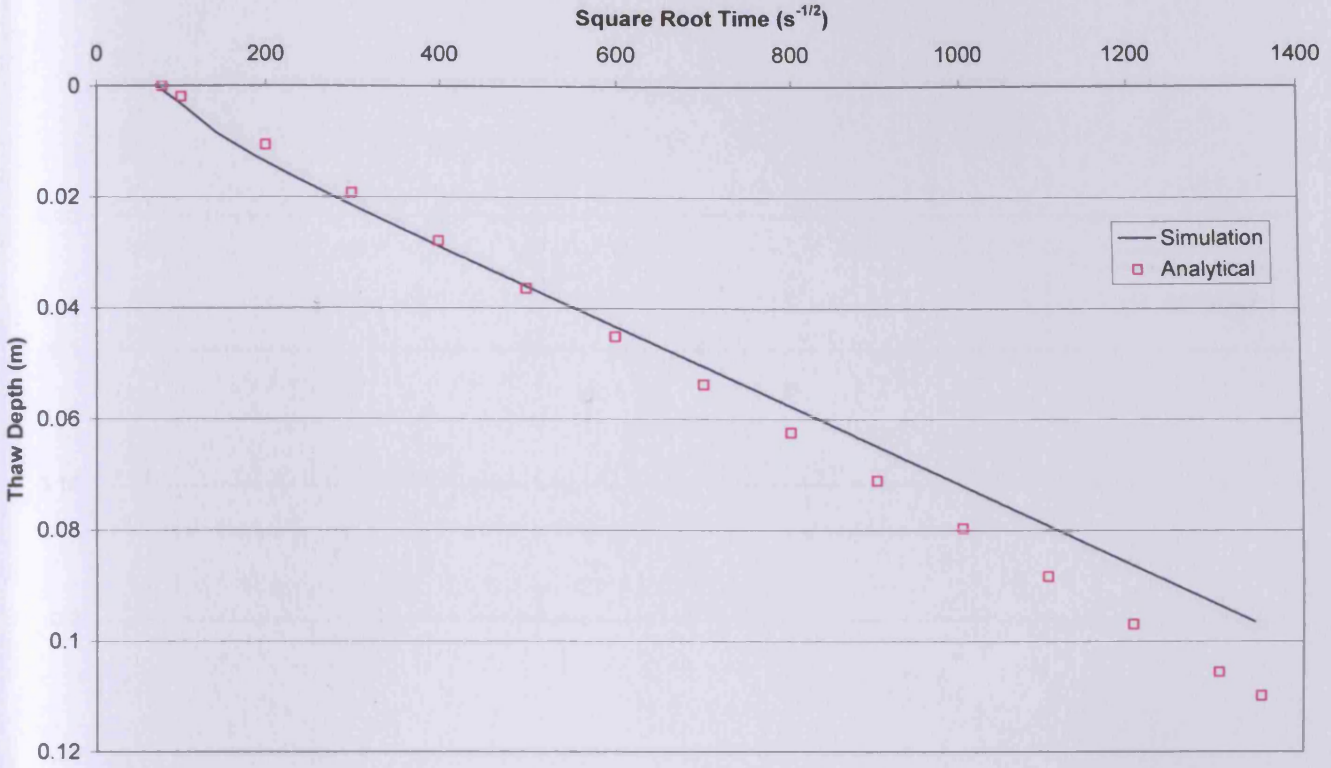

Figure 5.2-2 – Thaw depth vs. square root of time – T_s = 273.05K, T_{Step} = 0.5K

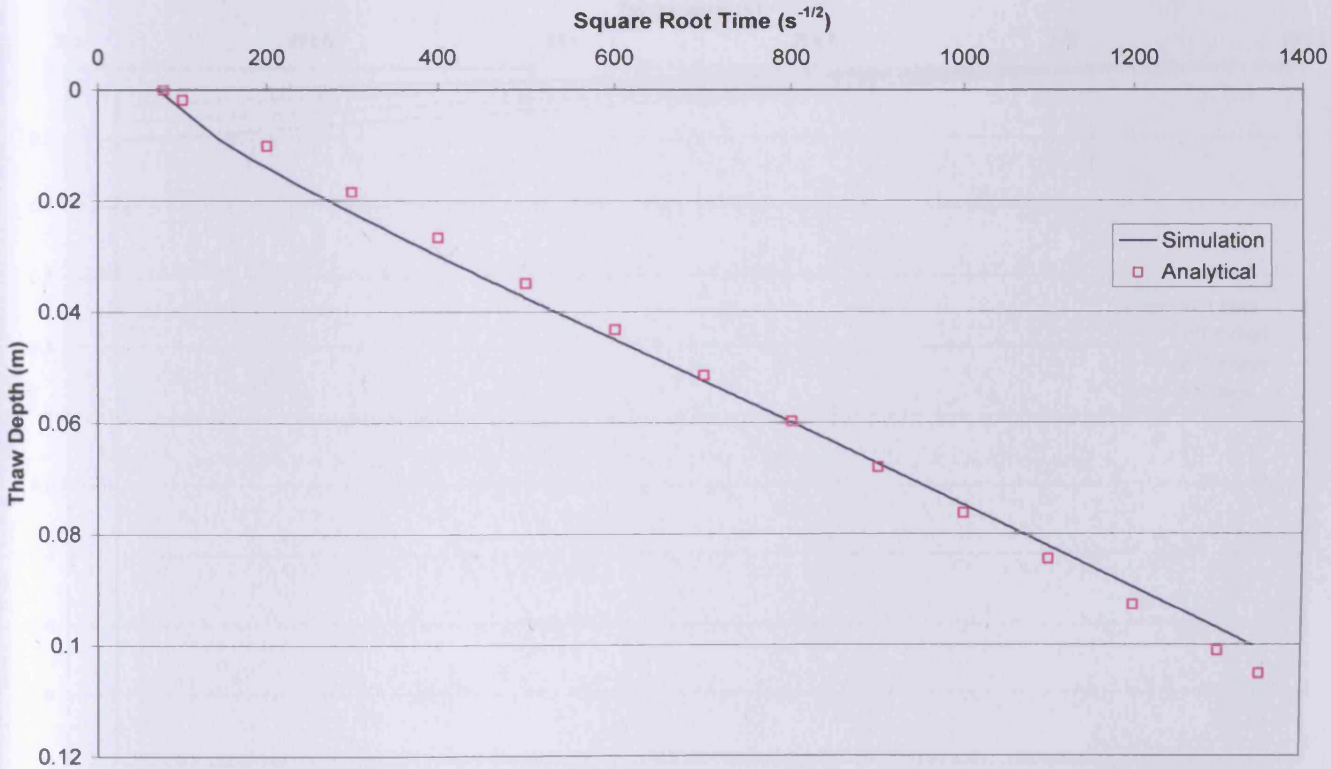

Figure 5.2-3 – Relative Thaw depth vs. square root of time – T_s = 273.10K, T_{Step} = 0.5K

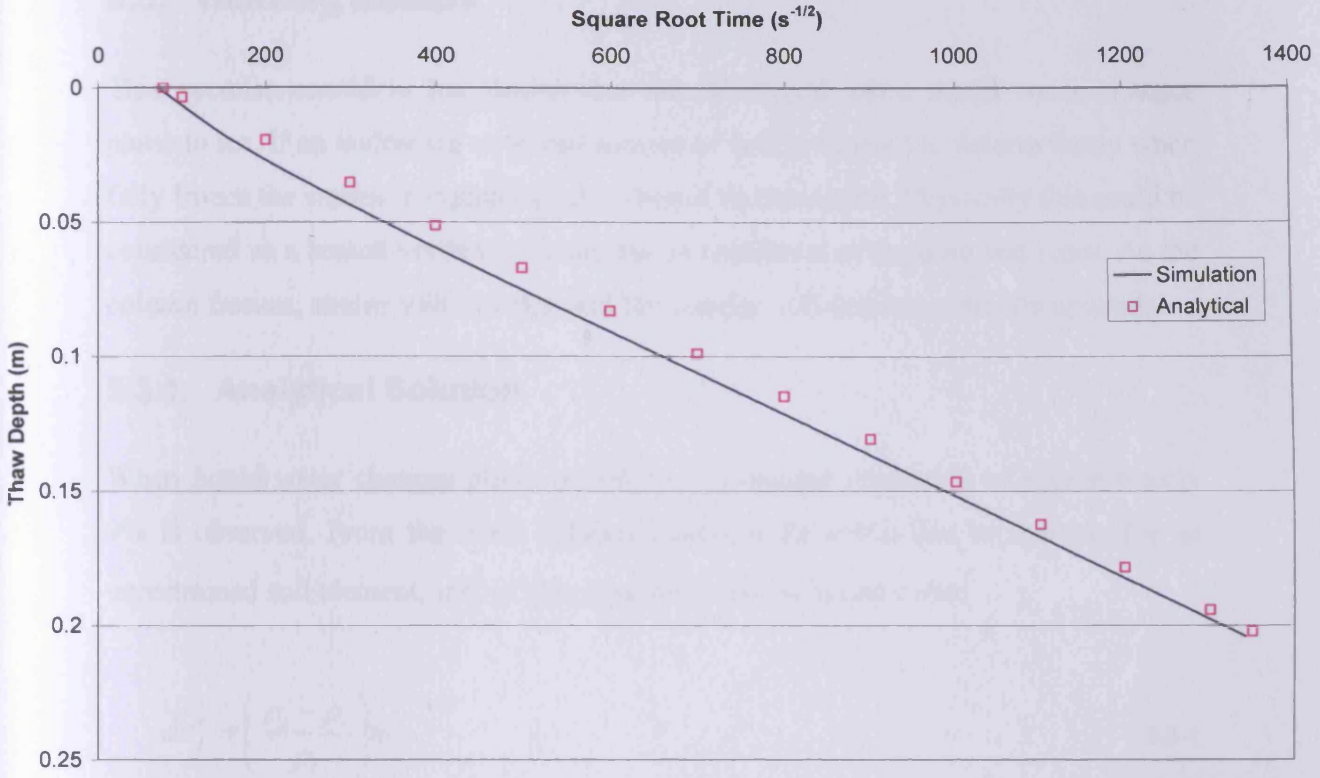

Figure 5.2-4 – Relative Thaw depth vs. square root of time – T_s = 273.10K, T_{Step} = 2.0K

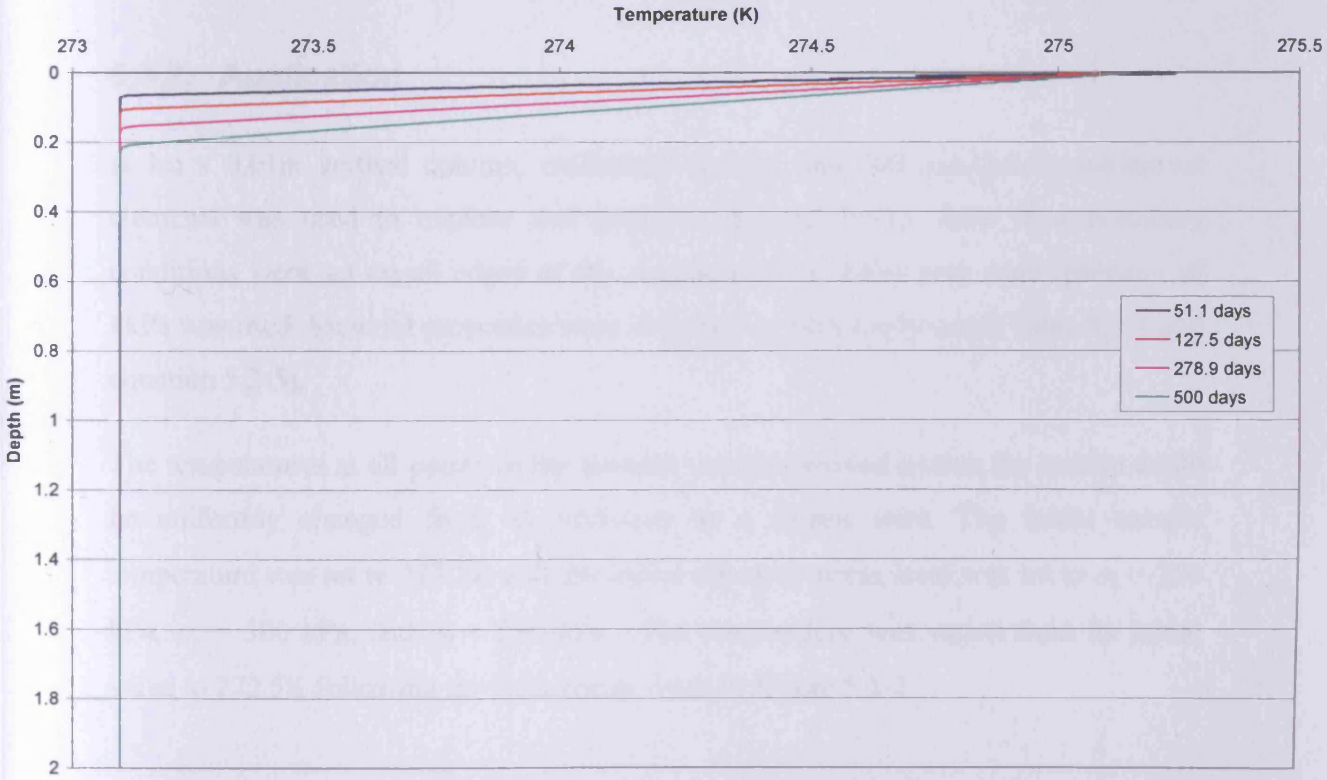

Figure 5.2-5 – Temperature profile across sample during thaw – T_s = 273.10K, T_{Step} = 2.0K

5.3. Heaving Strains

This exercise considers the strains that are developed when liquid water changes phase to ice. If an undrained unfrozen sample of soil is allowed to deform freely when fully frozen the strains in equation 5.3-1 should be developed. Physically this could be considered as a sealed vertical column that is restrained at the base and sides. As the column freezes, strains will develop and the sample will deform vertically upwards.

5.3.1. Analytical Solution

When liquid water changes phase to solid ice a volume expansion of approximately 9% is observed. From the mass balance equation the strain due to freezing for an unrestrained soil element, $d\varepsilon_f^e$ of given porosity can be found to be:

$$d\varepsilon_f^e = \left(\frac{\rho_l - \rho_i}{\rho_l} \right) n \qquad \textbf{5.3-1}$$

where ρ_l and ρ_i is the density of liquid water and ice respectively and n the porosity.

5.3.2. Application

A 1m x 0.01m vertical column, uniformly divided into 100 quadratic quadrilateral elements was used to explore this problem (Figure 5.3-1). Zero flow boundary conditions were set on all edges of the sample and an initial pore water pressure of 1kPa was used. Material properties were the same as previously used (Table 5.2-1 and equation 5.2-5).

The temperatures at all points in the domain were controlled so that the system could be uniformly changed from an unfrozen to a frozen state. The initial sample temperature was set to 273.5K and the initial effective stress level was set to σ_x = 250 kPa, σ_y = 500 kPa, and σ_z = 250 kPa. The temperature was varied from its initial value to 272.5K following the time curve given in Figure 5.3-2.

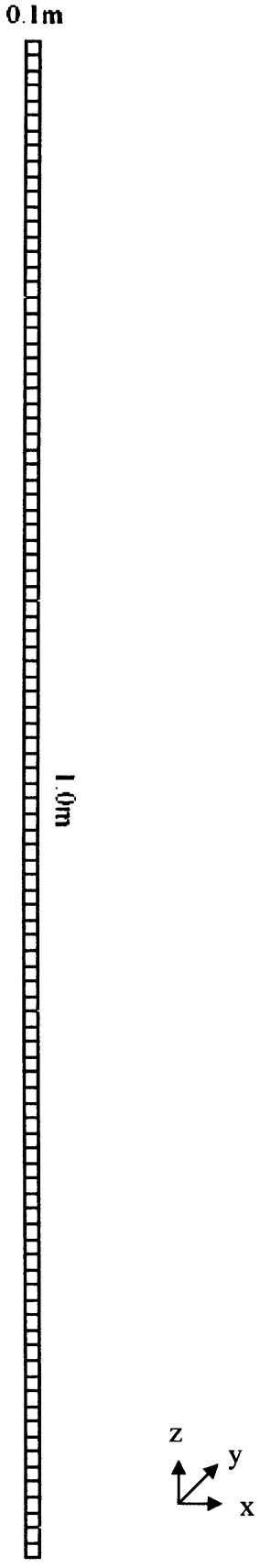

Figure 5.3-1 – Mesh Used in Simulation

The simulation was run for 3000s and a time step of 100s was used. For each test the spatial and temporal convergence was checked. A number of tests have been considered which vary how the problem is restrained and also considers the geometry. Eight noded isoparametric quadrilaterals were used in all tests; two tests used axisymmetric element geometry and the other two used plane strain element geometry. Horizontal and vertical restraints were applied as per the schedule in Table 5.3-1.

Test H1 considers a vertical column of soil which is allowed deform with vertical and horizontal displacements restrained at the base. H2 considers the same column with the addition of horizontal displacements restrained on the perimeter. Test H3 considers an arbitrary rectangular domain of soil of unit breadth with vertical and horizontal displacements restrained at the base and horizontal displacements restrained on one side. H4 considers the same rectangular domain with vertical and horizontal displacements restrained at the base and horizontal displacements restrained on both sides. In all cases a zero flux moisture flow boundary condition is applied on all sides of the sample to maintain undrained conditions.

Table 5.3-1 – Heaving strain test conditions

Test	Geometry	Displacement Restraint
H1	Axisymmetric	Base (h,v)
H2	Axisymmetric	Base (h,v) and Right (h)
H3	Plane Strain	Base (h,v) and Left (h)
H4	Plane Strain	Base (h,v), Left (h) and Right (h)

*** For axisymmetric problems the axis of rotation is the left hand side of the sample**
**** h – horizontal, v – vertical**

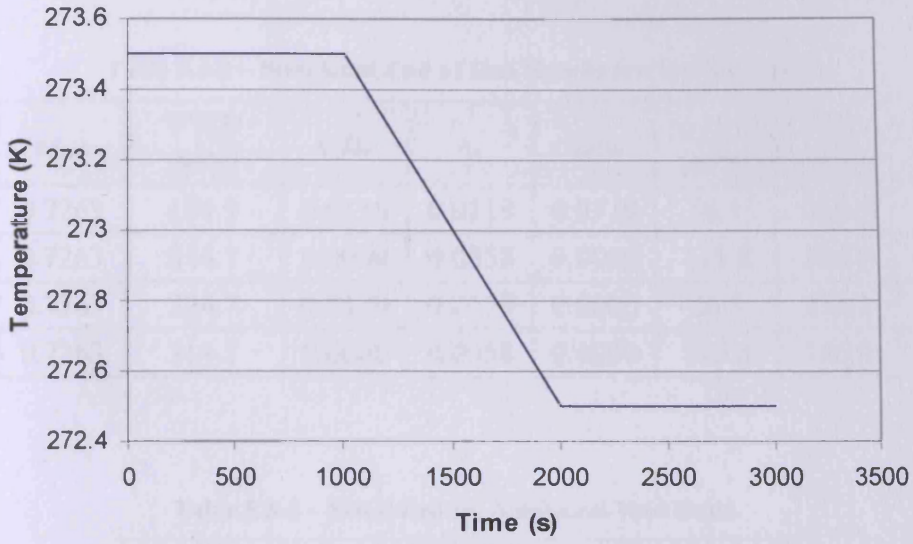

Figure 5.3-2 – Temperature time curve applied to nodes in heaving strain exercise

5.3.3. Results and Conclusions

Heave simulation results are presented in Table 5.3-2, Table 5.3-3, and Figure 5.3-3. The first point to note from the results is that where strain is permitted to develop it is isotropic. It is also clear that freezing of soil systems causes significant changes in the effective stress and pore water pressures.

Table 5.3-3 shows the simulated void ratio versus the analytically calculated value from 5.3-1 for tests H1 to H4. A very good agreement between the simulated and analytical values exists for all tests carried out giving confidence in the implementation.

The tests were designed to explore a variety of restraint conditions and the ability of the model to correctly use axisymmetric and plane strain element types. The results from these tests confirm that heaving due to freezing is correctly incorporated into the model and both element types function correctly.

Table 5.3-2 – Simulated End of Run Results for Test H1 – H4

Test	e_{final}	PWP (kPa)	$\varepsilon_x/\varepsilon_r$	ε_y	$\varepsilon_z/\varepsilon_\theta$	σ_x/σ_r (kPa)	σ_y (kPa)	σ_z/σ_θ (kPa)
H1	0.7263	194.9	0.0119	0.0119	0.0119	56.1	306.1	56.1
H2	0.7263	314.1	0.0000	0.0358	0.0000	115.8	186.9	115.8
H3	0.7263	224.7	0.0179	0.0179	0.0000	26.3	276.3	115.8
H4	0.7263	314.1	0.0000	0.0358	0.0000	115.8	186.9	115.8

Table 5.3-3 – Simulated vs. Analytical Void Ratio

Test	$e_{simulation}$	$e_{analytical}$	%err
H1	0.7263	0.7270	0.096%
H2	0.7263	0.7270	0.096%
H3	0.7263	0.7270	0.096%
H4	0.7263	0.7270	0.096%

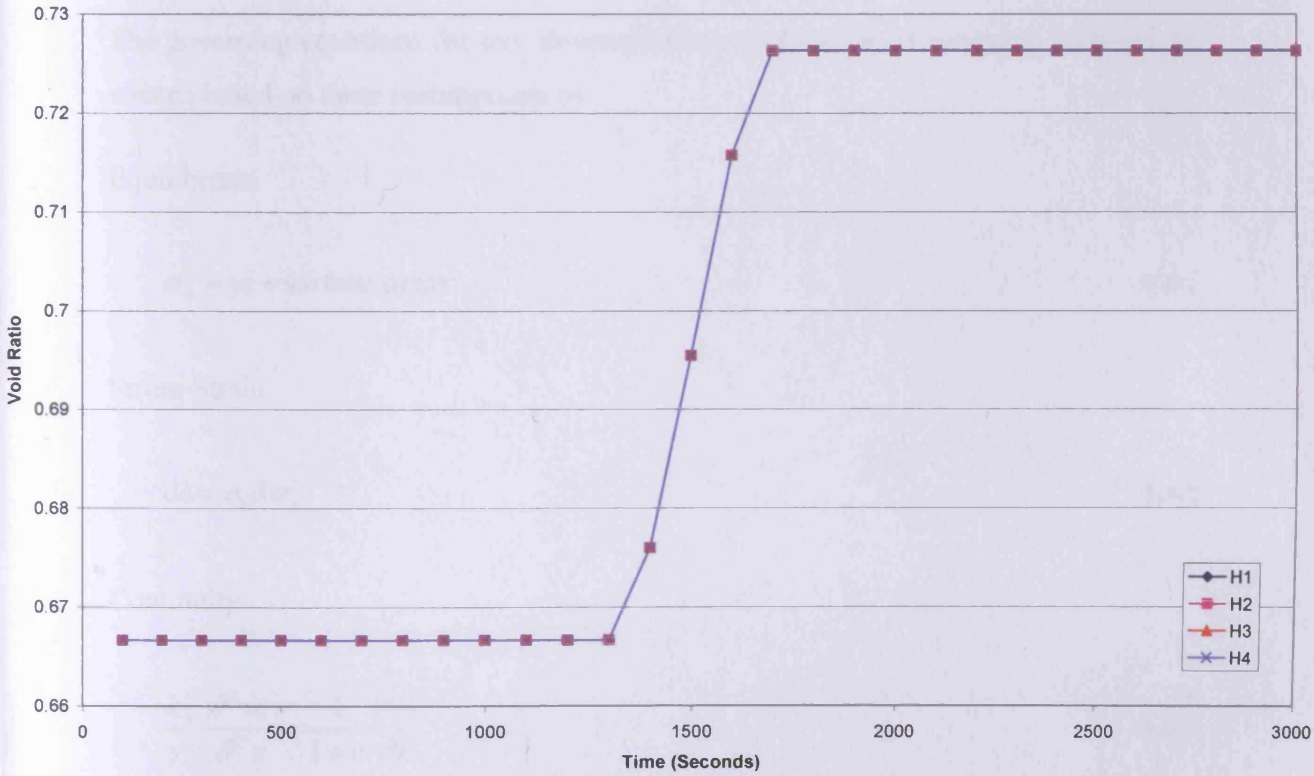

Figure 5.3-3 – Plot of Development of Void Ratio Due to Freezing

5.4. Transient Coupled Liquid Flow and Deformation Behaviour

Terzaghi's theory of one-dimensional consolidation in soil is used in this test to explore the transient coupled liquid flow and deformation behaviour of the proposed model. Terzaghi's theory produces an analytical solution that can be directly compared to the numerical results. This test is presented here as previously presented verification tests for the COMPASS model have not considered saturated consolidation.

The assumptions made in the Terzaghi theory of one dimensional consolidation are (Craig 1987): 1) the soil is homogeneous; 2) the soil is fully saturated; 3) the solid particles and water are incompressible; 4) compression and flow are one-dimensional (vertical); 5) strains are small; 6) Darcy's law is valid at all hydraulic gradients; 7) the coefficient of permeability and the coefficient of volume compressibility remain constant throughout the process and; 8) there is a unique relationship, independent of time, between void ratio and effective stress.

The governing equations for one dimensional consolidation in saturated soils can be written based on these assumptions as

Equilibrium

$$\sigma_z = \gamma z + \text{surface stress} \qquad \textbf{5.4-1}$$

Stress-Strain

$$\mathrm{d}e = a_v \mathrm{d}\sigma'_z \qquad \textbf{5.4-2}$$

Continuity

$$\frac{k_w}{\gamma_l}\frac{\partial^2 u_l}{\partial^2 z} = \frac{1}{1+e}\frac{\partial e}{\partial t} \qquad \textbf{5.4-3}$$

The effective stress is given by

$$\sigma_z' = \sigma_z - u_l \qquad \textbf{5.4-4}$$

where γ is the unit weight of soil, σ_z the effective vertical stress, and α_v is the coefficient of theoretical compressibility defined as the slope of the curve of the void ratio – pressure relationship.

Terzaghi's equation of consolidation is given by combining equations (5.4-1) to (5.4-4)

$$\frac{\partial u_l}{\partial t} = c_v \frac{\partial^2 u_l}{\partial z^2} \qquad \textbf{5.4-5}$$

The coefficient of consolidation, c_v, is defined by

$$c_v = \frac{k_w}{\gamma_l m_v} \qquad \textbf{5.4-6}$$

where

$$m_v = \frac{a_v}{1+e} \qquad \textbf{5.4-7}$$

m_v is the coefficient of volume change. The coefficient of volume change can be linked to Poisson's ratio and Young's modulus as during one dimensional K_0 consolidation the volumetric strain increment equals the vertical strain increment. m_v is thus defined as

$$m_v = \frac{(1+\nu)(1-2\nu)}{E(1-\nu)} \qquad \textbf{5.4-8}$$

The consolidation equation is normally used to solve for uniform initial excess pore water pressure resulting from an instantaneous application of load on the surface with drainage at either the surface or surface and base of the soil layer.

The problem considered is a soil layer of thickness H ($-H \leq z \leq 0$), with an impermeable base subject to an instantaneously applied uniform load on the surface ($z = 0$). At the time of application of the load the excess pore water pressure is equal to the applied consolidation stress throughout the layer. Drainage is only permitted through the upper surface. These boundary conditions can be expressed as

$$u_l(z,\ 0) = u_0 \qquad \textbf{5.4-9}$$

$$u_l(0,\ t) = 0 \qquad \textbf{5.4-10}$$

$$\frac{\partial u_l}{\partial z}(-H,\ t) = 0 \qquad \textbf{5.4-11}$$

The analytical solution to the problem described above is given as (Wang, 2000)

a) The excess pore water pressure in the consolidating soil layer:

$$u_l = \frac{4}{\pi} u_0 \sum_{n=0}^{\infty} \frac{1}{2n+1} e^{-(2n+1)^2 \pi^2 T_v/4} \sin\frac{(2n+1)\pi(-z)}{2H} \qquad \textbf{5.4-12}$$

where, T_v is a dimensionless number called the *time factor* and can be defined as

$$T_v = \frac{c_v}{H^2} t = \frac{k_w}{\gamma_l m_v} \frac{t}{H^2} \qquad \textbf{5.4-13}$$

b) The vertical displacement D in the soil layer:

$$D = -m_v u_0 H \left[\left(1 + \frac{z}{H}\right) - \frac{8}{\pi^2} \sum_{n=0}^{\infty} \frac{1}{(2n+1)^2} e^{-(2n+1)^2 \pi^2 T_v/4} \cos\frac{(2n+1)\pi(-z)}{2H} \right] \qquad \textbf{5.4-14}$$

5.4.1. Application

A 1m high, 20cm wide clay layer was considered to explore the transient coupled liquid flow and deformation behaviour of the model. The vertical column was

discretised into 50 equally sized 8 noded ispoarametric quadrilateral elements. The clay layer is considered to be a saturated, isotropic elastic medium with an impermeable base and laterally restrained in the horizontal direction on both edges. The base of the sample was restrained in the vertical direction. The effects of gravity were omitted from the analysis to allow easier interpretation of the results.

The initial pore water pressure was set at a value of 0 kPa and a uniform surface loading of -100 kN/m^2 was incrementally applied to the top of the sample over 10000s. The initial time step, t_0, was 1000s with a maximum time step, t_{max}, of 10000s. These spatial and temporal discretisations were used after a thorough investigation was undertaken to ensure converged results were obtained.

Arbitrary material properties were assumed for this simulation of

$$k_w = 1\times10^{-9}\, m/s,\ e_0 = 0.8,\ E = 1\times10^{6}\, Pa \text{ and } v = 0.3 \qquad \textbf{5.4-15}$$

Using the material properties in equation 5.4-15, the coefficient of volume change can be calculated from Equation 5.4-8 as

$$m_v = 7.42857\times10^{-7}\, Pa^{-1} \qquad \textbf{5.4-16}$$

5.4.2. Results and Conclusions

The variation of excess pore water pressure over various times is shown in

Figure 5.4-1. At the instant of application of load the pore water pressure rises to equal the load intensity of 100 kPa throughout the soil column. As the analysis progresses the sample is permitted to drain through the upper surface and the excess pore water pressure dissipates, consolidation occurs through the reduction in void ratio and the effective stress correspondingly rises as the pore water pressure drops. Dissipation of the excess pore water pressure in the lower part of the soil column takes longer due to the low permeability of the soil and the length of the drainage path. It can be seen that at the end of the analysis the pore water pressure throughout the soil column is tending to the initial value of 0 kPa as the excess pore water pressure fully dissipates. A good correlation between the simulated and analytical results was observed.

Figure 5.4-2 shows the vertical displacement of the surface and mid point of the soil column as the excess pore water pressure is dissipated. In the initial stages of the analysis a high pore water pressure gradient exists near the surface of the sample and the rate of consolidation is greater than at the mid point of the soil column. As the excess pore water dissipates over time the displacements approach their ultimate settlement value as the sample returns to its equilibrium state. Again a good correlation between the simulated and analytical results was observed.

These results verify that the proposed model correctly represents transient coupled liquid flow and deformation behaviour.

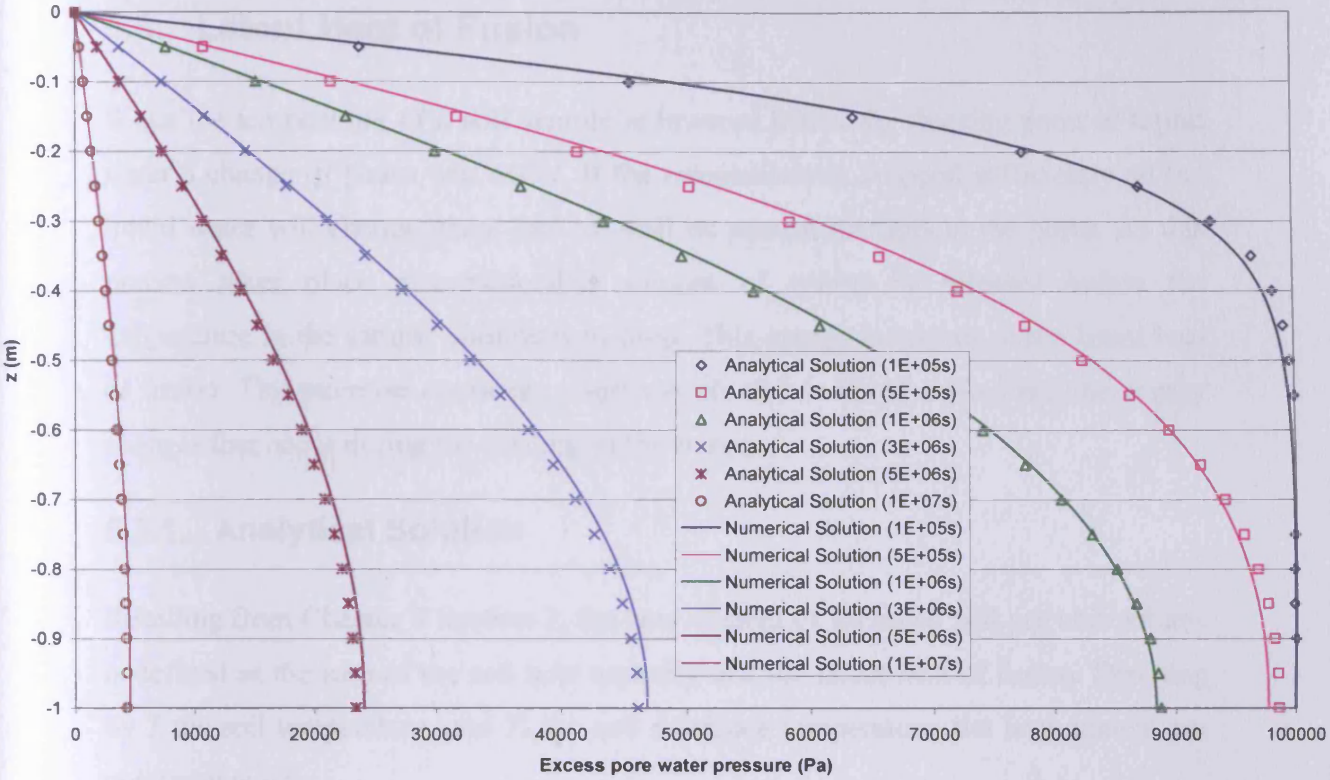

Figure 5.4-1 – Plot of dissipation of analytical and numerical pore water pressure against time.

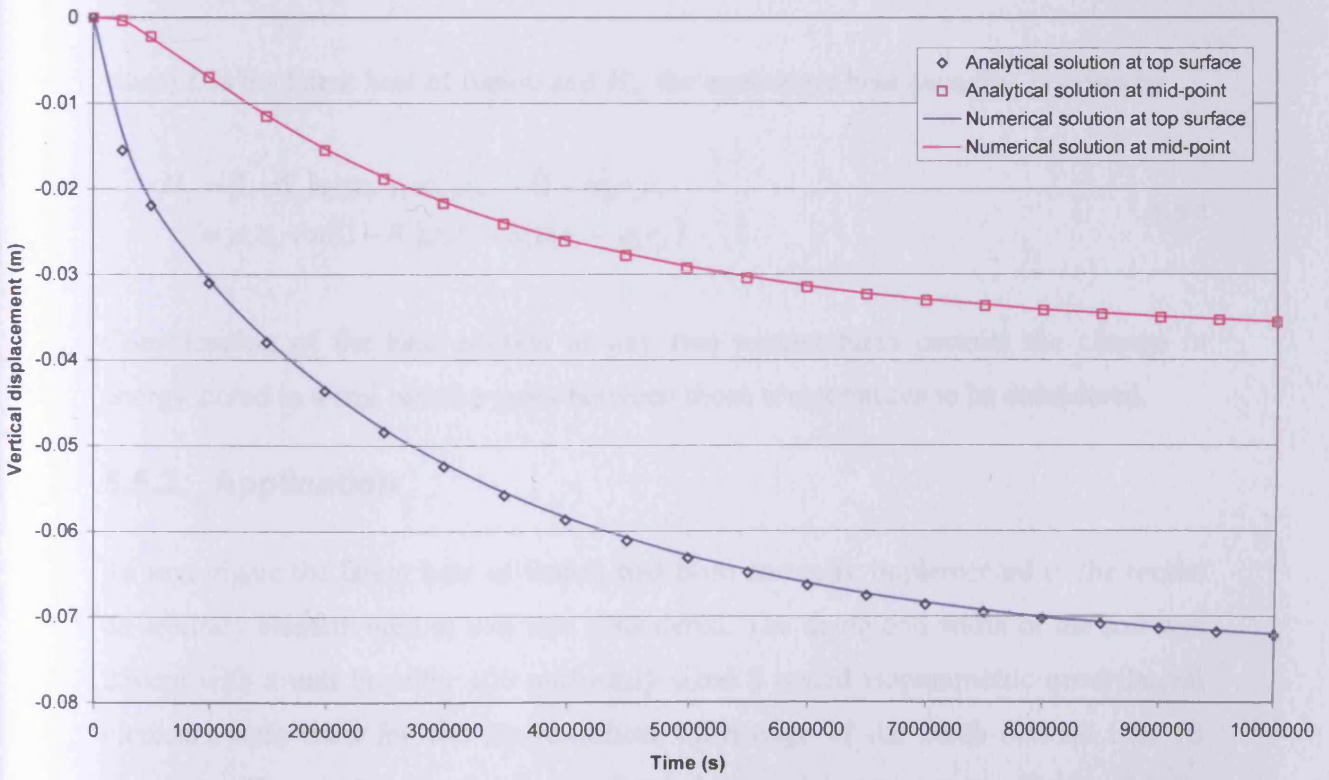

Figure 5.4-2 – Plot of analytical and numerical settlement of surface and mid layer over time.

5.5. Latent Heat of Fusion

When the temperature of a soil sample is lowered below the freezing point of liquid water a change of phase will occur. If the temperature is dropped sufficiently all the liquid water will change phase and ice will be present throughout the pores. As this process takes place a considerable amount of energy is released before the temperature in the sample continues to drop. This energy is known as the latent heat of fusion. This exercise considers a soil sample that is being cooled and the energy changes that occur during the cooling of the sample.

5.5.1. Analytical Solution

Recalling from Chapter 3 Section 3, the heat content of saturated soil per unit volume is defined as the sum of the soil heat capacity and the latent heat of fusion. Denoting by T the soil temperature, and T_r the soil reference temperature, the heat content per unit volume is:

$$\Omega = H_c(T - T_r) - LnS_i\rho_i \qquad \left(J/m^3\right) \qquad \textbf{5.5-1}$$

where L is the latent heat of fusion and H_c, the equivalent heat capacity, is given by

$$\begin{aligned} H_c &= (1-S_i)n\rho_l c_l + nS_i\rho_i c_i + (1-n)\rho_s c_s \\ &= \rho_s c_s + n((1-S_i)\rho_l c_l + S_i\rho_i c_i - \rho_s c_s) \end{aligned} \qquad \textbf{5.5-2}$$

Consideration of the heat content at any two temperatures permits the change in energy stored in a soil which moves between those temperatures to be considered.

5.5.2. Application

To investigate the latent heat of fusion had been correctly implemented in the model an arbitrary element area of soil was considered. The depth and width of the soil was 250cm with a unit breadth. 100 uniformly sized 8 noded isoparametric quadrilateral elements were used for the discretisation, each edge of the mesh divided into 10 elements (Figure 5.5-1). Arbitrary thermal material parameters (Table 5.5-1), segregation freezing temperature and hydraulic conductivity (5.5-3) were assumed for

the soil. A time step of 1000 seconds was chosen and this was allowed to vary according to the time stepping algorithm employed with a maximum time step of 1000s. These spatial and temporal discretisations were used after a thorough investigation was undertaken to ensure converged results were obtained.

A temperature flux was applied on faces AB and CD shown in Figure 5.5-1, to remove these predetermined quantities of energy from the system and then allow a comparison between the target and calculated temperatures. The initial temperature of the soil was set at 280K. Three final temperatures of 273.15K, 273.00K and 260.00K were chosen to represent the system just before freezing commences, just as the system becomes fully frozen and fully frozen respectively. The energy required to be removed to reach end temperatures based on equation 5.5-1 and 5.5-2 is shown in Table 5.5-2.

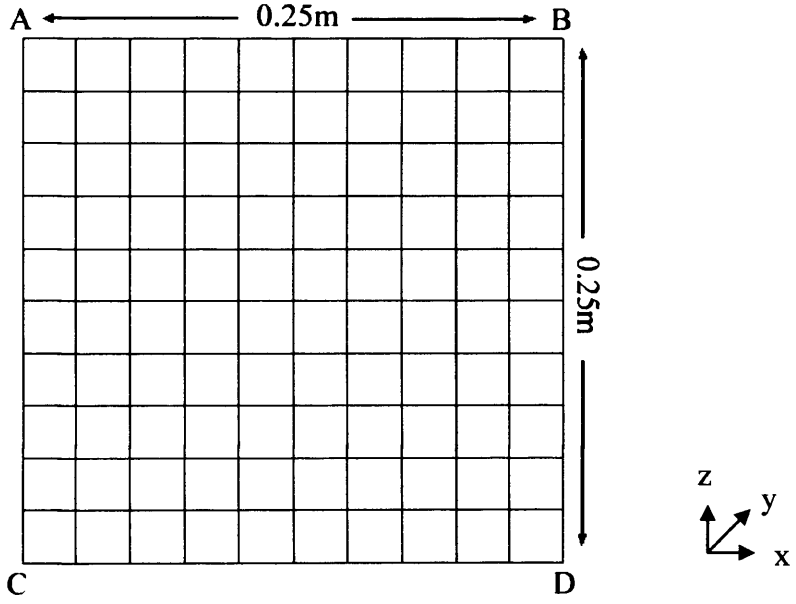

Figure 5.5-1 – Mesh used in Simulation

Table 5.5-1 – Thermal Constants Used in Calculation

	Soil	Liquid	Ice
c ($J/m^3°C$)	1000	4180	2050
ρ (kg/m^3)	2000	1000	917
λ ($W/m°C$)	1.00	0.58	2.22

$T_s = 273.0\text{K}; \qquad k = 1\text{x}10^{-8}\ \text{m/s} \quad k \rightarrow 0 \text{ as } S_i \rightarrow 1$ 5.5-3

Table 5.5-2 – Energy Requirements

Temperature Change	Energy Required
280.00K – 273.15K	-1229580J
280.00K – 273.00K	-7471540J
280.00K – 260.00K	-9061810J

5.5.3. Results and Conclusions

Table 5.5-3 shows the comparison between target and numerically calculated final temperatures of the three simulations. Figure 5.5-2 shows the time evolution of temperature at the centre of the sample as heat is extracted. In particular it is clear to see between 120 and 350 hours of the analysis the presence of a so called 'zero curtain' where the latent heat of fusion is being removed with little or no change in temperature of the system. It can be seen that a very good correlation exists between predicted and simulated temperatures indicating that the latent heat of fusion is correctly incorporated into the model.

Table 5.5-3 – Predicted vs. Simulated Finish Temperatures

Predicted Finish Temperature	Simulated Finish Temperature
273.150K	273.157K
273.000K	273.001K
260.000K	260.070K

The excellent correlation between predicted and simulated temperatures achieved in this exercise confirm the ability of the numerical model to account for the latent heat of fusion associated with freezing and thawing soil systems.

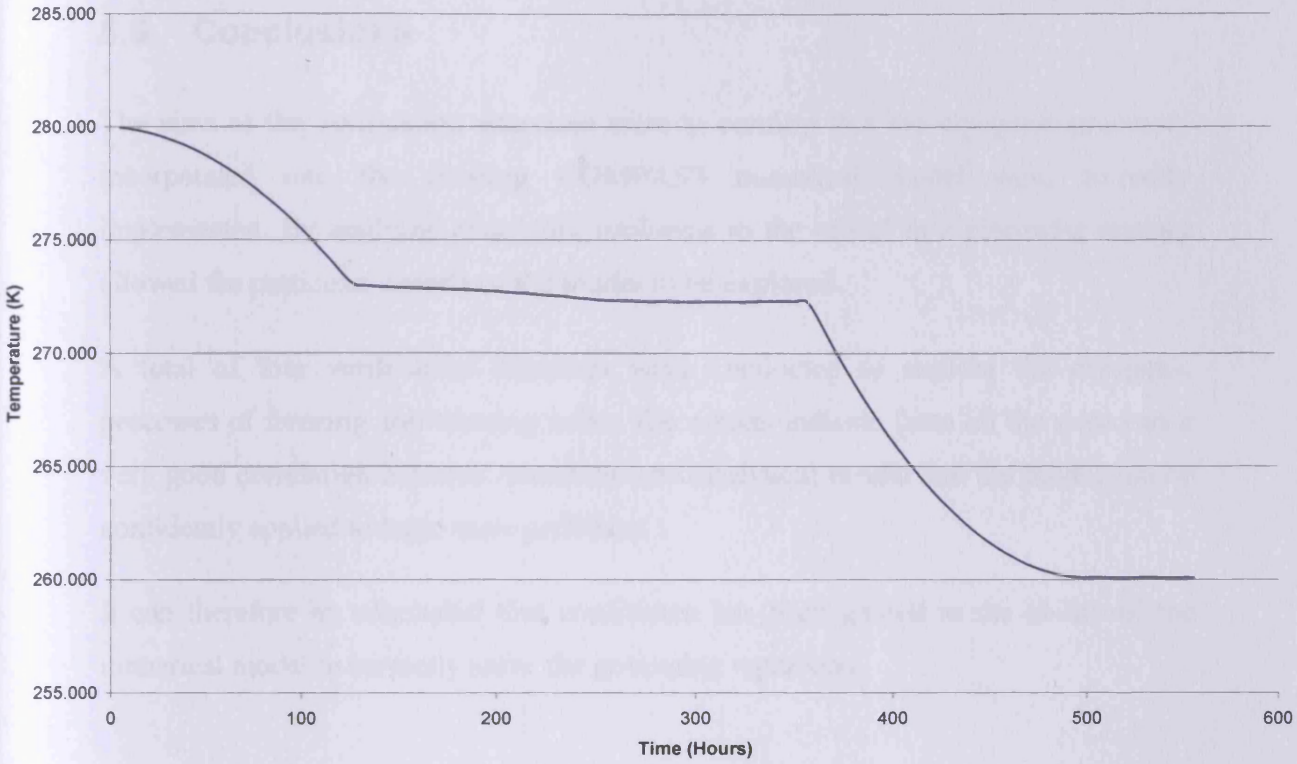

Figure 5.5-2 – System fully frozen.

5.6. Conclusions

The aims of the verification exercises were to confirm that the cryogenic processes incorporated into the existing COMPASS numerical model were correctly implemented. By applying controlled problems to the model in a piecewise manner allowed the particular aspects of the model to be explored.

A total of four verification exercises were conducted to explore the cryogenic processes of freezing and thawing soils. The results indicate from all the exercises a very good correlation between numerical and analytical results and the model can be confidently applied to large scale problems.

It can therefore be concluded that confidence has been gained in the ability of the numerical model to correctly solve the governing equations.

5.7. References

Andersland, O. B. and Ladanyi, B., 2003. *Frozen ground engineering*. 2nd Edition. New York; Chichester: Wiley. UK

Craig , R. F., 1987 "Soil Mechanics" 4th Edition. Van Nostrand Reinhold, UK

Johnston, G. H., 1981 "Permafrost – Engineering Design and Construction". John Wiley & Sons, Chichester. UK.

Mitchell, H. P., 2002 "*An investigation into the thermo / hydro / mechanical interactions involved in high level nuclear waste disposal*" Ph.D thesis. University of Wales, Cardiff. UK.

Nixon, F. M. and McRoberts, E. C., 1973. "A Study of Some Factors Affecting the Thawing of Frozen Soils". *Canadian Geotechnical Journal* **10**, 439-452.

Wang, J., 2000 "Transient and dynamic thermo/hydraulic/mechanical behaviour of partially saturated soil". PhD Thesis, University of Wales, Cardiff. UK.

Chapter 6

Validation and Sensitivity Analysis

6.1. Introduction

This chapter focuses on the impact of the cryogenic related processes included within the proposed theoretical formulation. In particular the development of ice lenses and the movement of moisture under cryogenic suction is investigated, firstly in an extension of the verification exercises presented in Section 5.3 of Chapter 5 and secondly in a validation exercise. The performance of the proposed model with respect to a number of variables is subsequently explored in order to determine their effect on the magnitude and growth of ice lenses in a freezing soil.

An analysis of a one dimensional, one sided, undrained freezing soil column is conducted in Section 6.2 to investigate the impact of cryogenic suction effects within the theoretical formulation. Section 6.3 validates the implementation of ice lensing within the model by numerically simulating the experimental growth of ice lenses in a one dimensional frost cell (Penner 1986).

The sensitivity of the model to a series of variables which largely control the formation, magnitude and growth of ice lenses in a freezing soil are investigated in Sections 6.4 to 6.9. The variables investigated are the thermal gradient, rate of cooling, hydraulic conductivity, segregation freezing temperature, and stress level. Each variable is explored separately to assess its effect on the development of the

thermal, hydraulic and mechanical fields of a freezing soil. The one dimensional frost heave experiment by Penner (1986) used in the validation exercise in Section 6.3 is used as the basis of this sensitivity investigation.

Finally in Section 6.10 conclusions of the validation and sensitivity analyses are drawn.

6.2. Moisture Movement in the Frozen Fringe and Ice Lensing

In Chapter 3 a modification to the moisture flow equation was introduced to account for the movement of moisture due to thermal gradients that occurs in the frozen fringe as a result of the coexistence of ice and water. These are repeated here;

$$\mathbf{v}_l = -k_l\left[\nabla\left(\frac{u_l}{\gamma_l}\right)+\frac{\rho_l L}{T_0}\nabla\left(\frac{T}{\gamma_l}\right)+\nabla z\right] \qquad \textbf{6.2-1}$$

$$\mathbf{v}_l = -k_l\left[\nabla\left(\frac{u_l}{\gamma_l}\right)+\nabla z\right] \qquad \textbf{6.2-2}$$

In this section two undrained, one sided freezing simulations; the first using the modified moisture flow equation which includes the movement of moisture in the frozen fringe due to cryogenic potentials (Equation 6.2-1) and the second using the more standard Darcy's Law (Equation 6.2-2) which excludes cryogenic potentials are presented to verify the application of this component of the numerical model. The verification component of this analysis is based on a mass balance check, a check on the quantity of strain developed and on an assessment of development of the various fields of behaviour considered.

6.2.1. Analytical Solution

When liquid water changes phase to solid ice a volume expansion of approximately 9% is observed. From the mass balance equation the strain due to freezing for an unrestrained soil element, $d\varepsilon_f^e$, of given porosity can be found to be:

$$d\varepsilon_f^e = \left(\frac{\rho_l - \rho_i}{\rho_i}\right) n \qquad \text{6.2-3}$$

where ρ_l and ρ_i is the density of liquid water and ice respectively and n the porosity.

6.2.2. Analysis

The problem considered is the behaviour of an unfrozen cylindrical 0.1m x 0.05m radius soil column which is then fully frozen. The numerical simulation undertaken used a mesh of 8 noded isoparametric axisymmetric quadratic elements divided vertically into 250 elements and horizontally into 1 element (Figure 6.2-1). A time step of 100 seconds was chosen and this was allowed to vary according to the time stepping algorithm employed with a maximum time step of 250 seconds. These spatial and temporal discretisations were used after a thorough investigation was undertaken to ensure converged results were obtained.

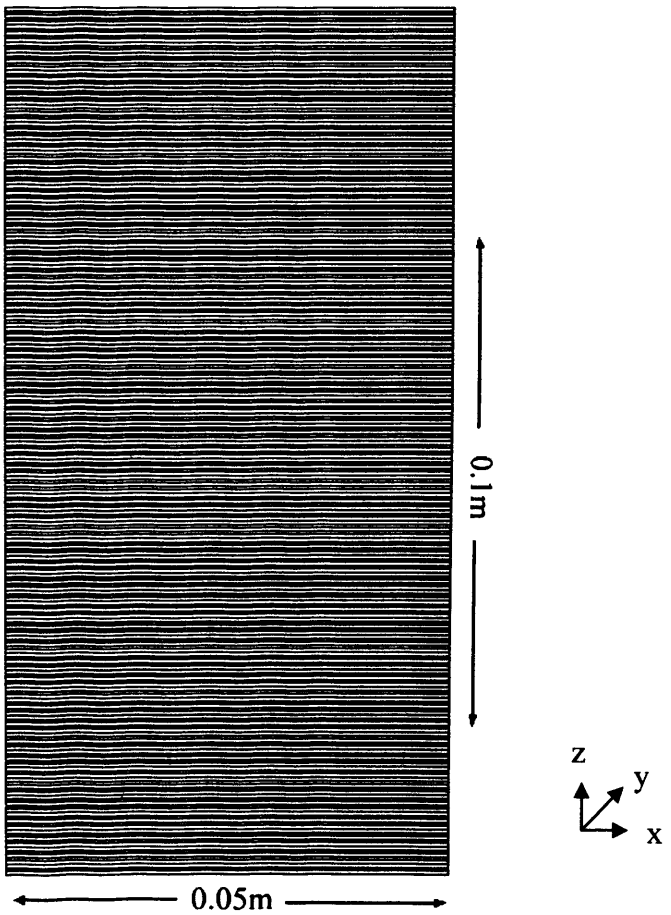

Figure 6.2-1 – Mesh used in Simulation

Material parameters for heat capacity, density and thermal conductivity used in the test are taken from Harlan and Nixon (1978) and are given in Table 6.2-1. Constant values were assumed for Poisson's ratio and initial porosity.

$$v = 0.3; \quad n = 0.35 \qquad \textbf{6.2-4}$$

Table 6.2-1 – Thermal Constants Used in Calculation

	Soil	Liquid	Ice
c (J/m^{3}K)	1257	4140	2105
ρ (kg/m^3)	1750	1000	917
λ (W/mK)	1.950	0.602	2.220

Assuming the in-situ earth pressure coefficient, K_0, is given by Equation 6.2-5 (Barnes 2000) gives $K_0 = 0.429$ and the initial stress levels were set to $\sigma_z = 50.00$ kPa, and $\sigma_r = 21.43$ kPa.

$$K_0 = \frac{v}{(1-v)} \qquad \textbf{6.2-5}$$

The elastic stiffness parameter of the soil, κ, is calculated based on data presented by Selvadurai et al (1999) for a silty frost susceptible soil, as

$$\kappa = 0.005127 \qquad \textbf{6.2-6}$$

The hardening parameter, p_0, is set a high value to ensure that the material remains in the elastic region of the stress space.

The following representative hydraulic conductivity of a frost susceptible soil based on the relationship proposed in Chapter 3 (Equation 3.3-13) is used.

$$k = \begin{cases} 3.07\times10^{-11} e^{13.44T} & -0.3°C < T < T_0 \\ 5.45\times10^{-13} & T \le 0.3°C \end{cases} m/\sec \qquad \textbf{6.2-7}$$

where T and T_0 are in degrees Celsius

The initial temperatures at the top and bottom of the sample were set at values of 274.2K and 273.2K respectively with an initial non-uniform linear temperature profile

through the sample as shown in Figure 6.2-2. The end temperatures were varied at a rate of -0.02 K/day for 10 days as shown in Figure 6.2-3.

Zero flow boundary conditions were set on all edges of the sample and an initial pore water pressure of 0kPa was used. Gravity effects were not included in the analysis. The sample was laterally restrained in the vertical direction at the base of the sample and in the radial direction on the right hand edge. This could be considered as a soil column in an oedometer type cell.

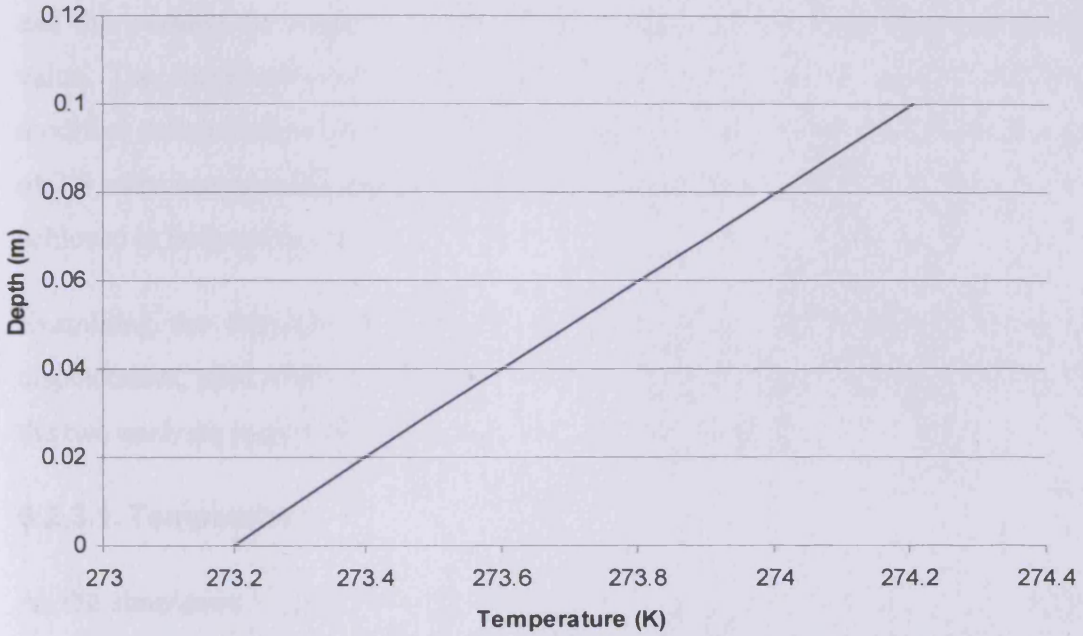

Figure 6.2-2 – Initial temperature profile through sample for mass balance test.

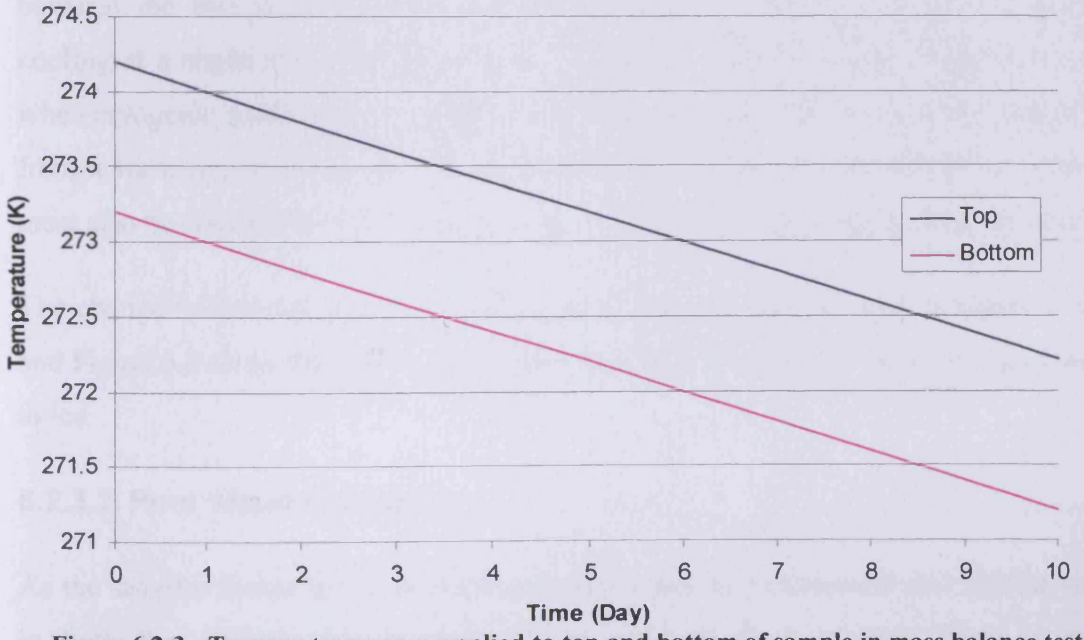

Figure 6.2-3 - Temperature curve applied to top and bottom of sample in mass balance test.

6.2.3. Results and Conclusions

The variation of displacement, pore water pressure, temperature, effective stress and void ratio with respect to time are shown in Figure 6.2-4a to Figure 6.2-8a respectively for the analysis considering the impact of cryogenic potentials in the frozen fringe and in Figure 6.2-4b to Figure 6.2-8b for the analysis considering moisture flow defined by Darcy's law.

Both simulations involve the entire domain changing phase from unfrozen to frozen and this permits the magnitude of freezing strains to be compared against a known value. The simulated results show a total heave of 3.14mm and 3.11mm for the modified moisture flow and Darcy's law respectively. Both are within a relative error of 2% when compared to the analytical solution and verify that mass balance has been achieved in both cases.

Examining the transient development of the results reveals different profiles for displacement, pore water pressure, effective stress and void ratio during freezing from the two analyses undertaken. These are now discussed below.

6.2.3.1. Temperature

As the simulation is driven by the thermal field, significant variations in the thermal results between the two analyses would not be expected. A slight variation was noted between the two tests with the simulation using the modified moisture equation cooling at a slightly slower rate (Figure 6.2-4a and Figure 6.2-4b). This is because, when cryogenic suctions are considered, water is drawn to the frozen fringe and flows from a warmer part of the sample and due to convection this additional heat energy must also be cooled which accounts for the retardation of the thermal field observed.

The change in thermal gradient through the fringe can also be seen in Figure 6.2-4a and Figure 6.2-4b as the thermal conductivity changes due to the ratio of liquid water to ice.

6.2.3.2. Pore Water Pressure

As the samples freeze the pore water pressure tends to a maximum and similar value in both the analyses irrespective of the moisture flow regime. What is most

pronounced is that when cryogenic potentials are considered a significant depression of the pore water pressure occurs which coincides with the 273.15K isotherm. This is illustrated in Figure 6.2-5a. The process of ice lensing has been described as a cryogenic suction and although the samples remain fully saturated flow occurs from regions of higher potentials to regions of lower potentials. Both samples are undrained and therefore the total mass of liquid is constant but local redistribution of water can occur.

The pore water pressure profile given by Darcy's law (Figure 6.2-5b) shows that an upwards flow of moisture will occur during freezing and a corresponding increase in void ratio should be observed towards the top of the sample. The pore water pressure profile for when cryogenic potentials are considered (Figure 6.2-5a) indicates that there will be a downward flow of water and an increase in void ratio at the freezing zone. The displacement profile (Figure 6.2-6a) shows an accumulation occurring at the freezing zone corroborating this prediction of water redistribution towards the freezing zone due to the coexistence of liquid water and ice.

6.2.3.3. Displacement

Excluding the initial and final stages the simulations heave at constant rates. The ice lensing formulation (Figure 6.2-6a) shows a much greater rate of heave and it can be seen that the sample is experiencing a greater displacement in the central region. When a soil is freezing it will create a potential which will attempt to draw water towards the partially frozen zone. As the hydraulic conductivity drops this water will then accumulate and freeze. Comparing the displacements to that predicted by Darcy's law (Figure 6.2-6b) shows no accumulation taking place in this region.

A greater rate of heave occurs at the beginning of the test which coincides with the establishment of the frozen fringe. The rate slows once the frozen fringe has fully formed and the base of the sample becomes completely frozen. In this early stage, where the fringe is being established, in the region of soil at the base of the sample, cryogenic suctions are being developed but the hydraulic conductivity remains relatively high as the applied temperature is keeping the soil in a partially frozen state. This results in a large accumulation of moisture in this region. The rate is also affected at the end of the simulation due to the constraints on the available free water.

6.2.3.4. Effective Stress

The increase in pore water pressure due to phase change of liquid water to ice results in a drop in the effective stress. In the theoretical formulation a non-linear elastic model has been implemented and as the effective stress drops the stiffness of the soil reduces. As the effective stress tends to zero the soil becomes very soft as Young's modulus also tends to zero and so very small changes in pore water pressure can result in large changes in displacement.

Both simulations reflect the changes in pore water pressure observed (Figure 6.2-5a and Figure 6.2-5b) and as the systems fully freeze a condition of zero effective stress results throughout the soil. In Figure 6.2-5b (Darcy's law) the stiffness of the soil drops throughout the sample due to a decrease in the effective stress across the entire sample as the soil freezes. Even the unfrozen zone becomes softer as the lower zone freezes and causes a change in the pore water pressure in the upper zone.

Figure 6.2-7a (moisture flow due to cryogenic suction) shows the reverse of that observed using Darcy's law. As freezing progresses the effective stress in the unfrozen zone increases and the soil becomes stiffer until the frozen fringe passes through. A depression in the pore water pressure profile can be seen (Figure 6.2-5a) due to the cryogenic suction created by the presence of the frozen fringe and this drop in pore water pressure must be accompanied by an increase in the effective stress as noted.

6.2.3.5. Void Ratio

The simulations were run under undrained conditions; the mass of water in the system remained constant and so any changes in volume are due to the change of phase from liquid water to solid ice. This has been verified using the mass balance equation by comparing the predicted and simulated displacements. Averaging the void ratio across the domain also verifies that the predicted 9% strain has occurred in both examples (Figure 6.2-8a and Figure 6.2-8b).

Although the global mass of water is constant due to the undrained boundary conditions applied, local redistribution of water may take place. Depending on the thermal regime causing the freezing to occur, three possibilities exist; primary heave,

secondary heave and no heave. (This has been previously discussed in Chapter 2, section 2.2 and is not repeated here). Most practical situations exhibit the secondary heave mode where there is a combination of in-situ freezing and moisture movement.

Examining the pore water pressure profiles (Figure 6.2-5a and Figure 6.2-5b) the direction of flow can be determined. The simulation using Darcy's law (Figure 6.2-5b) shows that an upward movement of water is occurring as the pore water pressure is higher at the freezing zone and lower at the surface. The void ratio plot confirms this and as freezing progresses water flows upwards until the frozen fringe passes where it fully freezes. The greatest amount of strain is observed at the surface where the largest increase of water accumulation has taken place as a result of the effect the frozen zone has on the moisture flow. This is also consistent with the effective stress plot (Figure 6.2-7b) which shows a reduction in the effective stress in the unfrozen zone which is due to the additional water that is now present in the upper regions.

Using the modified moisture equation the flow gradients are opposite of those using Darcy's law and the flow of water is now towards the freezing zone. The pore water pressure profile (Figure 6.2-5a) shows that the flow of water is occurring from the base and top of the sample towards the frozen fringe. A small amount of water is expected to be drawn up from the base but will be insignificant as a result of the considerably reduced hydraulic conductivity of the frozen soil.

At the onset of freezing a large increase in the void ratio (Figure 6.2-8a) is noted and this continues until the frozen fringe is fully developed. This is due to the considerable potentials for flow that exist in a soil that has just started to freeze which results in a large increase in the void ratio. During the simulation a constant rate of increase in void ratio is observed with a notable decrease in the void ratio at the surface. This decrease is due to a lack of water present in the upper layers as water has been drawn downwards to the freezing zone and this zone consolidates. This kind of behaviour is typical of frost susceptible soils with an ice rich layer over laid by a layer of soil that has experienced some consolidation.

6.2.3.6. Conclusions

The introduction of an additional term to the moisture flow equation to include the effect of cryogenic potentials has been verified through a mass balance exercise. The freezing response due to the modification of the moisture flow equation has been discussed with respect to displacement, pore water pressure, temperature, effective stress and void ratio.

Initial observations show that the cryogenic potential component has been implemented correctly and the numerical model exhibits the cryogenic suction that is critical in frozen soils to attract the additional water to the frozen fringe.

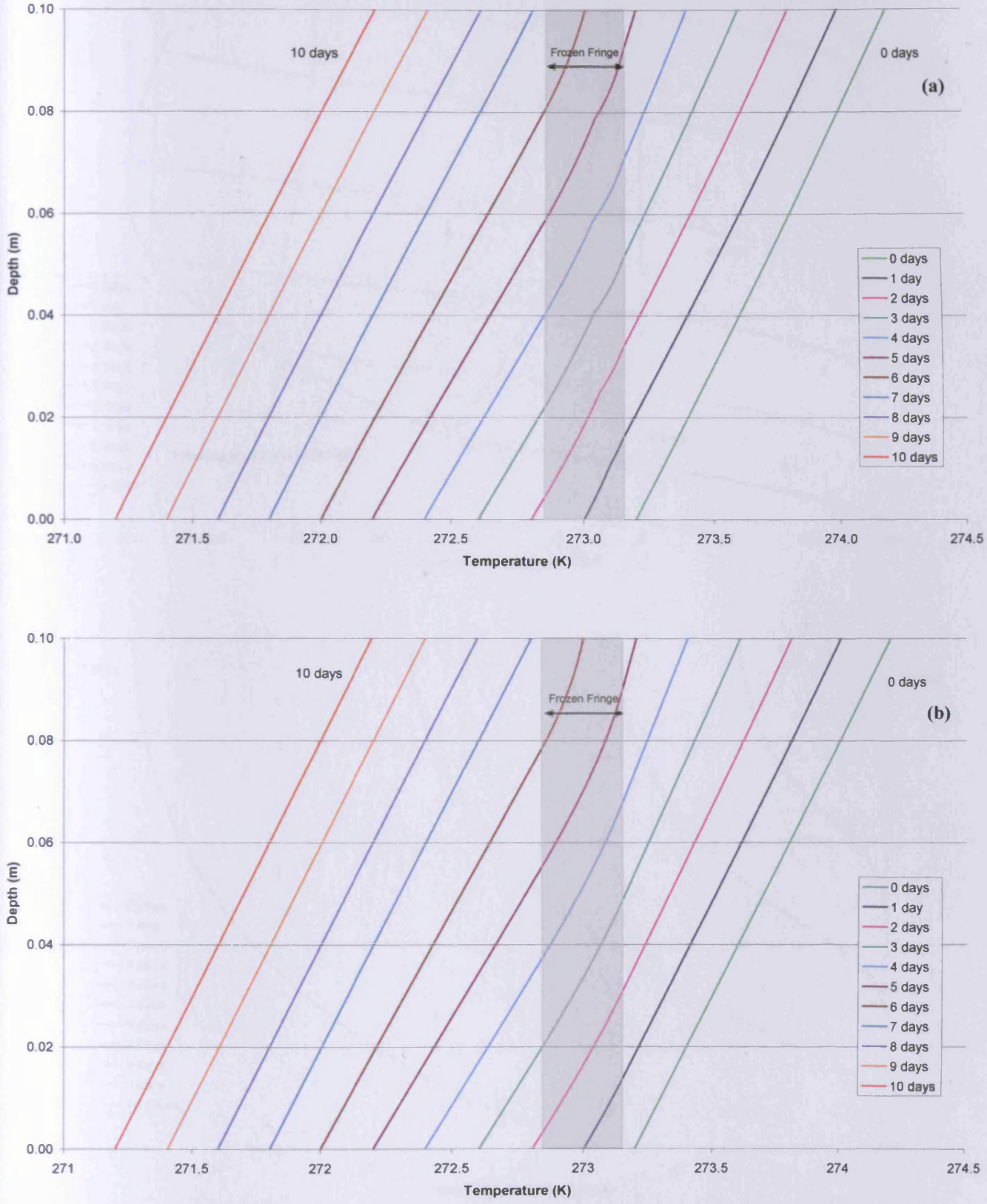

Figure 6.2-4 – Temperature profiles – undrained freezing test; a) moisture flow including cryogenic suction. b) moisture flow defined by Darcy's law

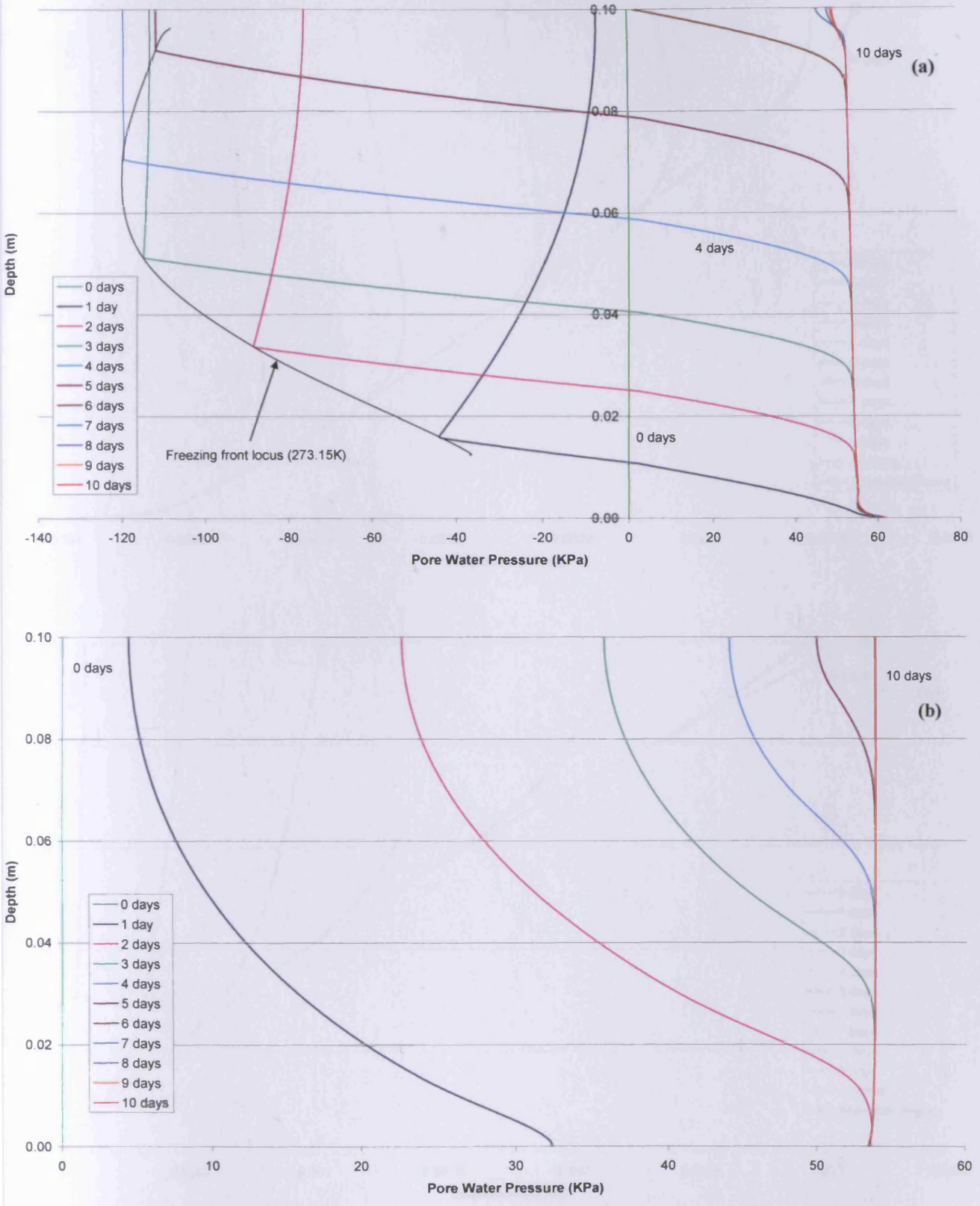

Figure 6.2-5 – Pore water pressure profiles – undrained freezing test; a) moisture flow including cryogenic suction. b) moisture flow defined by Darcy's law

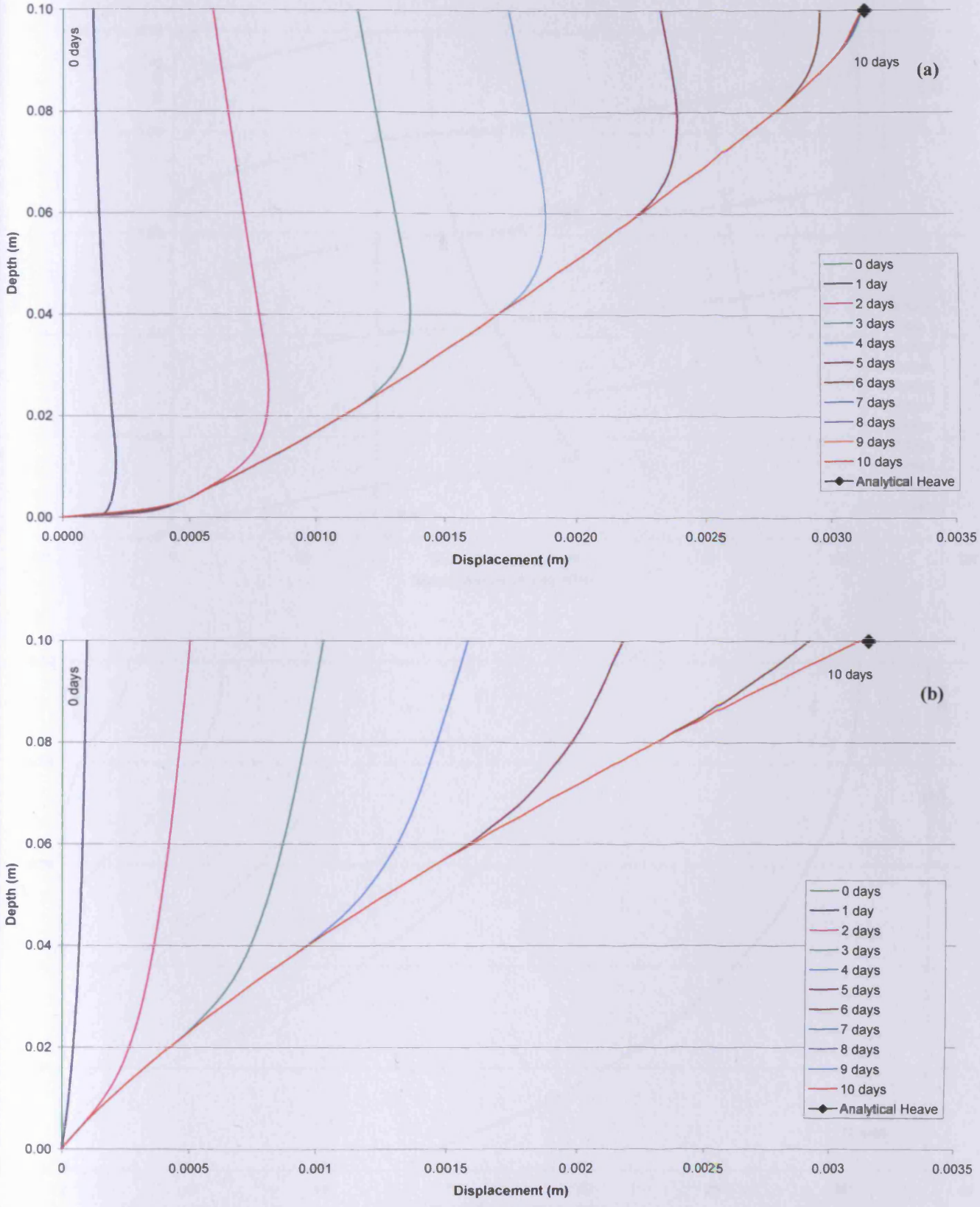

Figure 6.2-6 – Displacement profiles – undrained freezing test; a) moisture flow including cryogenic suction. b) moisture flow defined by Darcy's law

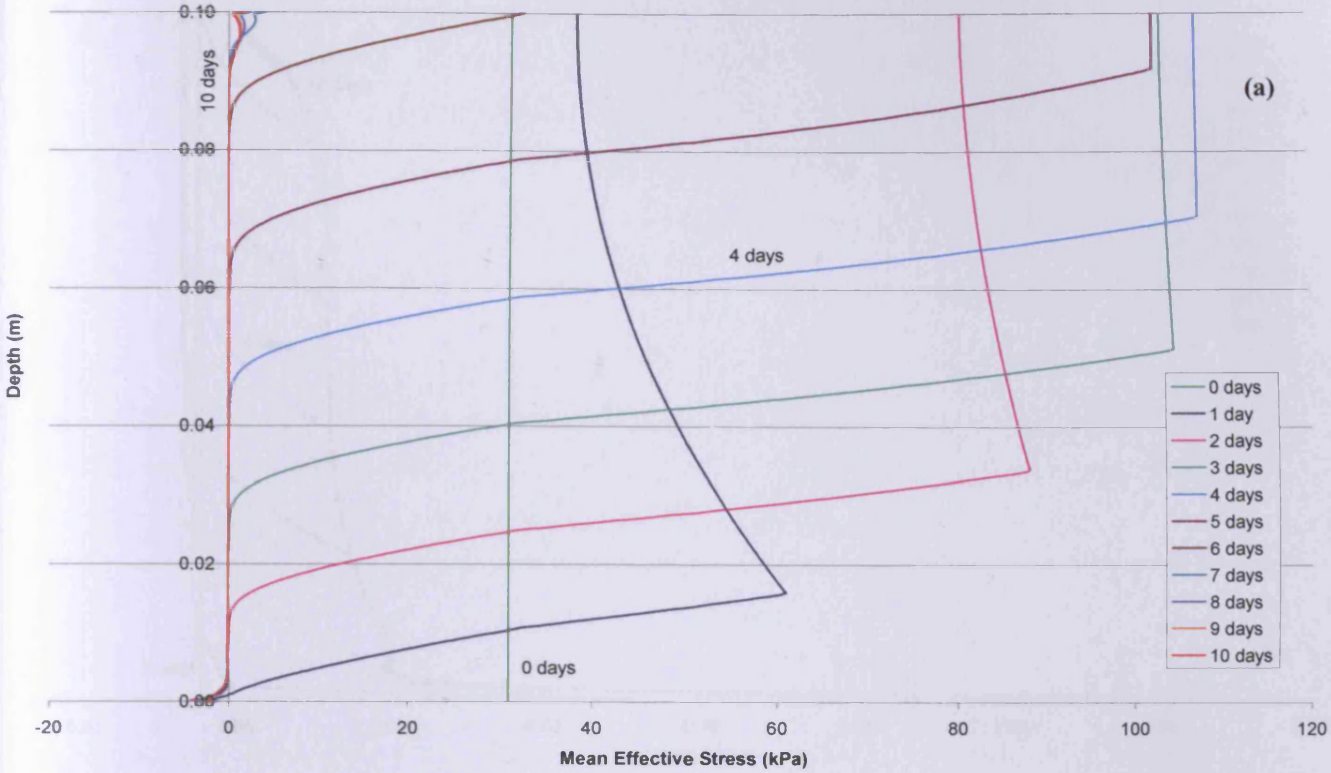

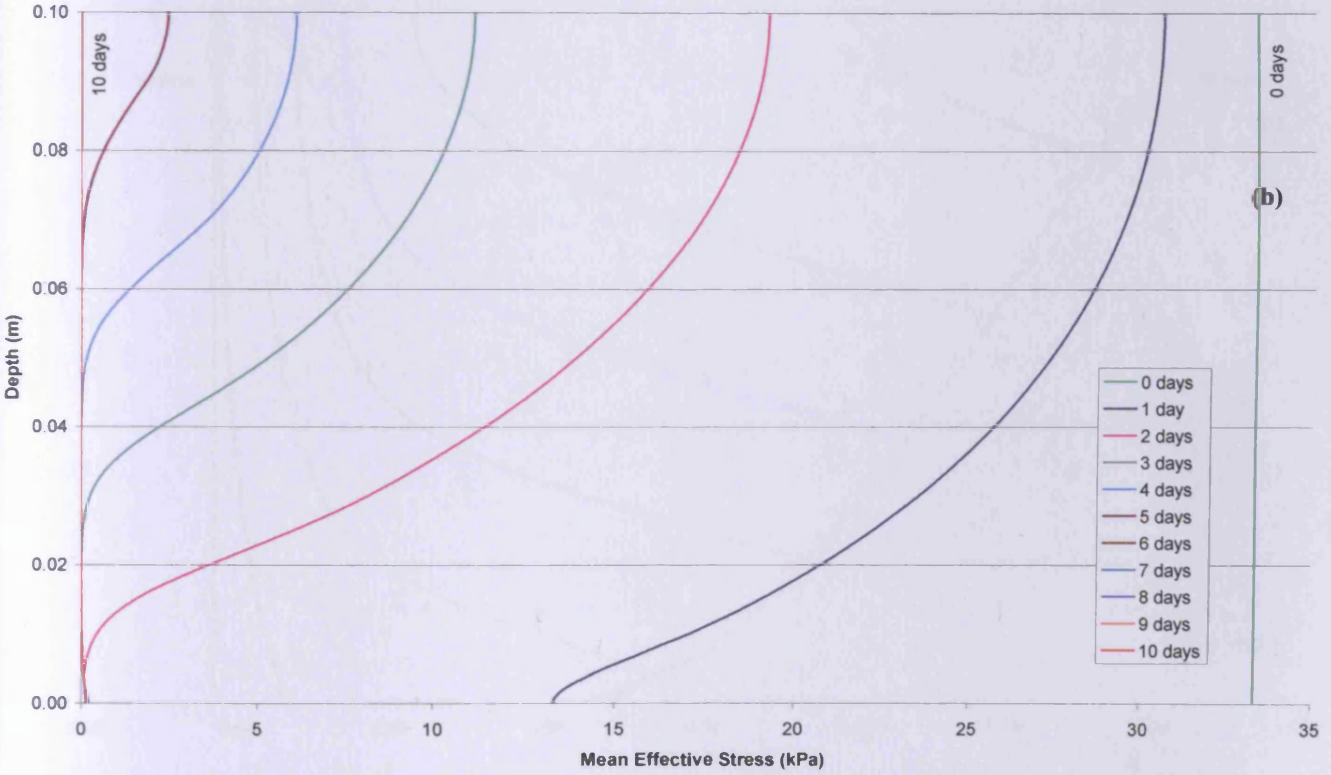

Figure 6.2-7 – Mean effective stress profiles – undrained freezing test; a) moisture flow including cryogenic suction. b) moisture flow defined by Darcy's law

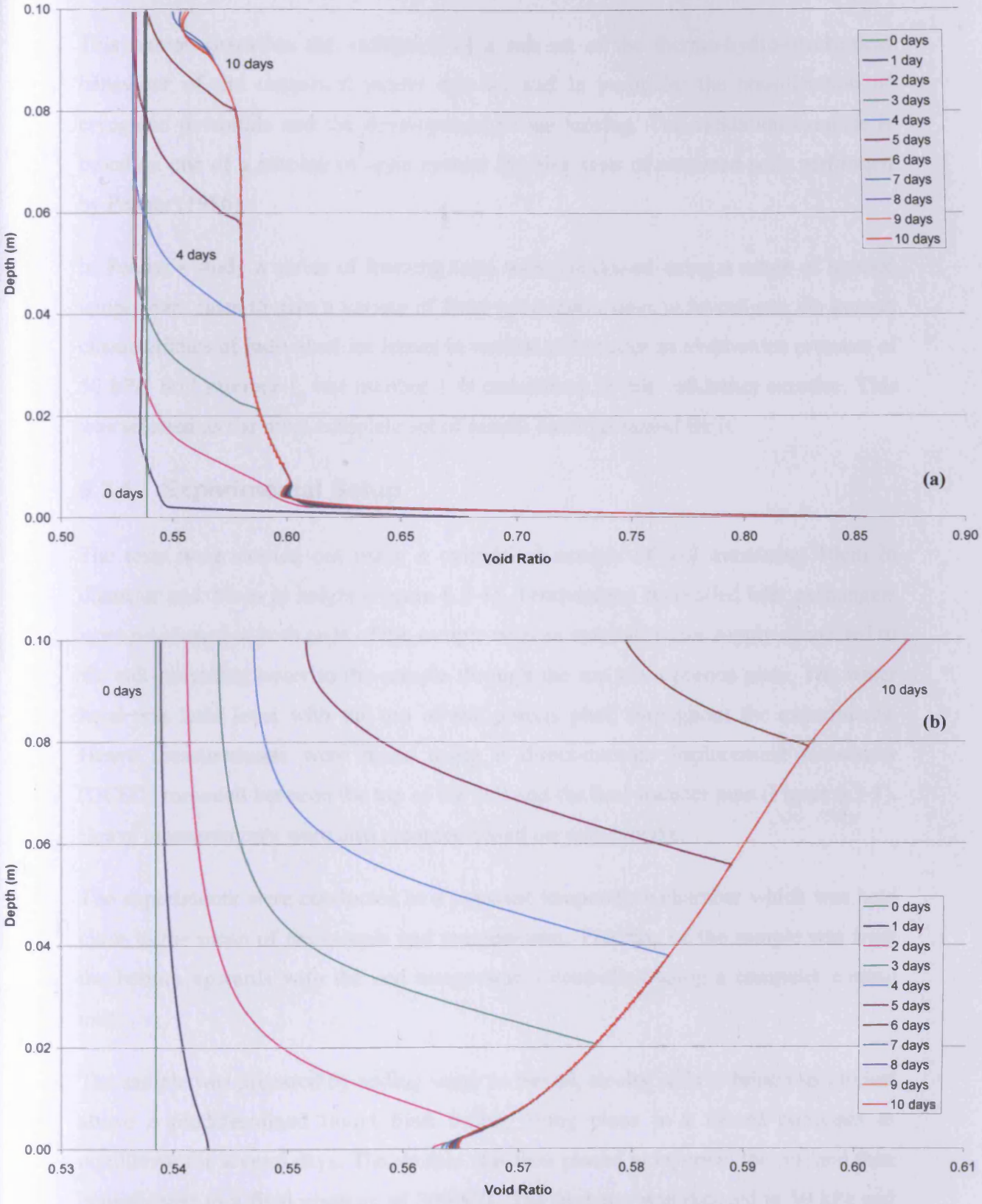

Figure 6.2-8 – Void ratio profiles – undrained freezing test; a) moisture flow including cryogenic suction. b) moisture flow defined by Darcy's law

6.3. One Dimensional Ramped Freezing Test

This section describes the validation of a sub set of the thermo-hydro-mechanical behaviour of the numerical model due to, and in particular the consideration of cryogenic potentials and the development of ice lensing. The validation exercise is based on one of a number of open system freezing tests of saturated soils performed by Penner (1986).

In Penner's study a series of freezing tests were conducted using a range of ramped temperature rates to give a variety of frost penetration rates to investigate the growth characteristics of individual ice lenses in natural soils under an overburden pressure of 50 kPa. Soil number 1, test number 1 is considered in this validation exercise. This was selected as the most complete set of results were presented for it.

6.3.1. Experimental Setup

The tests were carried out using a cylindrical sample of soil measuring 10cm in diameter and 10cm in height (Figure 6.3-1). Temperature controlled heat exchangers were positioned at both ends of the sample with an external water supply connected to the cell providing water to the sample through the top via a porous plate. The water level was held level with the top of the porous plate throughout the experiments. Heave measurements were made using a direct-current displacement transducer (DCDT) mounted between the top of the cell and the heat transfer pipe (Figure 6.3-1). Heave measurements were also recorded based on water intake.

The experiments were conducted in a constant temperature chamber which was held close to the mean of the sample end temperatures. Freezing of the sample was from the bottom upwards with the end temperatures controlled using a computer control unit.

The sample was prepared by adding water to sieved, air-dry soils to bring them to just above a predetermined liquid limit before being place in a closed container to equilibrate for several days. The sample was then placed in layers in the cell and then consolidated to a final pressure of 500 kPa. The pressure was reduced to 50 kPa and allowed to reach its equilibrium volume before the test commenced.

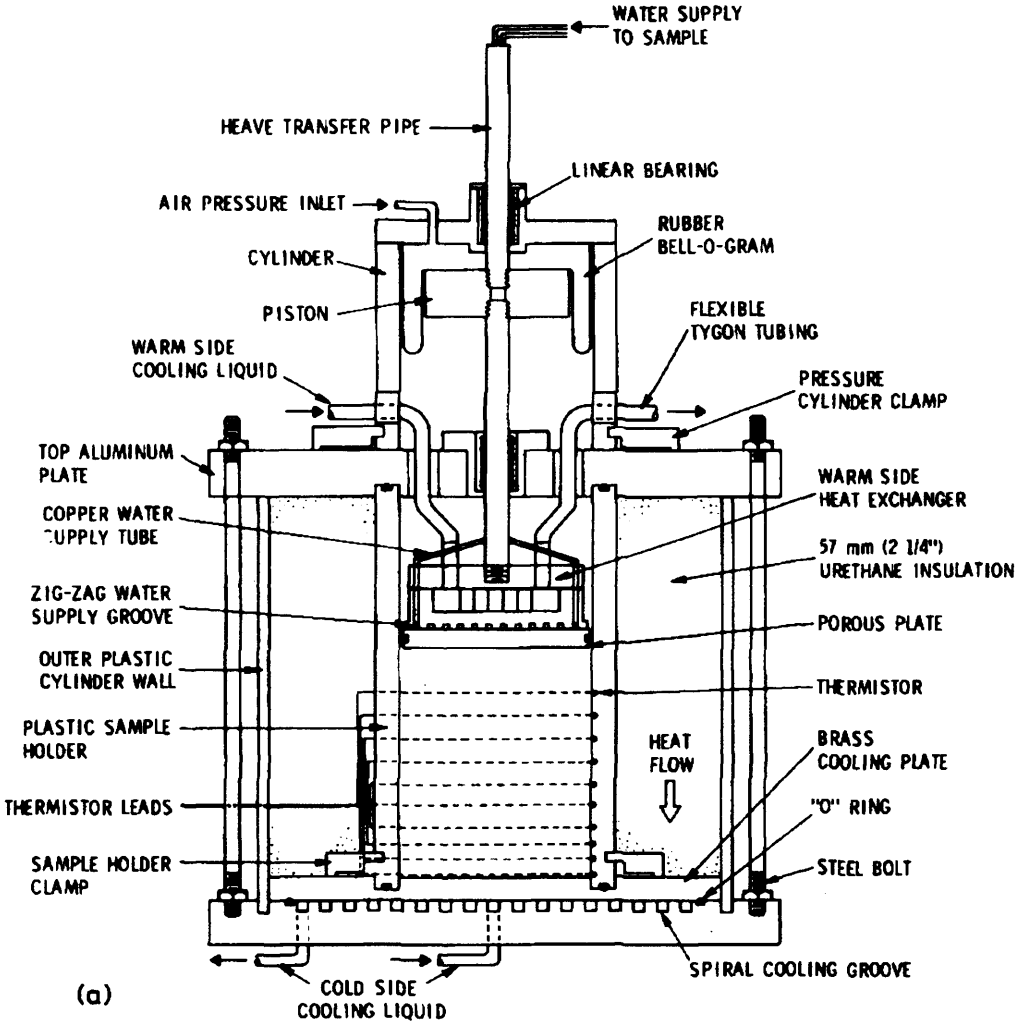

Figure 6.3-1 – Frost cell used to explore aspects of ice lens growth in soils (Penner 1986)

6.3.2. Material Parameters

Material parameters for the test conducted by Penner (1986) were not reported in the author's paper. The soil is quoted as being a frost susceptible soil passing the 100 sieve with a clay-size content of 29% by weight. A number of material parameter values have been proposed by Shen and Ladanyi (1987) in an analysis of the soil. These values have been taken from Harlan and Nixon (1978) and were given previously in Table 6.2-1. The dry density was taken to be 1750 kg/m^3 according to other experiments on the sample under similar conditions published by Penner and Ueda (1977).

The elastic stiffness parameter of the soil, κ, is calculated based on data presented by Selvadurai et al (1999) for a similar silty frost susceptible soil, as

$$\kappa = 0.005127 \qquad \textbf{6.3-1}$$

A constant value is assumed for Poisson's ratio (Selvadurai et al, 1999).

$$\nu = 0.3 \qquad \textbf{6.3-2}$$

The hardening parameter, p_0, is set a high value to ensure that the material remains in the elastic region of the stress space.

The hydraulic conductivity relationship for a frost susceptible soil can be presented in a generic form as;

$$k = \begin{cases} k_u e^{\alpha T} & T_s < T < T_0 \\ k_f & T \le T_s \end{cases} \qquad \textbf{6.3-3}$$

where

k_u, k_f are the unfrozen and frozen hydraulic conductivities respectively.

α is an experimentally determined constant from the regression analysis.

T_0, T_s are the freezing temperature of pure water and segregation freezing temperature respectively. All temperatures are in degrees Celsius.

From experimental data published (Horiguchi and Miller, 1983; Dallimore and Williams, 1984), the relationship between the hydraulic conductivity and temperature has been determined using equation 6.3-3 and successfully applied to frost heave problems (Shen and Ladanyi, 1986; Selvadurai et al, 1999). Unsaturated hydraulic conductivity values for similar soils have been reported as 3.072×10^{-11} m/s (Shen and Ladanyi, 1986), 2.918×10^{-10} m/s (Selvadurai et al, 1999) and 1.075×10^{-9} m/s (Shen and Ladanyi, 1991) with frozen hydraulic conductivity values reducing to 5.453×10^{-13} m/s, 5.1804×10^{-12} m/s, and 8.0499×10^{-13} m/s respectively.

As no information about the saturated unfrozen and frozen hydraulic conductivity of the soil was presented by Penner (1986), the hydraulic conductivity of the soil was assumed to decrease exponentially by approximately two orders of magnitude with temperature according to the following relationship.

$$k = \begin{cases} 9.0\times10^{-11} e^{15.743T} & -0.3°C < T < T_0 \\ 8.0\times10^{-13} & T \le -0.3°C \end{cases} m/\sec \qquad \textbf{6.3-4}$$

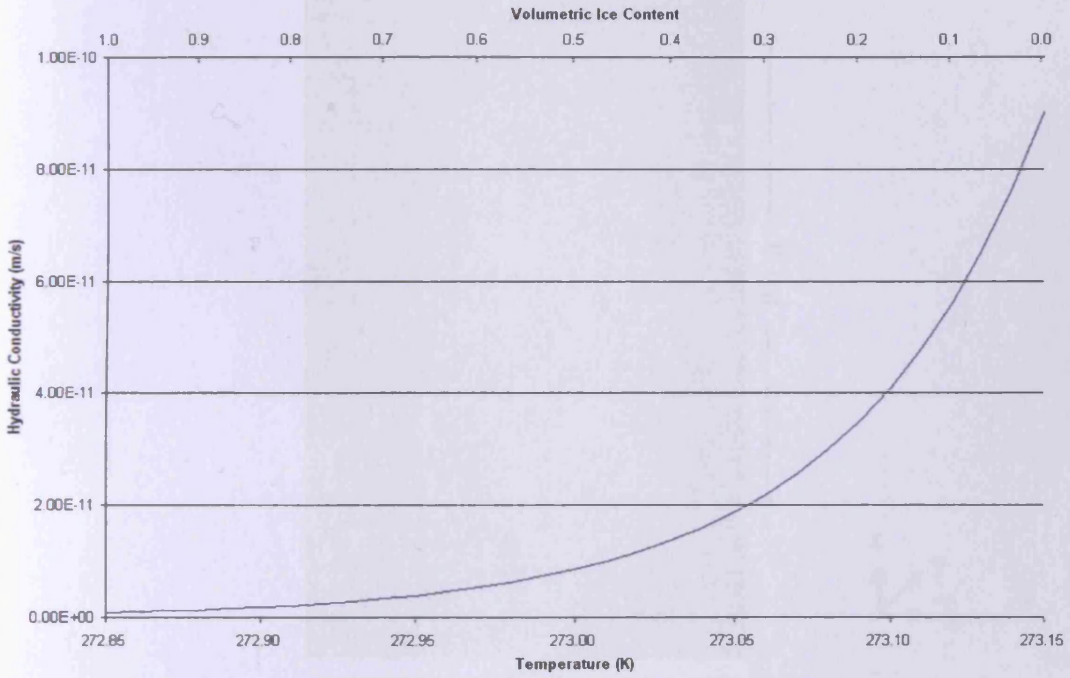

Figure 6.3-2 – Variation of hydraulic conductivity with temperature and volumetric ice content used for the ramped freezing test.

The porosity of the soil was estimated as n = 0.35 based on the work of Shen and Ladanyi (1987).

6.3.3. Numerical Simulation

The frost cell was numerically modelled as an axisymmetric column using 8 noded isoparametric axisymmetric quadratic elements divided vertically into 250 elements and radially into 1 element (Figure 6.3-3). Heat and moisture flow and deformation

all occur in the vertical direction where a fine mesh is required. In the radial direction these processes do not occur due to the symmetry of the problem and a courser mesh has been used. An initial time step of 10 seconds was chosen and this was allowed to vary according to the time stepping algorithm employed with a maximum time step of 1000s. These spatial and temporal discretisations were used after a thorough investigation was undertaken to ensure converged results were obtained.

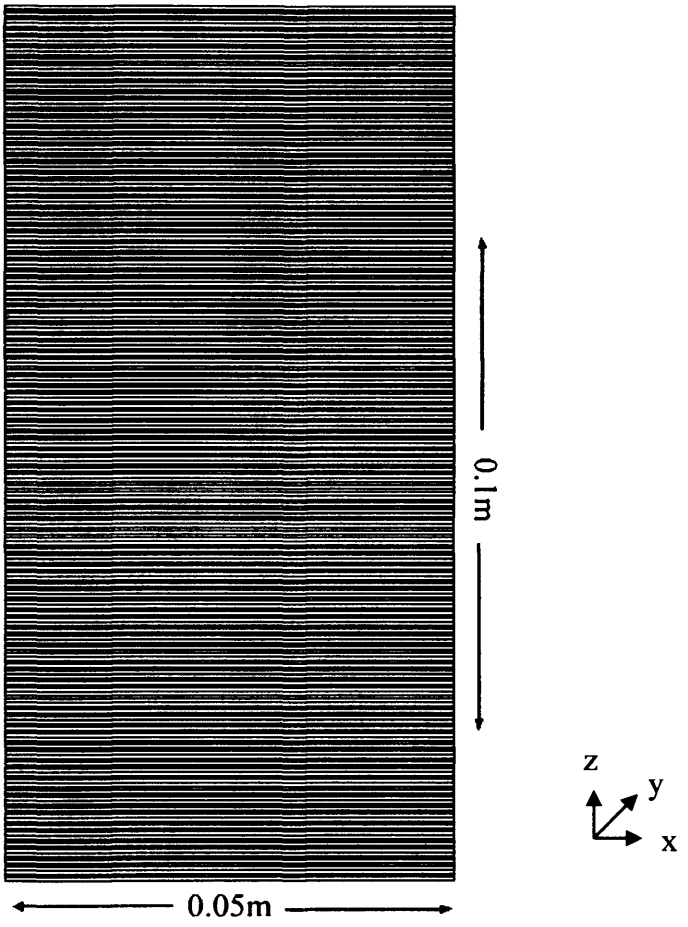

Figure 6.3-3 – Mesh used in Simulation

Following the experimental condition (Penner 1986) an initial temperature of 273.25K has been applied throughout the sample. The initial pore water pressure was set to 0 kPa and the upper surface fixed to this value for the duration of the simulation to represent the presence of the porous plate. The sample was restrained in the vertical direction at the base of the sample and in the radial direction on the right hand vertical edge of the domain.

Taking an insitu earth pressure coefficient, K_0, of 0.429 the initial stress levels were set to σ_z = 50.00 kPa, and σ_r = 21.43 kPa.

It is unclear in Penner's report of the experiment as to the length of time the sample was allowed to temper overnight in the cold temperature chamber. A period of "overnight" is reported, therefore a time of 12 hours has been assumed for this initial phase of the experiment. During this time the sample was connected to the water supply and the end temperatures were brought to their initial conditions. Having tempered in the cold chamber overnight the experiment was commenced and the sample end temperatures were varied at a rate of -0.02 K/day for a total of 10 days. (Figure 6.3-4)

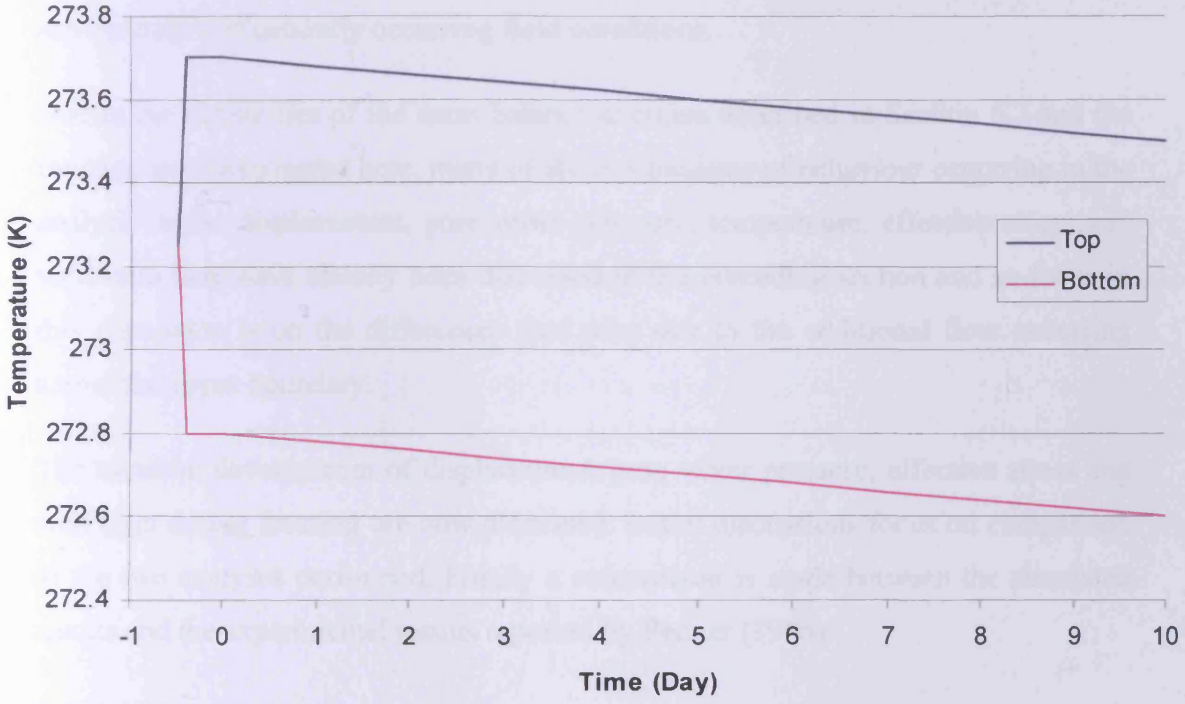

Figure 6.3-4 – Temperature curve applied to top and bottom of sample in ramped freezing test.

Two analyses are performed; the first using the formulation presented in Chapter 3 which includes the effect of cryogenic suctions, and the second using the same formulation but with the effect of cryogenic suctions removed, thereby reducing the moisture flow equation to a standard Darcy's Law form. These two analyses allow the impact of cryogenic suction on the formation of ice lenses to be assessed.

6.3.4. Results and Conclusions

The variation of displacement, pore water pressure, temperature, effective stress and void ratio with respect to time are shown in Figure 6.3-5a to Figure 6.3-9a for the

analysis which considers the effect of cryogenic suction and Figure 6.3-5b to Figure 6.3-9b for the analysis which only considers Darcy's Law. Profiles of surface heave and frost penetration with respect to time for simulated and experimental results are shown in Figure 6.3-10 and Figure 6.3-11.

The exercise conducted earlier in Section 6.2 was based on the freezing test performed by Penner (which is considered here) with boundary conditions changed to ensure that the sample froze completely and was under undrained conditions. In this exercise, with flow permitted through the top, the sample was free to draw in (or expel) water allowing the ice lensing phenomenon to be explored in a scenario representative of naturally occurring field conditions.

Due to the similarities of the mass balance exercise described in Section 6.2 and the freezing test investigated here, many of the mechanisms of behaviour occurring in the analysis in the displacement, pore water pressure, temperature, effective stress and void ratio field have already been discussed in the preceding section and so focus in this discussion is on the differences that arise due to the additional flow occurring across the upper boundary.

The transient development of displacement, pore water pressure, effective stress and void ratio during freezing are now discussed. Initial discussions focus on comparison of the two analyses performed. Finally a comparison is made between the simulated results and the experimental results reported by Penner (1986).

6.3.4.1. Temperature

In comparison to the undrained analysis presented in Section 6.2 a greater variance between the two analyses (the first including cryogenic suction effects Figure 6.3-5a and the second without these effects included Figure 6.3-5b) can be seen. This is due to the impact of the additional water that is flowing into the system due to ice lensing which then has to be cooled and frozen. There is a noticeable variation in the profile considering cryogenic suction effects at a temperature of 273.08K (Figure 6.3-5a); this is at the location where the moisture is accumulating and where lensing is taking place. This location can be considered to be the position of the frost front.

6.3.4.2. Pore Water Pressure

In profiles (Figure 6.3-7a and b) a similar maximum pore water pressure independent of the frozen region of the sample was obtained with a clear depression of the pore water pressure values developed when cryogenic suctions are considered. The pore water pressure gradients in both profiles confirm why the displacement profiles, discussed below, have been observed to occur. Using only Darcy's law the presence of a freezing front will expel water whilst in contrast, considering the additional effect of cryogenic suction results in a movement of moisture towards the freezing zone.

As a side note; under drained conditions the maximum depression in the pore water pressure when cryogenic suctions are considered is reduced compared to undrained conditions (Figure 6.3-6). Under drained conditions additional moisture is available to be drawn into the sample; the pore water pressure is then relieved due to this free water being available and as a result the pore water pressure depression to cause moisture movement towards the frozen fringe is reduced. In comparison in undrained conditions the pore water pressure is not able to be relieved by additional moisture flowing into the sample, the pore water pressure is therefore depressed further to cause the observed movement of moisture towards the frozen fringe.

6.3.4.3. Displacement

Comparison of the displacement results from the two analyses shown in Figure 6.3-7a and b illustrate the major impact that the consideration of cryogenic suction in the system has.

The most notable observation is with the displacement profile from the simulation using Darcy's law (Figure 6.3-7b) which shows almost no heave occurring in the sample. In this analysis as the soil progressively freezes water pressure in the fringe increases due to the impact of density variation between the two phases, leading to flow away from the frozen fringe. The allowance of moisture to flow across the upper boundary of the sample results in liquid water being expelled from the sample during freezing.

The reverse is true when cryogenic suctions are considered; in this case significant quantities of water are drawn towards the frozen fringe where it accumulates leading

to large quantities of surface heave as shown in Figure 6.3-7a. This can be seen in the displacement values where, even though the sample is not completely frozen, the displacement is already several times greater than that which would develop due to insitu phase change (i.e. if the whole soil was frozen in undrained conditions).

The freezing front locus and the lensing front locus have been plotted on Figure 6.3-7a to indicate where the simulated displacements relate to the position within the frozen fringe. The freezing front locus is plotted at the freezing temperature of pure water, T_0, of 273.15K. The lensing front locus is plotted where the accumulation of ice appears to be accumulating within the frozen fringe.

Ice lensing takes place in real soils within the frozen fringe at a location near to the coolest isotherm at which water can exist in the liquid form (O'Neill and Miller 1985). Ice lensing in real soils also occurs at discrete intervals, however, as the formulation is based on a continuum assumption; ice lenses will form throughout the fringe and typically a constant, smooth, gradual build up of heave will occur. This gradual build up of heave can be seen in the results. It can also be seen that ice lensing is taking place within the fringe when the freezing front and lensing front are superimposed onto the displacement plot (Figure 6.3-7a).

6.3.4.4. Effective Stress

The effective stress plots mirror the pore water pressure profiles as expected. As the samples freeze the effective stress tends to zero resulting in zero effective stress in the frozen soil. An increase in the effective stress is again seen at the warmest side of the frozen fringe coinciding with the maximum negative pressure generated when cryogenic suction effects are considered (Figure 6.3-8a). In the simulation using Darcy's law (Figure 6.3-8b) the effective stress slowly decreases linearly between the top of the sample and warm side of the frozen fringe with a much more pronounced decrease in profile through the frozen fringe tending to zero at the cold side.

6.3.4.5. Void Ratio

Considering the simulation using Darcy's law (Figure 6.3-9b) an increase in the void ratio is calculated towards the base of the sample where rapid freezing prevents the movement of moisture out of the fringe region and results in insitu freezing. When the

freezing rate drops after the initial 12 hour "overnight" tempering in the cold chamber and the test proper is commenced, the liquid water now has sufficient time to flow upwards in the sample away from the frozen fringe and insignificant quantities of heave occur. A very different picture is portrayed in the void ratio profile when cryogenic suction effects are considered (Figure 6.3-9a) and it is clear to see significant increases in the void ratio in the frozen fringe.

Ice lensing is predicted to occur as the effective stress tends towards 0kPa (Nakano 1986; Nakano 1990). As the sample freezes the effective stress tends towards 0kPa and as a result of this loss of strength the soil pores are no longer able to resist the forces generated due to cryogenic suctions and therefore swell to accommodate the additional moisture accumulation.

6.3.4.6. Experimental vs. Simulated

During the experimental programme Penner (1986) observed a change in the growth rate during ice lens formation (Figure 6.3-12). The heave rose to a maximum when a new ice lens was initiated and reduces to a minimum just before the next ice lens formed. Martin (1959) predicted falling ice lens temperatures during lens formation and so have Konrad and Morgenstern (1980); although the theories are significantly different they both predict a decreasing water supply to the growing ice lens. Penner (1986) hypothesised that the Miller frozen fringe is growing in thickness during ice lens formation since the lens and the 0°C isotherm is increasing and the reduced rate of lens growth could be attributed to the longer path the water must travel as a result of the thickening frozen fringe.

The results from the simulation show a steady rate of heave during the time period (Figure 6.3-10). While the observations by Penner are not unlike those occurring in the field under natural conditions, the ability of the model to represent these discrete ice lens is not possible. The approach adopted in this work assumes that the ice lensing is continuous and providing the conditions for ice lensing are met this process will steadily occur in the frozen fringe. The experimental results show a slightly higher rate of heave in the initial stages of the test, decreasing as the test progresses compared to an almost constant rate in the simulation. The time between ice lenses in the experimental sample increase as the test advances and would account for this

observation. Overall the comparisons between the calculated and measured results show a good correlation.

The frost penetration (Figure 6.3-11) is also affected by the location and magnitude of the ice lensing; a similar surface heave can be the result of a smaller quantity of ice lensing and a greater frost penetration as opposed to a larger quantity of ice lensing and reduced frost penetration. The extent of the frozen fringe would also impact on the results; as the silt or clay fraction increases so does the range over which the soil freezes. With a larger fringe there is a larger partially frozen soil zone which generates a greater cryogenic suction and hence more ice lensing and a slowing in the frost penetration rate.

The frost front in the simulated results penetrates to a slightly greater extent than the experimental results; this would indicate less ice lensing forming and more insitu water being frozen. This is also corroborated by the surface heave profile (Figure 6.3-10); the difference between the two representing the additional ice lensing taking place in the experiment while the frost penetration depth is less. Overall there is a good correlation between experimental and simulated results.

The results presented by Penner (1986) relate to the thermal field and the effect on heave rate and magnitude. Unfortunately no data are available for the pore water pressures as the only measuring devices installed were thermistors. There is also no data presented for the stress field. The remainder of the results of the simulation are therefore unable to be compared to the experimental ones.

Many of the parameters used in the analysis were not presented in the author's paper (Penner 1986) and so they have been drawn from previous work which considered the same or similar soil; where this was not possible representative values have been used. Experience in the development of the model has shown that parameters such as thermal conductivity, specific heat capacity and density can be estimated with reasonable accuracy and variations in these parameter values do not cause significant variations in the results. Parameters such as porosity, hydraulic conductivity and the stress-strain response are important and the results are far more sensitive to values used. The accurate determination of the hydraulic conductivity of the frost susceptible

soil is regarded as an essential pre requisite for the accurate estimation of frost heave (Selvadurai et al. 1999). Despite these limitations the results correlate extremely well.

6.3.4.7. Conclusions

The investigation undertaken in this section considered a drained analysis of a one dimensional ramped freezing test by Penner (1986) using the proposed numerical model with the intention of assessing the model's ability to simulate ice lensing.

A general discussion was presented comparing the calculation of the proposed model to the calculation using the proposed model with the effect of cryogenic suctions removed (i.e. Darcy's law) with respect to displacement, pore water pressure, temperature, effective stress and void ratio.

The results of the analysis showed that the proposed model is capable of simulating freezing with ice lensing in a frost susceptible soil. The determination of accurate parameters to use in the simulation is essential and in particular the hydraulic conductivity; however it is acknowledged that determining the hydraulic conductivity in a partly frozen soil is extremely difficult.

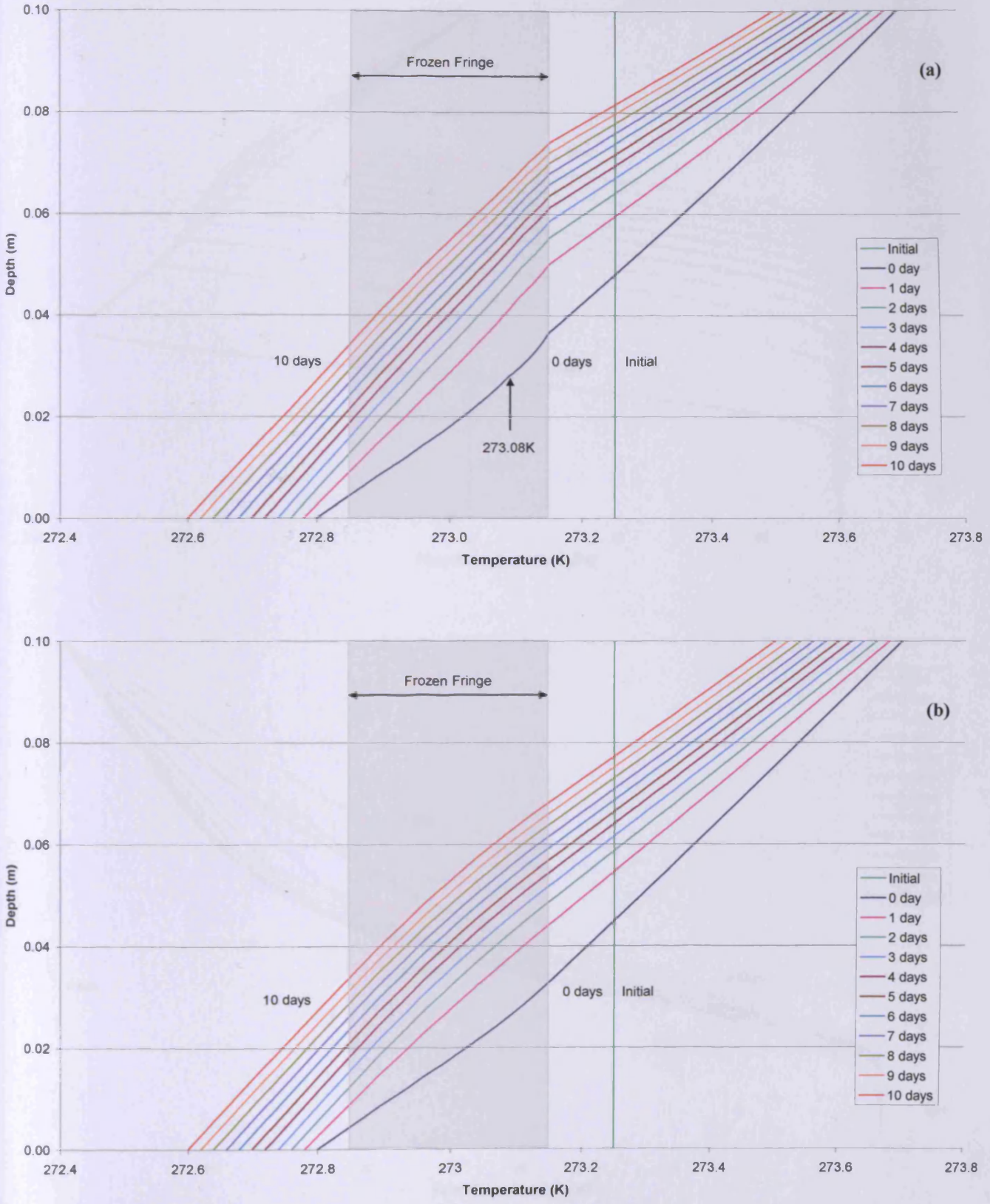

Figure 6.3-5 – Temperature profiles – ramped freezing test; a) moisture flow including cryogenic suction. b) moisture flow defined by Darcy's law

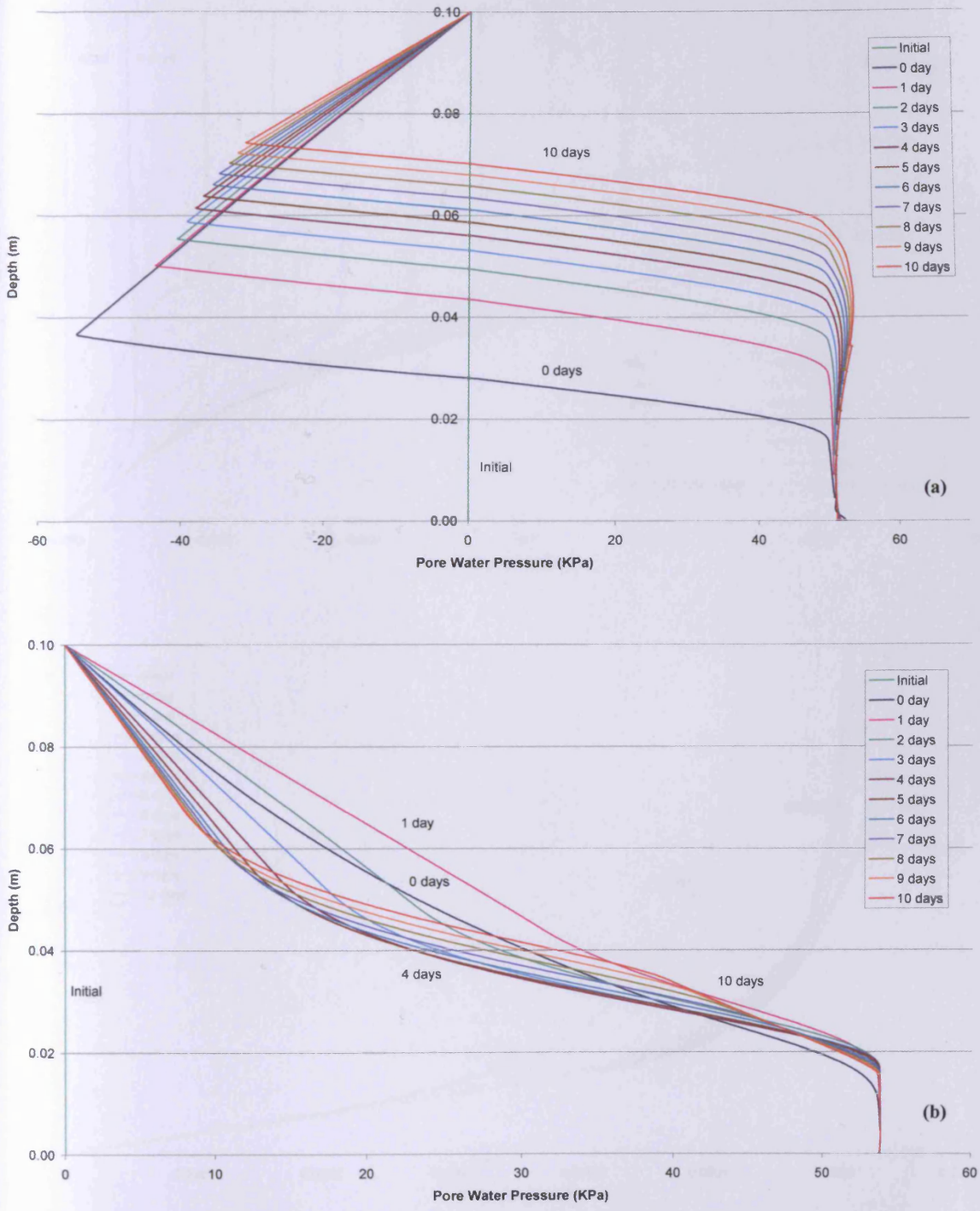

Figure 6.3-6 – Pore water pressure profiles – ramped freezing test; a) moisture flow including cryogenic suction. b) moisture flow defined by Darcy's law

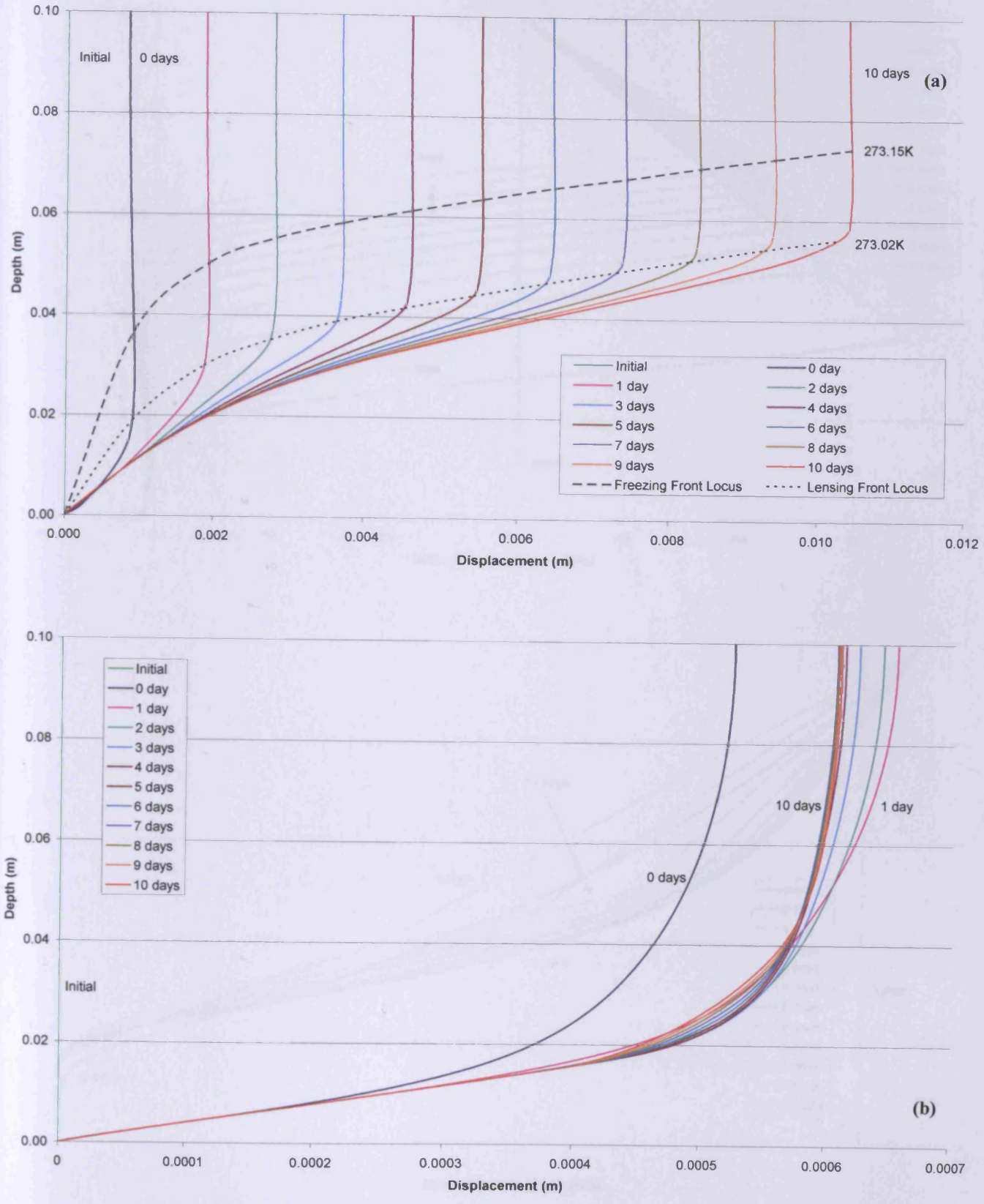

Figure 6.3-7 – Displacement profiles – ramped freezing test; a) moisture flow including cryogenic suction. b) moisture flow defined by Darcy's law

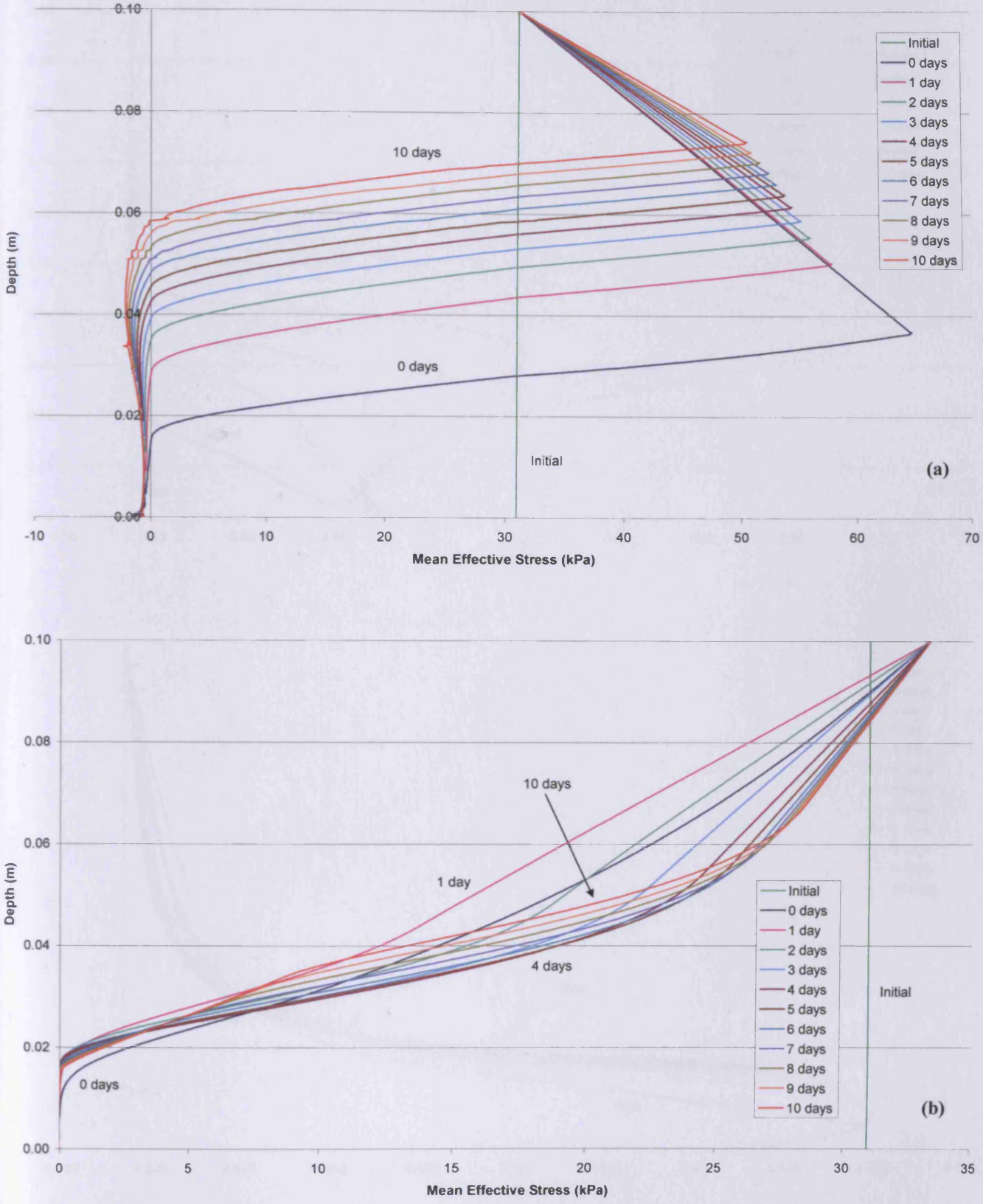

Figure 6.3-8 – Mean effective stress profiles – ramped freezing test; a) moisture flow including cryogenic suction. b) moisture flow defined by Darcy's law

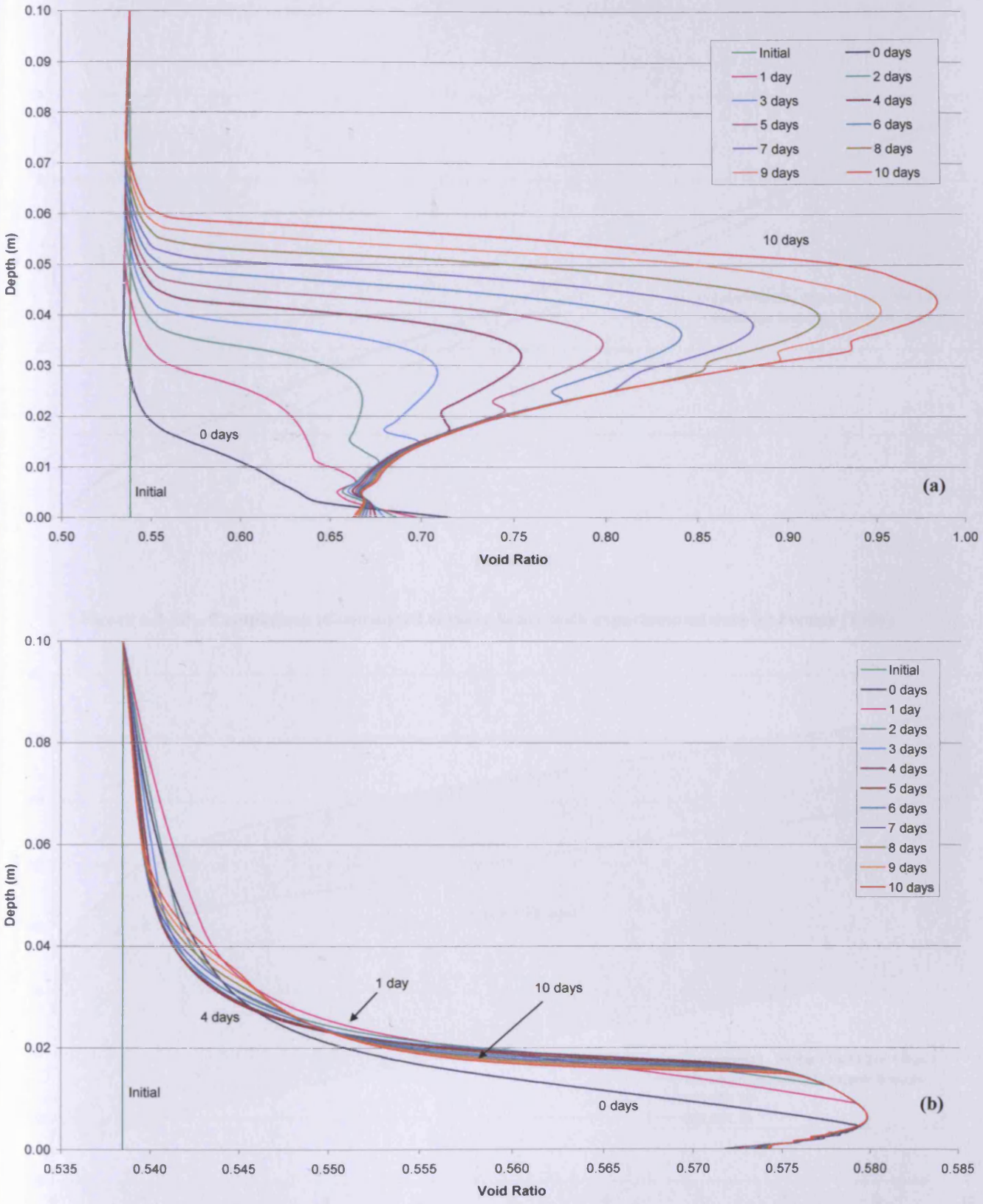

Figure 6.3-9 – Void rato profiles – ramped freezing test; a) moisture flow including cryogenic suction. b) moisture flow defined by Darcy's law

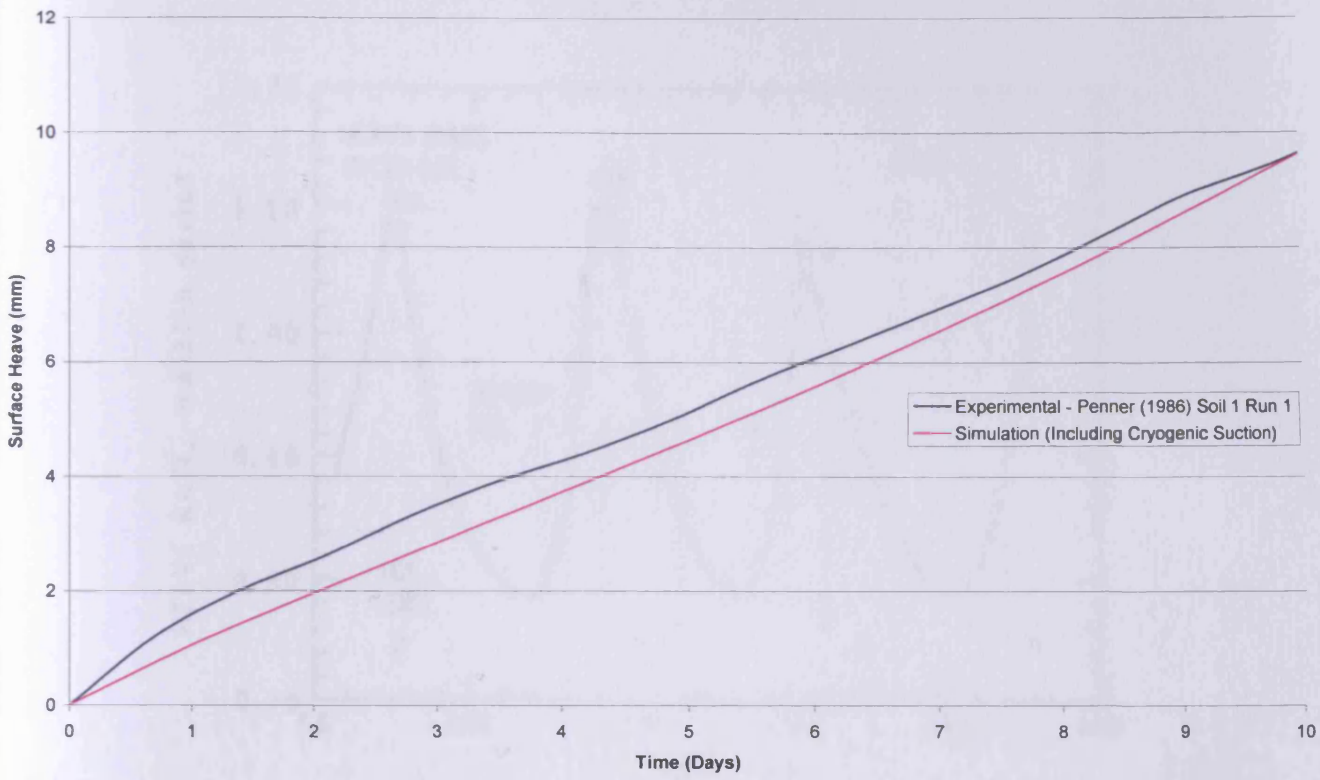

Figure 6.3-10 – Comparison of calculated surface heave with experimental data by Penner (1986)

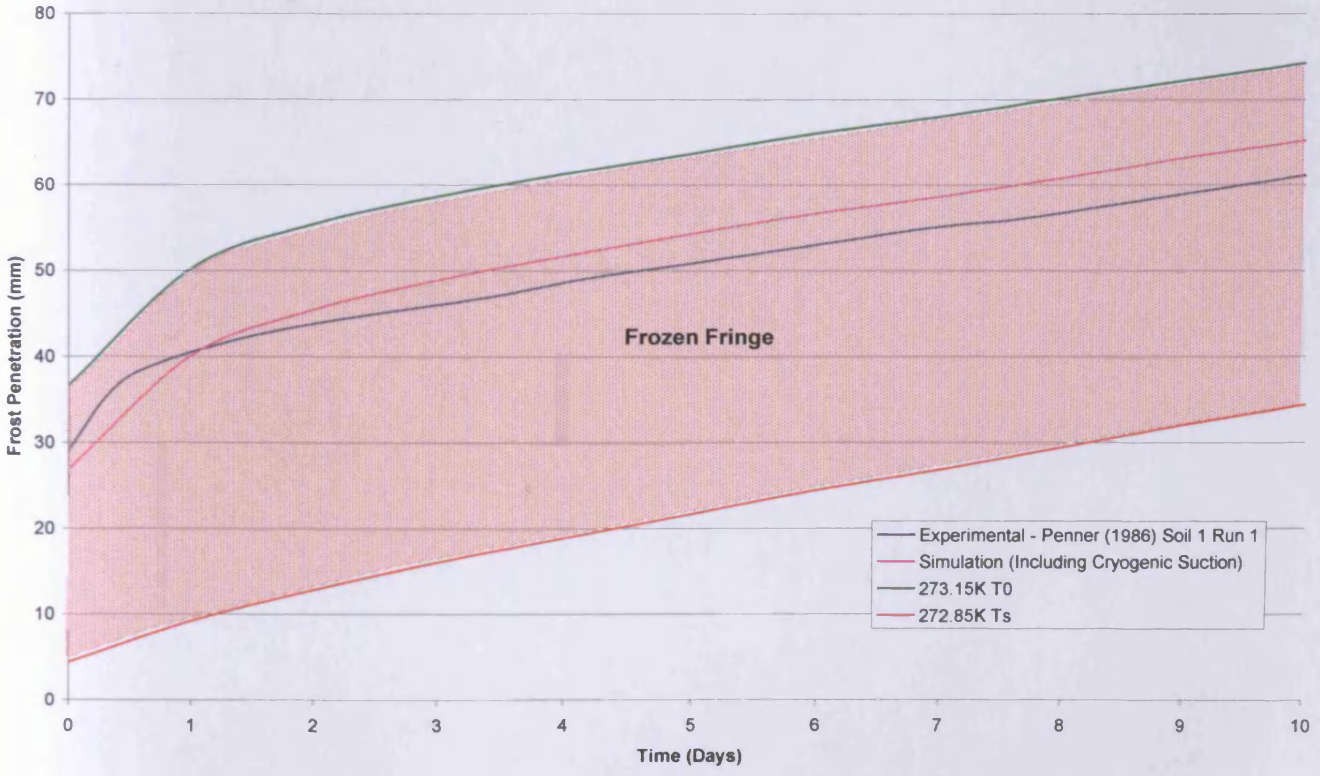

Figure 6.3-11 – Comparison of calculated frost penetration with experimental data by Penner (1986)

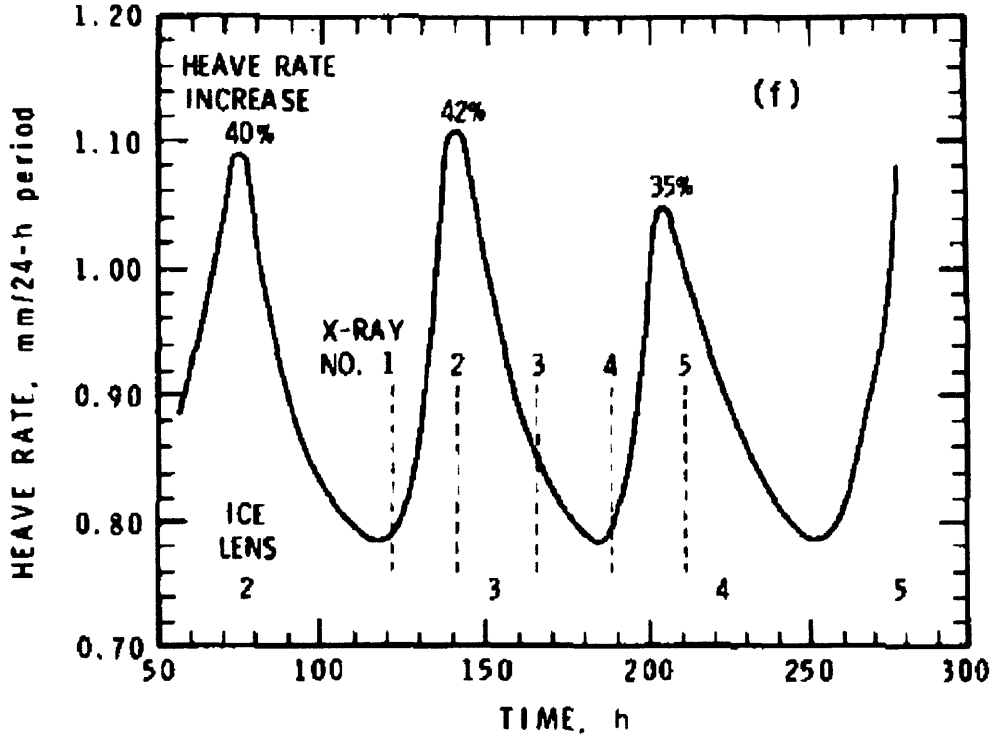

Figure 6.3-12 - Increase in heave rate during growth history of ice lenses, run No. 1, soil No. 1, ramped temperature rate 0.02°C/day (Penner 1986).

6.4. Overview of Sensitivity Analysis

In the following fives sections (6.5 to 6.9) a series of sensitivity analyses using the proposed numerical model are presented. In each case the analysis presented in Section 6.3 of Penner's experiment is used as a reference case. A specific parameter of the analysis is then varied. Of particular interest is the effect of these variables on the surface heave; i.e. will the sample experience more or less heave as a result of the variation in these parameters?

The five parameters considered are as follows;

- Thermal Gradient
- Rate of Cooling
- Hydraulic Conductivity
- Segregation Freezing Temperature, and
- Stress Level

All numerics of the problem; mesh, domain, boundary conditions and so forth, unless otherwise stated, remain unchanged from that presented in Section 6.3.3.

6.5. Thermal Gradient

6.5.1. Introduction

The concept of Segregation Potential (SP) (Konrad and Morgenstern, 1981) predicted that the formation of ice lenses is proportional to the thermal gradient. This was expressed by Konrad and Morgenstern in mathematical form in Equation 6.5-1. Recalling from Chapter 3; the rate of ice lensing in the proposed numerical model is analogous to the Segregation Potential (Equation 6.5-2).

$$\frac{dh}{dt} = SP \cdot \nabla T \qquad \textbf{6.5-1}$$

$$\frac{dh}{dt} = \frac{k_l L \rho_i}{g T_0 \rho_l} \nabla T \qquad \textbf{6.5-2}$$

Therefore according to (6.5-2) the magnitude of ice lensing is proportional to the gradient of temperature and the response of the numerical model is predicted to follow this trend.

Five simulations were run to explore this relationship with the thermal gradient of Table 6.5-1 applied across the domain (Figure 6.5-1); the original test by Penner (1986) is test T2.

Table 6.5-1 – Thermal gradient tests

Test	Thermal Gradient (K/m)
T1	4.5
T2	9.0
T3	13.5
T4	18.0
T5	36.0

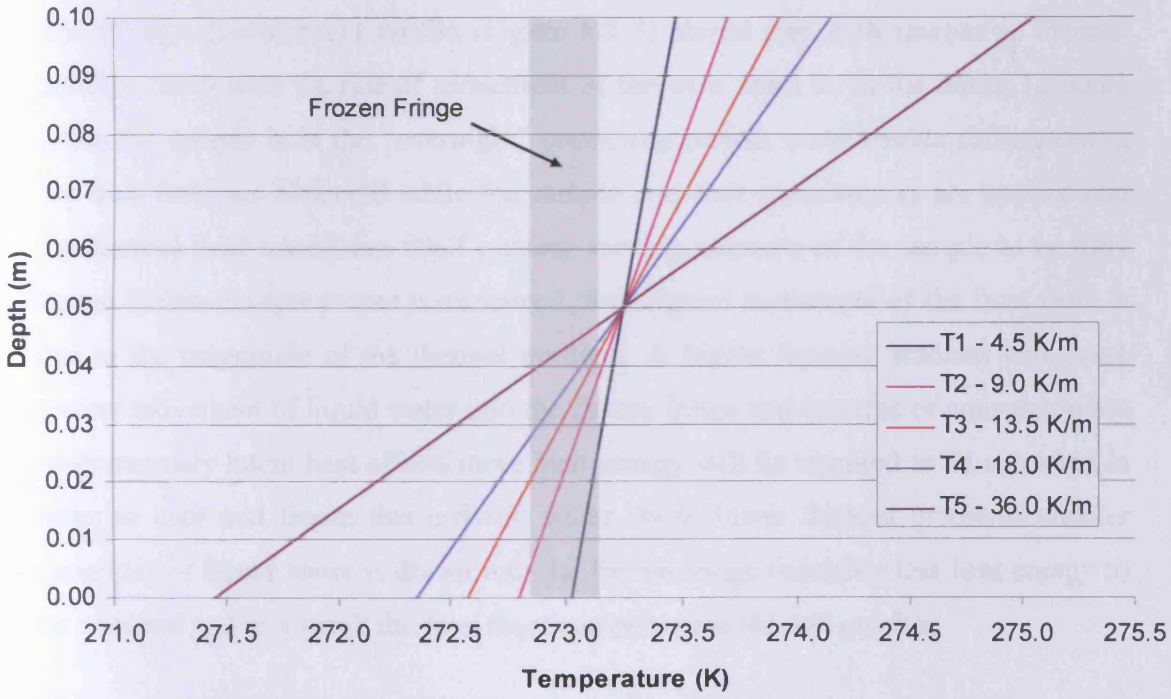

Figure 6.5-1 – Thermal gradient profile through sample after 12 hours.

6.5.2. Results and Conclusions

The magnitude of surface heave with varying thermal gradient is shown in Figure 6.5-2. Displacement profiles through the samples at the end of the simulations are shown in Figure 6.5-3.

As predicted; increasing the thermal gradient across the sample increases the magnitude of heave. Konrad and Morgenstern (1981) predicted a direct correlation of heave with thermal gradient; however this has not been reflected in the results. A reasonably linear variation of ice lens heave with thermal gradient is present but a gradual decrease in additional heave with each increase in thermal gradient is observed.

Konrad and Morgernstern (1981) assume that the heave due to ice lensing is governed by the thermal gradient. In this model the flow of moisture is governed by both thermal and pressure gradients (Equation 6.2-1) and it is known from earlier in this chapter that the pressure gradients developed due to phase change related density variations oppose the accumulation of moisture in a freezing soil. It would appear that with increasing thermal gradients the pressure term in the moisture equation has an increased opposing effect.

The 10 day displacement profile (Figure 6.5-3) shows that with increasing thermal gradient the slower the rate of movement of the frost front is. In the initial 12 hours while the sample is in the "overnight" tempering period, considerable differences in the frost front are observed while the sample end start temperatures are applied and the thermal field establishes itself causing varying amounts of the sample to be fully frozen before the test proper commenced. Subsequent movement of the frost front is due to the magnitude of the thermal gradient. A higher thermal gradient will cause greater movement of liquid water into the frozen fringe and because of convection but predominately latent heat effects more heat energy will be required to be extracted in order to cool and freeze this arriving water. With lower thermal gradients smaller quantities of liquid water is drawn into the frozen fringe requiring less heat energy to be removed and as a result the frost front can penetrate the soil quicker.

This exercise has shown that the model predicts that in a frost susceptible soil an increase in the thermal gradient will cause an increase in the magnitude of ice lensing. This is consistent with experimentally observed behaviour (Konrad and Morgernstern, 1981; Konrad and Nixon, 1994). Where frost susceptible soils are required to be frozen with a minimal amount of heave permitted a low thermal gradient should be considered and a longer freezing period used.

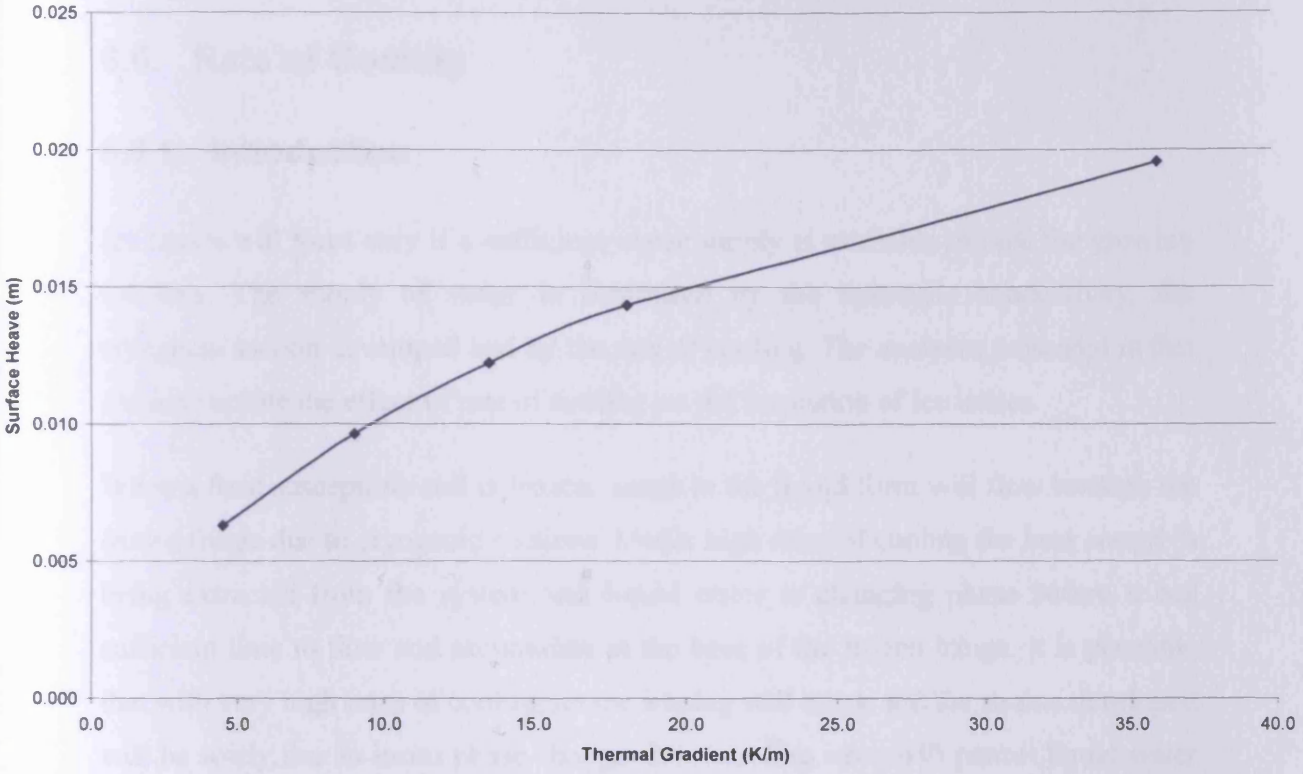

Figure 6.5-2 – Magnitude of surface heave with varying thermal gradient.

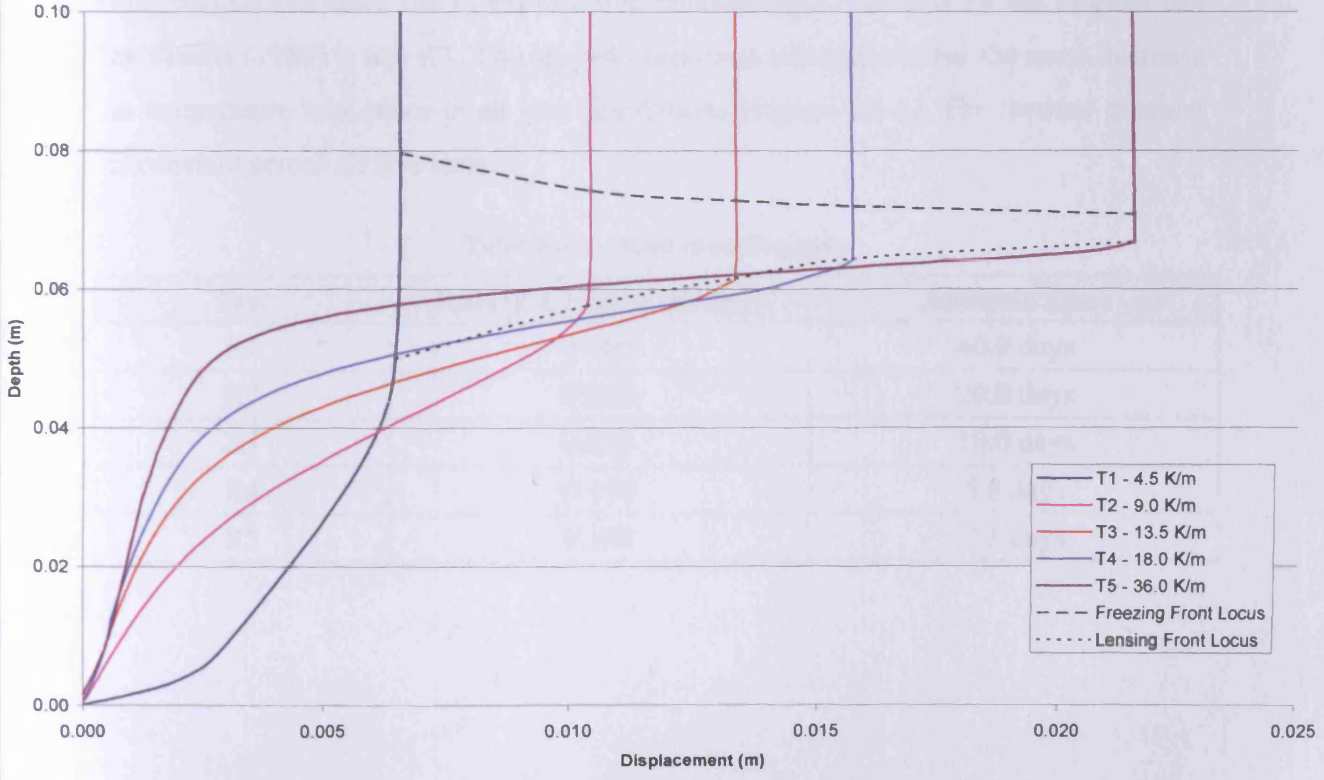

Figure 6.5-3 – 10 day displacement profiles through sample (variable thermal gradient).

6.6. Rate of Cooling

6.6.1. Introduction

Ice lenses will form only if a sufficient water supply is available to feed the growing ice lens. The supply of water is controlled by the hydraulic conductivity, the cryogenic suction developed and by the rate of cooling. The analyses presented in this section explore the effect of rate of cooling on the formation of ice lenses.

When a frost susceptible soil is frozen, water in the liquid form will flow towards the frozen fringe due to cryogenic suctions. Under high rates of cooling the heat energy is being extracted from the system and liquid water is changing phase before it has sufficient time to flow and accumulate at the base of the frozen fringe. It is plausible that with very high rates of cooling no ice lensing will occur and the strains developed will be solely due to insitu phase change. Low cooling rates will permit liquid water to flow and accumulate before it changes phase.

Five simulations were run to explore this relationship (Table 6.6-1); the original test by Penner (1986) is test R3. The analysis time was adjusted so that the same decrease in temperature took place in all five simulations (Figure 6.6-1). The thermal gradient is constant across all five tests.

Table 6.6-1 – Rate of cooling tests

Test	Rate of Cooling (K/day)	Analysis Time
R1	0.005	40.0 days
R2	0.010	20.0 days
R3	0.020	10.0 days
R4	0.050	5.0 days
R5	0.100	2.5 days

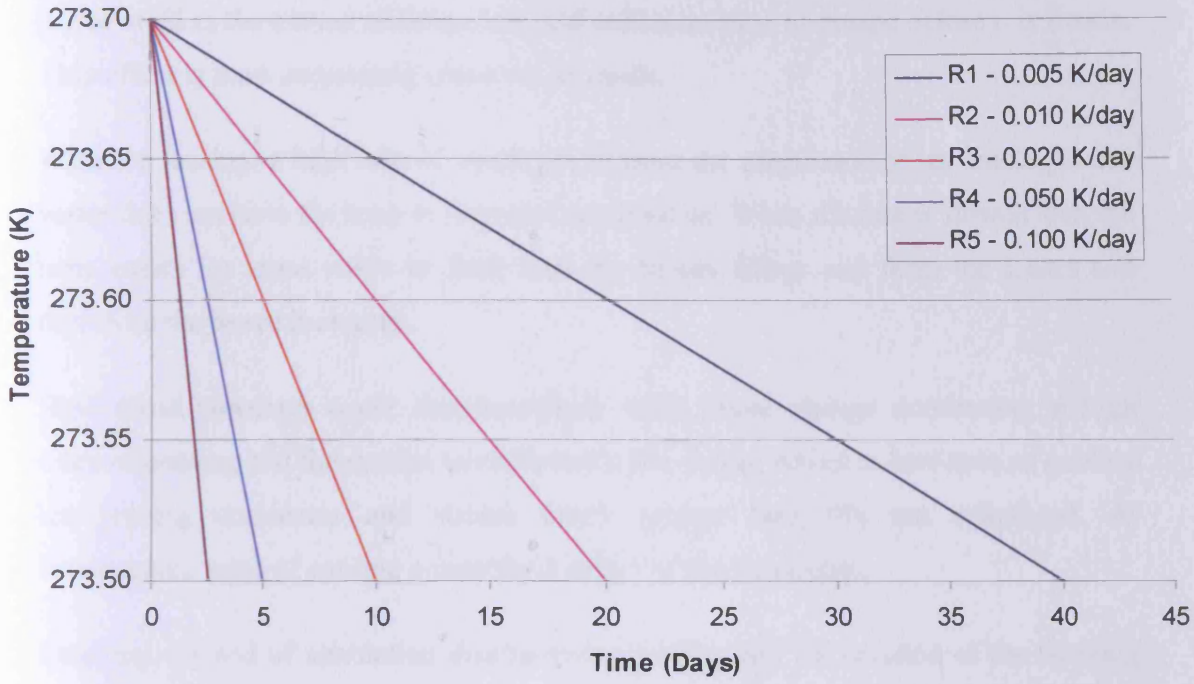

Figure 6.6-1 – Variation of surface temperature for rate of cooling tests

6.6.2. Results and Conclusions

The magnitude of surface heave with varying rates of cooling is shown in Figure 6.6-2. Displacement profiles through the samples at the end of the simulations are shown in Figure 6.6-3.

It is clear to see that as the rate of cooling is increased the magnitude of heave is significantly reduced (Figure 6.6-2). When saturated soils freeze not all the water will freeze in-situ and some water will be expelled during the freezing process. As a result of the expulsion of the water during the freezing process a 9% increase in the voids is not achieved.

There are two processes occurring simultaneously when a soil freezes; phase change and ice lensing. Considering the phase change component; a soil will achieve 9% strain if it is frozen very rapidly as the insitu pore water does not have time to flow away from the freezing zone before the latent heat is extracted and change phase occurs. When a slow rate of freezing is used, there is sufficient time for the moisture to escape and less strain is developed. At the extreme a sample may not exhibit any

heave at all as the excess moisture has had sufficient time to escape before it is frozen. This effect is most commonly observed in sands.

With ice lensing; a high rate of cooling will limit the magnitude of ice lensing as the water does not have the time to flow and accumulate. When the rate is slowed then the time exists for more water to flow into the frozen fringe and form ice lenses and therefore the heave increases.

Both these processes occur simultaneously with; phase change dominating at high rates of cooling and the system tends towards 9% strain; whilst at low rates of cooling ice lensing dominates and strains much greater than 9% are calculated. At intermediate rates of cooling a combined effect of the two exists.

Studying the end of simulation displacement profiles and the location of the freezing front and lensing front shows that the frost front tends towards a constant value as the cooling rate drops (Figure 6.6-3). This is due to the low rate analysis having more water coming in and needing more cooling and latent heat removed. Using equation 6.2-3 and the position of the frost fronts reveals that all tests have experienced a degree of ice lensing as the simulated heave exceeds that predicted by the in-situ pore water phase change alone.

This exercise has shown that the model predicts that in a frost susceptible soil a decrease in the rate of cooling will cause an increase in the magnitude of ice lensing. This is consistent with observed behaviour (Matsuoka 2001). Where frost susceptible soils are required to be frozen with a minimal amount of heave permitted a high rate of cooling should be considered.

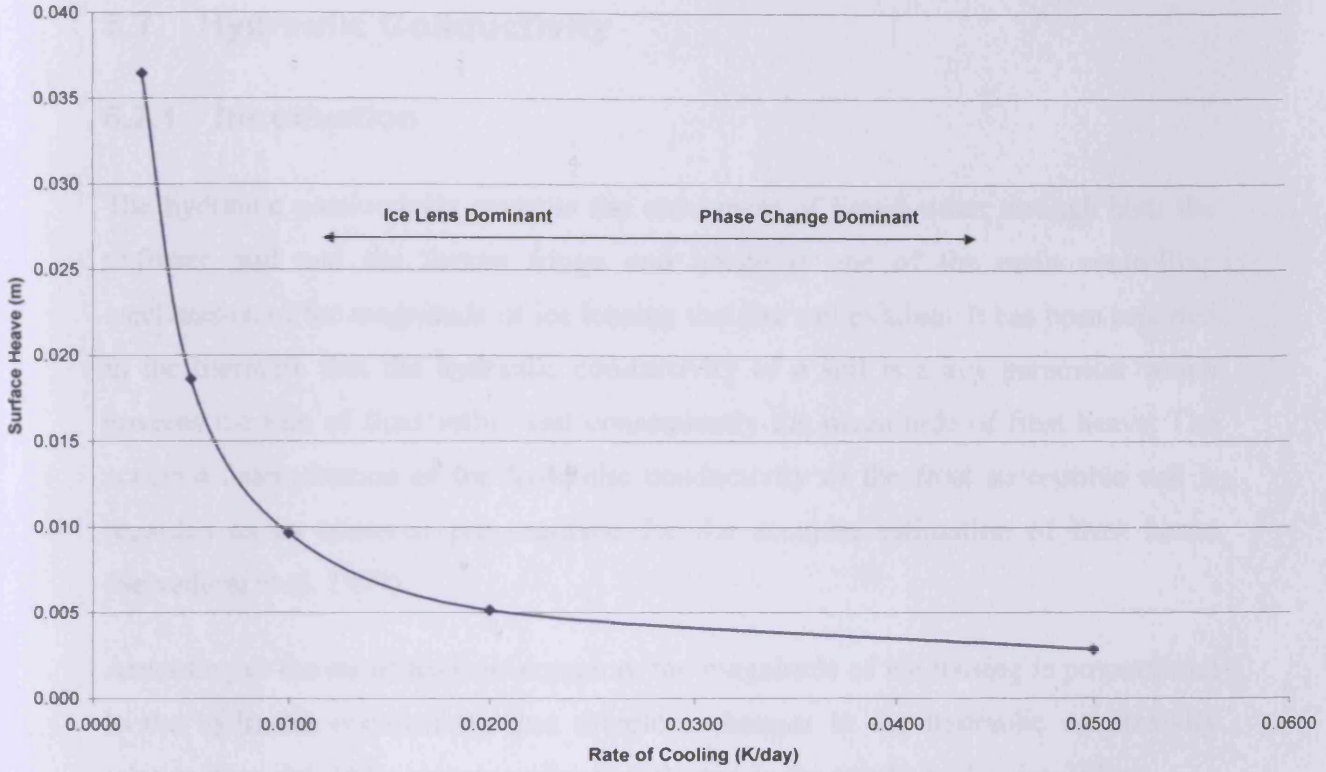

Figure 6.6-2– Magnitude of surface heave with varying rate of cooling.

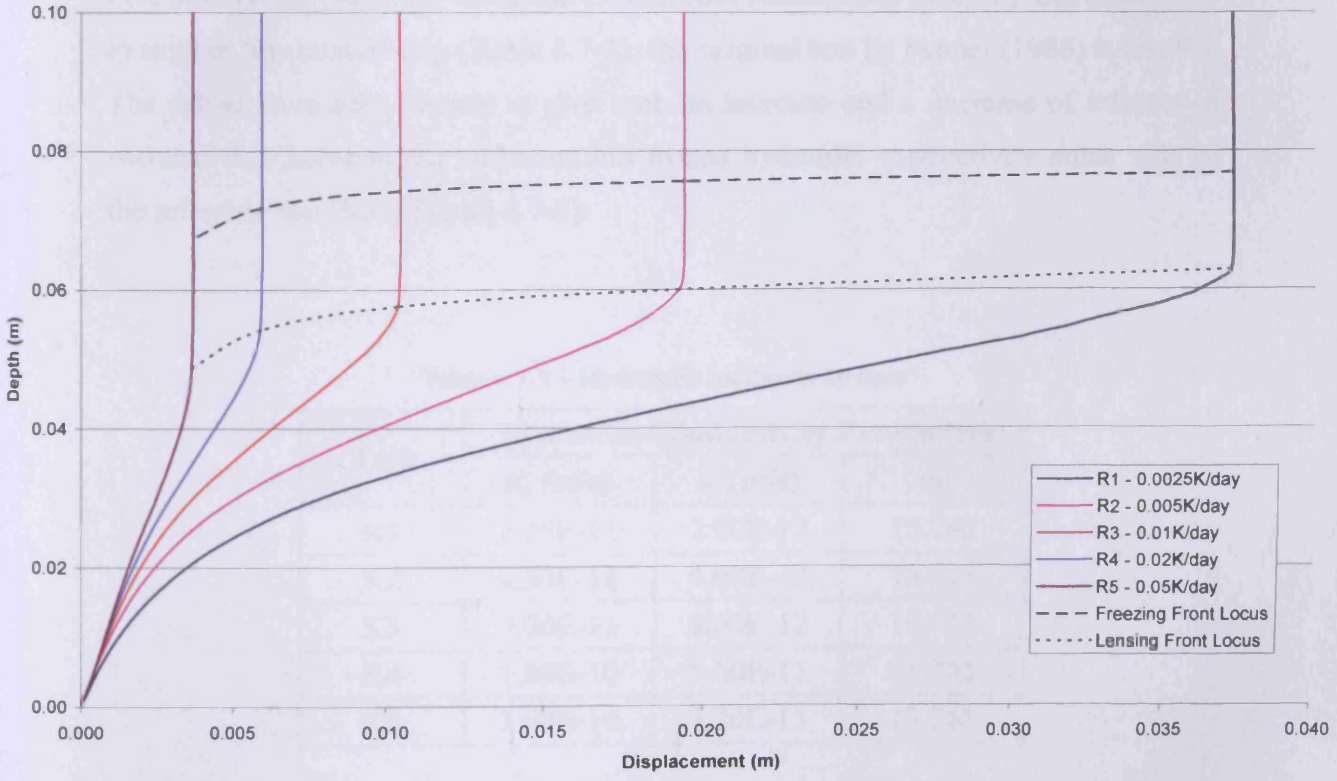

Figure 6.6-3 – End of simulation displacement profiles through sample (variable rate of cooling).

6.7. Hydraulic Conductivity

6.7.1. Introduction

The hydraulic conductivity controls the movement of liquid water through both the unfrozen soil and the frozen fringe and hence is one of the main controlling mechanisms of the magnitude of ice lensing that the soil exhibits. It has been reported in the literature that the hydraulic conductivity of a soil is a key parameter which governs the rate of fluid influx and consequently the magnitude of frost heave. The accurate determination of the hydraulic conductivity of the frost susceptible soil is regarded as an essential pre requisite for the accurate estimation of frost heave (Selvadurai et al. 1999).

According to the moisture flow equation, the magnitude of ice lensing is proportional to the hydraulic conductivity and therefore changes to the hydraulic conductivity relationships should be correspondingly reflected in the results of the simulation.

Five simulations were run using the exponential relationship given by Equation 6.3-3 to explore this relationship (Table 6.7-1); the original test by Penner (1986) is test K3. The values have been chosen to give both an increase and a decrease of a factor of two and four between the unfrozen and frozen hydraulic conductivity either side of the reference test (K3) (Figure 6.7-1).

Table 6.7-1 – Hydraulic conductivity tests

Test	Hydraulic Conductivity Parameters		
	k_u (m/s)	k_f (m/s)	α
K1	2.25E-11	2.00E-12	15.743
K2	4.50E-11	4.00E-12	15.743
K3	9.00E-11	8.00E-12	15.743
K4	1.80E-10	1.60E-11	15.743
K5	3.60E-10	3.20E-11	15.743

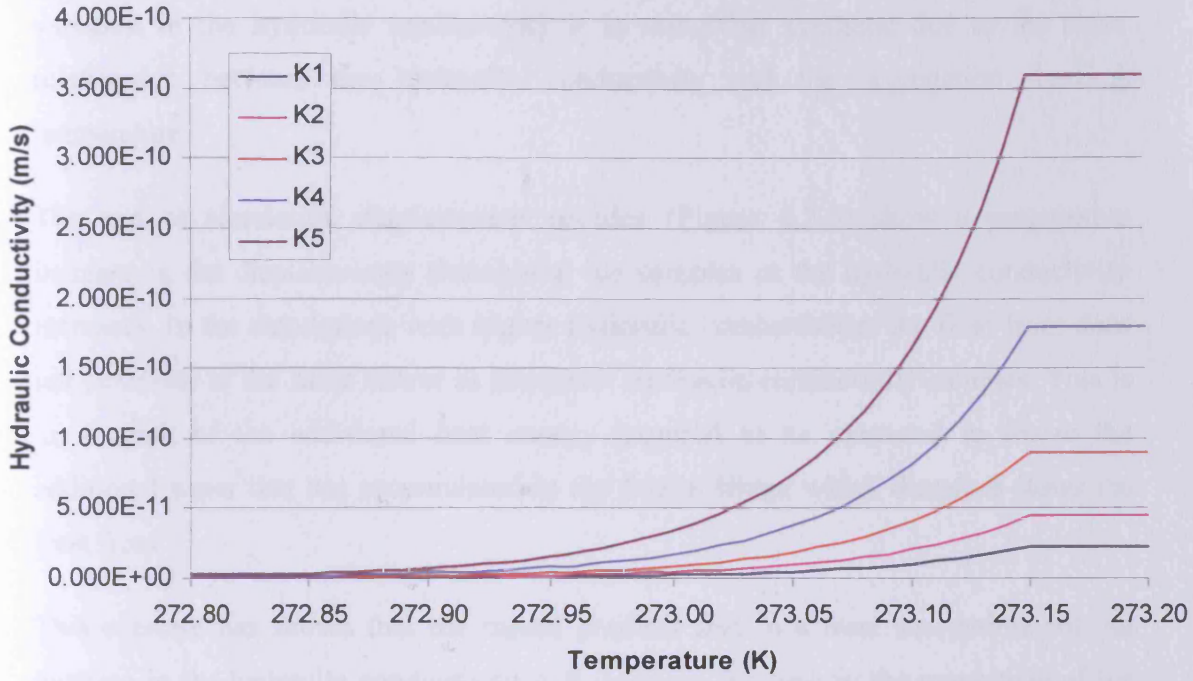

Figure 6.7-1 – Variation of hydraulic conductivity with temperature for simulations

6.7.2. Results and Conclusions

The magnitude of surface heave with varying unfrozen hydraulic conductivity is shown in (Figure 6.7-2). Displacement profiles through the samples at the end of the simulations are shown in Figure 6.7-3.

It can be seen from Figure 6.7-2 that relatively small changes in hydraulic conductivity can have pronounced effects on the magnitude of the heave predicted. The hydraulic conductivity is a key parameter in the prediction of heave due to ice lensing yet these variations are comparable with the acceptable errors of laboratory based tests that are used to determine this parameter in the first place. Caution must be exercised when this parameter is determined, particularly with the unfrozen hydraulic conductivity and the segregation freezing temperature.

The range of simulated hydraulic conductivities span less than two orders of magnitude but the differences in the quantity of heave is quite considerable. The segregation freezing temperature of a soil would also alter as the hydraulic conductivity changes and the combined effect of the two would ultimately determine the magnitude of heave. Whilst this exercise shows how sensitive the heave is to

variation in the hydraulic conductivity it is somewhat synthetic due to the close relationship between the hydraulic conductivity and the segregation freezing temperature.

The end of simulation displacement profiles (Figure 6.7-3) show a progressive increase in the displacements throughout the samples as the hydraulic conductivity increases. In the simulations with higher hydraulic conductivities the frost front does not penetrate to the same extent as the lower hydraulic conductivity samples. This is as a result of the additional heat energy required to be extracted to freeze the additional water that has accumulated in the frozen fringe which therefore slows the frost front.

This exercise has shown that the model predicts that in a frost susceptible soil an increase in the hydraulic conductivity will cause an increase in the magnitude of ice lensing. This is consistent with experimentally observed behaviour (Konrad and Morgenstern, 1980). As the hydraulic conductivity is a material property it is not possible to control this factor to reduce the heave when freezing frost susceptible soils. Factors such as the rate of freezing, thermal gradient and stress level should be considered to control the magnitude of heave when the soil type cannot be changed.

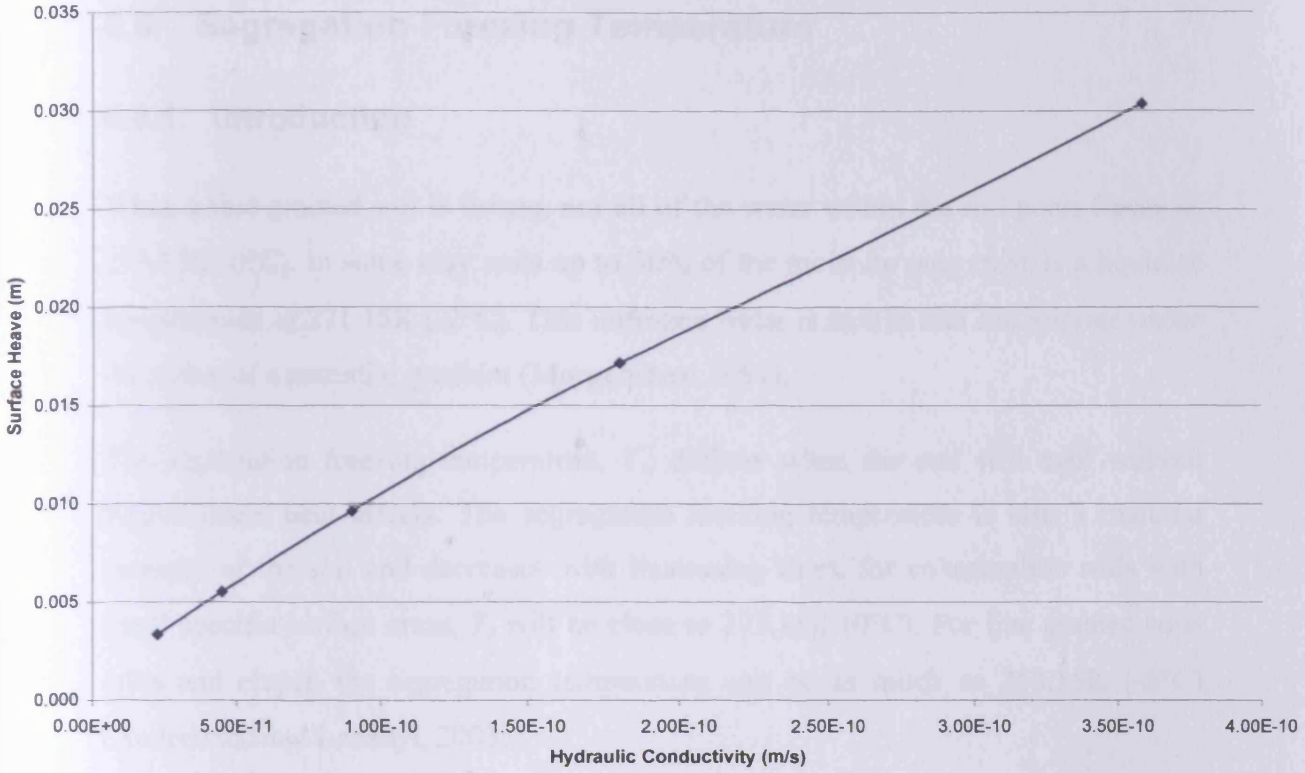

Figure 6.7-2– Magnitude of surface heave with varying hydraulic conductivity.

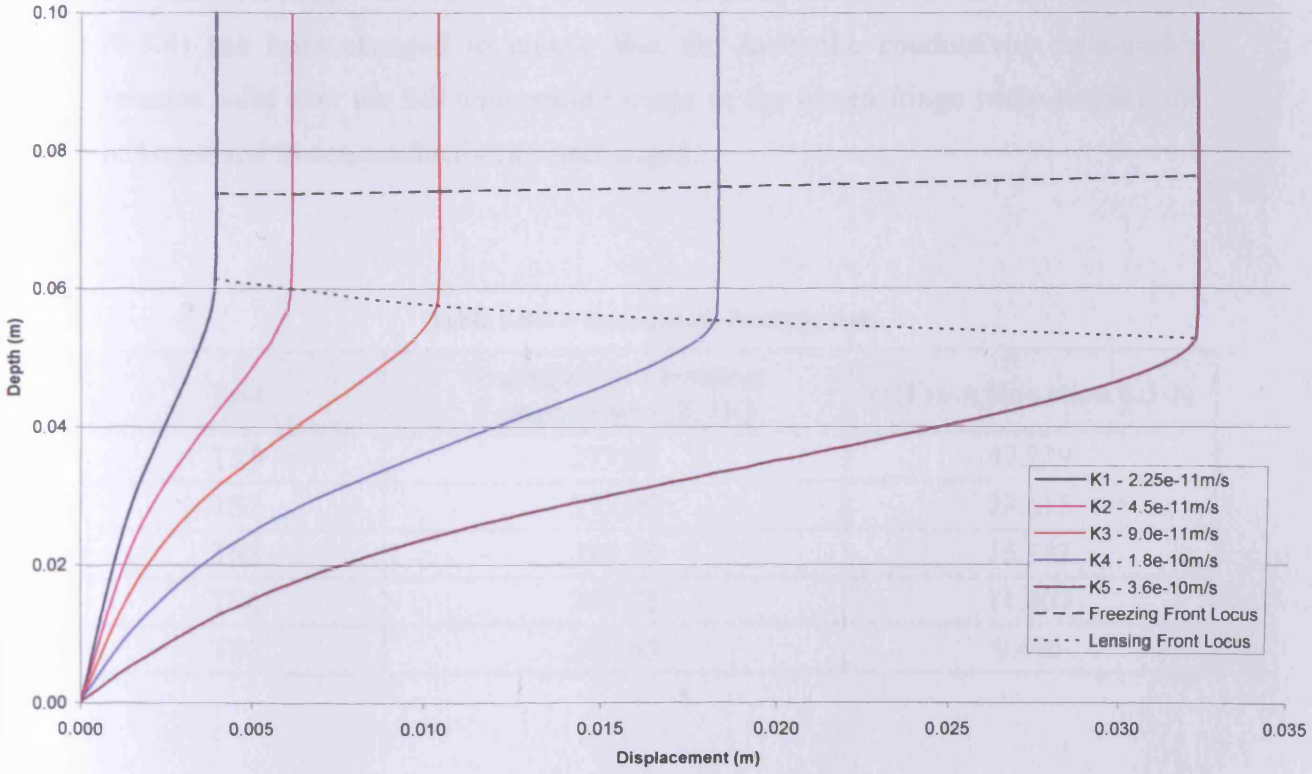

Figure 6.7-3– 10 day displacement profiles through sample (variable hydraulic conductivity).

6.8. Segregation Freezing Temperature

6.8.1. Introduction

When a fine grained soil is frozen, not all of the water within the soil pores freeze at 273.15K (0°C). In some clay soils up to 50% of the moisture may exist as a liquid at temperatures of 271.15K (-2°C). This unfrozen water is mobile and can migrate under the action of a potential gradient (Morgenstern 1981).

The segregation freezing temperature, T_s, defines when the soil will cool without further latent heat effects. The segregation freezing temperature is also a material property of the soil and decreases with increasing fines, for cohesionless soils with small specific surface areas, T_s will be close to 273.15K (0°C). For fine grained soils (silts and clays), the segregation temperature can be as much as 268.15K (-5°C) (Andersland and Ladanyi, 2003).

Five simulations were run to explore this relationship (Table 6.8-1); the original test by Penner (1986) is test TS3. The value of α in the hydraulic conductivity relationship (6.3-4) has been changed to ensure that the hydraulic conductivity relationship remains valid over the full temperature range in the frozen fringe while keeping the unfrozen and frozen conductivities unchanged.

Table 6.8-1 – Segregation freezing tests

Test	Segregation Freezing Temperature, T_s (K)	α (From Equation 6.3-3)
TS1	273.05	47.229
TS2	272.95	23.615
TS3	272.85	15.743
TS4	272.75	11.807
TS5	272.65	9.446

6.8.2. Results and Conclusions

The magnitude of surface heave with varying segregation temperature is shown in Figure 6.8-1. Displacement profiles through the samples at the end of the simulations are shown in Figure 6.8-2.

Figure 6.8-1 shows calculated heave behaviour with changing segregation freezing temperature and allows a comparison with expected patterns of behaviour to be made. Those soils with segregation freezing temperatures tending towards 273.15K (0°C) exhibit less heave, consistent with observations of the freezing of sands and similar cohesionless soils where little or no heave is observed (Andersland and Ladanyi, 2003). With increasing fines the segregation temperature decreases and the associated heave respectively increases as silt and clay types are simulated.

While decreasing the segregation freezing temperature increases the heave it should be noted that soils with very low segregation freezing temperatures, i.e. clays, do not exhibit an increase in heave when frozen. Soils such as clays which have very low segregation freezing temperatures also have low hydraulic conductivities and while there is a larger frozen fringe which creates the potential for flow, the hydraulic conductivity does not permit the flow of liquid water into the fringe which is also required for the accumulation of water and subsequent heave.

Sands; whilst having segregation freezing temperatures close to 273.15K (0°C) do not create the potentials that are needed to draw the moisture into the frozen fringe. Despite the high hydraulic conductivity of sands and the ability for large quantities of moisture to flow the heave does not result because the potential to accumulate water in the frozen fringe is much weaker.

Silts lie in between the sands and clays and exhibit the greatest amount of ice lensing due to the combined effect of segregation freezing temperature and hydraulic conductivity, a suitably sized fringe is able to create the potential for moisture to flow and the hydraulic conductivity permits the flow to occur. The result under such conditions is large accumulations of ice within the soil and why silts are particularly frost susceptible.

The 10 day displacement profiles (Figure 6.8-2) show a much greater depth of frost penetration in the sample with the smallest frozen fringe due to the smaller quantity of excess water accumulating and latent heat change required. It can also be seen that for each uniform decrease in the segregation freezing temperature the additional heave progressively reduces for each step.

This exercise has shown that the model predicts that in a frost susceptible soil a decrease in the segregation freezing temperature will cause an increase in the magnitude of ice lensing. This is consistent with experimentally observed behaviour (Konrad and Morgenstern, 1981). As the segregation freezing temperature is a material property it is not possible to control this factor to reduce the heave when freezing frost susceptible soils. Factors such as the rate of freezing, thermal gradient and stress level should be considered to control the magnitude of heave when the soil type cannot be changed.

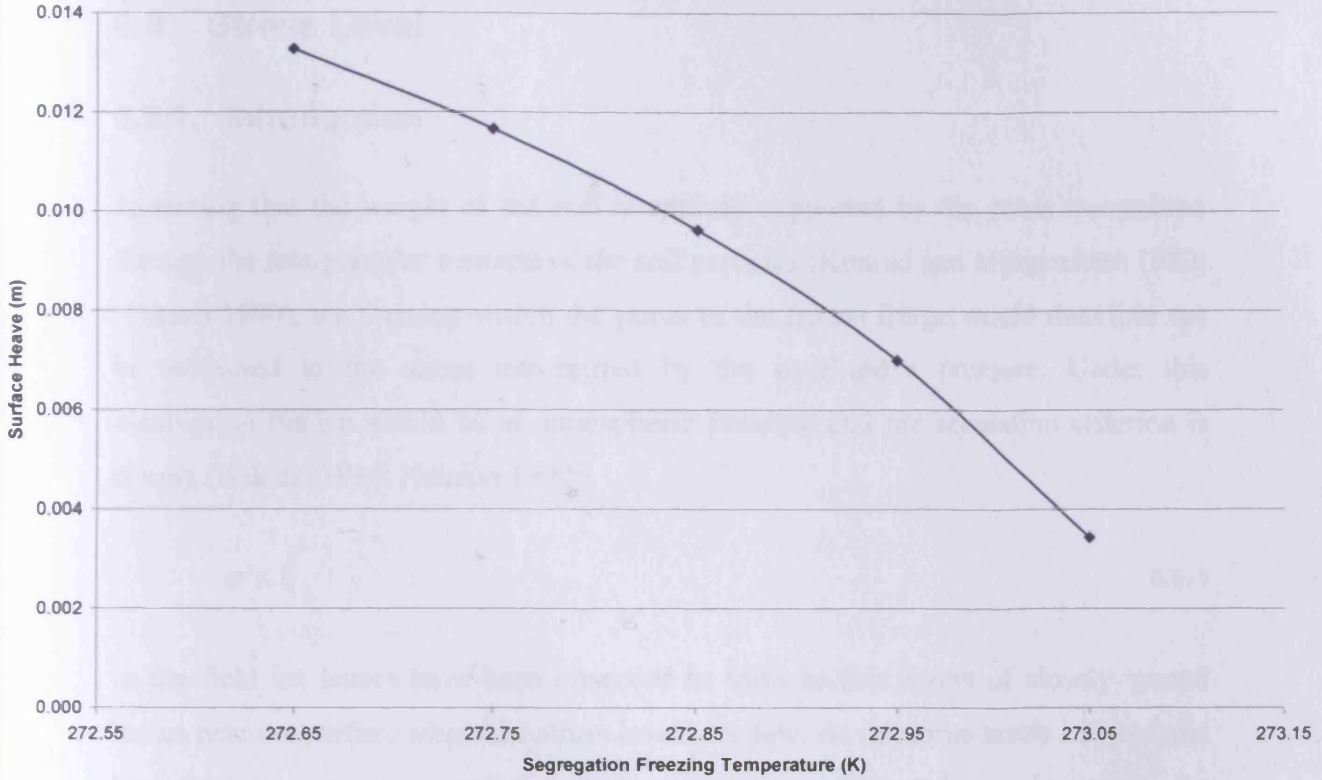

Figure 6.8-1– Magnitude of surface heave with varying segregation freezing temperature.

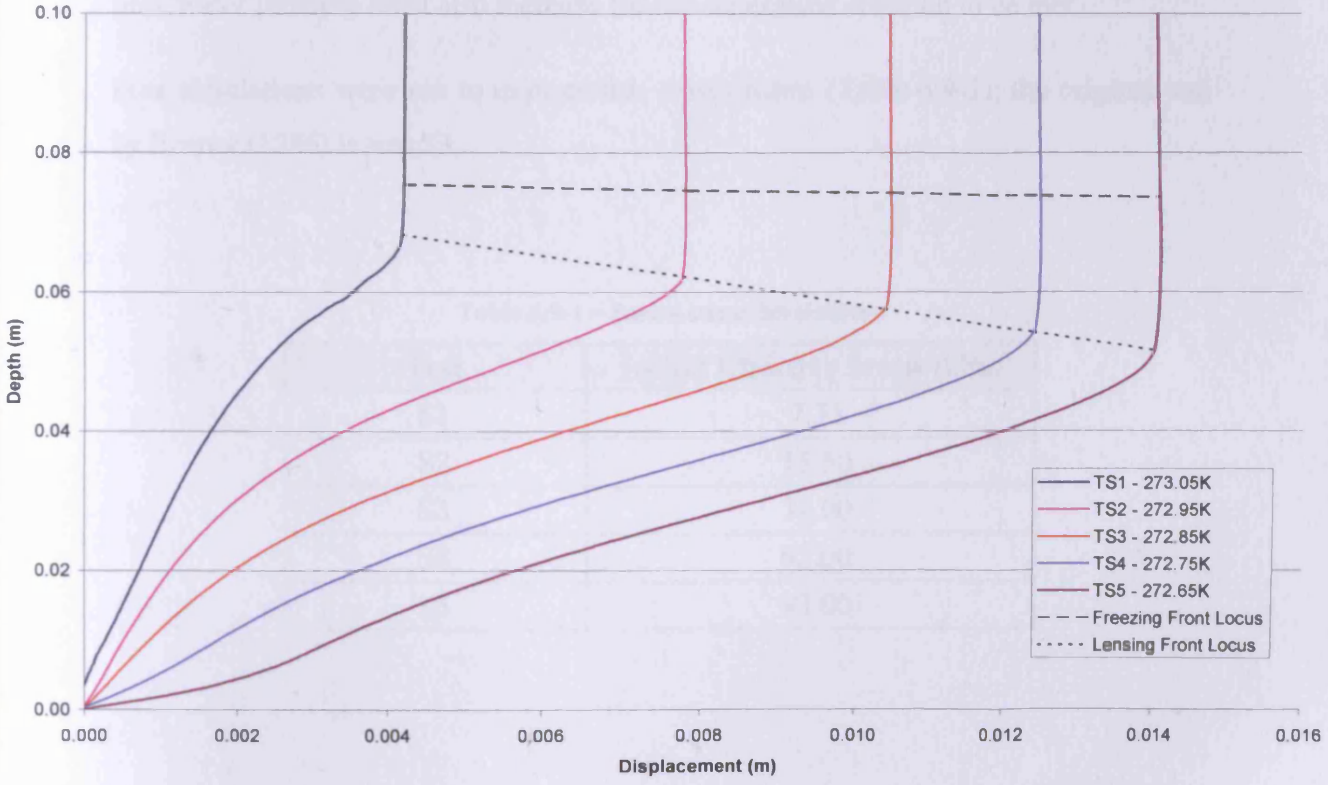

Figure 6.8-2– 10 day displacement profiles through sample (variable segregation freezing temperature).

6.9. Stress Level

6.9.1. Introduction

Assuming that the weight of the soil is entirely supported by the stress transmitted through the intergranular contacts of the soil particles (Konrad and Morgenstern 1980; Nakano 1990), ice forming within the pores of the frozen fringe would therefore not be subjected to the stress transmitted by the overburden pressure. Under this assumption the ice would be at atmospheric pressure and the separation criterion is simply (Nakano 1986; Nakano 1990):

$$\sigma' \leq 0 \qquad \textbf{6.9-1}$$

In the field ice lenses have been observed to form as thin layers of closely spaced lenses near the surface where the stress levels are low. As the stress levels increase the lens thickness increases and the distance between adjacent lenses increases. An increase in effective stress would generally retard the formation of ice lenses as the pore water pressure must also increase for the separation criterion to be met.

Five simulations were run to explore this relationship (Table 6.9-1); the original test by Penner (1986) is test S3.

Table 6.9-1 – Insitu stress level tests

Test	Initial Effective Stress (kPa)
S1	7.75
S2	15.50
S3	31.00
S4	62.00
S5	93.00

6.9.2. Results and Conclusions

The magnitude of surface heave with varying effective stress is shown in Figure 6.9-1. Displacement profiles through the samples at the end of the simulations are shown in Figure 6.9-2.

As the effective stress level is increased a corresponding decrease in heave can be seen in the surface heave profile (Figure 6.9-1). At low initial effective stresses the soil is softer and so it is easier for ice lenses to form. As the effective stress level increases the soil becomes stiffer and so the pore water pressure must increase to a greater extent for ice lensing to occur. It can be noted that under high initial effective stresses the heave is still greater than the in-situ phase change alone.

The displacement profiles at the end of the simulation (Figure 6.9-2) show that even with a high effective stress level in the soil, ice lensing is still taking place and the forces generated by freezing can be quite substantial. Observations based on the weight of buildings known to have been lifted by frost heaving soil indicate ice heaving forces in excess of 760 kPa being developed (Andersland and Ladanyi 2003).

This exercise has shown that the model predicts that in a frost susceptible soil an increase in the initial effective stress will cause a decrease in the magnitude of ice lensing. This is consistent with experimentally observed behaviour (Konrad and Morgenstern, 1982; Penner and Ueda, 1977). Where frost susceptible soils are required to be frozen with a minimal amount of heave permitted a high initial effective stress should be considered e.g. the use of surcharge loading prior to freezing.

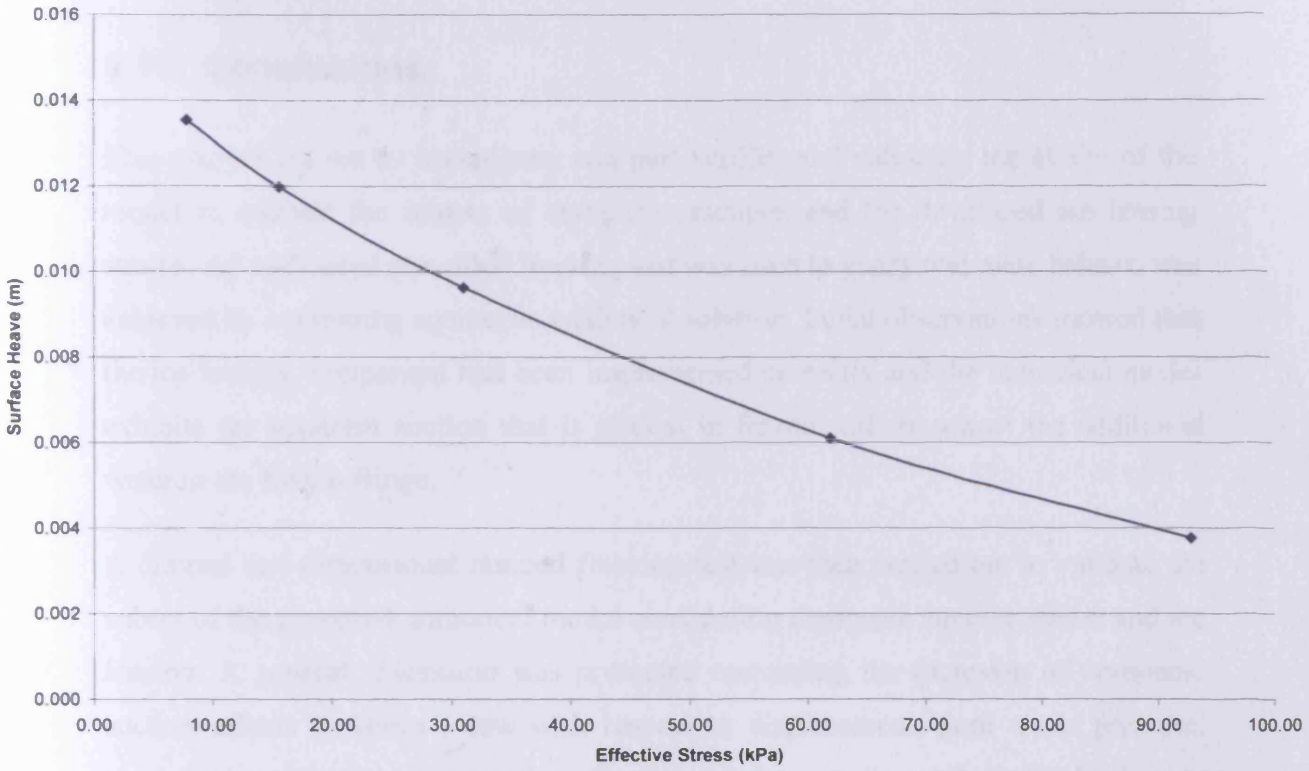

Figure 6.9-1– Magnitude of surface heave with varying segregation freezing temperature.

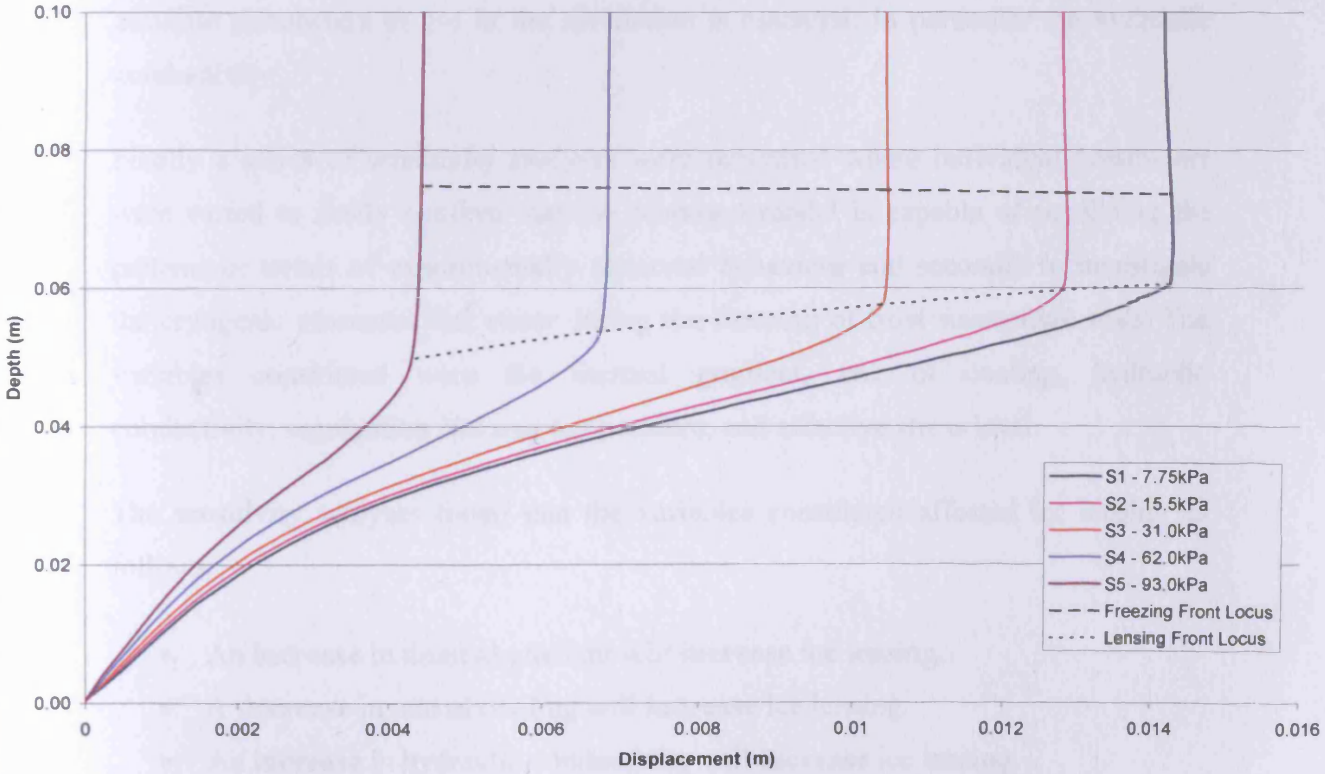

Figure 6.9-2– 10 day displacement profiles through sample (variable effective stress).

6.10. Conclusions

This chapter set out to investigate, and part verifies and validates, the ability of the model to include the impact of cryogenic suctions and the developed ice lensing strains. An undrained one sided freezing test was used to verify that mass balance was achieved by comparing against an analytical solution. Initial observations showed that the ice lensing component had been implemented correctly and the numerical model exhibits the apparent suction that is critical in frozen soils to attract the additional water to the frozen fringe.

A drained one dimensional ramped freezing test was then carried out to validate the subset of the proposed numerical model considering cryogenic suction effects and ice lensing. A general discussion was presented comparing the inclusion of cryogenic suction effects to Darcy's law with respect to displacement, pore water pressure, temperature, effective stress and void ratio and the experimental results by Penner (1986). The results of the analysis showed that the proposed model is capable of simulating freezing with ice lensing in a frost susceptible soil. The determination of accurate parameters to use in the simulation is essential; in particular the hydraulic conductivity.

Finally a series of sensitivity analyses were presented where individual parameters were varied to firstly confirm that the proposed model is capable of predicting the patterns or trends of experimentally observed behaviour and secondly to investigate the cryogenic processes that occur during the freezing of frost susceptible soils. The variables considered were the thermal gradient, rate of cooling, hydraulic conductivity, segregation freezing temperature, and effective stress level.

The sensitivity analyses found that the variables considered affected ice lensing as follows:

- An **increase** in thermal gradient will **increase** ice lensing.
- A **decrease** in rate of cooling will **increase** ice lensing.
- An **increase** in hydraulic conductivity will **increase** ice lensing.
- A **decrease** in segregation freezing temperature will **increase** ice lensing.
- A **decrease** in effective stress level will **increase** ice lensing.

In each case these trends of behaviour match the experimentally observed trends and patterns that were discussed in Chapter 2.

When control over the freezing process is possible the thermal gradient, rate of cooling and effective stress level can be manipulated to reduce the magnitude of ice lensing. A particular application where this knowledge would be used is in ground freezing applications where the ground is to be frozen with minimal disturbance to surrounding structures.

The hydraulic conductivity and segregation temperature are material properties and as such are more difficult to change to control the magnitude of ice lensing. It is generally not feasible to remove large volumes of soil; however there may be situations where this is the most cost effective option when constructing in frost susceptible soils. Certainly the knowledge on how these parameters perform is indispensable.

It can therefore be concluded that the development of ice lensing into the theoretical formulation has been correctly implemented into the finite element code COMPASS. The proposed model is capable of representing coupled flow and deformation processes including ice lensing in saturated freezing soils.

6.11. References

Andersland, O. B. and Ladanyi, B. 2003. "Frozen ground engineering". 2nd Edition. New York; Chichester: Wiley.

Barnes, G 2000. "Soil Mechanics – Principles and Practice". 2nd Edition. Macmillan Press LTD, London.

Dallimore, S.R., and Williams, P.J., 1984. "Pipelines and frost heave" A Seminar. Carleton University, Ottawa, **75**.

Harlan, R. L. and Nixon, J. F. 1978. "Ground thermal regime" In: *Geotechnical engineering for cold regions*. O. B. Andersland and D. M. Andersland (Eds), McGraw Hill. 103-150.

Horiguchi, K. and Miller, R.D. 1983. "Hydraulic conductivity functions of frozen materials". *Proceedings of the 4th International Conference on Permafrost*, 504-508.

Konrad, J. M. and Morgenstern, N. R. 1980. "A mechanistic theory of ice lens formation in fine-grained soils". *Canadian Geotechnical Journal* **17**, 473-486.

Konrad, J. M. and Morgenstern, N. R. 1981. "The segregation potential of a freezing soil". *Canadian Geotechnical Journal* **18**, 482-491.

Konrad, J.M. and Morgenstem, N.R., 1982. "Effects of applied pressure on freezing soils". *Canadian. Geotech. Journal*, **19,** 494-505.

Konrad J. M. and Nixon J. F. 1994 "Frost heave characteristics of a clayey silt subjected to small temperature gradients" *Cold Regions Science and Technology*, **22,** 299-310.

Martin, R. T. 1959 "Rhythmic ice bonding in soil" *Highway Research Record* **218**, 11-23.

Matsuoka, N. 2001 "Solifluction rates, processes and landforms: a global review" *Earth-Science Reviews*, **55**, 107-134.

Morgenstern, N. R. 1981. "Geotechnical engineering frontier resource development." *Geotechnique* **31(3)**, 305-365.

Nakano, Y. 1986. "On the stable growth of segregated ice in freezing soil under negligible overburden pressure". *Advances in Water Resources* **9(4)**, 223-235.

Nakano, Y. 1990. "Quasi-steady problems in freezing soils: I. Analysis on the steady growth of an ice layer." *Cold Regions Science and Technology* **17**, 207-226.

O'Neill, K. and Miller, R. D. 1985. "Exploration of a rigid ice model of frost heave." *Water Resources Research* **21(3)**, 281-296.

Penner, E. and Ueda, T. 1977 "The dependence of frost heaving on load application – preliminary results". *Proceedings of the International Symposium of Frost Action in Soils: Lulea.* **1,** 92-101.

Penner, E. 1986 "Aspects of Ice Lens Growth in Soils". *Cold Regions Science and Technology* **13**, 91-100.

Selvadurai, A. P. S., Hu, J. and Konuk, I. 1999 "Computational Modelling of Frost Heave Induced Soil – Pipeline Interaction. 1 Modelling of Frost Heave". *Cold Regions Science and Technology* **29**, 215-228.

Shen, M., and Ladanyi, B. 1987 "Modelling of Coupled Heat, Moisture and Stress Field in Freezing Soil". *Cold Regions Science and Technology* **14**, 237-246.

Shen, M. Ladanyi, B. 1991. "*Soil Pipeline Interaction During Frost Heave Around a Buried Chilled Pipeline*". Cold Regions Engineering, ASCE 6th International Speciality Conference. ASCE Publications, New York. 11-21.

Chapter 7

Simulation of a Freezing and Thawing Experiment

7.1. Introduction

This chapter presents the numerical simulation of a freezing and thawing experiment which was undertaken at the CNRS Centre de Géomorphologie in Caen, France (Harris 2007, personal communication). It should be clearly noted that the author of this study did not contribute to or have any involvement in the experimental work. The large scale experiment was designed to measure and record the timing and rate of: a) frost penetration, b) surface frost heaving, c) thaw penetration, d) pore water pressure changes and e) downslope surface soil displacements (Harris et al, 1996).

The numerical simulation undertaken in this chapter investigates the timing and rate of: a) frost penetration, b) surface frost heaving, c) thaw penetration, and d) pore water pressure changes. However the downslope surface soil displacements are not considered. In addition to the above specified timings and rates, the development of the deformation field within the soil is also considered.

Section 7.2 details the experimental setup of the work undertaken at the CNRS Centre de Géomorphologie. Material parameters are presented in Section 7.3 with the numerical simulation detailed in Section 7.4. Simulated profiles of temperature, pore water pressure and displacement with time are presented and discussed in Section 7.5.

Profiles with depth of temperature, pore water pressure, displacement, effective stress and void ratio for 5 distinct stages in the simulation are also presented, namely; just frozen, partially frozen (freezing), fully frozen, partially frozen (thawing), and thawed.

Finally conclusions from the simulation of the freezing and thawing experiment are drawn in Section 7.6.

7.2. Experimental Setup

The experiment was conducted on a slope of 12° which was constructed using a 5m x 1.2m x 0.35m strip of test soil. The test soil was laid over a 100mm thick layer of course sand which formed the sand basal layer and was connected to a metered water supply at the crest of the slope and was permitted to drain at the foot. A compacted loam was used to form the foundation of the slope which supported the basal drainage zone and test soil (Figure 7.2-1). The test soil was added in small layers, compacted and raked to help prevent formation of discontinuities along which ice segregation may occur. A double layer of polythene was placed between the soil and the polystyrene outer confining baffles. The polythene was lubricated with silicon oil to minimise the friction on the sides and to allow the slope to be more accurately modelled as an infinite slope.

No attempt was made during the experimental programme to remove the soil accumulating at the base of the slope or replace the soil moving away from the top.

Temperature sensors and Druck miniature pore pressure transducers filled with antifreeze were installed at depths of 0.5m 0.15m and 0.25m to monitor the soil temperature and pore water pressure respectively. Frost heave and downslope displacements were monitored using linear voltage displacement transformers (LVDTs) mounted on a slotted steel strip and supported by a wooden beam (Figure 7.2-1). All instruments were scanned at half hourly intervals and recorded using a PC controlled data logging system.

The soil was allowed to wet up from the basal sand layer by introducing water at the top of the slope. Once the soil had become saturated the slope was then frozen from the top down by covering the soil with a refrigerated lid. The air temperature was gradually lowered to around - 10°C. During the soil freezing phases an open hydraulic system was maintained. The water supply was shut off once the slope had fully frozen so that the thaw moisture content would be determined purely by the in-situ ice content.

Removal of the refrigerated lid allowed the soil to thaw from the surface downwards at ambient laboratory temperatures. The ambient temperatures varied from around 15°C in the summer to 5°C in winter.

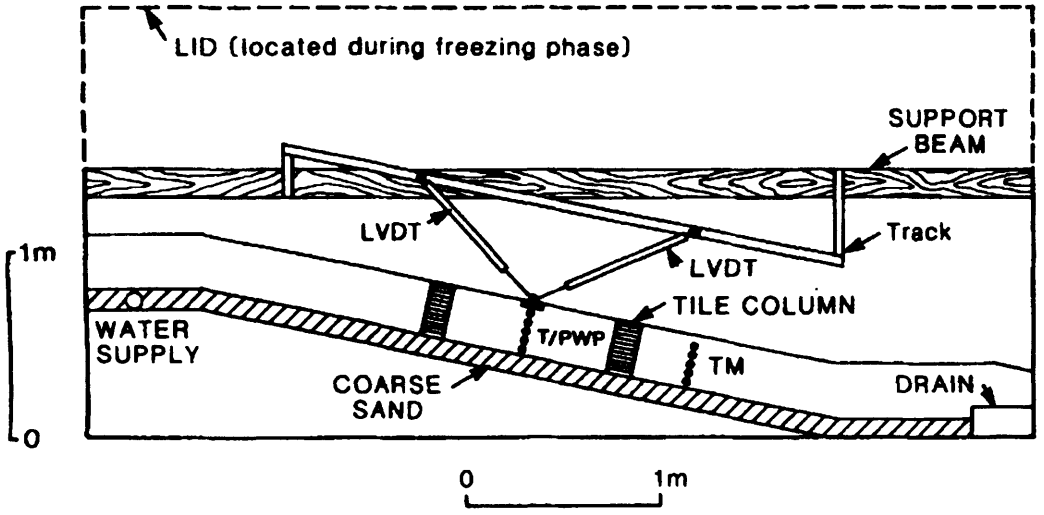

Figure 7.2-1 – Diagram of apparatus; TM, thermistors; T, semiconductor temperature sensors; PWP. Porewater pressure transducers (Harris et. al 1996)

7.3. Material Parameters

Detailed material parameters for the test conducted by Harris et al. (2001) were not reported in the author's paper. The soil used in the experiment comprised of a natural soil collected from a quarry face in Vire, Normandy, France. Vire silt was derived from Precambrian slate and consisted of a sandy silt. The soil was chosen for its good analogues for many arctic and alpine solifluction soils (Harris et al. 1997).

Selected geotechnical parameters for Vire silt are given in Table 7.3-2 (Harris et al 2001).

Table 7.3-1 – Test Soil Geotechnical Properties (Harris et al 2001)

Property	Value
% clay	15
% silt	72
% sand	13
LL (%)	31
PL (%)	18
Saturated bulk density (Mg/m^2)	2.04
C_v (m^2/yr)	64
ϕ' (degrees)	31

Representative material parameters for heat capacity, density and thermal conductivity used in the test are given in Table 7.3-2 based on Harlan and Nixon (1978).

Table 7.3-2 – Thermal Constants Used in Calculation

	Soil	Liquid	Ice
c ($J/m^3°C$)	1000	4180	2050
ρ (kg/m^3)	2500	1000	917
λ ($W/m°C$)	1.00	0.58	2.22

The porosity of the soil was estimated using the saturated bulk density (Table 7.3-1) and assumed solid and liquid densities (Table 7.3-2). Using the relationship in equation 7.3-1 and these values gives a porosity of $n = 0.31$.

$$\rho_u = (1-n)\rho_s + n\rho_l \qquad \textbf{7.3-1}$$

A constant value is assumed for Poisson's ratio (Selvadurai et al, 1999a).

$$v = 0.3 \qquad \textbf{7.3-2}$$

The elastic stiffness parameter of the soil, κ, is calculated based on data presented by Selvadurai et al (1999a) for a similar silty frost susceptible soil, as

$$\kappa = 0.005127 \qquad \textbf{7.3-3}$$

The hardening parameter, p_0, is set a high value to ensure that the material remains in the elastic region of the stress space.

As no information about the saturated unfrozen and frozen hydraulic conductivity of Vire silt is available, the hydraulic conductivity relationship for a similar soil, a Caen silt has been used. Estimates for the hydraulic conductivity applicable to Caen silt are as follows; (Shen and Ladanyi, 1991)

$$k = \begin{cases} 1.075\times10^{-9}\, e^{23.99T} & -0.3°C < T < T_0 \\ 8.0499\times10^{-13} & T \le -0.3°C \end{cases} m/\sec \qquad \textbf{7.3-4}$$

A grain size analysis indicated that Caen silt consists of 13%–20% clay, 65%–75% silt and 10%–20% sand (Selvadurai et al. 1999b). As the clay, silt and sand fractions for Caen silt are close to the Vire silt the use of the hydraulic conductivity relationship for Caen silt is an acceptable assumption.

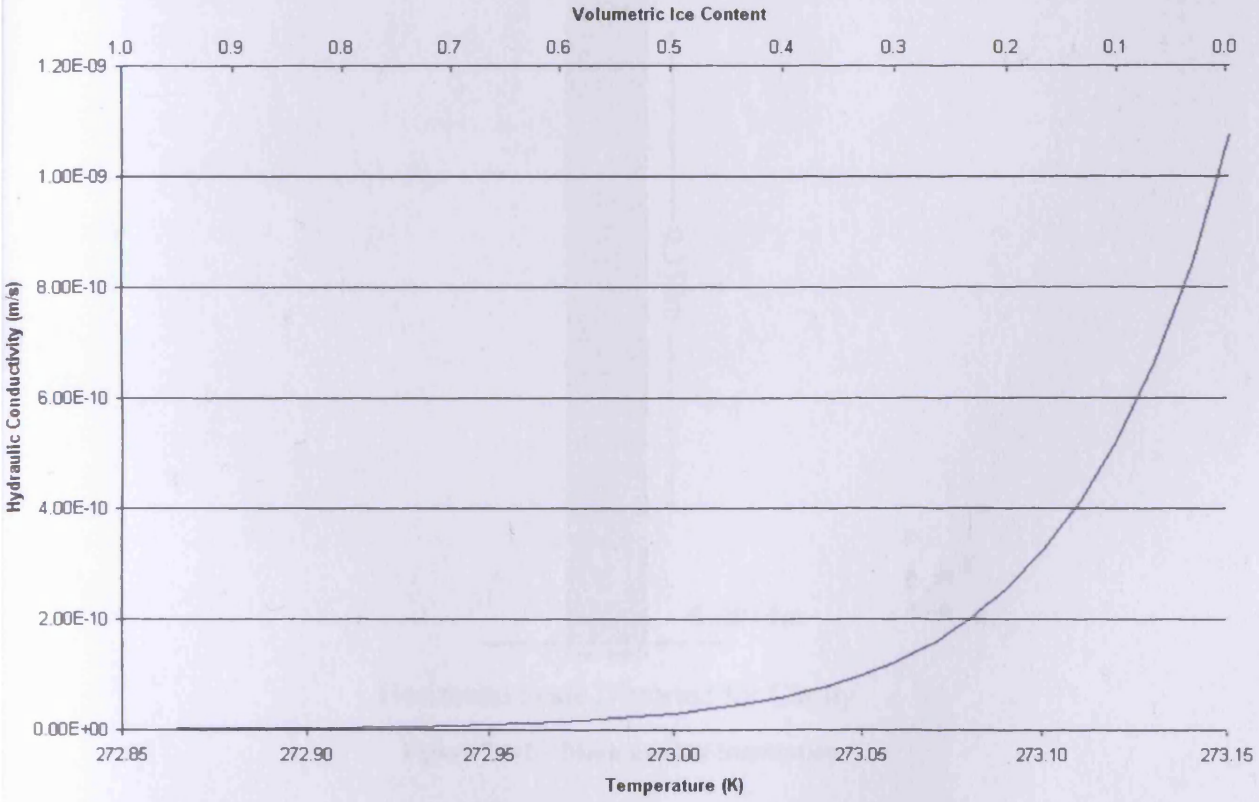

Figure 7.3-1 – Variation of hydraulic conductivity with temperature and volumetric ice content used for the freezing and thawing experiment.

7.4. Numerical Simulation

The experimental slope was constructed in such a way to be considered as an infinite slope. The simulation was set up as a vertical pseudo one dimensional problem which is in effect considering a thin vertical strip within the slope. The developed model however does not consider slope geometry, this is a known limitation with this analysis and that the downslope trends reported in the experimental results will not be able to be repeated in this exercise.

The domain was discretised using plane strain 8 noded quadratic elements divided vertically into 250 elements and horizontally into 1 element (Figure 7.4-1). In order to keep the elements square a domain width of 0.0014m was used.

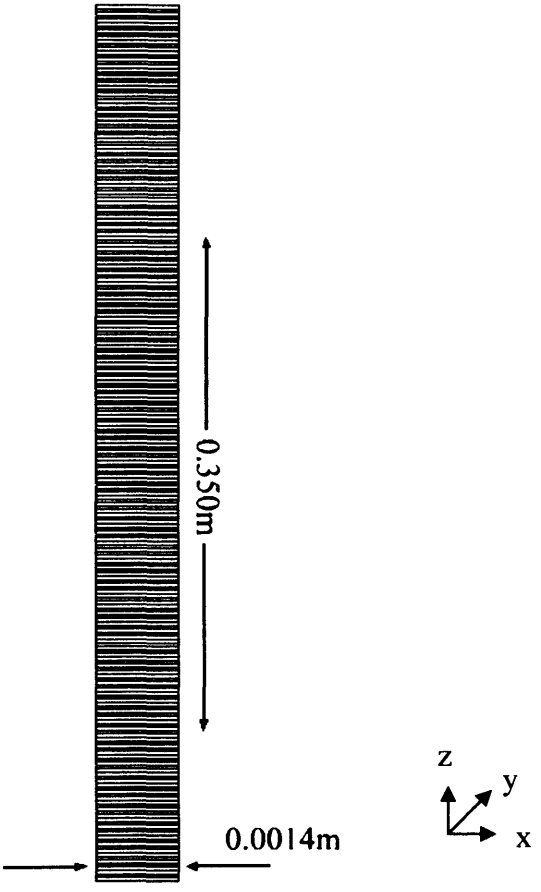

Figure 7.4-1 – Mesh used in Simulation

Experimental results for over 200 days of testing were taken during the experiments covering 3 cycles of freezing and thawing. In this simulation the second freeze / thaw cycle was simulated which lasted 40 days (78 days 8 hours – 118 days 8 hours). The second cycle has been chosen for this simulation as there were experimental problems freezing the slope in the first cycle; this meant that slope started to thaw prematurely before it had become fully frozen.

An initial time step of 100 seconds was used and this was allowed to vary according to the time stepping algorithm employed with a maximum time step of 100 seconds. These spatial and temporal discretisations were used after a thorough investigation was undertaken to ensure converged results were obtained.

Following the experimental condition an initial temperature of 293.60K has been applied throughout the sample. The initial pore water pressure was set to 0kPa and the base and surface fixed to this value for the duration of the simulation to represent the porous basal sand layer and the free draining surface respectively. The sample was laterally restrained in the vertical direction at the base of the sample and in the horizontal direction on both edges.

Assuming the in-situ earth pressure coefficient, K_0, is given by Equation 7.4-1 (Barnes 2000) gives $K_0 = 0.429$. The initial stress levels were calculated using the saturated bulk unit weight and assuming a constant value equal to the average stress of sample. The initial stress levels were set as $\sigma_z = 3500$ Pa, $\sigma_y = 1500$ Pa, and $\sigma_z = 1500$ Pa.

$$K_0 = \frac{v}{(1-v)} \qquad \textbf{7.4-1}$$

The temperatures at the top and bottom of the slope were varied according to the temperatures recorded by the data logger (Figure 7.4-2).

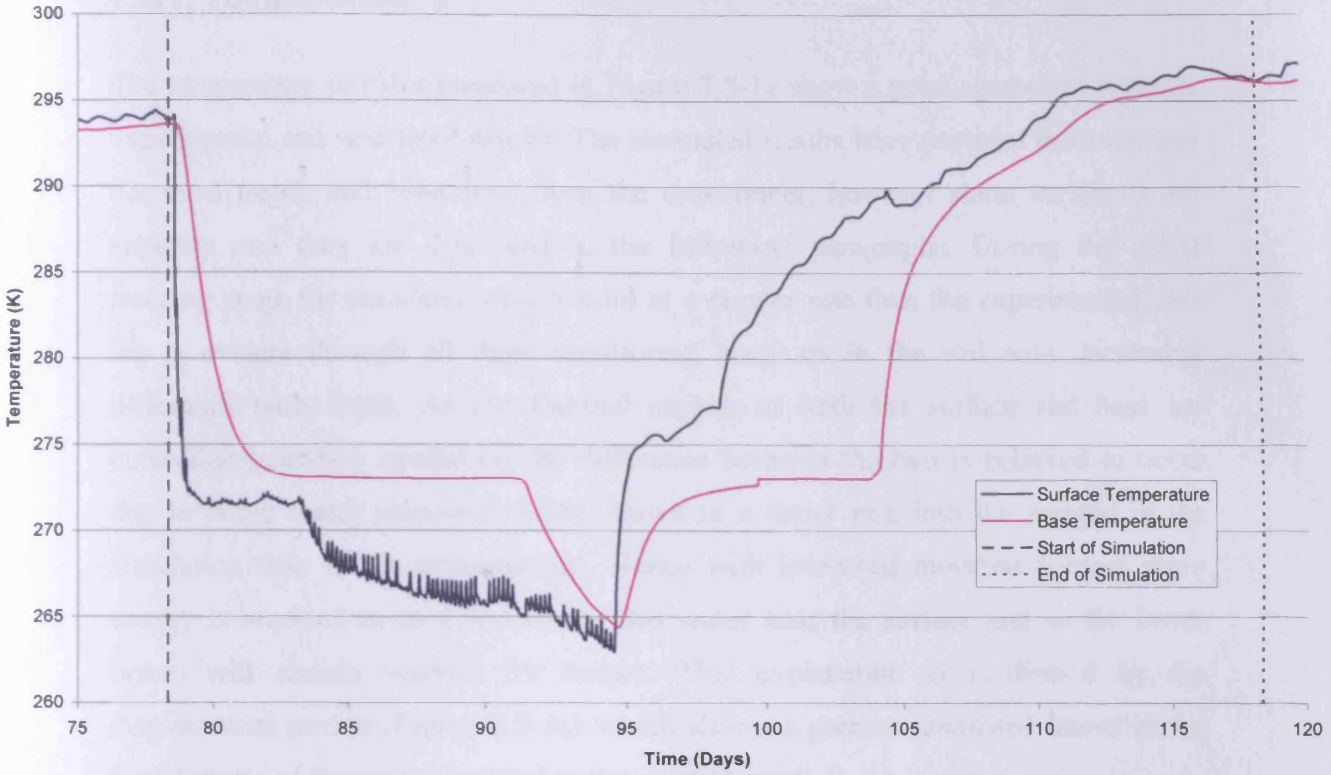

Figure 7.4-2 – Temperature time curve applied to surface and base of slope in simulation

7.5. Results

Variations in temperature, pore water pressure and displacement with time are shown in Figure 7.5-1a to Figure 7.5-3a. Variations with depth of temperature, pore water pressure, displacement, effective stress and void ratio are shown in Figure 7.5-1b to Figure 7.5-3b, Figure 7.5-4 and Figure 7.5-5 for 5 distinct stages in the simulation, namely; just frozen, partially frozen (freezing), fully frozen, partially frozen (thawing), and thawed.

The simulation involved one complete cycle of freezing and thawing where the domain changed state from fully unfrozen to fully frozen and back again. The results permit the comparison between a complex coupled laboratory experiment and the simulation of the proposed model. A discussion of the performance of the proposed model to represent a real world experiment is now presented.

7.5.1. Temperature

The temperature profiles presented in Figure 7.5-1a show a good agreement between experimental and simulated results. The simulated results have captured the important observed trends and behaviour from the experiment, however some variations are apparent and they are discussed in the following paragraphs. During the initial freezing stage the simulated results cool at a slower rate than the experimental, this lag is evident through all three monitoring locations in the soil with decreasing difference with depth. As the thermal regime of both the surface and base are controlled boundary conditions the difference between the two is believed to occur due to water being calculated to be drawn at a faster rate into the sample in the simulation than in the experimental. Hence with increased moisture content more energy is required to cool and freeze this water near the surface and so the lower layers will remain warmer for longer. This explanation is confirmed by the displacement profile (Figure 7.5-3a) which shows a greater calculated heave in the initial stages of freezing compared to the experimental.

Examining the calculated temperatures in the lower layers shows that they are cooling more rapidly than occurred in the experiment, most probably due to less water accumulating in the lower layers as lensing has increased in the uppermost layers. With less water accumulated in the lower layers, less heat has to be extracted for it to become fully frozen and so it cools more rapidly. The experimentally observed stationary profiles (zero curtain) in the 15cm and 25cm profiles at 86-88 days and 89-91 days respectively are also captured by the model and are be due to latent heat effects in the regions that are currently being frozen.

On thaw, the simulated and experimental profiles track well with each other. Although the experimental results thaw slightly faster. As expected with higher moisture content in the upper layers, as a result of the accumulation during freeze, the simulated results lag behind the experimental results as more water has to change phase and therefore warms more slowly.

Figure 7.5-1 shows temperatures profiles with depth and it can be seen that the model captures the general patterns well. However considering the profile at 80 days, an inconsistency between the experimental and simulated results can be seen with the

simulated results at the base of the sample cooling more rapidly than the region of soil above, whereas the experimental results record a decreasing temperature with depth. The difference arises due to the experiment being frozen and thawed from the surface only whereas the boundary conditions applied in the simulation are the measured experimental temperatures at the surface and base. This pattern of behaviour in the calculated results is a result of the prescribed lower boundary condition acting as a sink resulting in a flow of heat energy out of the soil.

During development of the proposed model it has been found that the sensitivity of the predicted results to the values of thermal conductivity and specific heat capacity are negligible providing they are of an approximate value. What appears to be occurring in the proposed model at this time (80 days) is that more moisture is accumulating in the upper layers due to a higher hydraulic conductivity and slowing the cooling of the sample as more energy is required to be removed to cool the additional water in the upper layers. Hence in the experimental results the base cools more rapidly as less moisture is drawn into the soil during this phase.

In the 80 day, 86 day and 99 day profiles (Figure 7.5-1b) it is clear to see the point at which the transition of the frozen fringe to unfrozen or frozen zone occurs by the gradient change in the thermal profile. At these points there is often the 'zero curtain' visible as latent heat effects are taking place.

Overall the reported trends and observations in the thermal field from the experiment have been replicated in the thermal field in the simulated results.

7.5.2. Pore Water Pressure

Before considering the results from the simulation it is worth discussing the pore water pressure transducers and the meaning of their results. As the formulation is based on a continuum assumption the results from the simulation refer to the pore water pressure field alone, however there are questions regarding the physical meaning of the recorded results from the transducers. The Druck miniature pore water pressure transducers were filled with antifreeze to prevent them from freezing but the question must be posed as to how effective this was at preventing phase change occurring within the ceramic tip. Even assuming that the transducer remains unfrozen throughout the experimental test there will be times when the transducer becomes

encased in ice and or an ice / soil composite. The physical meaning of the results under such conditions is not known as, by virtue of ice lensing, discrete impermeable ice barriers are formed and the pore water pressure is no longer continuous within the frozen soil and localised variations may be recorded. There is also the possibility that the transducers are in fact measuring an ice pressure rather than the pore water pressure in the frozen soil. In their discussion of a similar experiment; Harris and Davies (1998) argued that the rapid transition from negative to positive readings during freezing is in response to the sealing of the pressure transducer within an effectively closed frozen soil system. Considerable uncertainty was also raised as to the mechanism of pressure transfer from heaving soil to the transducer and it could not be assumed that the pressure readings necessarily accurately reflect ice pressures (Harris and Davies 1998).

Measured and simulated pore water pressure profiles are shown in Figure 7.5-2. The simulated results capture the significant trends of behaviour observed and reported in the experiment. The first point to note is the difference in magnitude of the cryogenic suctions that are generated; the simulated results are far in excess of the experimental readings. The initial rapid freezing of the surface causes a very large negative pore water pressure to be calculated and this can be seen to be transmitted down through the sample (Figure 7.5-2a and b). As freezing continues the pore water pressure becomes less negative, reaching a maximum positive pressure upon complete freezing (Figure 7.5-2a); consistent with the obtained maximum pore water pressure observed in previous chapters (Chapter 6). These trends are also shown in the 15cm and 25cm profiles where they reach a maximum negative pressure before rapidly rising to a positive maximum on complete freezing.

A rise in pore water pressure upon complete freezing is evident in the experimental 5cm and 15cm profiles and to a lesser extent it can be argued that the 25cm has also risen in magnitude although it has not obtained a positive pressure. What is clear is that in the upper layers of the soil the experimental pore water pressure has obtained a significant positive value; one possible explanation is that freezing has created a rigid soil / ice structure while unfrozen water still remains within the soil pores but not interconnected. As this water freezes the expansion of the liquid water to ice due to density changes is resisted by the rigidity of the ice / soil structure and the pore water

goes into compression. The lower layer, being the furthest from the cold side cools slower and sufficient time and proximity to the basal drainage layer exists as to drain preventing similar pore water pressure to build up. This again brings into question the physical meaning of the results which the pore water pressure transducers are measuring.

In the simulated results a rise in pore water pressure is predicted; however these values refer only to pore water pressure as ice is assumed to form within the pores and is at atmospheric pressure (Nakano 1986; Nakano 1990). The increase in pore water pressure on freezing predicted by the model is mostly due the initial stress level with a minor contribution due to the rate of freezing as has been observed in Chapter 6 (Section 6.6 and 6.9). The proposed numerical model is based on the assumption that continuity exists even in the fully frozen state whereas in reality discontinuities by virtue of ice lensing will exist.

During thaw at all three depths in the experimentally recorded pore water pressures variations are evident. These can be contributed to the pore matrix becoming reconnected as the ice changes phase and the transducers are no longer reporting local variations. Again Harris and Davies' (1998) discussion also concluded that the rapid response was attributed to the hydraulic continuity being re-established between the transducers and the mobile unfrozen water. In the simulated results a variation in the pore water is also observed on thaw and a temporary increase is predicted which falls upon complete thawing. A negative spike in the pore water pressure is predicted around 103-104 days where the majority of the sample has thawed with the lower most layers frozen or partially frozen. This would explain the trend in the temperature profile for the 25cm thermistor as previously discussed and that in the very lower layers the sample experiences a final spell of ice lensing before becoming fully thawed.

While ice lensing occurs during both the freezing and thawing stages of the test, it is only during the freezing stage that the large cryogenic suctions are observed (Figure 7.5-2b). As expected; considerable cryogenic suctions are developed when the thermal gradients are high and the potential for moisture flow is at its greatest. There is evidence that negative pore water pressures are developed in the thawing stage, just not to the same extent as those on freeze (103-104 days) (Figure 7.5-2a).

In both the simulation and experiment, once the samples had completely thawed, they continued to deform and consolidate as the excess pore water pressures were dissipated. Overall the reported pore water pressure trends and observations from the experiment have been replicated in the simulated pore water pressure results.

7.5.3. Displacement

This section discusses the simulated displacement profiles and compares them to the experimentally observed profile. Only experimental results for surface heave are available for comparison and these are discussed below. A correlation between experimental results and simulated results has been found with trends and behaviour correctly predicted.

During the initial period of freezing (79 days), both the experimental and simulated surface displacement can be seen to reduce in the very early stages of freezing (Figure 7.5-3a). This would indicate that appropriate conditions exist during this time for water expulsion to occur. It is known that soil water may either be expelled or attracted to the freezing front depending upon soil type, stress level, and rate of freezing when a freezing front advances through a saturated soil (Nakano, 1999). The problem of water expulsion was studied analytically (Nakano, 1999) based on a mathematical model called M_1 (Nakano, 1986, 1990) and the condition of water expulsion was derived. The assumptions on which the proposed model is based follows the approach proposed by Nakano (1986, 1990) and so under appropriate conditions water expulsion will be calculated in the proposed model.

As previously speculated from the temperature profile; the simulation appears to be calculating an accumulation of more moisture in the upper layers than was found in the experimental results during the beginning of the freezing phase (80 to 88 days). This can be clearly seen in the displacement plot with the surface heaving at a faster rate in the simulation. It can also be seen that the sample is consolidating in the layers beneath the frozen fringe. This is more pronounced just beneath the frozen fringe; which given the strong cryogenic suction generated is causing consolidation to occur as insufficient free water is available to feed the growing ice lens. This effect is transmitted down the entire sample until the frost front passes and lensing takes place.

The most plausible explanation for the increase in ice lensing in the upper layers compared to the experimental results is that the hydraulic conductivity relationship used is yielding too high conductivities and too much moisture is able to flow to the frozen fringe. With a reduced hydraulic conductivity, more specifically a reduced unfrozen hydraulic conductivity, less moisture will be able to accumulate and subsequently less heat energy is required to cool this additional moisture and the frost front will penetrate the soil quicker. It is well known that high water intake rates retard the frost penetration, whereas the frost front advances faster with small moisture migration rates (Konrad and Shen, 1996). With the frost front advancing faster the simulated temperatures would be closer to the reported experimental results.

On initial thaw (95 to 96 days) a drop in the calculated surface profile is observed which indicates that as the surface thaws a quantity of water is expelled (Figure 7.5-3a). A similar effect has been previously witnessed in Chapter 6 Section 2 where the frozen fringe is being established. In this instance the soil was freezing and due to the high hydraulic conductivity and the cryogenic suctions developed, a greater rate of heave occurred which reduces upon complete formation of the frozen fringe. With the thermal gradient reversed an opposite situation is observed with the partially formed frozen fringe where large amount of water appears to being expelled causing a drop in the surface profile. This stops once the fringe becomes fully formed. This phenomenon was not observed in the experiment.

Upon full formation of the frozen fringe (96 to 98 days) the surface heave profile starts to increase despite a surface temperature causing thaw to occur in both the experiment and the simulation. A process of simultaneous heave and expulsion appears to be taking place during this phase in the test. This observation is consistent with phenomenon of 'summer heave' where the ground heaves during thaw (Mackay, 1984).

After the maximum heave has been reached (98 days) expulsion of the thawed moisture exceeds the heave that is simultaneously taking place and the surface profile decreases in both the experiment and simulation. In the simulation this continues at a steady rate to day 103 where the rate rapidly increases with the surface reducing by approximately 20mm over a 24 hour period. The experimental results show a slightly more uniform settlement profile. This variation between the simulated and observed

behaviour is again connected with the hydraulic conductivity which sees the simulated results drawing in more moisture during the thawing phase.

Post 104 days all latent heat effects have ceased and the moisture rich mass dissipates the excess water which remains within the soil pores. The experimental trend is mirrored in the simulated results with both showing consolidation taking place as the excess pore water pressure generated on thaw is dissipated.

Displacements of internal points within the experiment were not measured due to the practicalities of installing experimental devices capable of measuring locations within the soil mass while not becoming connected to the surrounding soil as it freezes making such measurements extremely difficult. Despite no experimental readings to compare to, the simulated results provide an interesting insight into the processes that maybe taking place within the soil during freeze and particularly during thaw (Figure 7.5-3a and b). During freeze, as expected, the profiles show that as the freezing front penetrates deeper into the soil, moisture accumulates and freezes as ice lenses form within the frozen fringe and this process continues until the sample is completely frozen.

Examining the internal simulated displacement profiles during thaw indicates that a significant amount of ice lensing is occurring throughout the thawing phase. This is more prevalent in the upper layers, and while its impact is decreasing with depth it is still significant (Figure 7.5-3b). Direct observations of ice lensing and the composition of the unfrozen water within the frozen fringe can be routinely measured using nuclear magnetic resonance, differential scanning calorimetry or time domain reflectometry (Nakano 1999). X-Ray photography was effectively used by Penner (1986) to locate and infer the temperature at growing ice lenses showing the usefulness of these techniques for non-invasive investigations. That said; these techniques have been reported to be used on small laboratory samples rather than to full sized laboratory experiments where use would inevitably lead to some form of destructive interference. However the trends of behaviour calculated in this simulation are consistent with the observations made with these types of techniques in such laboratory experiments. At 5cm a further 9mm of heave occurs during thaw before the sample fully thaws and the frost front passes (Figure 7.5-3a).

Comparisons of the simulated and experimental surface thaw profile indicate that the experiment thaws more rapidly than the simulated results predict. It has been discussed as to why the simulated heave is greater than the experimentally reported results and that is believed to be due to the hydraulic conductivity used in the simulation being higher. It has also been proposed that significant ice lensing is continuing to take place during the thawing phase. The difference between the thaw profile of the simulated and experimental results is due to a combination of 1) more moisture accumulated in the sample during the freezing phase which requires more energy to thaw and 2) as the sample continues to lens during thaw a higher quantity of moisture will accumulate because of the higher hydraulic conductivity. These both result in a retardation of the speed of thaw and hence the surface profile falls more slowly in the simulation (Figure 7.5-3a and b).

Finally a period of rapid change throughout the sample takes place over two days (102 to 104 days) where ice lensing appears to stop and large quantities of water are expelled. The profiles of displacement across the sample reduce as the sample becomes entirely unfrozen and the sample tends to the initial displacement values as the residual pore water pressure dissipates (Figure 7.5-3b).

Overall the reported displacement trends and observations from the experiment have been replicated in the simulated displacement results.

7.5.4. Effective Stress and Void Ratio

As no results were recorded for effective stress and void ratio during the experimental programme, simulated results for effective stress and void ratio have therefore not been shown with time. Profiles with depth at 5 distinct stages during the simulation are shown in Figure 7.5-4 and Figure 7.5-5. The 5 stages serve to show the effective stress and void ratio during the simulation at initial freezing (80 days), partially frozen (freezing) (86 days), fully frozen (94 days), partially frozen (thawing) (99 days), and thawed (118 days). Each of these stages is now discussed.

7.5.4.1. Initial Freezing – 80 Days

As the temperature is rapidly dropped during the initial stage of the simulation an increase in the effective stress beneath the freezing layer is very evident (Figure

7.5-4). Considerable cryogenic suctions are created and this has a corresponding response with the effective stress rising. Confirmation of consolidation occurring is apparent in the displacement profile (Figure 7.5-3b) which shows a downward displacement which is greatest at the boundary of the unfrozen and partially frozen soil. This observation is consistent with other freezing tests where consolidation of the unfrozen soil in response to effective stress increase caused by cryogenic suctions has been recorded (Konrad and Nixon, 1994).

The void ratio plot reinforces those observations with a slight decrease in void ratio in the unfrozen soil and an increase in the frozen fringe where liquid water is accumulating (Figure 7.5-5).

7.5.4.2. Partially Frozen (Freezing) – 86 Days

Freezing continues down through the sample and the trends observed at initial freezing (80 days) are also evident in the 86 day profile. At this stage in the freezing, the thermal gradient in the sample has reduced and the cryogenic suctions generated are reduced in comparison to that of the initial stage (Figure 7.5-2b). This results in a smaller effective stress rise and reduced quantity of ice lensing despite being closer to the drainage boundary. However an increase in the void ratio in excess of the insitu 9% volumetric expansion due to freezing is produced.

7.5.4.3. Fully Frozen – 94 Days

During this period the temperature throughout the sample is below the segregation freezing temperature and no latent heat effects or cryogenic suctions are active. The void ratio plot shows that the majority of ice lensing has occurred in the upper 10cm of the soil (Figure 7.5-5). The additional liquid water for this accumulation has been drawn up through the sample from the base as the frozen hydraulic conductivity drops by approximately 4 orders of magnitude to the unfrozen value. The whole column has undergone some degree of ice lensing during the freezing cycle.

It is also evident that as the soil approaches its fully frozen state that a large accumulation of water occurs in the lowest 2cm. This has been observed before in Chapter 6, Section 2 where the frozen fringe is partially formed. During this stage as the fringe is vanishing, cryogenic suctions are still being developed, but the hydraulic

conductivity remains relatively high as the applied temperature is keeping the soil in a partially frozen state. During this time a greater rate of heave occurs which ceases when the frozen fringe vanishes.

7.5.4.4. Partially Frozen (Thawing) – 99 Days

In the upper layers that have become unfrozen the effective stress has tended to its initial value and a corresponding drop in void ratio has also occurred (Figure 7.5-4 and Figure 7.5-5). What is interesting to see is that within the frozen fringe, cryogenic suctions will still be developed, and while some of the melt water will be expelled through the surface some of this free water will be drawn down and accumulate lower down in the sample as new ice lenses. What can be seen from the void ratio plot is that a quantity of ice lensing is calculated to occur around a depth of 20cm even though the sample is thawing (Figure 7.5-5).

7.5.4.5. Thawed – 118 Days

At the end of the simulation the soil has completely thawed and the temperature is far in excess of the freezing point of water (Figure 7.5-1b). The void ratio has generally tended to its initial value although there is still an area within the centre of the column that still shows an accumulation of water (Figure 7.5-5). An examination of the pore water pressure profile at 118 days shows that positive pore water pressures still exist in this region and that over further time these will dissipate and the void ratio in this region will reduce as the sample drains (Figure 7.5-2b).

The calculated effective stress profile shows an increase in level to its initial value towards the extents of the sample; however remains lows in the centre of the sample (Figure 7.5-4). Given the elevated pore water pressure in the centre of the sample it is predicted that the effective stress level would increase as the pore water pressures dissipate.

7.5.5. Numerical Difficulties

Throughout the numerical work conducted as part of this study, continued numerical difficulties have been encountered. Due to the very small space that the frozen fringe occupies and the rapid changes that take place within this space leads to computation

instabilities. The developed theoretical formulation is highly dependant on the rate of change of the thermal field to achieve convergence in the numerical scheme. As a result oscillations have been encountered where the rate is high and this has forced the use of small time steps (< 5 seconds) to achieve convergence.

The amplitudes of the oscillations depend on the characterization of the transition between the frozen and unfrozen state in the soil. This arises from the fact that when the frost front crosses an element boundary, the resulting temperature gradient in the element is an average of the temperature gradients in the frozen and unfrozen portions of the element. Steps have been taken to improve the numerical scheme by introducing a pre-run to improve the estimate in the predictor-corrector scheme and this has made significantly improvements.

During the numerical work undertaken in this chapter these instabilities have been more prevalent as the data used is taken from an experimental programme and not derived under highly idealized conditions which have been taken to exist for the verification, validation and sensitivity analyses. Having said that the modifications made to the numerical scheme have made a positive impact to the ability to solve the governing equations. All told; the numerical model has performed well under these conditions.

7.6. Conclusions

The numerical simulation conducted in this chapter investigated the timing and rate of: a) frost penetration, b) surface frost heaving, c) thaw penetration, and d) pore water pressure changes for a large scale laboratory freezing and thawing experiment. In addition to the above specified timings and rates, the development of the deformation field within the soil was also considered.

The proposed numerical model has been applied to a complex coupled freezing and thawing experiment to explore one complete freezing and thawing cycle. The work undertaken in this chapter used the proposed numerical model and experimental

results from a freezing and thawing experiment to enable a comparison to take place with real world data.

The simulated results show a good correlation with the experimental results by predicting the patterns and trends of experimentally observed behaviour and the cryogenic processes that occur during the freezing and thawing of frost susceptible soils. The temperature field is able to predict the variations due to latent heat effects and act as the driver for the cryogenic processes. Cryogenic suctions are able to be generated in the pore water pressure field which draws moisture into the freezing zone although interpreting the physical meaning of experimental and simulated results requires some caution. Finally the displacements predict the experimentally observed behaviour in both the freezing and thawing phases.

As has been the case through this study the accurate determination of material parameters is paramount in order to accurately represent the behaviours and processes that occur. In particular the determination of the hydraulic conductivity and segregation temperature is vital.

It can be concluded that the inclusion of ice lensing and cryogenic processes into the theoretical formulation has resulted in a model that is capable of representing coupled flow and deformation processes including ice lensing in saturated freezing soils. Further use of the numerical model is required to gain confidence in the ability to provide accurate results with the ultimate aim to be able to be used to perform blind predictions.

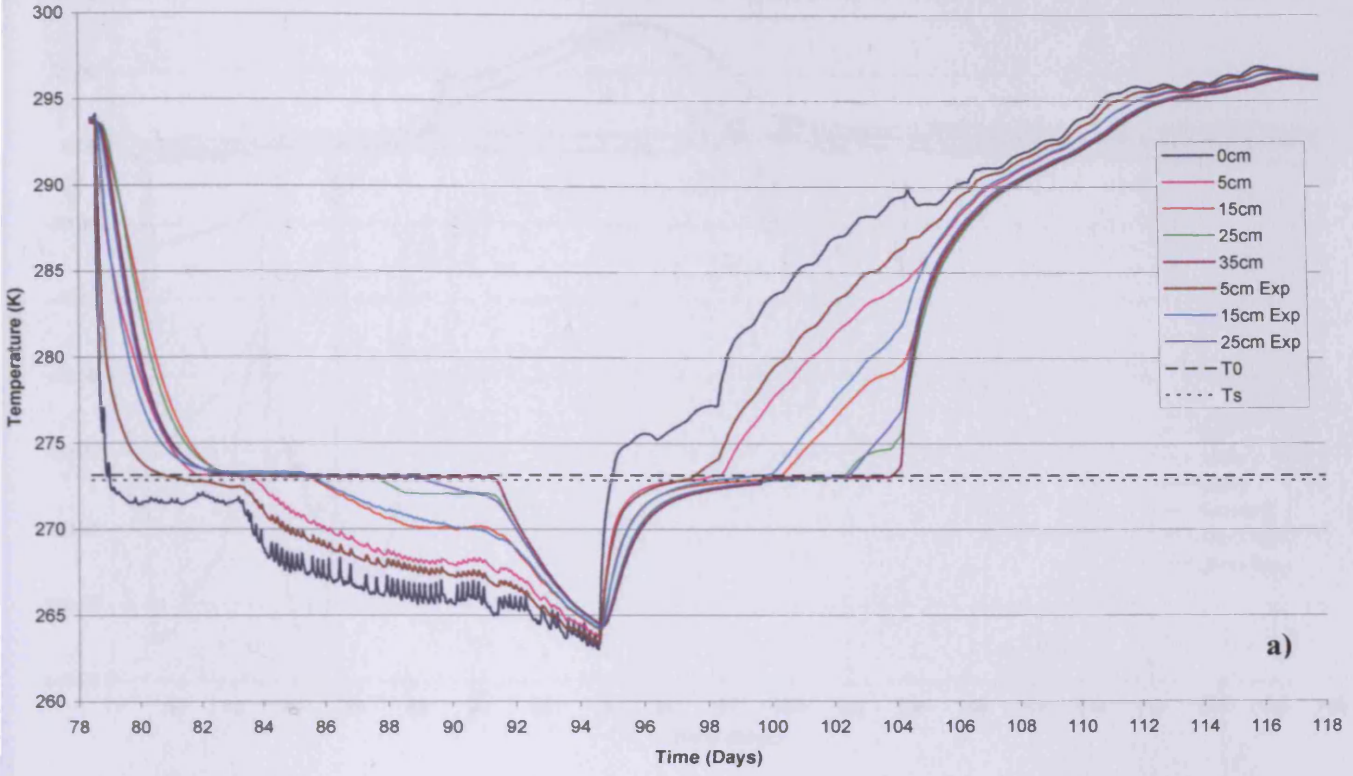

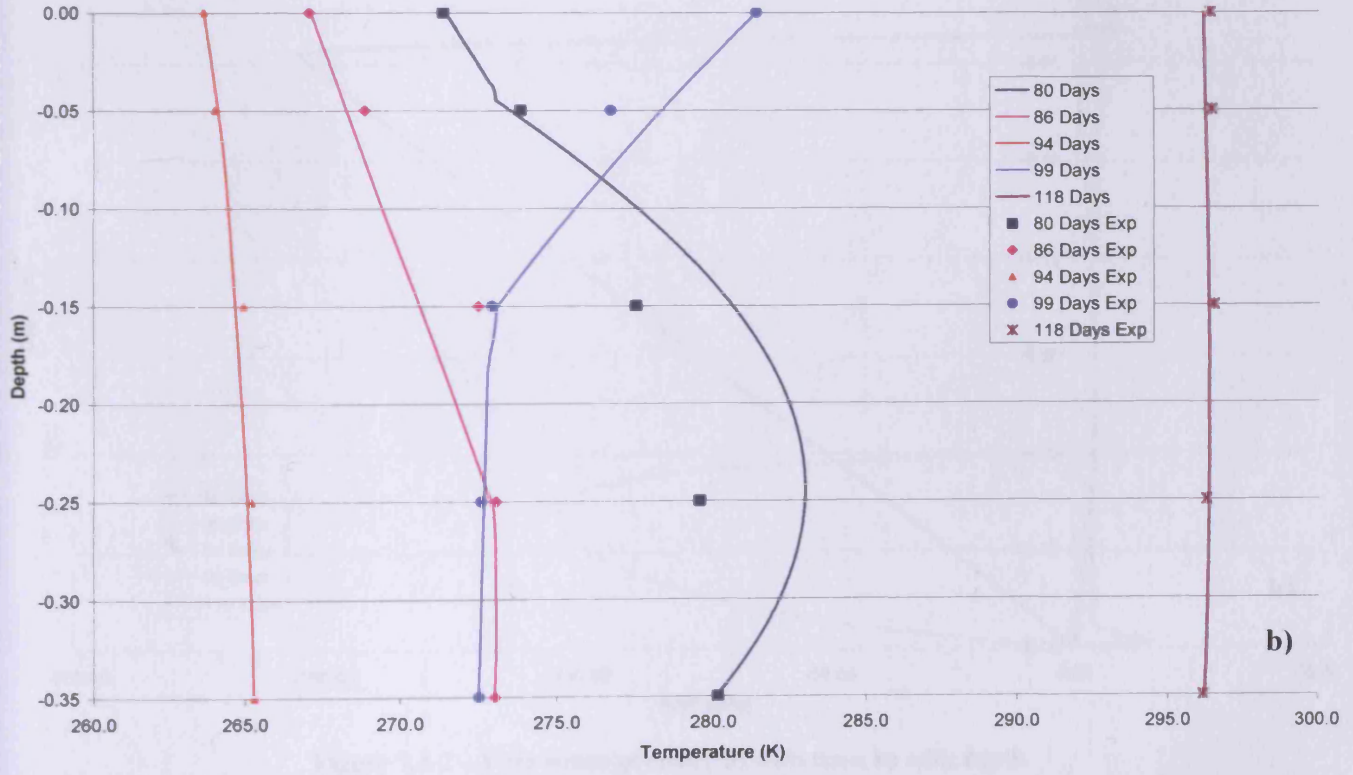

Figure 7.5-1 – Temperature profile a) with time, b) with depth.

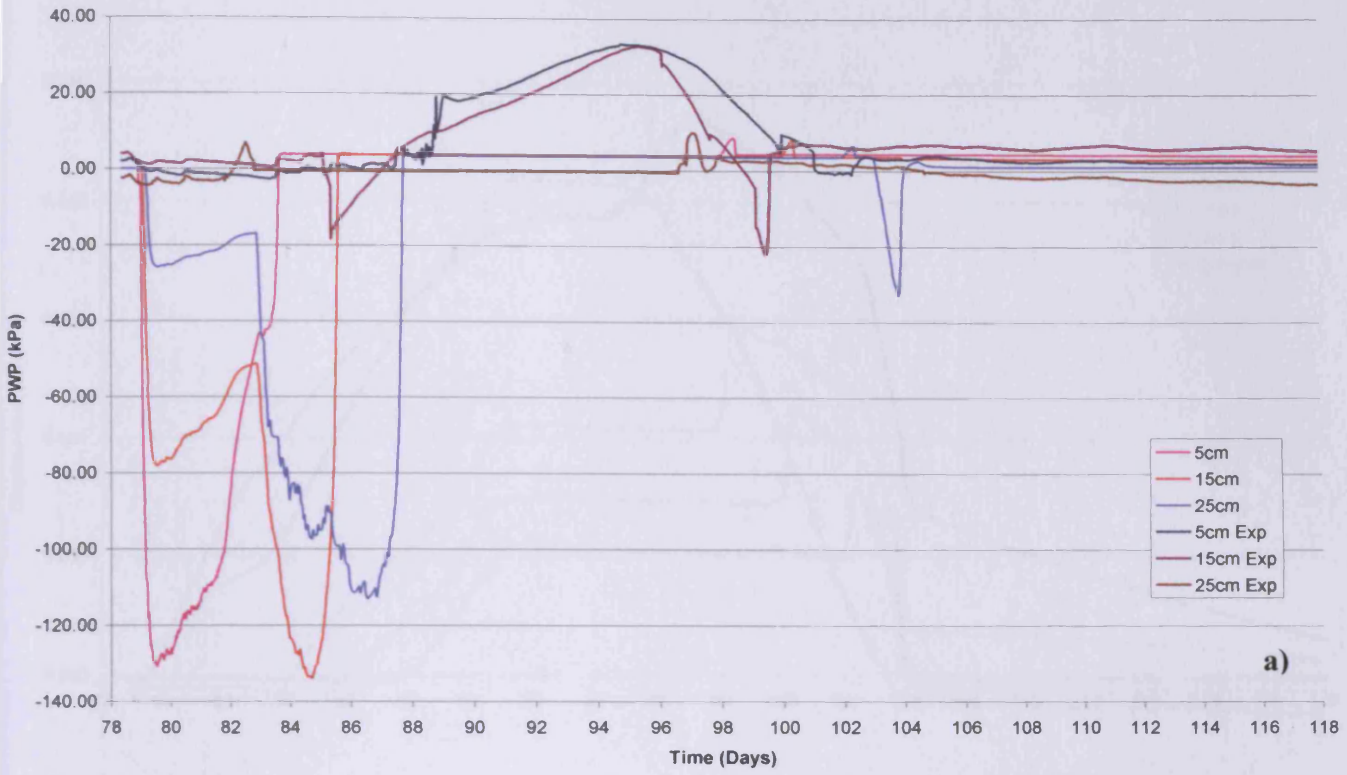

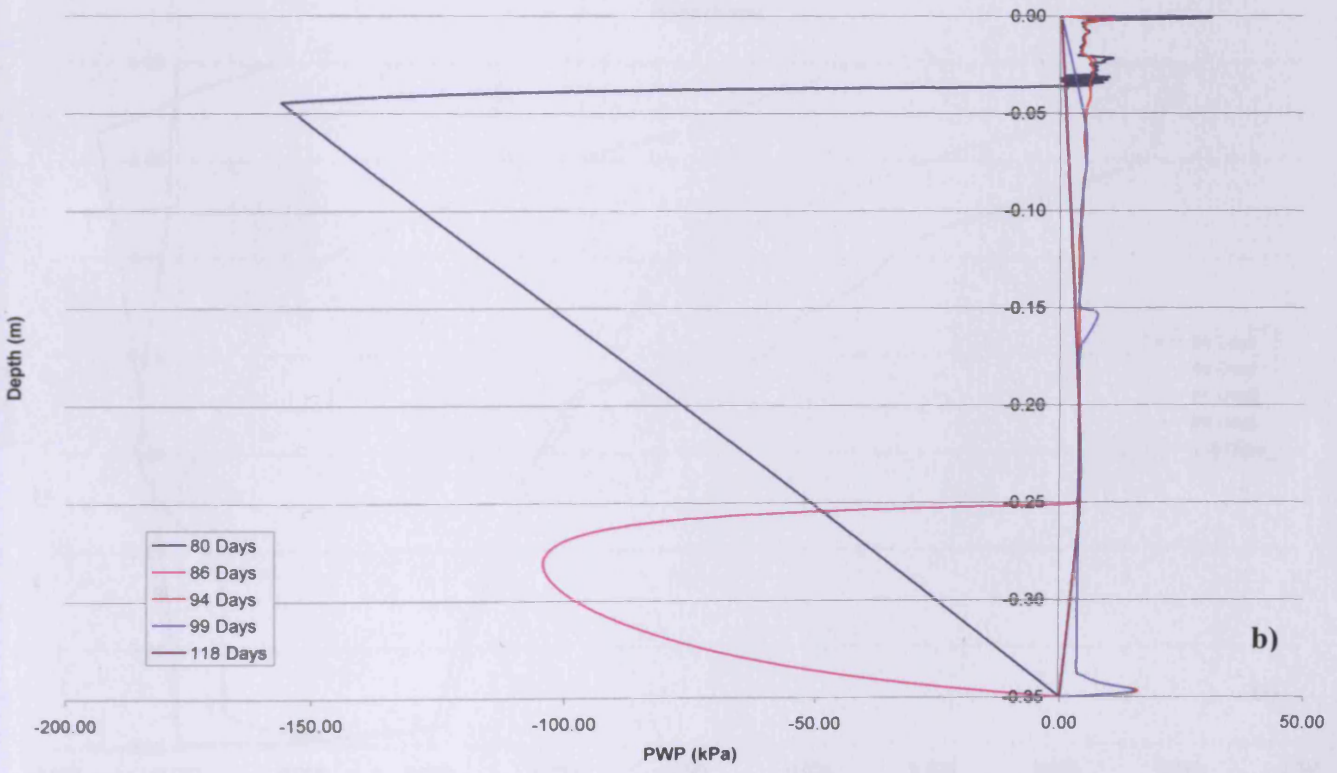

Figure 7.5-2 – Pore water pressure a) with time, b) with depth

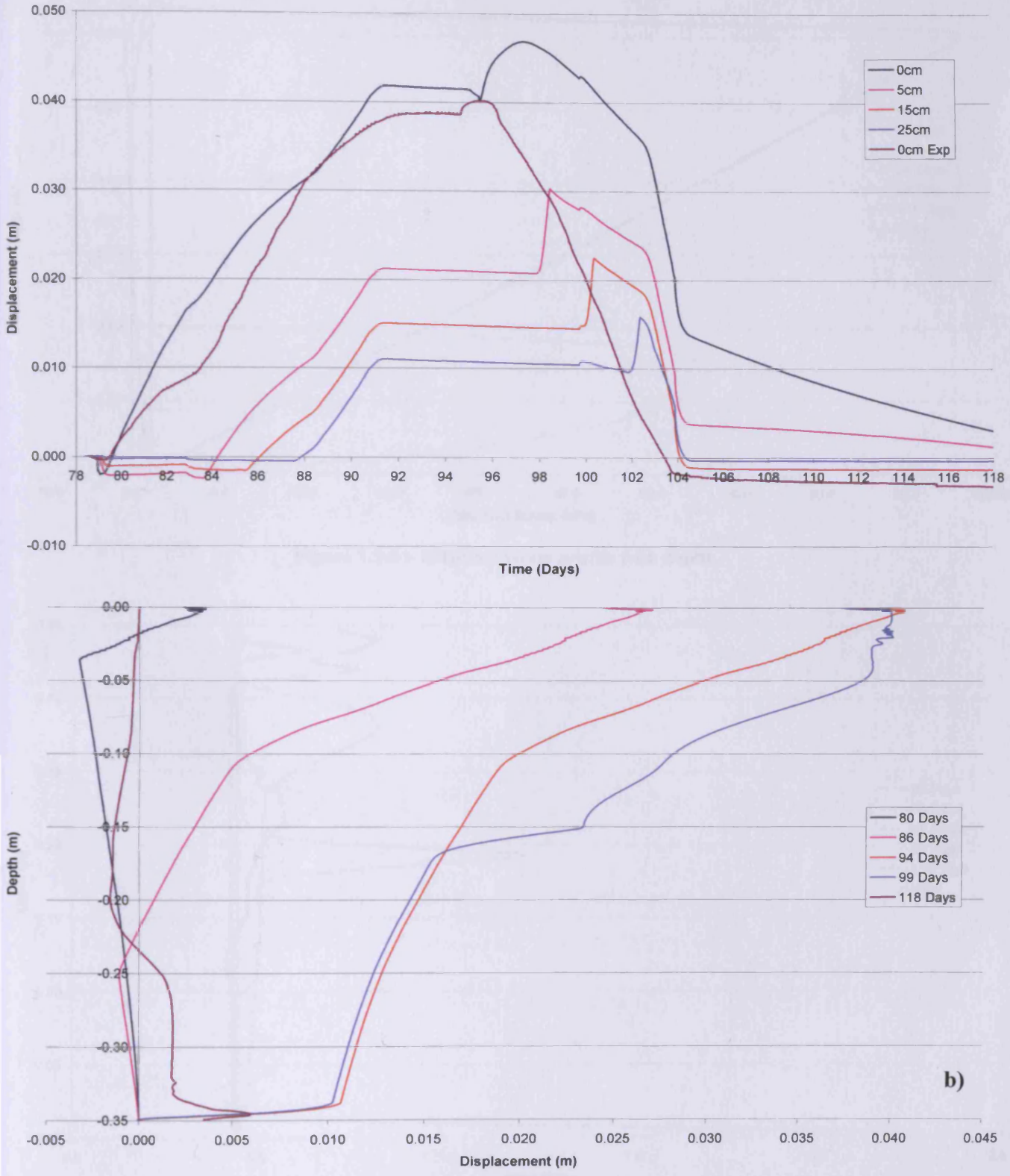

Figure 7.5-3 – Displacement profile a) with time, b) with depth

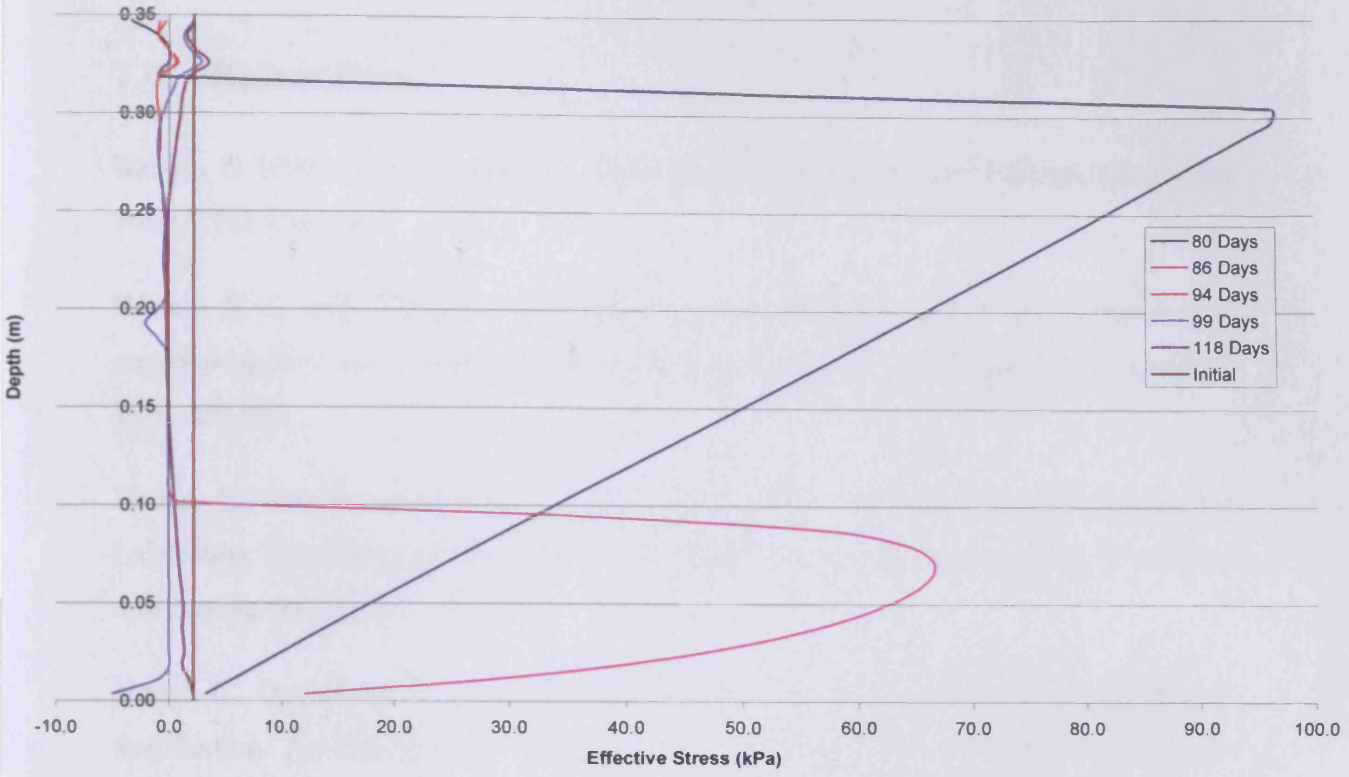

Figure 7.5-4 – Effective stress profile with depth

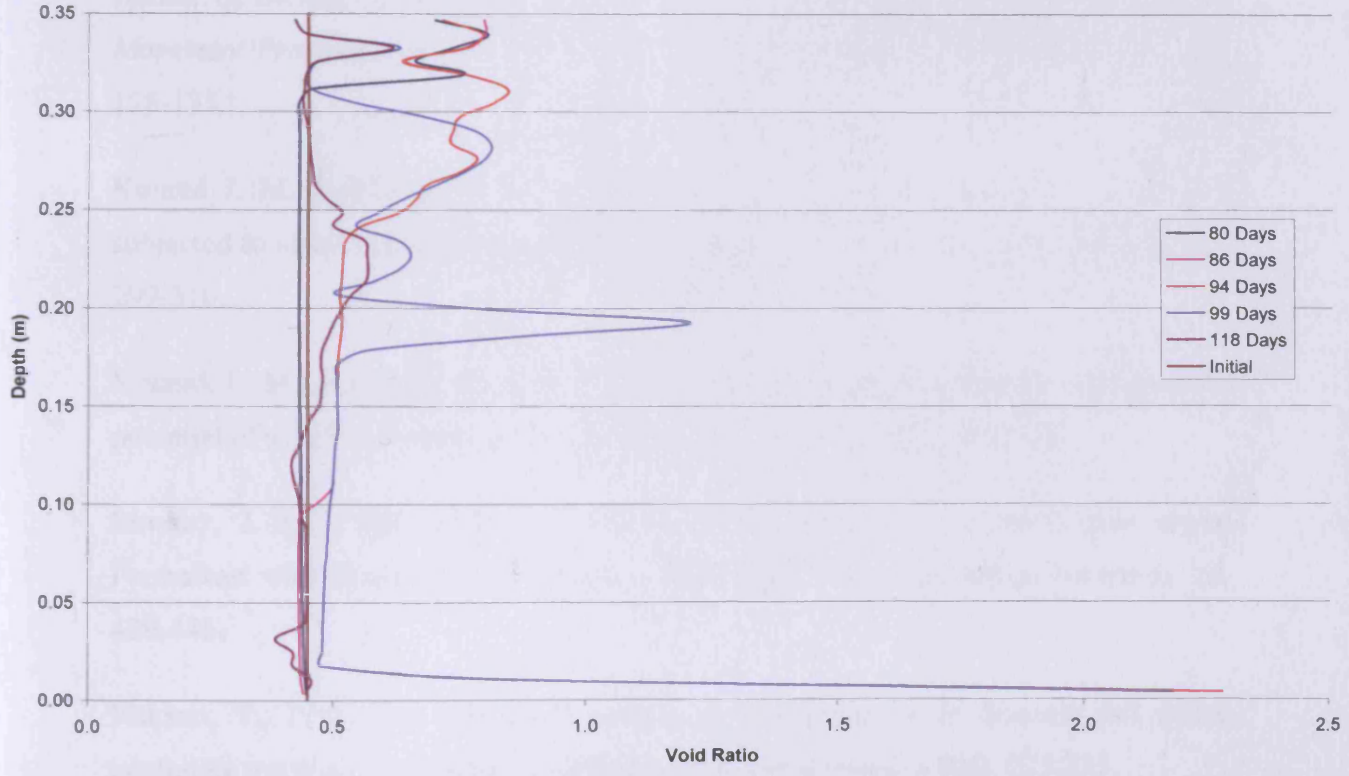

Figure 7.5-5 – Void ratio profile with depth

7.6. References

Barnes, G 2000. "Soil Mechanics – Principles and Practice". 2nd Edition. Macmillan Press LTD, London.

Harlan, R. L. and Nixon, J. F. 1978. "Ground thermal regime" In: *Geotechnical engineering for cold regions*. O. B. Andersland and D. M. Andersland (Eds), McGraw Hill. 103-150.

Harris, C., Davies, M. C. R, Coutard, J. P. 1996. "An Experimental Design for Laboratory Simulation of Periglacial Solifluction Processes". *Earth Surface Processes and Landforms* **21(1)**, 67-76.

Harris, C., Davies, M. C. R, Coutard, J. P. 1997. "Rates and Processes of Periglacial Solifluction: An Experimental Approach". *Earth Surface Processes and Landforms* **22**, 849-868.

Harris, C, Davies, M. C. R, Rea, B. R. 2001 "*Scaled Physical Modelling of Mass Movement Processes on Thawing Slopes*", Permafrost and Periglacial Processes. **12**, 125-135.

Konrad J. M. and Nixon J. F. 1994 "Frost heave characteristics of a clayey silt subjected to small temperature gradients" *Cold Regions Science and Technology*, **22,** 299-310.

Konrad. J. -M., and Shen. M., 1996, "2-D frost action modelling using the segregation potential of soils" *Cold Regions Science and Technology*, **24(3)**, 263-278.

Mackay, J. R., 1984, "The Frost Heave of Stones in the Active Layer above Permafrost with Downward and Upward Freezing" Arctic and Alpine Research, **16**, 439-446.

Nakano, Y., 1986. "On the stable growth of segregated ice in freezing soil under negligible overburden pressure". *Advances in Water Resources* **9(4)**, 223-235.

Nakano, Y., 1990 "Quasi-steady problems in freezing soils: 1. Analysis on the steady growth of an ice layer". *Cold Regions Science and Technology* **17,** 207-226.

Nakano, Y., 1999. "Water expulsion during soil freezing described by a mathematical model called M1" *Cold Regions Science and Technology* **29 (1),** 9-30.

Penner, E. 1986 "Aspects of Ice Lens Growth in Soils". *Cold Regions Science and Technology* **13**, 91-100.

Selvadurai, A. P. S., Hu, J. and Konuk, I. 1999a "Computational Modelling of Frost Heave Induced Soil – Pipeline Interaction. 1 Modelling of Frost Heave". *Cold Regions Science and Technology* **29**, 215-228.

Selvadurai, A. P. S., Hu, J. and Konuk, I. 1999b "Computational Modelling of Frost Heave Induced Soil – Pipeline Interaction: II. Modelling of experiments at the Caen test facility". *Cold Regions Science and Technology* **29**, 229-257.

Shen, M. Ladanyi, B. 1991. "*Soil Pipeline Interaction During Frost Heave Around a Buried Chilled Pipeline*". Cold Regions Engineering, ASCE 6th International Speciality Conference. ASCE Publications, New York. 11-21.

Chapter 8

Conclusions and Suggestions for Further Work

8.1. Introduction

The principal aim of this study was to develop a coupled heat, moisture and deformation model which incorporates cryogenic effects and to undertake adequate verification and validation work on the model to demonstrate its suitability for modelling cryogenic effects in saturated soils. In order to achieve this, specific objectives were set out in Chapter 1, these are;

i. The investigation and development of a coupled theoretical model of saturated soil with cryogenic effects including the effects of moisture flow, heat flow and deformation.

ii. The development of two-dimensional thermo / hydro / mechanical governing equations.

iii. The development of a numerical solution of the theoretical formulation.

iv. The development of a computer programme, based on the existing model COMPASS, of the numerical solution for saturated soil with cryogenic effects.

v. To verify and validate the numerical code via comparisons with analytical solutions and existing experimental results.

vi. An investigation into the cryogenic behaviour of frost susceptible soils.

It is claimed that each one of these objectives has been achieved and completed successfully. The following sections details the main conclusions drawn from this work, and suggestions for further research are made.

8.2. Current State of the Art

A review of developments and understanding in the field of freezing soil behaviour in the numerical modelling of coupled heat and mass transport in freezing and thawing soil was presented. The concept of the frozen fringe, the region between the frozen and unfrozen soil, was introduced and found to be a pivotal part in the ability to model freezing and thawing soil but despite the number of years of research, no definitive answer to date has been reached about the exact processes that occur in this region. While the need account for the energy release due to the latent heat of fusion is required; two very distinct processes occur during freezing and thawing. It is the ice lensing that defines the uniqueness in freezing systems with the attraction and large accumulation of solid water in the soil matrix. The uniqueness of thawing soils is in the conditional stability while the excess water accumulated thaws and dissipates, too fast and the soil suffers from major strength losses and certain failure will result.

With such complex processes to consider the numerical developments of solutions have changed considerably over time. Most of this in part is due to large amount of computing power required to solve highly coupled finite element analysis involving moving boundary problems which were simply to costly to run. Still recently the models developed were for one-dimensional use and did not employ full coupling between variables and opted to solve the equations sequentially. Freezing and thawing processes from a geological point of view was also considered and with the current situation with global warming; temperatures are rising and this has very significant bearing on those parts of the world which are covered in permafrost and those that experience seasonal freezing and thawing. The need for numerical models that are able to be applied to a variety of scenarios where freezing and thawing of soil is

concerned was clearly identified and that a numerical model that has the physical processes defined in a generic way is an extremely useful tool.

8.3. Theoretical Formulation and Numerical Solution

Chapter 3 presented the theoretical formulation for the thermo / hydro / mechanical behaviour which represents the flow of moisture and heat in a deformable saturated soil which may be subjected to freezing. The significant developments are the governing equations for moisture and heat transfer which have been modified to include the latent heat of fusion and the equation for moisture flow which has been modified to include the flow of moisture due to the thermal gradient.

Chapter 4 presented an approximate solution to the developed coupled flow and deformation formulation give in Chapter 3. Spatial discretisation of the governing differential equations for moisture, heat and deformation has been accomplished through the use of the Galerkin weighted residual finite element method. Temporal discretisation has been achieved by employing a backwards difference mid-interval time stepping algorithm.

A pre-run was introduced into the model with the objective of enabling the determination of an initial approximation to the thermal field across the domain. By incorporating a pre run to improve the initial estimate in the predictor-corrector scheme a good approximation to the thermal field known was possible which significantly improved the accuracy of the latent heat effects that occurred during any given time step.

8.4. Verification of the Numerical Model

The aim of the verification exercises was to confirm that the cryogenic processes integrated into the existing COMPASS numerical model were correctly implemented. Four verification exercises were presented to explore the cryogenic processes of freezing and thawing soils which have been incorporated into the theoretical formulation. Analytical solutions were used to verify the mathematical correctness of

the model. Verification tests were carried out to check the following cryogenic components; i) coupled thermo-hydraulic response, ii) deformation behaviour of the fully coupled thermo-hydro-mechanical model, iii) transient coupled liquid flow and deformation behaviour, and iv) latent heat of fusion.

The results indicate from all the exercises a very good correlation between numerical and analytical results and the model can be confidently applied to large scale problems. It was therefore concluded that confidence has been gained in the ability of the numerical model to correctly solve the governing equations.

8.5. Validation and Sensitivity of the Numerical Model

Chapter 6 focused on the impact of the cryogenic related processes included within the proposed theoretical formulation. In particular the development of ice lenses and the movement of moisture under cryogenic suction were investigated. The performance of the proposed model with respect to a number of variables was subsequently explored in order to determine their effect on the magnitude and growth of ice lenses in a freezing soil. The variables investigated were the thermal gradient, rate of cooling, hydraulic conductivity, segregation freezing temperature, and stress level.

An undrained one sided freezing test was used as an extension of the verification exercises previously presented to verify that mass balance was achieved by comparing against an analytical solution. Initial observations showed that the ice lensing component had been implemented correctly and the numerical model exhibits the apparent suction that is critical in frozen soils to attract the additional water to the frozen fringe. A simulation of a drained one dimensional ramped freezing test performed by Penner (1986) was then carried out to validate the subset of the proposed numerical model considering cryogenic suction effects and ice lensing. The results of the analysis showed that the proposed model is capable of simulating freezing with ice lensing in a frost susceptible soil.

Finally a series of sensitivity analyses were presented where individual parameters were varied to firstly confirm that the proposed model is capable of predicting the

patterns or trends of experimentally observed behaviour and secondly to investigate the cryogenic processes that occur during the freezing of frost susceptible soils

The sensitivity analyses found that the variables considered affected ice lensing as follows:

- An **increase** in thermal gradient will **increase** ice lensing.
- A **decrease** in rate of cooling will **increase** ice lensing.
- An **increase** in hydraulic conductivity will **increase** ice lensing.
- A **decrease** in segregation freezing temperature will **increase** ice lensing.
- A **decrease** in effective stress level will **increase** ice lensing.

In each case these trends of behaviour match the experimentally observed trends and patterns that were discussed in Chapter 2.

It was concluded that the development of ice lensing into the theoretical formulation has been correctly implemented into the finite element code COMPASS. The proposed model is capable of representing coupled flow and deformation processes including ice lensing in saturated freezing soils.

8.6. Simulation of Freezing Experiments at Caen

A large scale freezing experiment conducted at the Caen CNRS Centre de Géomorphologie in Caen, France was considered in Chapter 7. The large scale experiment was designed to measure and record the timing and rate of: a) frost penetration, b) surface frost heaving, c) thaw penetration, d) pore water pressure changes and e) downslope surface soil displacements. The results from the numerical simulation of the experiment were presented and compared against the experimental data.

A good correlation was achieved with the experimental results by predicting the patterns and trends of experimentally observed behaviour and the cryogenic processes that occur during the freezing and thawing of frost susceptible soils. The accurate determination of material parameters is paramount in order to accurately represent the

behaviours and processes that occur. In particular the determination of the hydraulic conductivity and segregation temperature is vital.

It was concluded that the development of ice lensing and cryogenic processes into the theoretical formulation has been correctly implemented into the finite element code COMPASS. The proposed model is capable of representing coupled flow and deformation processes including ice lensing in saturated freezing soils. Further use of the numerical model is required to gain confidence in the ability to provide accurate results with the ultimate aim to be able to be used to perform blind predictions.

8.7. Overall Summary and Conclusions

General relationships are well established for cryogenic processes but field studies have not as yet provided the necessary precision of monitoring or experimental control to enable a more detailed exploration of the mechanisms of freezing and thawing. By adopting a laboratory based experimental approach it is possible to measure these processes with greater precision and detail while reducing the annual cycle of freeze and thaw to a few weeks. Several years of freezing and thawing can therefore be modelled in a matter of months.

Numerical modelling is the next step in the development and understanding of these processes. Large scale experiments and centrifuge modelling offer a good understanding and give good agreement with field conditions but are however expensive and time consuming activities to undertake.

A theoretical approach to describe the fully coupled transient moisture, heat and deformation processes in saturated soils which incorporates cryogenic effects has been presented. A numerical solution of the theoretical formulation was achieved spatially via the use of the Galerkin residual weighted finite element method and temporally via a backward difference mid interval finite difference scheme. The model developed in this study uses the framework for transient THM analysis provided by COMPASS to implement the numerical solution of the proposed model.

A verification and validation programme was conducted to test the integrity and soundness of the model. The verification exercises focused on the cryogenic processes that have been incorporated into the existing COMPASS numerical model. A sensitivity analysis on key model variables was then implemented to explore the model performance in order to determine their effect on the magnitude and growth of ice lenses in a freezing soil

Finally the numerical model was applied to experimental work carried at Caen on one, one sided freezing test. The simulated results showed a good correlation with the experimental results by predicting the patterns and trends of experimentally observed behaviour and the cryogenic processes that occur during the freezing and thawing of frost susceptible soils.

It is therefore concluded that the proposed model is capable of providing a good representation of the fully coupled THM behaviour of saturated soils with cryogenic effects.

8.8. Suggestions for Further Research

The proposed model has been shown to be capable of representing the coupled thermo / hydro / mechanical behaviour of saturated soil with cryogenic effects. However, the numerical code is under constant development and the following suggestions are made for further research.

1) In this work for a limited number of material parameters, no direct experimental data was available, and assumed or estimated values were used. Further experimental work would be beneficial to more accurately define the material parameters. In particular, the hydraulic conductivity relationship is a key material parameter in the prediction of heave due to cryogenic suctions.

2) It is well documented that ice segregation leads to a negative pore water pressure gradient which flows towards the growing ice lens. As a result this raises the effective stress in the continuous matrix of soil surrounding the ice lens so consolidation results in the soil matrix (Morgenstern and Nixon 1971).

If the soil is normally consolidated or slightly over consolidated, the freezing process will result in an increase in the pre-consolidation pressure and irreversible plastic deformation will occur. During the investigations conducted in this work, the pre-consolidation pressure, p_0, was set a high value to ensure that the material remained in the elastic region of the stress space. Allowing non-recoverable plastic strains to develop will permit the representation of additional observed deformation trends to be reproduced using the numerical model.

3) In periglacial environments; seasonal variations in temperatures and the effects of climate change and global warming result in the widespread gradual downslope displacement (solifluction) of the mountain landscape. The ability to quantify the changes in solifluction rates in these environments is of considerable importance. Initial investigations using the proposed numerical model were unable to capture the downslope displacements from laboratory experiments and work to enable slope geometries to be modelled and the pre-failure shear strains that result is required. This is currently being investigated within the Geoenvironmental Research Centre at Cardiff University.

4) When solutes are present in unfrozen water it can be seen that they tend to be excluded from ice as the water freezes and as a result accumulate in the unfrozen water. Solute behaviour is of importance to the energy status of unfrozen water and therefore to the unfrozen water content. The influence of solutes on liquid water pressure and on unfrozen water content can have major effects on the transport of water in freezing soils. The effects of solutes on freezing have been published in the literature (Padilla and Villeneuve, 1992; Ostroumov et a., 2001) and inclusion into the theoretical formulation would lead to a more complete representation of the physics of freezing and thawing.

5) Frozen soil is usually stronger than unfrozen soil or ice; it displays time-dependant creep behaviour similar to ice and like unfrozen soil, frozen soils display a frictional behaviour (Hohmann-Porebska and Czurda 1997). In order to model the effects of frozen soil it is necessary to introduce creep effects into the theoretical formulation. Creep strain is composed of primary, secondary

(steady-state), and tertiary creep and any expression introduced must be capable of representing each stage.

6) Exclusive use of 8 noded isoparametric elements was made in this work. Alternative element options are available and their applicability to freezing and thawing problems should be considered. The use of triangular elements would permit the discretisation of complex domains to be generated with greater ease than isoparametric elements e.g. problems such as buried chilled pipelines. Before triangular elements can be used it is necessary to conduct the verification and validation tests presented for isoparametric elements. Numerical instabilities have also been encountered during this work and the use of higher order elements and interpolation functions may make the solution more stable. The use of 12 noded isoparamteric elements is currently being investigated within the Geoenvironmental Research Centre at Cardiff University.

7) The work presented here used two dimensional axisymmetric and plane strain formulations although the majority of problems investigated have all been with one dimensional boundary conditions. The extension to two dimensions would simply require an appropriately defined example as the theoretical formulation and numerical implementation is for a multidimensional approach. A three dimensional formulation is also incorporated in the numerical code COMPASS; however before a three dimensional example is simulated, the verification tests must be also completed using the three dimensional elements.

8) The proposed model has been partially verified and validated using existing experimental data, and analytical solutions. In order to fully test the capabilities of the model it is suggested that the numerical code should be used to provide blind predictions of material response for comparison against experimental data.

8.9. References

Hohmann-Porebska, M. and Czurda, K. A. 1997. "Cryogenical alterations of fabric and shear strength of clayey soils" *Ground freezing and frost in geotechnical engineering* Lulea; Sweden: Balkema. 317-326.

Morgenstern, N. R. and Nixon, F. M. 1971. "One-dimensional consolidation of thawing soils." *Canadian Geotechnical Journal*, **8**, 558-565.

Ostroumov. V., Hoover. R., Ostroumova. N., Van Vliet-Lanoë. B., Siegert. Ch., and. Sorokovikov. V., 2001 "Redistribution of soluble components during ice segregation in freezing ground" *Cold Regions Science and Technology*, **32**, 175-182.

Padilla. F., and Villeneuve. J-P., 1992. "Modelling and experimental studies of frost heave including solute effects" *Cold Regions Science and Technology*, **20**, 183-194.

Penner, E. 1986 "Aspects of Ice Lens Growth in Soils". *Cold Regions Science and Technology*, **13**, 91-100.